

Developing new imaging biomarkers in multiple sclerosis

Niamh Cawley

MB BCh BAO MRCPI

A thesis submitted to the University College of London for the degree of

Doctor of Philosophy

July 2016

Department of Neuroinflammation,

Queen Square MS Centre

UCL Institute of Neurology

Queen Square

London

WC1N 3BG

Declaration

I, Niamh Cawley, confirm that the work presented in this thesis is my own. Where work has been derived from other sources, I confirm that this has been indicated in my thesis.

Abstract

The overall aim of this thesis is to investigate the development of new imaging biomarkers for clinical application in multiple sclerosis (MS).

To date, there have been significant advances in the use of magnetic resonance imaging (MRI) in the initial diagnostic work-up of patients suspected of having MS and also in the monitoring of disease activity during active treatment. However, there is often a discrepancy between the clinical and conventional MRI findings which arises due to the complex heterogeneous features of MS pathology. The development of imaging biomarkers, which are directly linked to the pathological processes underlying progressive and relapsing forms of MS, are vital to developing a better understanding of the pathological mechanisms driving the disease.

In order to address this, I performed clinical studies in both progressive and relapsing forms of MS with both innovative imaging techniques and with other more established imaging measures. After the introduction (where I review the main characteristics of MS (Chapter I) and of conventional and advanced MRI techniques employed in the studies presented in this thesis (Chapter II)), I present the following studies:

- (A) Pilot studies with innovative imaging techniques – this included a gamma-aminobutyric acid (GABA) magnetic resonance spectroscopy study in patients with secondary progressive multiple sclerosis (SPMS) (Chapter III) and a novel diffusion study (neurite orientation dispersion and density imaging, NODDI) in the brain of patients with relapsing remitting multiple

sclerosis (RRMS) (Chapter IV). The main results of these investigations are that GABA may be a marker of neurodegeneration and NODDI may better characterise microstructural changes in the brain than standard diffusion tensor imaging.

(B) Clinical studies with more established imaging measures including an MRI follow-up spinal cord study in primary progressive multiple sclerosis (PPMS) (Chapter V) using ¹H-Magnetic resonance spectroscopy (¹H-MRS), Q-space imaging (QSI) and spinal cord area. Another study looked at the development of spinal cord atrophy in a progressive MS cohort of patients over 1 year to determine the sample sizes required to demonstrate a reduction in spinal cord cross-sectional area as a primary outcome measure in clinical trials (Chapter VI). Both of these studies demonstrated spinal cord atrophy occurred over 1 year and it may be a useful outcome measure in phase II neuroprotective trials in early PPMS.

In the final chapter (Chapter VII), I will summarise the results of the studies presented in the thesis and propose future directions for the research.

Acknowledgements

I would like to thank all the patients with multiple sclerosis and healthy controls who volunteered their time to take part in the studies carried out as part of this thesis.

I would also like to thank the radiographers at the NMR Unit, Marios Yiannakas, Chichi Ugorji and Luke Hoy. They took great care when imaging subjects to ensure optimal results, as well as the patience and compassion they displayed towards those who participated in the studies.

The help and support I received from the physics team was invaluable, from setting up and developing the GABA spectroscopy and NODDI protocols, to the post-processing of the diffusion and spectroscopy data, in particular from Drs. Bhavana Solanky, Torben Schneider, Francesco Grussu and Claudia Wheeler-Kingshott.

I am extremely grateful to Dr. Carmen Tur and Dr. Dan Altmann, for her support and advice on the statistics used in this thesis, and for her help in performing more complex statistical analyses for the studies carried out as part of this thesis.

A special thank you to Dr. Ferran Prados, for his patience and endless support, which he provided me for the analysis of my data. His willingness to help, with nothing ever being a problem, no matter how big or small, will always be remembered.

My time at UCL was enhanced by the great colleagues I worked with, Dr. Khaled-Abdel-Aziz, Dr. Rhian Raftopolous, Dr. Wallace Brownlee, Dr. Shahrukh Mallik,

Dr. Becky Samson, Dr. Sara Collorone and Ifrah Lidow for their friendship and support during my time at UCL.

I am extremely grateful to my principal supervisor, Professor Olga Ciccarelli, for her guidance, motivation and ongoing support throughout my PhD. She has supported me throughout all the twists and turns which I have encountered in completing this thesis and I am forever grateful for this. Professor Alan Thompson, has been an excellent mentor to me, from identifying my goals early on in my PhD, ensuring I kept focussed on them and his invaluable input and advice in the final stages of my thesis. I wish to thank Professor David Miller for his thoughtful comments to my papers and abstracts.

I would like to thank my family for their ongoing love and encouragement, in particular to my mother, for her unconditional love and her sustained support and help throughout my life. Finally, a big thank you to my husband, Rob. His patience and support has been endless over the last number of years. He has always been there for me, through the ups and downs, and has made London my second home. I look forward to the next stage of our life together.

Publications associated with this thesis

Papers:

Cawley, N., Solanky, B. S., Muhlert, N., Tur, C., Edden, R. A., Wheeler-Kingshott, C. A. M., Miller, D. H., Thompson, A. J. & Ciccarelli, O. Reduced gamma-aminobutyric acid concentration is associated with physical disability in progressive multiple sclerosis. 2015. Brain 138, 2584-95.

Cawley, N., Tur, C., Prados, F., Plantone, D., Kearney, H., Abdel – Aziz, K., Ourselin, S., Gandini Wheeler – Kingshott, C. A. M., Miller, D. H., Thompson, A. J., O. Ciccarelli. Spinal cord atrophy as a primary outcome measure in phase II trials of progressive multiple sclerosis. Awaiting resubmission to MSJ over the next few weeks.

Cawley, N., Abdel – Aziz, K., Tur, C., Prados, F., Solanky, B. S., Schneider, T., Wheeler-Kingshott, C. A. M., Miller, D. H., Thompson, A. J. & Ciccarelli, O. Longitudinal changes in advanced imaging measures in the cervical cord in PPMS. In preparation for submission.

Book Chapter:

Cawley, N., Ciccarelli, O. MR Spectroscopy in Multiple Sclerosis. In: Magnetic Resonance Spectroscopy of Degenerative Brain Diseases. Publisher: Springer, June 2016. Editor: Dr Gülin Öz, University of Minnesota.

Prize:

Awarded best bedside Teacher of the Year (the Djamshidian-Chinthapalli award for outstanding contribution to teaching) 2015/16, Institute of Neurology, UCL.

Table of contents

Declaration	2
Abstract	3
Acknowledgements	5
Publications associated with this thesis	7
Table of contents	9
List of Tables	14
List of Figures	17
List of Abbreviations	20
Chapter I	
Introduction to multiple sclerosis	23
1.1 Introduction	24
1.2 MS Phenotypes	24
1.3 Clinical presentation and disease course	28
1.3.1 Environmental Factors	31
1.3.2 Genetic Factors	35
1.4 Comorbidities & MS	37
1.5 Pathology	38
1.5.1 White Matter	Error! Bookmark not defined.
1.5.2 Grey Matter	39
1.6 Diagnosis of multiple sclerosis	42
1.7 Therapy in MS	48
Chapter II	
Principles of magnetic resonance imaging	49
2.1 Principles of MRI	50
2.2 T1 – longitudinal relaxation	53
2.3 T2 – transverse relaxation	53
2.4 Image contrast	54
2.4.1 T1-weighted imaging	55
2.4.2 T2-weighted imaging	55
2.4.3 Proton density imaging	55
2.5 Pulse sequences	56
2.5.1 Spin Echo Imaging	57
2.5.2 Fast spin-echo (FSE) sequences	57
2.5.3 Gradient echo imaging	58
2.6 Magnetic Resonance Spectroscopy (MRS)	60
2.6.1 Chemical Shift	61

2.6.2 Shimming	62
2.6.3 Spin-Spin Coupling (J-Coupling)	62
2.6.4 Localisation	63
2.6.4.1 PRESS (Point RESolved Spectroscopy)	63
2.6.4.2 MEGA-PRESS (MEscher-GARwood Point RESolved Spectroscopy)	63
2.6.5 Clinical Application of MR Spectroscopy in Multiple Sclerosis	65
2.7 Diffusion Imaging	71
2.7.1 Basic principles	71
2.7.2 Effects of diffusion on the MRI signal	71
2.7.3 Pulsed gradient spin echo	72
2.7.4 Diffusion tensor	73
2.7.5 Q-Space Imaging	77
2.7.5.1 Clinical application of Q-space imaging in MS	78
2.7.6 NODDI (Neurite Orientation Dispersion and Density Imaging)	79
2.7.6.1 Clinical application of NODDI in MS	82
2.8. Brain atrophy	82
2.8.1 Background	82
2.8.2 Technical	83
2.8.3 Clinical application	84
2.9 Spinal cord imaging	86
2.9.1 Spinal cord ¹ H-MR spectroscopy	86
2.9.2 Q-space imaging in the spinal cord	87
2.9.3 Spinal Cord Atrophy	88
2.9.3.1 Background	88
2.9.3.2 Technical	89
2.9.3.3 Clinical application	91
2.10 Conclusion	92

Chapter III

Gamma-aminobutyric acid concentration in progressive multiple sclerosis	93
--	-----------

3.1 Introduction	94
3.2 Materials and methods	97
3.2.1 Subjects	97
3.2.2 Cognitive Tests	98
3.2.3 Clinical Assessments	99
3.2.4 Magnetic Resonance Imaging Protocol	100
3.2.4.1 Structural MR Imaging	100
3.2.4.2 Single-Voxel Spectroscopy	101
3.2.5 Spectral Quantification	103
3.2.6 Statistical analysis	104
3.2.6.1 Differences in cognitive and clinical performance and metabolite concentrations between groups	104

3.2.6.2 Associations between clinical disability and regional GABA levels in patients and controls	104
3.7 Results	105
3.7.1 Participant demographics and characteristics	105
3.7.2 Clinical disability	105
3.7.3 Structural MRI Measures	107
3.7.4 GABA concentration in the hippocampus and sensorimotor cortex was lower in patients than controls	110
3.7.5 Associations between GABA levels in the sensorimotor cortex and clinical scores	111
3.7.6 Associations between tNAA levels in the sensorimotor cortex and clinical scores	112
3.8 Discussion	113
3.8.1 Evidence of GABAergic dysfunction in SPMS	113
3.8.2 Association between lower GABA levels and physical disability	115
3.8.4 Limitations and future directions	117
3.8.5 Conclusion	119
Chapter IV	
Application of NODDI, a novel diffusion MRI technique in RRMS	120
4.1 Introduction	121
4.2 Materials & Methods	124
4.2.1 Study	124
4.2.2 Cognitive Assessments	126
4.2.3 Clinical Assessments	126
4.2.4 MRI protocol	126
4.3 Image Post Processing	127
4.3.1 T2 hyperintense lesions	127
4.3.2 Brain segmentation	128
4.3.4 NODDI processing	128
4.4 Statistical Analysis	129
4.5 Results	130
4.5.1 Participant demographics and characteristics	130
4.5.2 Clinical disability	131
4.5.3 Difference in MRI metrics between RRMS and controls	133
4.5.4 Difference in MRI metrics between cervical myelopathy subjects and controls	137
4.5.5 Differences between MRI parameters in T2 lesions and normal appearing white matter in RRMS	139
4.5.6 Associations between MRI metrics and clinical disability scores in patients with RRMS and cervical myelopathy	140
4.6 Discussion	142
4.6.1 Difference in MRI metrics between RRMS and controls	143
4.6.1.1 Normal appearing white matter	143

4.6.1.2 T2 lesions	144
4.6.2 Difference in MRI metrics between cervical myelopathy subjects and controls	146
4.6.3 Associations between MRI metrics and clinical disability scores in RRMS	147
4.6.4 Associations between MRI metrics and clinical disability scores in cervical myelopathy patients	148
4.7 Conclusion	149
4.8 Limitations	149

Chapter V

Longitudinal changes in advanced imaging measures in the cervical cord in PPMS	151
---	------------

5.1 Introduction	152
5.2 Materials and Methods	154
5.2.1 Study participants	154
5.2.2 Clinical Assessments	155
5.2.3 MRI Protocol	157
5.2.3.1 MRS protocol	157
5.2.3.2 Spinal cord atrophy protocol	158
5.2.3.3 QSI protocol	159
5.2.3.4 Brain MRI protocol	159
5.3 Image Post Processing	161
5.3.1 Spinal cord metabolite quantification	161
5.3.2 Spectral Quality	161
5.3.3 Spinal cord cross sectional area measurement	162
5.3.4 Spinal cord QSI and ROI analysis	162
5.3.5 Brain T2 Lesion Volumes and grey matter and white matter volumes	164
5.3.6 Brain atrophy	164
5.4 Statistical Analysis	165
5.5 Results	168
5.5.1 Participant demographics and characteristics	168
5.5.2 Cross-sectional difference in spinal cord measures between patients and controls at 1 year	170
5.5.3 Longitudinal changes in MRI metrics over 1 year	176
5.5.4 Associations between change in Q-space imaging measures and change in clinical disability over 1 year	179
5.5.5 Associations between change in ¹ H-MRS measures and change in clinical disability over 1 year	180
5.5.6 Predicting clinical status at 1 year with baseline MRI measures	186
5.7 Discussion	189
5.7.1 Differences in spinal cord area, metabolite concentrations and Q-space imaging measures between patients and controls	189

5.7.2 Associations between whole cord imaging measures and clinical disability	192
5.7.3 Associations between change in column-specific q-space imaging measures and change in clinical disability	193
5.7.4 Predicting clinical status at 1 year with baseline MRI measures	194
5.8 Limitations	194
5.9 Conclusion	195
Chapter VI	
Spinal cord atrophy in progressive multiple sclerosis	196
6.1 Introduction	197
6.2 Methods	199
6.2.1 Subjects	199
6.2.2 Clinical Assessments	200
6.2.3 MRI acquisition	201
6.3 MRI analysis	201
6.3.1 Spinal cord area measurement	201
6.3.2 Brain atrophy measurement	202
6.3.3 Brain T2 lesion volume	203
6.4 Statistical analysis	203
6.5 Results	204
6.5.1 Participant demographics and characteristics	204
6.5.2 Spinal cord atrophy	207
6.5.3 Brain atrophy	208
6.5.4 Associations between change in cord area and change in clinical scores	208
6.5.5 Sample size calculations for a neuroprotective clinical trial	211
6.6 Discussion	211
6.6.1 Clinical correlations	213
6.6.2 Sample size	215
6.7 Conclusion	217
CHAPTER VII	
Conclusions and future directions	218
7.1 Conclusions	219
7.2 Future directions	224
References	228

List of Tables

CHAPTER 1

Table 1.1 2010 Revised McDonald Criteria – Diagnosing RRMS

CHAPTER 2

CHAPTER 3

Table 3.1 Mean (SD) demographics, clinical and cognitive performance of patients and controls.

Table 3.2 MRI measures in patients and controls.

Table 3.3 Comparison of GABA, tNAA and Glx concentration (mean (SD) in mM) in the prefrontal cortex, right hippocampus and left sensorimotor cortex between the control group and the patient group.

CHAPTER 4

Table 4.1 Mean (SD) demographics and clinical characteristics of patients and controls.

Table 4.2 Mean (SD) clinical and cognitive performance of RRMS patients and controls.

Table 4.3 Mean (SD) clinical and cognitive performance of cervical myelopathy subjects and controls.

Table 4.4 Mean (SD) of diffusion MRI measures in RRMS patients and controls.

Table 4.5 Mean (SD) of diffusion MRI measures in cervical myelopathy patients and controls.

Table 4.6 Mean (SD) of NODDI MRI measures in T2 lesions and in normal appearing white matter in RRMS patients.

CHAPTER 5

Table 5.1	Mean (SD) demographic of patients and volunteers.
Table 5.2	Mean (SD) clinical characteristics of patients.
Table 5.3	Summary of mean (SD) diffusivity from the anterior column of the cervical cord in patients and controls at baseline and at 12 months follow-up.
Table 5.4	Summary of mean (SD) diffusivity from the lateral column of patients and controls as baseline and as 12 months follow-up.
Table 5.5	Summary of mean (SD) diffusivity from the whole cord of patients and controls as baseline and at 12 months follow-up.
Table 5.6	Summary of mean (SD) diffusivity from the posterior column of patients and controls at baseline and at 12 months follow-up.
Table 5.7	Cross-sectional summary of mean (SD) metabolite concentrations (mmol/l) from the cervical cord of patients and controls.
Table 5.8	Sample size calculations required to detect significant changes in MRI metrics in patients over time compared to changes observed in controls with 80% power.
Table 5.9	Summary of significant associations between: (A) change in QSI metrics and change in clinical disability scores, (B) change in metabolites and change in clinical disability scores and (C) predictors of clinical status at 1 year with baseline MRI measures.
Table 5.10	Associations between change in Q-space metrics (predictors) and change in clinical scores (dependent variables) in patients.
Table 5.11	Associations between change in ¹ H-MRS measures (predictors) and change in clinical scores (dependent variables) in patients.
Table 5.12	Predictors of clinical status at 1 year with baseline MRI measures.

CHAPTER 6

- Table 6.1** Mean (SD) of main demographic and clinical findings in the progressive MS, healthy controls, PPMS and SPMS cohort at 1 year.
- Table 6.2** Mean (SD) of the clinical scores at baseline and 1 year follow-up.
- Table 6.3** calculations for a neuroprotective clinical trial in progressive (5% significance).

List of Figures

CHAPTER 1

Figure 1.1 2013 multiple sclerosis phenotype descriptions for relapsing disease.

Figure 1.2 2013 multiple sclerosis phenotype descriptions for progressive disease.

CHAPTER 2

Figure 2.1 Alignment of spins after the application of an external magnetic field. There is net longitudinal magnetisation in the direction of B_0 .

Figure 2.2 T1 recovery curve - T1 relaxation time refers to the time taken for 63% of the longitudinal magnetisation to recover.

Figure 2.3 T2 relaxation curve - T2 relaxation time refers to the time taken for transverse magnetisation to decay to 37%.

Figure 2.4 Spin echo sequence diagram. An 180° pulse is applied at time t ($TE/2$) and an echo is detected at time $2t$ equal to TE .

Figure 2.5 Gradient echo sequence diagram. A radiofrequency pulse producing a flip angle $<90^\circ$ is applied, which is followed by a dephasing and rephrasing gradients to produce the echo.

Figure 2.6 Example of a post-processed spectrum from the spinal cord of a healthy control. The chemical shift is on the x-axis in ppm and signal intensity on the y-axis. Cho – choline; Cr – creatine; Ins – myo-inositol; NAA – n-acetylaspartate.

Figure 2.7 Example of an MRS GABA post-processed spectrum from the left sensorimotor cortex from a healthy control. GABA – gamma-aminobutyric acid; tNAA – total N-acetylaspartate.

Figure 2.8 Pulsed gradient spin echo sequence for diffusion weighting. Δ represents the interval between centres of the two diffusion gradients corresponding to the diffusion time, δ represents the pulse width and g is the magnitude of the diffusion-weighting gradient.

Figure 2.9 Example of an AD, RD, FA and MD maps from an MS patient with reduced FA and increased diffusivity seen in lesional tissue (white arrows).

Figure 2.10 Steps involved in Q-space analysis. (A) The signal attenuation curve from the raw Q-space data is Fourier transformed. (B) This gives the probability density function. (C) Summary statistics (P0 and FWHM) are derived from the probability density function.

Figure 2.11 Example of NODDI maps from an MS patient (A) orientation dispersion index (ODI) (B) neurite density index (NDI) and (C) isotropic volume fraction (isoFV).

Figure 2.12 Orientation dispersion index (ODI), which is the spread of neurite orientations, ranging from 0 (on the left) and 1 (on the right).

Figure 2.13 Example of an axial 3D-FFE image (resolution 0.5 x 0.5 x 5mm³) through the C2/3 intervertebral disc from a healthy control showing the cord volume using the active surface model.

CHAPTER 3

Figure 3.1 Placement of MR Spectroscopy (MRS) voxels (left) with their example MRS spectra (right) in the prefrontal cortex (A), right hippocampus (B) and the left sensorimotor cortex (C).

CHAPTER 4

Figure 4.1 Boxplots of the NODDI metrics (ODI, NDI and isoVF) in: (A) normal appearing white matter (NAWM), (B) cortical grey matter (CGM), (C) deep grey matter (DGM) in RRMS and cervical myelopathy patients when compared to healthy controls, and (D) in NAWM compared to T2 lesions in RRMS patients only.

Figure 4.2 Example of NODDI maps from a control (top row) and a patient with RRMS (27 year old male, with an EDSS of 3.5) (bottom row), (A) orientation dispersion index (ODI), (B) neurite density index (NDI) and (C) isotropic volume fraction (isoVF). Visually there is a reduction in NDI in normal appearing white matter of the RRMS subject when compared to the control. Absolute values of NDI in the NAWM in the control is 0.5839 and 0.5642 in the RRMS patient.

Figure 4.3 Example of NODDI maps from T2 lesions in an MS subject. (A) Axial T2 scan with T2 hyperintense lesions outlined in red, (B) an NDI map of the T2 lesions demonstrating a reduction in NDI and (C) an ODI map of the T2 lesions demonstrating a reduction in ODI.

CHAPTER 5

Figure 5.1 Example of the spectroscopy voxel placement in the coronal (A) and sagittal planes (B) and the diffusion weighted image volume in the sagittal (C) and coronal plane (D) in the cervical cord.

Figure 5.2 Examples of a 3D-FFE axial image of the cervical cord outlined using the active surface model, P0xy map, FWHMxy map and a post processed spectra in a PPMS patient at baseline and then at 1 year follow-up. The graphs represent differences in height and width of the displacement distribution function from the posterior (left) and lateral column (right) from a patient at baseline and 1 year. The FFE image shows a reduction in cross-sectional cord area, increased FWHMxy in the lateral column, reduced P0xy in the posterior columns and reduced tNAA at 1 year.

Figure 5.3 Scatter plot demonstrating the association between change in vibration perception thresholds and change in diffusivity in the posterior columns (FWHMz) in patients (unadjusted).

Figure 5.4 Scatter plot demonstrating the association between perpendicular diffusivity in the posterior column at baseline predicting EDSS at 1 year (unadjusted).

CHAPTER 6

Figure 6.1 Spinal cord outline using the active surface model on the axial FFE images.

Figure 6.2 FFE image at baseline (A) and 1 year follow-up (B) with visible evidence of cord atrophy in a subject with PPMS (47 year old male, baseline: EDSS 4.0, cord area = 85.95mm²; 1 year: EDSS 6.0, cord area 82.37mm²).

Figure 6.3 Scatterplot showing the association between changes in spinal cord area (mm²) with changes in EDSS in the PPMS cohort (unadjusted analysis).

Figure 6.4 Scatterplot showing the association between changes in spinal cord area (mm²) with changes in 9-HPTz scores in the PPMS cohort (unadjusted analysis).

List of Abbreviations

AD	Axial diffusivity
ADC	Apparent diffusion coefficient
ASIA	American spinal injury association
BPF	Brain parenchymal fraction
BVMT-R	Brief visual memory test-revised
CVLT-II	California verbal learning test – second edition
Cho	Choline
CIS	Clinically Isolated Syndrome
CNS	Central nervous system
Cr	Creatine
CRLB	Cramér rao lower bounds
CSA	Cross-sectional cord area
CSF	Cerebrospinal fluid
DIR	Double inversion recovery
DTI	Diffusion tensor imaging
DWI	Diffusion weighted imaging
ECL	Echo chain length
EDSS	Expanded Disability Status Scale
FA	Fractional anisotropy
FFE	Fast field echo
FOV	Field of view
FSE	Fast spin echo
FWHM	Full width at half maximum
GABA	Gamma-aminobutyric Acid

Gln	Glutamine
Glu	Glutamate
Glx	Glutamate + glutamine
GMF	Grey matter fraction
HADS	Hospital anxiety and depression scale
Ins	Myo-inositol
isoVF	Isotropic volume fraction
MD	Mean diffusivity
MHC	Major Histocompatibility Complex
MRI	Magnetic resonance imaging
MS	Multiple sclerosis
MRS	Magnetic resonance spectroscopy
MEGA-PRESS	MErscher GARwood Point RESolved Spectroscopy
NAA	N-acetylaspartate
NAWM	Normal appearing white matter
NDI	Neurite density
NODDI	Neurite orientation dispersion and density imaging
ODI	Orientation dispersion imaging
PASAT	Paced Auditory Serial Addition Test
PBVC	Percent brain volume change
PPMS	Primary progressive multiple sclerosis
Ppm	Parts per million
PRESS	Point RESolved Spectroscopy
QSI	Q-space imaging
RD	Radial diffusivity
RF	Radiofrequency

RIS	Radiologically Isolated Syndrome
RRMS	Relapsing remitting multiple sclerosis
SDMT	Symbol digit modalities test
STEAM	STimulated Echo Acquisition Mode
SE	Spin Echo
TE	Echo Time
TR	Repetition Time
TWT	Timed 25-Foot Walk Test
VOI	Volume of interest
WMF	White matter fraction
9-HPT	9-Hole Peg Test

Chapter I

Introduction to multiple sclerosis

1.1 Introduction

Multiple sclerosis (MS) is a chronic demyelinating disease, of the brain and spinal cord, with both demyelinating and degenerative components. It is the most common cause of neurological disability in young adults world-wide. Jean-Martin Charcot was the first to describe the clinicopathological features of MS in 1868. However there had been case presentations as early as the 1820s. Despite the pathological characteristic lesions being described over 150 years ago, the aetiology and pathophysiology of the disease course remains unclear.

MS is a global disease with an estimated 2.1 million sufferers worldwide in 2008, which increased further to 2.3 million in 2013 (Browne *et al.*, 2014). The increase in MS prevalence is likely to be due to increased survival of people with MS, improved diagnosis of MS and increased MS incidence in some countries (Browne *et al.*, 2014). The prevalence of MS varies greatly, with the highest in North America and Europe (140 and 108 per 100,000 respectively) (Browne *et al.*, 2014). The UK prevalence of MS is estimated to be around 125 per 100,000 (Mackenzie *et al.*, 2014).

1.2 MS Phenotypes

The initial phase of relapsing-remitting MS (RRMS) is characterised by episodes of active disease with neurological dysfunction (relapse), during which demyelinating lesions form in the central nervous system, interspersed with periods of clinical inactivity. There is a variable degree of recovery between relapses. The disease course for RRMS is highly unpredictable with the frequency of relapses as well as the accumulation of disability linked to the sex of the patient as well as the age at disease onset. About 85% of patients present

with relapses and remissions. After a variable number of years, a proportion of patients show a gradual deterioration in function, independent of relapse activity, which is called secondary progressive MS (SPMS) (Weinshenker *et al.*, 1989a&b). SPMS is diagnosed retrospectively by a history of gradual worsening, after an initial relapsing remitting course, with or without acute exacerbations during the progressive course (Lublin *et al.*, 2014). There is no clear clinical, imaging, immunological, or pathological criteria to help determine the transition point from RRMS to SPMS. The median time to the development of SPMS was 19.1 years from first diagnosis in the Lyon cohort data (Vukusic *et al.*, 2003) and 21.4 years in the British Columbia cohort data (Koch *et al.*, 2010). The study by Koch *et al.* found that the main factors influencing the onset of SPMS in untreated RRMS patients included male gender, age at onset and motor onset symptoms, which were associated with both a shorter time to and a younger age at SPMS onset (Koch *et al.*, 2010). A more recent study found that pre and post-progression relapses accelerated the time to severe disability in progressive MS (Novotna *et al.*, 2015).

A minority of patients with MS (10%) have a slow accumulation of disability from disease onset without relapses, and are described as having primary progressive MS (PPMS) (Koch *et al.*, 2009). 3-10% of patients with PPMS have relapses (Hawker *et al.*, 2009; Andersson *et al.*, 1999). Primary progressive MS differs from other types of MS as the age of symptom onset is typically older (fourth-fifth decade) compared with RRMS (second-third decade). Studies to date show that PPMS has an equal sex distribution. This is in contrast to RRMS which has a female preponderance at 2-3:1 (Compston and Coles, 2008, Miller and Leary, 2007a). Previously it was felt that PPMS may represent a distinct, non- (or less)

inflammatory form of MS (Lassmann *et al.*, 2012). However, now it is felt that PPMS is part of the spectrum of progressive MS phenotypes, based on clinical, imaging and genetic data (Lublin *et al.*, 2014). A recent study in radiologically isolated syndrome (RIS) found a similar prevalence (at 12%) and age at onset of PPMS to the general MS population (Kantarci *et al.*, 2015). In this RIS cohort the presence of spinal cord lesions and being male predicted the evolution to PPMS (Kantarci *et al.*, 2015).

MS can be divided into different sub-types (RRMS, PPMS and SPMS) as described above, characterised by a different clinical course defined by the National Multiple Sclerosis Society of the USA Advisory Committee (Lublin & Reingold, 1996). These definitions have recently been modified (Lublin *et al.*, 2014), with the inclusion of two new disease courses: clinically isolated syndrome (CIS) and radiologically isolated syndrome (RIS). CIS is defined as the first clinical presentation of a disease that shows characteristics of inflammatory demyelination that could be MS, but has yet to fulfil the criteria for dissemination in time (Miller *et al.*, 2005). RIS is defined as the incidental imaging finding suggestive of demyelination without a corresponding history or physical examination findings typical for MS (Okuda *et al.*, 2009). Further modifications to the diagnostic criteria include the use of MRI scans to detect disease activity and to determine if progression of disability has occurred over a given time period (Lublin *et al.*, 2014). Disease activity is determined by clinical relapses and/or MRI activity (contrast-enhancing lesions; new or unequivocally enlarging T2 lesions assessed at least annually) (Lublin *et al.*, 2014). While progression is measured by clinical evaluation assessed at least annually (Lublin *et al.*, 2014).

The progressive relapsing disease subtype has also been redefined as PPMS with disease activity (Lublin *et al.*, 2014) as outlined below.

2013 description for relapsing disease

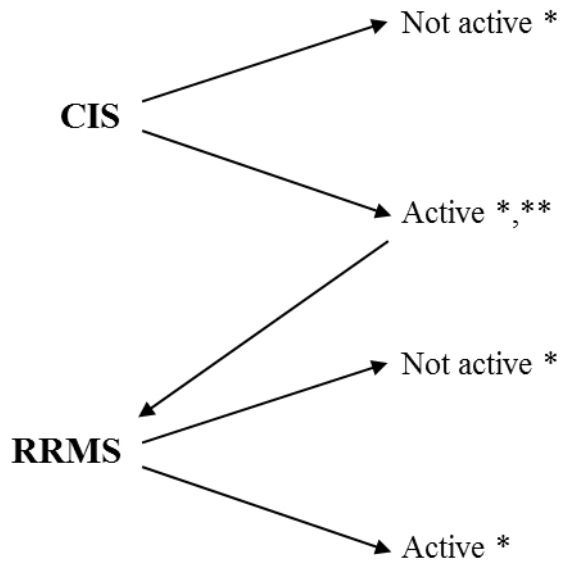


Figure 1.1: 2013 multiple sclerosis phenotype descriptions for relapsing disease.
 * Activity determined by clinical relapses and/or MRI activity (contrast-enhancing lesions; new or unequivocally enlarging T2 lesions assessed at least annually).
 ** CIS, if subsequently clinically active and fulfilling current MS diagnostic criteria, becomes RRMS (Lublin *et al.*, 2014).

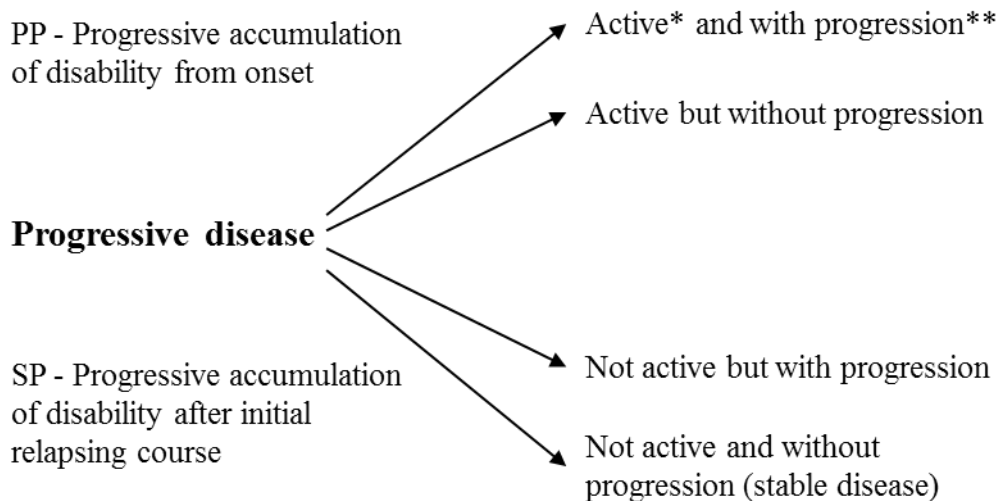
2013 description for progressive disease

Figure 1.2: 2013 multiple sclerosis phenotype descriptions for progressive disease. * Activity determined by clinical relapses assessed at least annually and/or MRI activity (contrast enhancing lesions; new and unequivocally enlarging T2 lesions). ** Progression measured by clinical evaluation, assessed at least annually. If assessments are not available, activity and progression are indeterminate (Lublin *et al.*, 2014).

1.3 Clinical presentation and disease course

The symptoms and signs of MS are variable and can result from injury to any part of the central nervous system (CNS), from the spine to the brain. The symptoms and signs of MS merely reflect the functional anatomy of impaired saltatory conduction at affected sites (Compston & Coles, 2002). The cerebrum is almost always involved when assessed with MRI, however most white matter abnormalities cannot be linked to specific events or clinical symptoms. Some areas are more affected than others such as the optic nerve, cerebellum, brain stem and the posterior and lateral columns of the spinal cord. Typical symptoms in RRMS include optic neuritis, sensory symptoms, motor deficits, diplopia, vertigo, balance problems, and fatigue (Weinshenker *et al.*, 1989a).

Cognitive impairment is very common in MS, with prevalence ranging from 40% to 70% (Chiaravalloti *et al.*, 2008), and typically is more common in the progressive forms of MS (Chiaravalloti *et al.*, 2008). MS detrimentally affects various aspects of cognitive functioning in particular attention, information processing speed, working memory, verbal memory and executive function (Rocca *et al.*, 2015). It has been demonstrated that white matter lesions only play a partial role on cognitive performance compared to damage to normal appearing white and grey matter (Rocca *et al.*, 2015). Cortical lesion number and volume are associated with cognitive deficits in MS patients, with damage to deep grey matter structures, such as the thalamus, having an early role in cognitive impairment in MS (Rocca *et al.*, 2015). It is thought that cognitive deficits in MS patients may be related to a disconnection syndrome involving white matter tracts (Rocca *et al.*, 2015). It has been found that some MS patients who have considerable disease burden do not have cognitive impairment. It is thought that this may be due to brain reserve and cognitive reserve (Sumowski *et al.*, 2013). The theory of brain reserve suggests that people with larger maximal life-time brain growth are able to withstand a greater disease burden, before reaching a critical threshold of brain volume loss, when cognitive impairment then emerges (Sumowski *et al.*, 2014). Cognitive reserve refers to enriching life experiences that are associated with more efficient patterns of cognitive processing, which helps to preserve cognition (Sumowski *et al.*, 2014). Based on these more recent findings, important factors which may help predict future risk of cognitive decline in MS are lower maximal life-time brain growth and intellectual enrichment (Sumowski *et al.*, 2014). These at risk subjects may benefit from early cognitive

rehabilitation and to engage in intellectual enrichment activities (Sumowski *et al.*, 2014).

Fatigue is reported to affect 50% to 80% of people with MS (Krupp, 2006) and it may be the most disabling symptom for some people with MS (Giovannoni, 2006). It is more common in people with PPMS and SPMS compared to RRMS and it tends to be worse in the afternoon (Patrick *et al.*, 2009). The pathophysiology of fatigue is not fully understood but potential mechanisms include pro-inflammatory cytokines e.g IFN- δ , tumour necrosis factor- α and interleukin 1, 6 and 10 (Heesen *et al.*, 2006), over activity of neural circuits (Thickbroom *et al.*, 2008) and/or diffuse axonal damage (Tartaglia *et al.*, 2004).

80% of PPMS cases have spinal cord involvement, progressing to quadriparesis with associated autonomic dysfunction. The PPMS phenotype implies a worse prognosis than RRMS (Noseworthy *et al.*, 2000). Natural history studies demonstrate a large variation in the rate of disability in PPMS, as measured by the number of years taken to reach an Expanded Disability Status Scale (EDSS) of 6 (Kurtzke, 1983). The evaluation of disease course in PPMS and SPMS (once established), are similar (Miller and Leary, 2007a). Natural history studies in RRMS have shown that the average annual relapse frequency is approximately one per year (Confavreux *et al.*, 1980). Due to the potential for treatment during the RRMS phase, studies have looked at factors which predict long-term disability. However, to date our ability to predict the disease course remains weak. A study by Weinshenker *et al.*, (Weinshenker *et al.*, 1989a) found that a high number of relapses in the first two years following the onset of MS correlated with long-term disability. Another study found relapse frequency after 2 years

does not seem to predict the onset of secondary progression or times to EDSS 6.0, 8.0 or 10, which may be related to neurodegeneration (Scalfari *et al.*, 2010). The number of relapses and the location of relapses did not correlate with progression to SPMS (Kremenutzky *et al.*, 2006).

The exact aetiology of MS is unknown but it is widely recognised that it has a complex causation that involves both genetic and environmental factors (Compston & Coles, 2008). Each of these factors are clearly implicated in the disease, with a complex interaction between genes and the environment occurring at a critical age (Compston & Coles, 2008). The four main factors thought to contribute to causality include (i) latitude, sunlight exposure (UVR) and Vitamin D, (ii) prior Epstein-Barr Virus (EBV) infection timing and adaptive immune response to EBV, (iii) cigarette smoking and (iv) hygiene hypothesis (Taylor *et al.*, 2011).

1.3.1 Environmental Factors

Multiple epidemiological studies have shown a definite role for environmental factors in determining the disease risk for MS. The latitude gradient is the most obvious example of how the environment affects the risk of MS (Kurtzke, 1975). Kurtzke divided areas into high, medium and low risk, which correlated with latitude. He found that there were very few cases of MS near the equator, with high risk zones in northern Europe and in the USA. This has been reproduced in more recent studies, with increases in prevalence seen with increasing distance north or south of the equator (Taylor *et al.*, 2011). MS is common in regions populated by northern Europeans but the risk of disease is modified depending on where the individual lives early in life (Compston & Coles, 2008). Migration

from high-risk to low-risk regions in childhood is associated with a reduced risk, while migration from low-risk to high-risk parts of the world is associated with an increased risk of developing MS compared with the population of origin (Compston & Coles, 2008).

The incidence of MS has been rising around the world over the last few decades. This is likely due to a rising incidence in women, which may support a sex-linked environmental factor (Compston & Coles, 2008). Potential explanations for this include a rise in female smoking, later age of first pregnancy, declining birth rates and obesity (Koch-Henriksen & Sorensen, 2010).

A large number of viruses but in particular Epstein Barr Virus (EBV) have been implicated in the pathogenesis of MS. About 90% of the population is infected by EBV and the infection typically occurs in early childhood. In comparison almost all patients (>99%) with MS are infected with EBV and the infection mostly occurs in adolescence (Ascherio *et al.*, 2000). The exact mechanism of how EBV is involved in the pathogenesis of MS is not fully understood. It is thought that MS may result from deficient control of EBV infection, resulting in EBV infected B cells accumulating in the central nervous system (Fernández-Menéndez *et al.*, 2016). EBV may have a direct role in inflammation and/or it may reactivate T cells contributing to the pathological process (Fernández-Menéndez *et al.*, 2016).

It has been proposed that EBV may be a simple confounder in epidemiological studies and it may not be a causative agent in MS pathogenesis. Even though EBV and other viral antibody titres are raised in MS subjects compared to the general population as outlined above, this may reflect immune dysregulation rather than being a true causative factor (Hunter *et al.*, 2000). A pathological

study of acute and chronic MS plaques as well as CSF, did not find EBV in the B lymphocytes and there was no evidence of intrathecal EBV antibody production (Sargsyan *et al.*, 2010). Therefore, it may be that EBV is association with other risk factors, such as smoking, which may alter the host's response to EBV and increase the overall risk of MS (Simon *et al.*, 2010).

Smoking has been identified as a risk factor for the subsequent development of MS. Cigarette smokers have a higher risk of developing MS compared to those who have never smoked (Ascherio & Munger, 2007). It has been demonstrated that smoking is associated with more severe disease, faster disability progression, and faster progression to SPMS (Hernan *et al.*, 2005; Manouchehrinia *et al.*, 2013). A retrospective study found that those who smoked had a higher risk of conversion from CIS to clinically definite MS (Di Pauli *et al.*, 2008). The mechanisms underlying the association between cigarette smoking and the risk of developing MS are not clear but one theory is the presence of neurotoxic compounds in cigarettes, such as nitric oxide (Hernan *et al.*, 2005). The presence of nitric oxide in MS lesions caused by smoking may accelerate axonal loss and the progression of disability in MS patients (Hernan *et al.*, 2005).

Additional environmental factors implicated in the development of MS include sunlight exposure and vitamin D status. The main source of Vitamin D for most people is sunlight (Holick *et al.*, 2004; Ascherio *et al.*, 2010), with people living at least 40° north or south of the equator having low sunlight for 4 months of the year and an associated reduction in Vitamin D levels (Webb *et al.*, 1988). Places such as Canada, Northern Europe, New Zealand and Tasmania have the highest

prevalence rates of MS in the world and have lower sunshine exposure (Goodin *et al.*, 2009).

Variability in UVB exposure and vitamin D status during pregnancy was thought to explain why season of birth affects MS risk (Disanto *et al.*, 2012), with births in November having the lowest risk of MS and births in May having the highest risk of MS (Willer *et al.*, 2005). However, a recent study has demonstrated that the apparent seasonal patterns for month of birth thought to be specific for MS are expected by chance alone, as the month of births varies significantly with geographical location and over time in the normal population (Fiddes *et al.*, 2013). Therefore, the prior association of MS with month of birth are likely due to a false positive association.

Overall, a number of studies have found a higher MS risk in subjects with low Vitamin D levels (Munger *et al.*, 2004; Salzer *et al.*, 2012) as well as a poorer prognosis in patients with MS who have low levels of Vitamin D (Ascherio *et al.*, 2014; Simpson *et al.*, 2010). One study demonstrated that Vitamin D levels in the first 12 months after a CIS strongly predicted MS activity and progression during the following four years (Ascherio *et al.*, 2014). More recently a study found that higher Vitamin D levels in RRMS patients treated with interferon beta-1b were associated with lower rates of disease activity on MRI (Fitzgerald *et al.*, 2015).

It is unlikely that any one of the environmental factors discussed above is solely responsible for the development of MS. It is very likely that a complex interaction of a number of environmental factors in association with genetic factors contribute to the development of MS.

1.3.2 Genetic Factors

The role of genetics in MS is clear given the difference in prevalence in populations of different ethnic backgrounds living in close proximity. Familial studies have demonstrated a familial recurrence rate of about 20% (Compston & Coles, 2002). Population based twin studies show higher clinical concordance rates in monozygotic (25%) than in dizygotic pairs (5%) (Willer *et al.*, 2003; Mumford *et al.*, 1994). The concordance rate for MS is similar in half-siblings raised together and apart (1.2% vs 1.5% respectively) which indicates that changes in environment have little influence on this group (Ebers *et al.*, 1995). In individuals adopted early in life and who went on to develop MS later, the new family did not incur any extra risk of MS, while the biological parents were found to be at an increased risk (Ebers *et al.*, 1995). The risk of MS changes from 3% in first degree relatives, to 1% in second-degree and third-degree relatives, indicating the risk of developing MS increases with the degree with which they are related to them (Dyment *et al.*, 2006). Overall, there is no clear pattern of inheritance apparent in MS, but it is clear that genes play a definite role in its pathogenesis (Compston, 2006).

Several genetic loci are associated with an increased risk of developing MS. Initial studies found a link between MS and major histocompatibility complex (MHC) (Compston *et al.*, 1976), with genes for the Human Leukocyte Antigen (HLA) located within the MHC area, which contains a high number of polymorphisms (Horton *et al.*, 2004). A number of HLA genes have been identified with an association between the DR2 haplotype HLADRB1*1501 in the class II region of the MHC on the short arm of chromosome 6 and the development of MS (Olerup

and Hillert, 1991). The genes inside this region encode cell-surface glycoproteins which are key components of the immune system (Munoz-Culla *et al.*, 2013).

Linkage studies have been replaced with Genome-Wide Association Studies (GWAS), which uses a hypothesis-free strategy that screens the whole genome by tagging linkage disequilibrium blocks (Munoz – Culla *et al.*, 2013). It uses single-nucleotide polymorphism (SNP) data as a reference to scan the whole genome and identify parts of the genome associated with the disease (Munzo–Culla *et al.*, 2013). The main progress since the identification of the MHC, has been the identification of the association with variants in both IL7R and IL2R (Hafler *et al.*, 2007/IMSGC 2007). To date 14 GWAS have now been completed in MS and the success of these studies are directly related to the number of samples screened. Collaboration between the International Multiple Sclerosis Genetic Consortium (IMSGC) and the Wellcome Trust Case Control Consortium (WTCCC2) ended in the largest study to date and confirmed the 23 previously reported associations and identified 34 new association variants, and 29 of these had genome significance (Sawcer *et al.*, 2011). These novel susceptibility loci identified modestly increase disease susceptibility in MS, such as VCAM1, PLEK, CD86 and IL12B, as well as replicating previously suggested associations (Sawcer *et al.*, 2011). These risk alleles tend to be involved in T-cell maturation, therefore suggesting the critical disease mechanisms mainly involve immune dysregulation (Sawcer *et al.*, 2011).

There are a number of limitations with the genetic analysis in MS. The IL7R association identified to date has a frequency of 72% in white Europeans, with the allele estimated to increase the risk of disease by only a factor of 1.2 (Sawcer,

2008). Therefore, the vast majority of people carrying this allele will never develop MS. Overall MS is not a common disease in the whole population and studies of less than 600 cases and 600 controls are unlikely to identify significant associations (Sawcer, 2008). The work to date provides substantial evidence of a genetic component to MS, however like the environmental factors, it involves complex interactions which are very challenging to disentangle.

1.4 Comorbidities & MS

Comorbidities in patients with MS can be divided into 3 areas: 1) MS and diseases which may have a common pathogenic origin e.g. thyroid dysfunction, psoriasis and inflammatory bowel disease, 2) MS and diseases which occur as a consequence of MS e.g. psychiatric disorders and 3) MS and disease that are very common e.g. cardiovascular disease and cancer (Capkun *et al.*, 2015; Marrie *et al.*, 2015). The existence of comorbidities in MS have been associated with diagnostic delays, disability progression and progression of lesion burden on MRI and this is becoming more clear with time (Marrie *et al.*, 2009; Marrie *et al.*, 2010; Weinstock-Guttman *et al.*, 2013). A population-based administrative data study in an MS population found survival was lower (median of 7 years lower) for those with MS than in a population matched for age, sex-and socioeconomic status (Marrie *et al.*, 2015). The study by Marrie *et al.*, 2015 found that a number of conditions were associated with increased risk of mortality, specifically depression, diabetes, hypertension, ischaemic heart disease and chronic lung disease. Excluding MS-related mortality, the most common causes of death were due to circulatory system disease, cancer and respiratory disease (Marrie *et al.*, 2015). The early detection and management of comorbidities in patients with MS is extremely important, as it can reduce premature death and improve quality of

life (Capkun *et al.*, 2015). Looking at the whole care of a patient with MS, including physical and mental comorbidities, will improve management of this complex disease (Ciccarelli & Thompson, 2016).

1.5 Pathology

The pathological features of MS were first described by Carswell and Cruveilhier (Carswell, 1838, Cruveilhier, 1841). They were later summarised by Frommann and Charcot (Frommann 1878, Charcot 1880). The sclerotic plaque has been the most important finding in MS, since it was first described. The pathological hallmarks of MS are inflammation, demyelination, remyelination, gliosis and neurodegeneration, which occur either focally or diffusely throughout the grey and white matter of the brain and spinal cord. The sclerotic plaque arises due to a complicated interplay of inflammation, demyelination and repair, with a variable degree of axonal loss (Compston & Coles, 2008).

1.5.1 White Matter

Oligodendrocytes in the CNS manufacture myelin. In MS, the oligodendrocytes are damaged by inflammatory T lymphocytes, which are not being regulated, resulting in immune dysregulation (Compston & Coles, 2008). Traditionally MS was considered to be an autoimmune inflammatory disorder, which was mediated by a T cell attack against CNS elements, in particular myelin. Patients with RRMS display a compelling autoimmune and inflammatory phenotype on laboratory and radiological tests (Stys *et al.*, 2012). These features are present in all forms of MS but they vary both quantitatively and qualitatively between the three forms (RR, SP and PP) of MS (Lassmann *et al.*, 2012), with the degree of inflammation

higher during the early relapsing stage of the disease and lower in the later phase of the disease (Frischer *et al.*, 2009).

Pathological examination of biopsied or post-mortem brains of patients with MS shows characteristic perivascular inflammatory infiltrates, which consist mainly of lymphocytes and macrophages. Inflammatory infiltrates mainly contain CD8+ T lymphocytes, which are clonally expanded in active lesions (Babbe *et al.*, 2000). CD4+T cells and B lymphocytes are less numerous than CD8+T cells and mainly accumulate in the perivascular space and meninges (Ozawa *et al.*, 1994; Serafini *et al.*, 2004). Microglial activation in the initial lesions is associated with demyelination and neurodegeneration with subsequent recruitment of macrophage as a result of myelin breakdown (Frischer *et al.*, 2009; Lassmann *et al.*, 2011).

Early RRMS is predominantly a disease of the white matter, characterised by confluent plaques of demyelination. The active demyelination is associated with inflammation and blood-brain barrier leakage (Lassmann *et al.*, 2014). The progressive stage of the disease is characterised by the gradual expansion of white matter lesions in the absence of blood-brain barrier leakage, with degeneration of chronically demyelinated axons a prominent feature in the progressive stages of MS and a major cause of irreversible disability (Mahad *et al.*, 2015).

1.5.2 Grey Matter

The understanding of MS has evolved significantly over recent years. Traditionally it was thought that MS was solely a disease of the white matter, however improvements in radiology and pathology in more recent years indicates

that grey matter structures (that is, neuronal somas and synapses) of the brain are also affected (Geurts *et al.*, 2009).

Extensive pathology is seen in the grey matter in all types of MS. Grey matter pathology is characterised by demyelination with a relative absence of immune cell infiltrates. The number of cortical lesions increases at a significantly greater rate in patients with actively progressive disease and correlates with increasing disability (Calabrese *et al.*, 2010a). Therefore, there is increasing evidence that accumulating cortical grey matter pathology plays an important role in the severity of both physical and cognitive disability (Calabrese *et al.*, 2010b; Mahad *et al.*, 2015). This ultimately results in extensive brain tissue loss and injury (Lassmann *et al.*, 2014). The degree of cortical atrophy is not constant throughout the brain, with marked regional variations in cortical involvement. There is more extensive involvement seen in the hippocampus, frontal and temporal cortices as well as the cingulate gyrus, and less extensive involvement in the occipital lobe and primary motor cortex (Gilmore *et al.*, 2009). The predilection for the frontal lobe and the hippocampus is likely to account for the predominance of cognitive over motor disability related to cortical pathology (Gilmore *et al.*, 2009).

Little is known about the mechanism of lesion formation in the cortical grey matter and how the accumulation of cortical pathology may contribute to clinical progression (Reynolds *et al.*, 2011). Post-mortem studies have shown that inflammatory infiltrates are commonly found in the cerebral leptomeninges in SPMS (Frischer *et al.*, 2009). In a proportion of SPMS cases, large B cell aggregates have been identified in the subarachnoid space with some characteristics of ectopic B cell follicles (Frischer *et al.*, 2009; Magliozzi *et al.*,

2007). The ectopic B cell follicle-like structures can be found distributed throughout the cerebral meninges and they are variable in number and size (Magliozzi *et al.*, 2007). They are mainly present in the cerebral sulci which suggests that reduced CSF flow and the microenvironment of these locations, favours the homing and retention of inflammatory cells which gives rise to an inflammatory milieu in the CSF (Magliozzi *et al.*, 2007). MS cases with these meningeal lymphoid-like structures are associated with a younger age at disease onset, a shorter time to disease progression and wheelchair use, and shorter disease duration (Magliozzi *et al.*, 2010). This raises the possibility that CSF-mediated factors may play an important role in cortical pathology. More recently a similar finding in white matter has been demonstrated, where a gradient in magnetisation transfer ratio (MTR) abnormalities from periventricular to deep normal appearing white matter (NAWM) in MS patients were found, which was most marked in the periventricular region. This further raises the possibility of CSF-mediated factors are involved in the pathogenesis in MS (Liu *et al.*, 2015). In the past, the majority of the evidence suggested that the disease began due to an immune dysregulation. This is based on the “outside-in” model of MS (Stys *et al.*, 2012). The resulting inflammatory reaction, which typically follows a RR course in the initial stages, causes further demyelination and tissue injury (Stys *et al.*, 2012).

In more recent years, doubt has been cast on this model due to some inconsistencies and an “inside-out” model of MS has been proposed. This model proposes that the initial malfunction occurs within the CNS, like other neurodegenerative conditions, for example Parkinson’s and Alzheimer’s disease. Primary neurodegeneration, possibly involving the oligodendrocyte-myelin

complex, resulting in Wallerian degeneration may be the initiating event. This then releases highly antigenic constituents along the degenerated tracts, which promotes secondary autoimmune and inflammatory responses in the predisposed individual (Hauser *et al.*, 2006; Trapp *et al.*, 2008; Sato *et al.*, 2015).

Progressive stages of MS remain largely refractory to treatment. It is widely suggested that accumulating axonal loss is responsible for irreversible clinical progression. Pathological changes associated with clinical progression include inflammatory changes becoming increasingly compartmentalised in the perivascular and subarachnoid spaces behind a relatively intact blood-brain barrier (Meinl *et al.*, 2008).

Pathological studies have significantly enhanced our understanding of the mechanisms underlying MS over the last number of years. It is most likely that MS starts as a result of inflammation, which then initiates a number of neurodegenerative mechanisms as the disease progresses, including changes related to age.

1.6 Diagnosis of multiple sclerosis

Over the last 50 years, the diagnostic criteria for MS have evolved, with successive modifications, due to technological advances which improve the accuracy of diagnosis. MS cannot be diagnosed in an asymptomatic individual based on MRI findings alone. The criteria have evolved and more recent criteria allow MRI evidence of dissemination of lesions in space and time, while the earlier criteria required clinical evidence of dissemination. The first criteria was proposed by Schumacher *et al* in 1965 and stated that definite MS was classed as having objective evidence for disease affecting two or more regions of the

CNS white matter (dissemination in space), with episodes separated at least 1 month apart or with progression over six months (dissemination in time), in a person aged 10-50 years at onset. The authors recommended routine laboratory tests to exclude alternative conditions and a lumbar puncture was also included, to look for an increase in cerebrospinal fluid (CSF) gamma globulin and mononuclear cells.

Subsequent to this, the new Poser criteria (Poser *et al.*, 1983) introduced laboratory features to improve the diagnostic classification in patients. This included visual evoked potentials (VEPs), CSF and MRI imaging. These criteria included the presence of unmatched oligoclonal bands (OCBs) in the CSF but not in the serum, indicating an immunological process in the CNS. Their presence is supportive of an MS diagnosis. However, they may be present in other CNS inflammatory conditions such as sarcoid, systemic lupus erythematosus (SLE) and syphilis. The age is restricted to between 10 and 59 years of age and progressive onset of disease is excluded from making an MS diagnosis.

The widespread use of MRI in MS and other neurological conditions was subsequently reflected in the diagnostic criteria for the disease proposed by Paty (Paty *et al.*, 1988). Paty included MRI in the diagnostic criteria, as well as computerised tomography (CT), OCBs, VEPs and somatosensory evoked potentials (SSEPs). The criteria developed by Paty *et al.*, included abnormalities in the above parameters, as well as a history of dissemination in time and space. The MRI was either strongly suggestive of MS, was suggestive of possible MS or was not MS, based on the number of lesions seen. An MRI strongly suggestive of MS has four lesions or three, one of which is periventricular; for possible MS

two lesions must be present with one lesion in a periventricular location. If there is one lesion or none, then another diagnosis should be considered. The authors included in the criteria that a single appropriate lesion could be used to demonstrate dissemination in space. In individuals over 40 years of age, it was recommended that OCBs are a prerequisite for a diagnosis of MS due to the increase in non-specific lesions seen with advancing age.

In 2001, there was a further revision of the criteria with the widespread use of MRI (McDonald *et al.*, 2001) and certain imaging features suggestive of MS. The work of Barkhof (Barkhof *et al.*, 1997) and Tintore (Tintore *et al.*, 2000) had shown that patients with CIS with three or four of the following brain MRI features had a high specificity for developing clinically definite MS (Barkhof *et al.*, 1997; Tintore *et al.*, 2000):

- Nine T2 hyperintense lesions or one gadolinium-enhancing lesion
- At least three periventricular lesions
- At least one infratentorial lesion
- At least one juxtacortical lesion

Following publication of the 2001 McDonald criteria, a number of studies confirmed higher sensitivity and specificity compared with the previous criteria. These criteria were subsequently revised in 2005, by the International Panel on Diagnosis of MS (Polman *et al.*, 2005). The modified criteria again incorporated CSF analysis, VEPs and clinical findings as well as three of the MRI criteria as outlined in the 2001 criteria with some modifications. Any number of cord T2 lesions could substitute for a brain lesion, while only one could in 2001. Cord

lesions were not recognised as having the same significance as an infratentorial lesion. The originally proposed time period of three months for dissemination in time (DIT) was reduced to one month for a new T2 lesion to satisfy DIT. The detection of a contrast-enhancing lesion, at least three months after the onset of the clinical event also constituted evidence for DIT.

The European multicentre collaborative research network that studies MRI in MS (MAGNIMS) (Montalban *et al.*, 2010) reviewed the requirements for demonstrating dissemination in space (DIS) and DIT, which proposed a new criterion for MS based on a single MRI scan. The proposed MRI criteria included: (i) one or more lesion (s) in at least two of four characteristic topographies: periventricular, juxtacortical, infratentorial and spinal cord, as outlined before, to satisfy DIS; and (ii) simultaneous presence of gadolinium-enhancing and non – enhancing lesions or a new enhancing lesion or T2 weighted lesion on any follow up scan, which provided evidence of DIT.

These MAGNIMS criteria were subsequently incorporated into the 2010 revisions to the McDonald criteria (Polman *et al.*, 2011), with the addition of symptomatic lesions in the brainstem or spinal cord excluded from DIS. The DIT criteria proposed by MAGNIMS was confirmed.

The criteria for a diagnosis of PPMS was also included, whereby patients must have a one year of progression with two of the following: (i) evidence of DIS in the brain (≥ 1 T2 lesion in following locations: periventricular, juxtacortical or infratentorial), (ii) evidence of DIS in the spinal cord (based on ≥ 2 T2 lesions in the cord), (iii) positive unmatched OCBs (Polman *et al.*, 2011).

The benefits of the 2010 McDonald criteria included the focus on lesion location rather than lesion count, the elimination of a mandatory interval between clinical attack and baseline reference scan and the acceptance of the concomitant presence of gadolinium-enhancing and gadolinium-nonenhancing lesions as evidence of DIT (Rovira *et al.*, 2015). The new 2010 diagnostic criteria does not require CSF testing to support the diagnosis of MS but CSF findings may be helpful in certain individuals when the MRI scan is not entirely diagnostic and/or there are MRI features which are atypical for MS (Dobson *et al.*, 2013). Overall, the 2010 McDonald criteria have improved the diagnostic process for RRMS, resulting in an easier and earlier diagnosis. However, there are some limitations for PPMS (Rovira *et al.*, 2015), as brain MRI can be normal in people with PPMS and small spinal cord lesions may not be picked up on spinal MRI (Kelly *et al.*, 2013).

The group made a few key recommendations which may guide future diagnostic criteria, including the addition of biomarkers (Awad *et al.*, 2010, Orbach *et al.*, 2013), the inclusion of newer MRI sequences to detect cortical lesions and microstructural tissue injury in NAWM.

Overall, MS is a very heterogeneous disease and no criteria are fully reliable on their own. A detailed clinical evaluation by an experienced neurologist is an essential part of the diagnostic process.

Clinical Presentation	Additional requirements for a diagnosis of MS
≥2 attacks; objective clinical evidence of ≥2 lesions or objective clinical evidence of 1 lesion with reasonable historical evidence of a prior attack	None
≥2 attacks; objective clinical evidence of 1 lesion	Dissemination in space (DIS), demonstrated by: ≥1 T2 lesion in at least 2 of the 4 MS-typical regions of the CNS (periventricular, infracortical, juxtacortical or spinal cord); Or Await a further clinical attack implicating a different CNS site.
1 attack; objective clinical evidence of ≥2 lesions	Dissemination in time (DIT), demonstrated by: Simultaneous presence of asymptomatic gadolinium-enhancing and non-enhancing lesions at any time; Or A new T2 and/or gadolinium-enhancing lesion(s) on follow-up MRI, irrespective of its timing with reference to a baseline scan; or await a second clinical attack
1 attack; objective clinical evidence of 1 lesion (clinically isolated syndrome)	Dissemination in space (DIS) can be demonstrated by: ≥1 T2 lesion in at least 2 areas of the CNS (periventricular, infracortical, juxtacortical or spinal cord); Or Await a second clinical attack implicating a different CNS site. DIT can be demonstrated with either: (A) Simultaneous presence of asymptomatic gadolinium-enhancing and non-enhancing lesions at any time. (B) A new T2 and/or gadolinium-enhancing lesion(s) on follow-up MRI, irrespective of the timing of the baseline MRI Or Await a second clinical attack

Table 1.1: 2010 Revised McDonald Criteria – Diagnosing RRMS (Polman *et al.*, 2011).

1.7 Therapy in MS

There have been significant advances in the treatment of patients with RRMS over the last decade, with new and effective drugs now available e.g natalizumab, alemtuzumab and fingolimod. Unfortunately, the same cannot be said for progressive forms of MS, with all trials of anti-inflammatory agents essentially negative to date (Ontaneda *et al.*, 2015), apart from one phase 2 trial in SPMS which significantly reduced the annualised rate of whole-brain atrophy on high dose simvastatin (Chataway *et al.*, 2014). The pathological process driving disability progression in progressive MS is not fully understood, but it likely involves compartmentalised inflammation, mitochondrial dysfunction and neurodegeneration (Mahad *et al.*, 2015). The lack of a clear understanding of the underlying pathology in progressive MS, in addition to the lack of sensitive outcome measures and fully validated biomarkers in progressive MS, make the development of effective treatments a big challenge (Ontaneda *et al.*, 2015). The key to the successful development of treatments in progressive MS is in the development of biomarkers that are linked to the pathological processes underlying progression (Thompson, 2015).

Therefore, the studies presented in Chapters III – VI aim at looking for reliable imaging biomarkers in progressive and relapsing MS, which may be useful in detecting clinically meaningful pathology which may have a role in clinical trials in the future.

Chapter II

Principles of magnetic resonance imaging

This chapter will focus initially on the basic principles of magnetic resonance imaging (MRI). The latter part of the chapter discusses the MRI sequences employed in the studies described in the remainder of this thesis.

2.1 Principles of MRI

Magnetic resonance imaging is a non-invasive technique used to image tissues in the human body in vivo with high spatial resolution. Two-thirds of the human body is made up of water, therefore the human body is abundant with water hydrogen atoms. It is the nucleus of the hydrogen atom, which is fundamental to the generation of conventional MR and consists of a single proton surrounded by one electron. The proton has a net positive charge and spins on its own axis, resulting in the production of a small magnetic field. These protons acquire a magnetic moment and can align with an external magnetic field.

When an external magnetic field (B_0) is applied to a hydrogen atom, the protons will align in either the same direction (parallel), or in the opposite direction (anti – parallel) with the magnetic field. This is similar to the way in which a compass oscillates about the earth's magnetic field. Protons aligned in the magnetic field gyrate around their own axis in a motion known as precession. The frequency at which the protons precess is described by the Larmor equation, where ω_0 is the Larmor Frequency given in Hz, B_0 is the strength of the externally applied magnetic field given in Tesla and γ is the gyromagnetic ratio given in Hz/Tesla. The gyromagnetic ratio is the ratio between the magnetic dipole moment to the angular momentum of each MR active nucleus, which is unique for each MR

active nucleus. The gyromagnetic ratio is an intrinsic property of the nucleus of interest.

$$\omega_0 = \gamma B_0$$

From this equation, the resonant frequency is proportional to the externally applied magnetic field and is determined by the gyromagnetic ratio. This ratio is different for different nuclei. The stronger the magnetic field the higher the Larmor frequency. For a 3 Tesla MRI scanner, the hydrogen nuclei precess at a frequency of 128 MHz.

At equilibrium each hydrogen nucleus is either aligned parallel to B_0 , in a low energy state or anti-parallel to the magnetic field, in a high energy state. These two alignments of the hydrogen proton with the B_0 result in two distinct energy levels. At room temperature a slight excess of protons align in the low energy state, this results in the net magnetisation (M) being in the direction of B_0 , as shown in **Figure 2.1**.

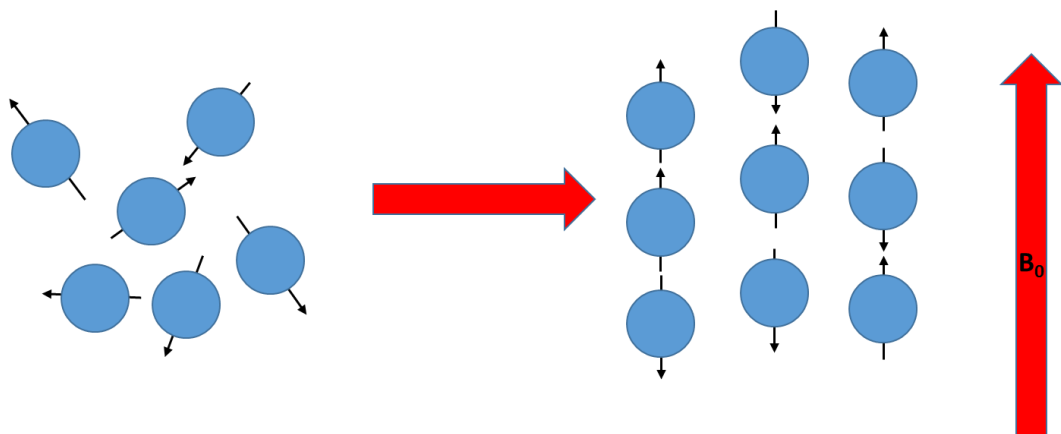


Figure 2.1: Alignment of spins after the application of an external magnetic field. There is net longitudinal magnetisation in the direction of B_0 .

The application of energy in the form of a radiofrequency (RF) pulse to the protons within an external magnetic field, induces them to flip to a higher energy state. Low energy spins originally aligned parallel to B_0 gain enough energy to re-align anti-parallel to B_0 , resulting in the reduction of net longitudinal magnetisation. Both the duration and amplitude of the RF pulse determines the flip angle. The flip angle is the angle at which the net magnetisation deviates from B_0 . An example of this is a RF pulse with a 90° flip angle which converts all the longitudinal magnetisation into transverse magnetisation. This induces a voltage in the MR receiver coil and this forms the basis of the MRI signal.

As the RF pulse is switched off, spins release energy to their surroundings in a process known as relaxation, and as a result the excited protons relax back to their equilibrium position, releasing electromagnetic energy which is detected by a coil that acts as an antenna. After the RF pulse is switched off, protons lose coherence and spins de-phase. This results in an increase in magnetisation in the longitudinal plane, with the spins returning to their original energy levels, aligning with B_0 . This is known as T1 recovery, and there is a decrease in the transverse plane, known as T2 decay. As transverse magnetisation decays, there is also decay of the voltage induced in the receiver coil. This reducing signal is known as free induction decay (FID).

The RF pulse is not continuous and the time from one excitation pulse to the next is known as the repetition time (TR) and the time from RF pulse to maximum signal induction is known as the echo time (TE) (Hahn, 1950).

2.2 T1 – longitudinal relaxation

Longitudinal relaxation or spin-lattice relaxation is the process whereby the protons return to their lower energy state and is due to spins releasing energy obtained from the RF pulse to the surrounding lattice and therefore to their original equilibrium state (Bloch, 1946). T1 is defined as the time required for longitudinal magnetisation to restore to 63% of its final value, as show in **Figure 2.2**.

2.2.

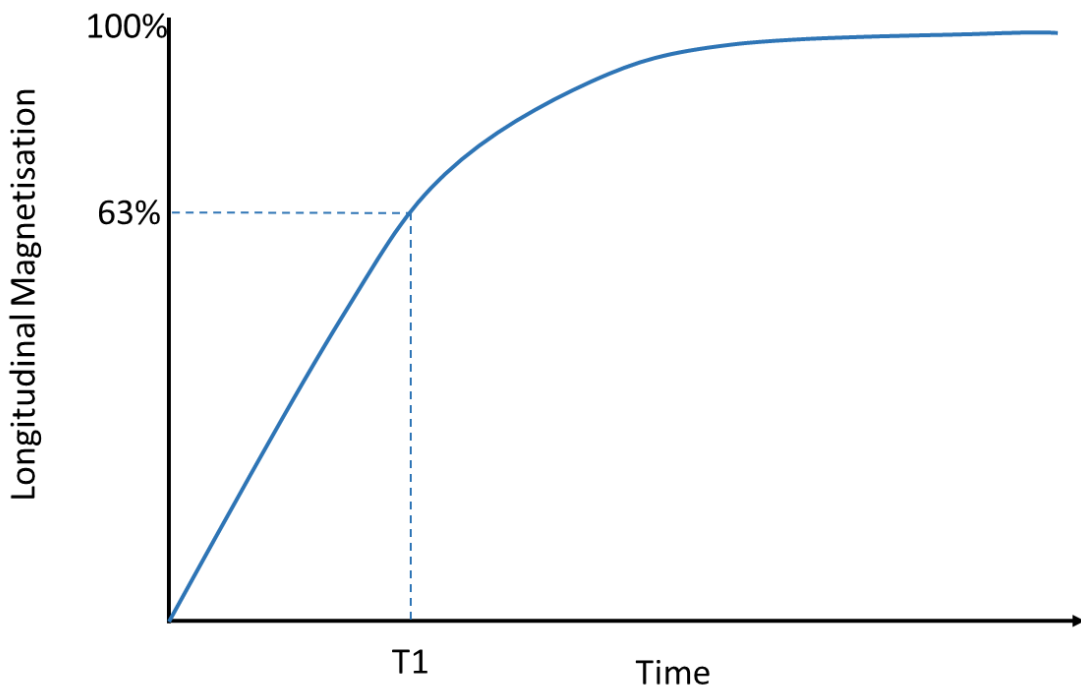


Figure 2.2 T1 recovery curve – T1 relaxation time refers to the time taken for 63% of the longitudinal magnetisation to recover.

2.3 T2 – transverse relaxation

Transverse relaxation or spin-spin relaxation is the process whereby protons lose phase coherence and the transverse magnetisation starts to disappear. It arises from the exchange of energy between spins. No energy is actually lost from the spin system but the decay of transverse magnetisation arises from the loss of

phase coherence between spins, which arise from magnetic field inhomogeneities (T_2^* relaxation) (Bloch 1946). T_2 is defined as the time required for the transverse magnetisation to decrease to a value of 37% of its maximum, as show in **Figure 2.3**.

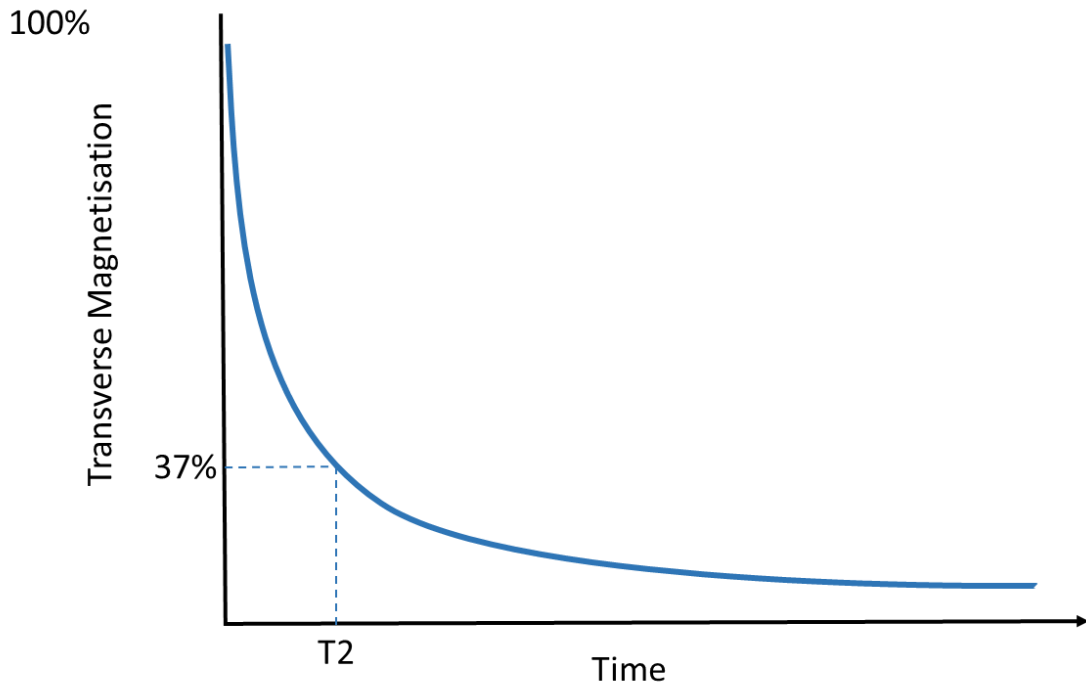


Figure 2.3 T_2 relaxation curve – T_2 relaxation time refers to the time taken for transverse magnetisation to decay to 37%.

2.4 Image contrast

Contrast is of importance in MRI so that abnormalities in normal appearing tissue can be readily determined, such as demyelination in MS. Different tissues in the body have intrinsic contrast parameters that are fixed, however by altering parameters such as TR and TE, amongst others, extrinsic contrast can be changed. When viewing the image areas of high signal appear brighter and low signal are darker.

2.4.1 T1-weighted imaging

The time constant T1 refers to the recovery of longitudinal magnetisation. As transverse relaxation is faster than longitudinal relaxation, T2 is always shorter than T1. Different tissues will have different relaxation times due to their different chemical constituents. For example, water is highly mobile with high inherent energy, while large molecules, like fat, have low inherent energy. Large molecules can transfer energy more efficiently, therefore T1 relaxation time is shorter in fat than in water. Also, molecules which are more tightly packed together, like fat, have greater spin-spin interactions and as a result protons in fat de-phase more rapidly and consequently have a shorter T2 relaxation time than water. The T1-weighting is determined by the TR and is characterised by short TE and short TR.

2.4.2 T2-weighted imaging

The time constant T2 refers to the time constant for decay of the transverse magnetisation in a uniform/homogenous magnetic field. T2 imaging decay varies depending on the tissue being imaged as decay is determined by the magnetic fields of nuclei interacting with each other. Water has a long T2 and fat has a short T2, due to slow dephasing of water molecules. T1 effects are diminished by selecting a long TR, to allow full recovery between excitations. T2-weighted images are characterised by long TE and long TR, in order to detect differences between tissues due to their difference in T2 relaxation times.

2.4.3 Proton density imaging

The proton density (PD) of a tissue depends on the number of protons in the tissue, which determines the signal of the PD weighted image. High signal is

produced by greater numbers of protons by increasing the transverse component of magnetisation. Decreasing the effects of T1 and T2, results in increased PD weighting of the image, which is achieved using a spin echo sequence with a long TR and a short TE.

After a RF excitation pulse, the net magnetisation returns from the transverse plane to the longitudinal plane, and induces a voltage in the MR receiver coil. The magnitude of the transverse component decays and hence this reducing signal is known as FID, as described above. The time constant of this decay is called T2*. In theory one would expect the decay of the MR signal to occur with a time T2, however, in practice it occurs with the shorter T2*. This occurs due to the magnetic field inhomogeneity, imperfections in the windings of the coil itself and also due to the differences in magnetic susceptibility between adjacent regions. T2* is always shorter than T2. In a perfect magnetic field, the value of T2* can approach that of T2.

2.5 Pulse sequences

MRI pulse sequences are composed of a set of pre-defined RF pulses, re-phasing pulses and gradient pulses. They are applied in a controlled fashion to form an MR pulse sequence. The main parameters of a pulse sequence are the TE and the TR as described above. The TE determines the amount of transverse magnetisation decay, therefore determining the amount of T2 weighting.

There are two principle types of pulse sequence, called spin echo (SE) and gradient echo (GE).

2.5.1 Spin Echo Imaging

The spin echo (SE) phenomenon was first described by Erwin Hahn in 1950 (Hahn 1950). It was later enhanced by Carr and Purcell when they reported the benefit of an 180° refocusing pulse (Carr and Purcell 1954). This imaging sequence initially uses a 90° RF pulse, rotating the longitudinal magnetisation into the transverse plane, maximising the transverse magnetisation, with all the spins in phase. When the RF pulse is switched off, there is recovery of longitudinal magnetisation (T_1 recovery) and decay of transverse magnetisation (T_2 decay). It is not possible to reverse the loss of phase coherence due to the intrinsic effect of neighbouring spins within the tissue. However, it is possible to reverse the loss of phase coherence which arises due to the magnetic field inhomogeneities (T_2^* decay), by applying a second RF pulse, with an 180° flip angle to the de-phased nuclei, which results in flipping of the magnetic moments. After a time interval ($TE/2$), equal to the time between the first and the second RF pulse, the nuclei return to being in phase, and as a result the NMR signal increases again. This is described as a spin echo. Spin echo imaging is not sensitive to the presence of magnetic field inhomogeneities due to the refocusing following an 180° pulse. Therefore, the SE image intensity depends on T_2 rather than on T_2^* . The spin echo diagram (**Figure 2.4**) demonstrates the timing and amplitude of the RF pulses.

2.5.2 Fast spin-echo (FSE) sequences

The fast spin echo (FSE) sequence is slightly different to the conventional spin echo, as multiple 180° RF pulses are applied after the initial 90° RF pulse. This results in a series of echoes, resulting in reduction in the total acquisition time.

FSE allows different TEs, therefore PD and T2 weighted images can be acquired from one sequence.

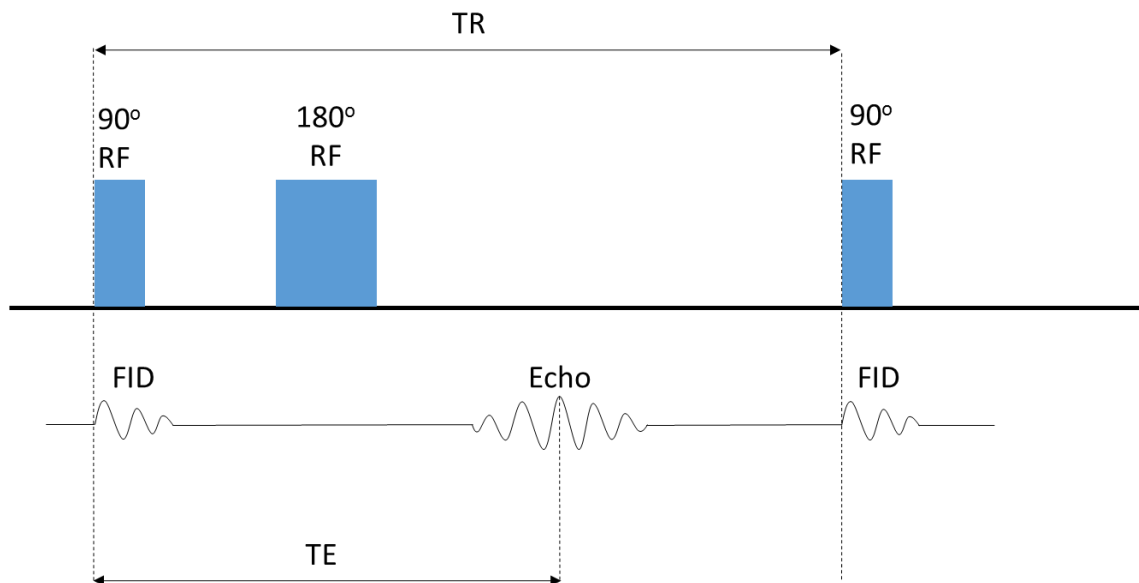


Figure 2.4: Spin echo sequence diagram. An 180° pulse is applied at time t ($TE/2$) and an echo is detected at time $2t$ equal to TE .

2.5.3 Gradient echo imaging

Gradient echo sequences are an alternative means to rephase the spins compared to SE sequences. It differs from SE sequences in that the initial RF pulse produces a flip angle which is typically less than 90°, and there is no 180° pulse. A flip angle less than 90° results in a reduction to the magnetisation in the transverse plane as not all the longitudinal magnetization is converted to transverse magnetization. After the RF pulse is turned off, spins in the transverse plane begin to dephase due to T_2^* effects. Rather than a RF pulse, re-phasing is achieved using gradients. After the excitation pulse a negative gradient is applied which causes rapid dephasing of the transverse magnetisation which has the effect of speeding up fast spins and slowing down slow spins. A positive gradient

is then applied which speeds up the slow spins and slows down the fast spins, hence spins which were previously dephasing, now begin to rephase, and after a certain time they will all come back into phase along the y-axis forming the gradient echo. The positive gradient only compensates for the dephasing caused by the negative gradient and it does not refocus dephasing due to the main magnetic field inhomogeneities. This is illustrated in **Figure 2.5**.

Gradient echo imaging often suffers from signal loss due to dephasing of spins in the presence of magnetic field inhomogeneities. The gradient echo image intensity (that is the height of the echo), depends on $T2^*$ rather than on $T2$. As the dephasing of spins increases with increasing TE, gradient echo imaging is typically acquired with a very short TE (several milliseconds). The use of smaller flip angles in gradient echo imaging enables longitudinal magnetisation to recover faster, allowing shorter repetition times and hence lending gradient echo sequences for rapid in vivo MRI, reducing scan time and motion artefacts (Haase *et al.*, 1985). A commonly used gradient echo sequence in investigation of multiple sclerosis is the T1 weighted magnetically prepared rapid acquisition gradient echo sequence (MP-RAGE) (Mugler and Brookeman, 1990).

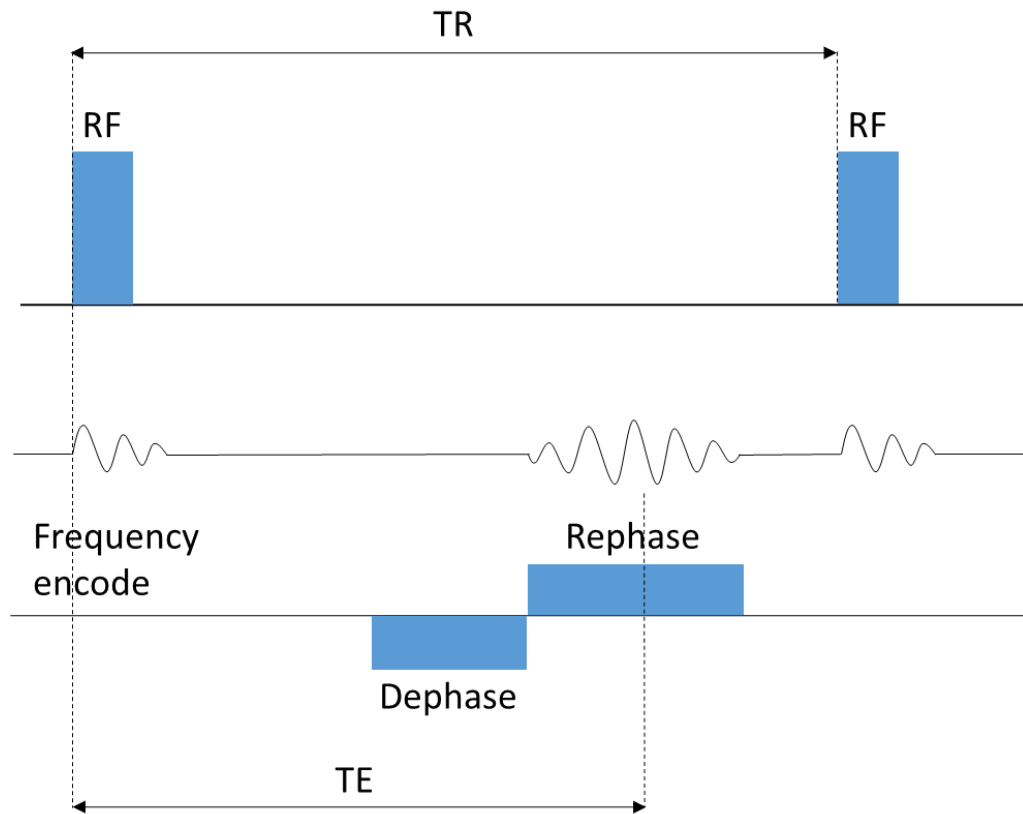


Figure 2.5: Gradient echo sequence diagram. A radiofrequency pulse producing a flip angle $<90^\circ$ is applied, which is followed by a dephasing and rephrasing gradients to produce the echo.

The following section will discuss advanced MRI techniques, which have been used in the studies in the following chapters of this thesis.

2.6 Magnetic Resonance Spectroscopy (MRS)

The discovery of chemical shift and spin-spin coupling in the early 1950s, was a result of the resonant frequency of the nuclear magnetic resonance (NMR) signal differing by small amounts in different molecules. This is due to differences in the local magnetic field surrounding each nucleus which depends on both the chemical structure of the molecule, as well as the magnetic properties of adjacent nuclei. Therefore, nuclei in different chemical environments will have different

resonant frequencies, allowing for the identification of both structure and relative concentrations of the molecules within an MR sample using MR spectroscopy (Proctor and Yu, 1950; Gutowsky and McCall, 1951). MRS therefore allows the non-invasive detection and identification of endogenous metabolites in vivo. The majority of in-vivo studies performed to date have used the proton (^1H) nucleus due to its high sensitivity and favourable relaxation times (Barker *et al.*, 2010). Other nuclei which are MR sensitive include phosphorus (^{31}P) and carbon (^{13}C). These nuclei have lower sensitivity, resulting in longer scan times and increased voxel size (Barker *et al.*, 2010). The remainder of this section will deal with ^1H -MRS.

2.6.1 Chemical Shift

Nuclei are susceptible to changes within their local environment. The applied external magnetic field (B_0) opposes the local magnetic field which arises from neighbouring electrons and nuclei. As a result, a current is induced which generates a small magnetic field to shield ^1H spins from B_0 which opposes the external magnetic field.

The degree of shielding, and hence resonant frequency, will differ due to the unique chemical environment, resulting in different metabolites having slight shifts in resonant frequency. This phenomenon is known as chemical shift. MRS is based on this principle and so nuclei within compounds can be distinguished on the basis of the resonant frequencies.

The x-axis of the spectra is displayed in parts per million (ppm), of the resonance frequency of the metabolites of interest relative to the resonant frequency of a reference compound. For ^1H and ^{13}C , tetramethylsilane (TMS) is widely used as

a reference compound, having its resonant frequency of 0ppm. Peaks in the spectrum are called resonances.

2.6.2 Shimming

Shimming refers to the process of optimizing the magnetic field homogeneity over the volume of interest. It is performed by making slight adjustments to the field gradients prior to acquiring the data. The homogeneity of the voxel is measured as the linewidth (the full-width of the peak at half its height) of the water resonance and can be quoted in ppm or hertz (Hz). Poor shimming results in a reduction in the homogeneity and it produces a broad line width and good shimming produces a narrow linewidth. Poor shimming results in rapid T2* decay, with broad spectral lines, while good shimming, increases the time it takes for the signal to decay, resulting in a spectrum with smaller linewidths and therefore higher peaks.

2.6.3 Spin-Spin Coupling (J-Coupling)

One common feature of the MR spectrum is the appearance of multiplets - doublet or triplet peaks, which are signals associated with a single hydrogen environment which are split into a number of subsets. This arises when adjacent spins align parallel or anti-parallel to B_0 and this effects the local field of the spin of interest (Barker *et al.*, 2010). This is known as spin-spin or J-coupling. The splitting due to coupling result in signals that have lower peak intensity and a broader footprint along the chemical shift axis, both of which makes coupled species more difficult to detect, for example Gamma-aminobutyric acid (GABA) (CH_2) groups in the molecule and glutamate (Puts *et al.*, 2012).

2.6.4 Localisation

In single voxel spectroscopy a number of localisation techniques are used to excite a predefined voxel like the PRESS (Point RESolved Spectroscopy) (Bottomley, 1987) or STEAM (STimulated Echo Acquisition Mode) (Frahm *et al.*, 1989). Localisation techniques are used to excite predefined voxels which are prescribed by the operator in single-voxel MRS. Not using localising techniques results in contamination of the metabolite of interest by large signals, e.g lipids from surrounding tissues. Good localisation techniques significantly improve spectral quality.

2.6.4.1 PRESS (Point RESolved Spectroscopy)

PRESS is based on the spin-echo sequence and a 90° pulse is followed by two 180° pulses so that the primary spin echo is refocused by the third pulse (Bottomley, 1987). Each of the pulses has a slice-selective gradient on one of the three principle axes, so that the protons within the voxel are the only ones to experience all three radiofrequency pulses. The signal intensity is twice as high as STEAM, therefore spectra can be acquired with a good signal-to-noise (SNR) in a relatively short time. Newer sequences allow short echo times compared with when PRESS was originally developed, when longer echo times were needed to allow for good visualisation of metabolites.

2.6.4.2 MEGA-PRESS (MEscher-GARwood Point RESolved Spectroscopy)

Mescher and Garwood first described the MEGA suppression scheme in 1998 and it was found the technique could be applied to editing gamma-aminobutyric acid (GABA) from an MR spectrum (Mescher *et al.*, 1998). It quickly became the standard technique for the measurement of GABA in MRS. It allows the GABA

signal at 3.02ppm to be separated from other overlying metabolites, which are at a stronger concentration, by utilising the known couplings within the GABA molecule (Mullins *et al*, 2014). J- coupling as described above describes the interaction between different hydrogen nuclei within the same molecule. MEGA-PRESS exploits the knowledge of known couplings within a molecule by applying an RF pulse to one coupled spin, which consequently modifies the time evolution of a coupling partner and the appearance of the resulting peak in the spectrum. The use of MEGA-PRESS in GABA detection, is a focus of one of the pathways described in this thesis (Chapter III).

GABA is present in the brain at a concentration of about 1mM (Puts *et al.*, 2012). The chemical structure and MR spectrum of GABA consists of three different multiplets, which correspond to the three methylene (CH₂) groups in the molecule (Puts *et al.*, 2012). MEGA-PRESS (Mescher *et al.*, 1998) works by collecting two interleaved datasets which differ in their treatment of the GABA spin system. In one dataset, the ON editing pulses is applied to the GABA spins at 1.9ppm, which selectively refocuses the evolution of J-coupling to the GABA spins at 3ppm (Mullins *et al.*, 2012). While in the second dataset, the inversion pulse is applied elsewhere so that the J-coupling evolves freely throughout the echo time and is called the OFF editing pulse (Mullins *et al.*, 2012). As the RF pulse is frequency selective, peaks which are not around 1.9ppm or at the resonance of the OFF pulse are not affected by the editing pulses. Subtraction of the refocused ON spectrum from the non-refocused OFF spectrum removes all the peaks from the spectrum and retains only those that are affected by the editing pulses. Subtraction occurs in the post-processing and the ON and OFF spectra are collected in an interleaved way to reduce the potential problem of subject and

hardware instabilities. The resulting edited spectrum contains signals close to 1.9ppm, which were directly affected by the pulses and the GABA signal at 3 ppm, which is coupled to the GABA spins at 1.9 ppm. In this way the GABA resonance, which had a large overlap from the tCr resonance, has been selectively edited from the spectrum offering clear identification of GABA at 3.02ppm.

In addition to this, the edited spectrum also contains, the combined Glx peaks (sum of glutamate and glutamine) at 3.75ppm which is coupled to the Glx resonances at 2.1ppm.

One disadvantage of J-difference, is their reliance upon subtraction to remove overlapping signals from the spectrum, as it can result in subtraction artefacts which can obscure the intended edited GABA signals (Puts *et al*, 2012).

2.6.5 Clinical Application of MR Spectroscopy in Multiple Sclerosis

MRS can be seen as a complementary technique to MRI because it helps to enhance sensitivity to pathology; it also provides chemical and biophysical information about the microenvironment of tissues. MRS has the unique ability to characterize the chemical pathology of brain and spinal cord lesions in MS, as well as regions of the brain or spinal cord that are not associated with evident structural abnormalities on conventional MRI (Gass *et al.*, 2015). This results in improved diagnosis and it helps to better define the natural history of the disease process (Lin *et al.*, 2005).

Quantitative MRI techniques, such as MRS, have been used to measure disease burden within focal lesions, both acute and chronic, as well as in normal

appearing white and grey matter of MS patients at different stages of the disease. ¹H-MRS has demonstrated that although grey and white matter may appear normal on conventional MRI, they may be affected in the early phases of the disease (Miller *et al.*, 2003). ¹H-MRS has the specificity to detect and differentiate between neuronal and glial abnormalities in the absence of distinct structural injury. ¹H-MRS can be helpful in improving our understanding in vivo of the neurobiological mechanisms of injury and repair in MS (Gass *et al.*, 2015).

Studies carried out to date in MS, have demonstrated changes in various metabolites, including N-acetylaspartate (NAA) (usually this refers to total NAA (tNAA), which is equal to the sum of NAA and N-acetylaspartate-glutamate (NAAG)), choline (Cho)(usually this refers to total Cho (tCho) = choline + phosphocholine), myo-inositol (Ins), glutamate (Glu), and creatine (Cr) (usually this refers to total Cr (tCr) = creatine + phosphocreatine) (De Stefano *et al.*, 2007a; Bakshi *et al.*, 2008) in the brain and spinal cord, which suggest the presence of specific pathological abnormalities.

An example of an MR spectrum is shown in **Figure 2.6** below.

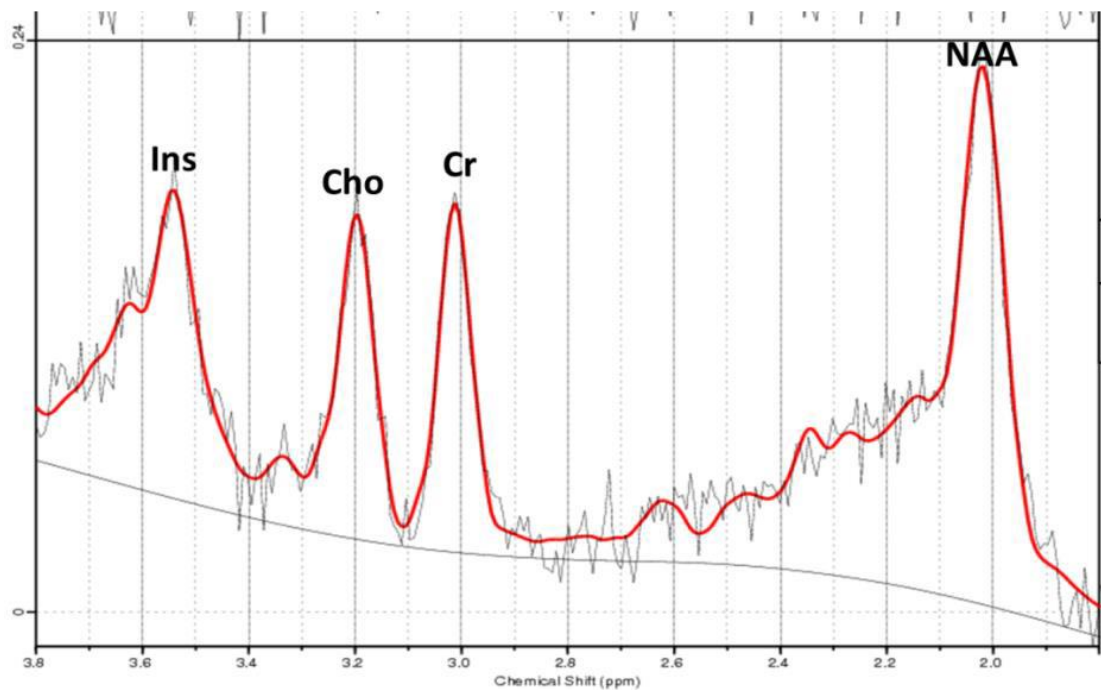


Figure 2.6: Example of a post-processed spectrum from the spinal cord of a healthy control. The chemical shift is on the x-axis in ppm and signal intensity on the y-axis. Cho – choline; Cr – creatine; Ins – myo-inositol; NAA – n-acetylaspartate

A decrease in NAA in the brain has been reported in all phases of the disease, including radiologically isolated syndrome, indicating neuronal dysfunction and/or axonal loss occurring at the earliest stage of MS (Stromillo *et al.*, 2013). It is thought that NAA levels may reflect both axonal loss and metabolic dysfunction (Moffett *et al.*, 2007). The discordant relationship between NAA and markers of structural damage (Cader *et al.*, 2007), as well as the partial recovery of NAA after a relapse (Ciccarelli *et al.*, 2010), suggests that NAA may reflect neuronal energy metabolism (Ciccarelli *et al.*, 2014).

It has been proposed that Ins is a glial specific cell marker and increases in Ins are associated with astrocytic activation and proliferation (Brand *et al.*, 1993; Chard *et al.*, 2002). Increased Ins, is believed to reflect increased gliosis in patients with CIS which is associated with clinical conversion to MS (Fernando *et al.*, 2004).

It has been shown that Cr remains relatively constant in the ageing brain (Saunders *et al.*, 1999) and it was thought that Cr remains relatively constant in diseases. As a result, Cr has been used as an internal reference to normalise the intensity of other metabolites. However, more recently it has been demonstrated that Cr levels are higher in the brain of MS patients (Inglese *et al.*, 2003), therefore one needs to be careful if using Cr as an internal reference in MS patients. It is thought that increased Cr represents increased gliosis (Inglese *et al.*, 2003).

Cho is a normal constituent of cell membrane and myelin phospholipids. Increases in Cho is thought to represent myelin breakdown, which occurs in active demyelination (De Stefano *et al.*, 2007b; Moore *et al.*, 2012). In RRMS, one study found increased Cho in NAWM (Inglese *et al.*, 2003), which is likely to reflect myelin breakdown.

Glutamate (Glu) is the major excitatory neurotransmitter in the central nervous system and it is the precursor for the major inhibitory neurotransmitter GABA. Glu and glutamine (Gln) can be difficult to distinguish at 3T (Tkac *et al.*, 2001), however a modification of the PRESS localisation at 3T enabled the separation of Glu and Gln in the brain (Hurd *et al.*, 2004). Most studies carried out to date have quantified the glutamate + glutamine (Glx) complex (Hattori *et al.*, 2002). Increased Glu has been found in acute MS brain lesions (Srinivasan *et al.*, 2005)

and an association has been demonstrated between memory and glutamate levels in the hippocampal, thalamic and cingulate regions in RRMS patients, which may be related to Glu excitotoxicity and neuroaxonal loss (Muhlert *et al.*, 2014).

GABA is the main inhibitory neurotransmitter in the CNS and it is produced from glutamate by glutamic acid decarboxylase (GAD) within GABAergic neurons (Chang *et al.*, 2003). GABA is then metabolised to succinic acid semialdehyde by GABA transaminase (GABA-T) and then to succinate within astrocytic mitochondria (Chang *et al.*, 2003). A number of clinical studies have been carried out to date using MRS to quantify GABA. Altered GABA concentrations in the brain have been detected in a number of conditions including epilepsy (MacDonald *et al.*, 2010), schizophrenia (Reynolds *et al.*, 2002) and depression (Hasler *et al.*, 2007). One study carried out in MS found reduced motor function was associated with increased GABA levels in the sensorimotor cortex and increased motor activation on functional MRI in patients with RRMS (Bhattacharyya *et al.*, 2013). Chapter III of this thesis will present the results of an MRS study, which quantified GABA in a number of regions in the brain in a cohort of patients with SPMS. An example a post processed MRS GABA spectrum is shown in **Figure 2.7**.

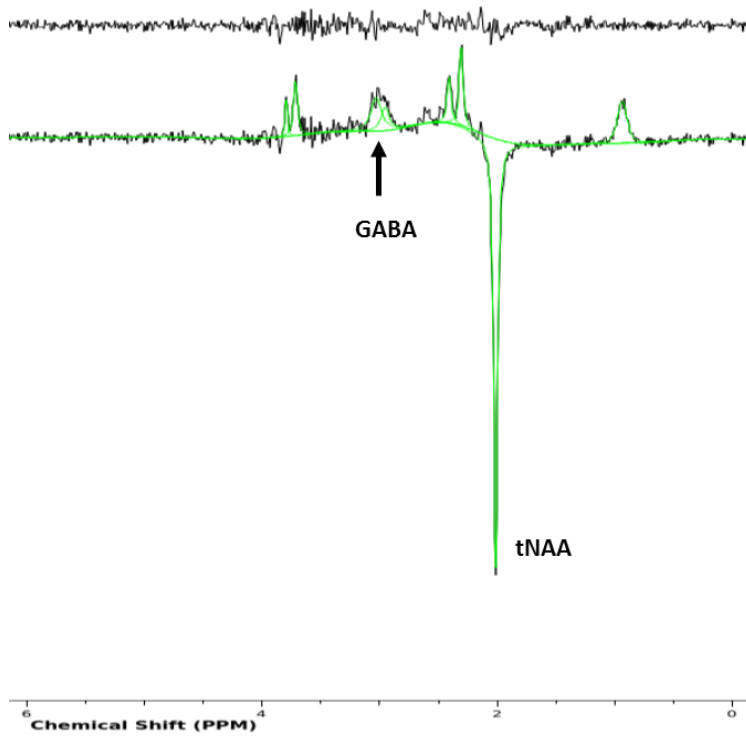


Figure 2.7: Example of an MRS GABA post-processed spectrum from the left sensorimotor cortex from a healthy control. GABA - gamma-aminobutyric acid; tNAA – total N-acetylaspartate.

2.7 Diffusion Imaging

2.7.1 Basic principles

Diffusion can be defined as the random translational movement of molecules in a fluid system, including biological tissue (Le Bihan *et al.*, 2001). When the concentration of fluid is uniform, diffusion is described statistically, by measuring the probability of a molecule travelling a given distance in a given diffusion time (Wheeler-Kingshott *et al.*, 2003). In an isotropic fluid, such probability has a Gaussian distribution and the molecules are free to diffuse in any direction without restrictions (Wheeler-Kingshott *et al.*, 2003). In biological tissue, white matter tracts contain closely packed, myelinated axons, orientated in a similar direction. Typically, diffusion of water molecules within axons and in the extracellular space tends to occur parallel to fibres, rather than perpendicular to the fibres, as the cell membranes and extracellular structures act as barriers (Wheeler-Kingshott *et al.*, 2003). This ordered, directional diffusion is called anisotropic diffusion. By measuring the degree of anisotropic diffusion, it provides useful biological information on the tissue's microstructure. A reduction in anisotropy reflects disruption to the microstructural integrity of white matter tracts, therefore allowing the diffusion of water molecules to occur more freely other than in the main orientation of the tract.

2.7.2 Effects of diffusion on the MRI signal

Diffusion of protons can affect the MR signal (Wheeler-Kingshott *et al.*, 2003). Normally in tissue, there is a delay between the excitation and the refocusing of the magnetisation, when spins are diffusing due to thermal agitation. When there is no motion or diffusion of water molecules, the dephasing which occurs after the

first pulse is exactly rephased after the 180° pulse. If there is random motion of the spins between dephasing and rephasing, then the refocusing of the spins is incomplete. This results in loss of transverse magnetisation and a reduction in the signal amplitude. Typically, the effects of diffusion are nearly always present, but these effects tend to be very small and do not contribute significantly to the signal attenuation in a standard spin-echo sequence. The amount of signal attenuation in a diffusion-weighted sequence depends on the diffusion properties of the tissue, the sequence parameters which determine the magnetic field gradients and the time during which the diffusion process takes place.

2.7.3 Pulsed gradient spin echo

The pulsed gradient spin echo (PGSE) was proposed by Stejskal and Tanner (Stejskal *et al.*, 1965) to apply diffusion weighting to an MRI acquisition. It consists of a 90° and 180° spin echo pair of radiofrequency pulses, then large and equal gradient pulses are applied on either side of the 180° refocusing pulse. The first gradient pulse induces a phase shift for all spins and then the second gradient pulse reverses this phase shift. As a result, the phase shift for static spins is cancelled and spins which have changed location due to diffusion of molecules during the time period between the two gradients (Δ in **figure 2.8**), are not fully refocussed by the second gradient pulse and this determines the signal attenuation. The net displacement of water molecules is called the apparent diffusion coefficient (ADC). By manipulating the strength of the gradient (G), the pulse width (δ) and the diffusion time (Δ), the degree of weighting or the b-factor can be controlled. The b-factor has units of s/mm^2 . Values of up to 1000s/mm^2 are required to obtain good contrast. Two acquisitions are performed, one without

superimposed diffusion gradient (b value = 0) and one with a diffusion gradient (b value $\neq 0$).

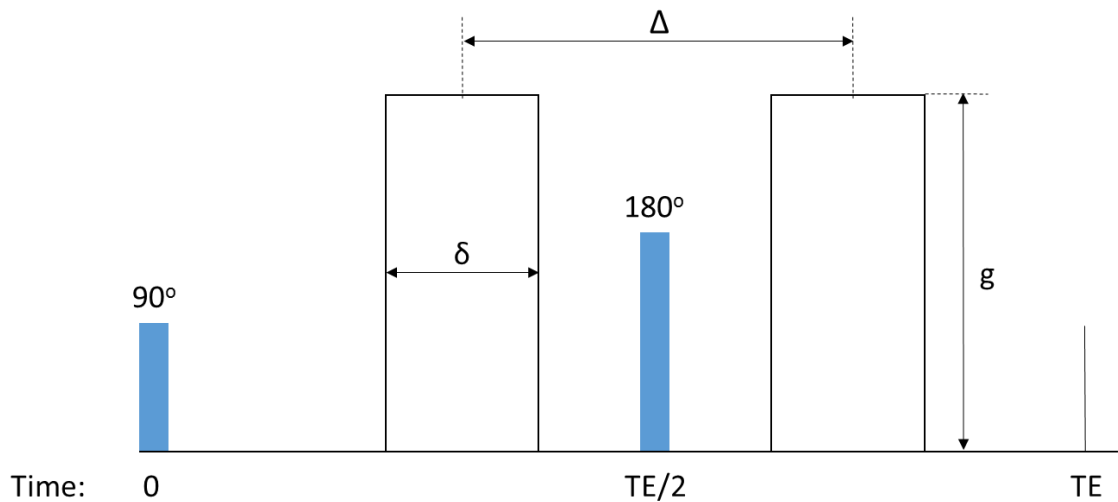


Figure 2.8: Pulsed gradient spin echo sequence for diffusion weighting. Δ represents the interval between centres of the two diffusion gradients corresponding to the diffusion time, δ represents the pulse width and g is the magnitude of the diffusion-weighting gradient.

2.7.4 Diffusion tensor

The diffusion tensor model is a superior mathematical model of water diffusion within white matter tracts than the simple ADC, as it also provides information about the direction of diffusion, therefore it can characterise multi directional diffusion. The diffusion tensor model is represented mathematically by a 3x3 tensor, which is a matrix of values. The diffusion tensor is made up of nine values, with each value corresponding to a gradient orientation and a cell orientation (Basser *et al.*, 1994). However, only six elements need to be measured to estimate the full diffusion tensor as it is symmetric around the diagonal (Basser *et al.*, 1994).

The diffusion tensor records the full direction of molecules, from which fractional anisotropy (FA) (a measure of the directional dependence of apparent diffusion, ranging from 0, when diffusion is equal in all directions and 1, when the apparent diffusion is along one direction only), mean diffusivity (MD) (the average diffusivity), radial diffusivity (RD) (index of diffusivity perpendicular to the main axis of the diffusion tensor i.e. perpendicular to the main fibre direction, increased RD relates to demyelination and decreased RD relates to remyelination) and axial diffusivity (AD) (diffusion parallel to the main axis) (Basser *et al.*, 1996) are derived. These diffusion tensor imaging (DTI) measures have been used as measures of microstructural tissue changes. Pathological processes, which lead to a reduction in the barriers that restrict diffusion, can result in an increase in apparent diffusion coefficient (ADC) values (Gass *et al.*, 2015). The structure, for example myelin in the brain, alters the direction of movement of the water molecules, providing information about the microstructure of tissues along a diffusion direction (Filippi *et al.*, 2003). A reduction in FA can arise due to a reduction in neurite density, an increase in the dispersion of neurite orientation dispersion, in addition to other microstructural changes (Beaulieu *et al.*, 2002).

In general MS lesions have an increased ADC to reflect expanded free water content within lesions due to a combination of oedema, demyelination and axonal loss (Horsfield *et al.*, 1998). FA tends to decrease in MS lesions which is likely to be due to a reduction in white matter tract integrity and with an increase in the extracellular space as a result of disruption to myelin and axonal structures (Hygino da Cruz *et al.*, 2011). Abnormalities in NAWM have been detected with DTI, with increases in ADC and MD and a decrease in FA (Ciccarelli *et al.*, 2003) (increased diffusivity and reduced anisotropy). This is represented in **Figure 2.9**.

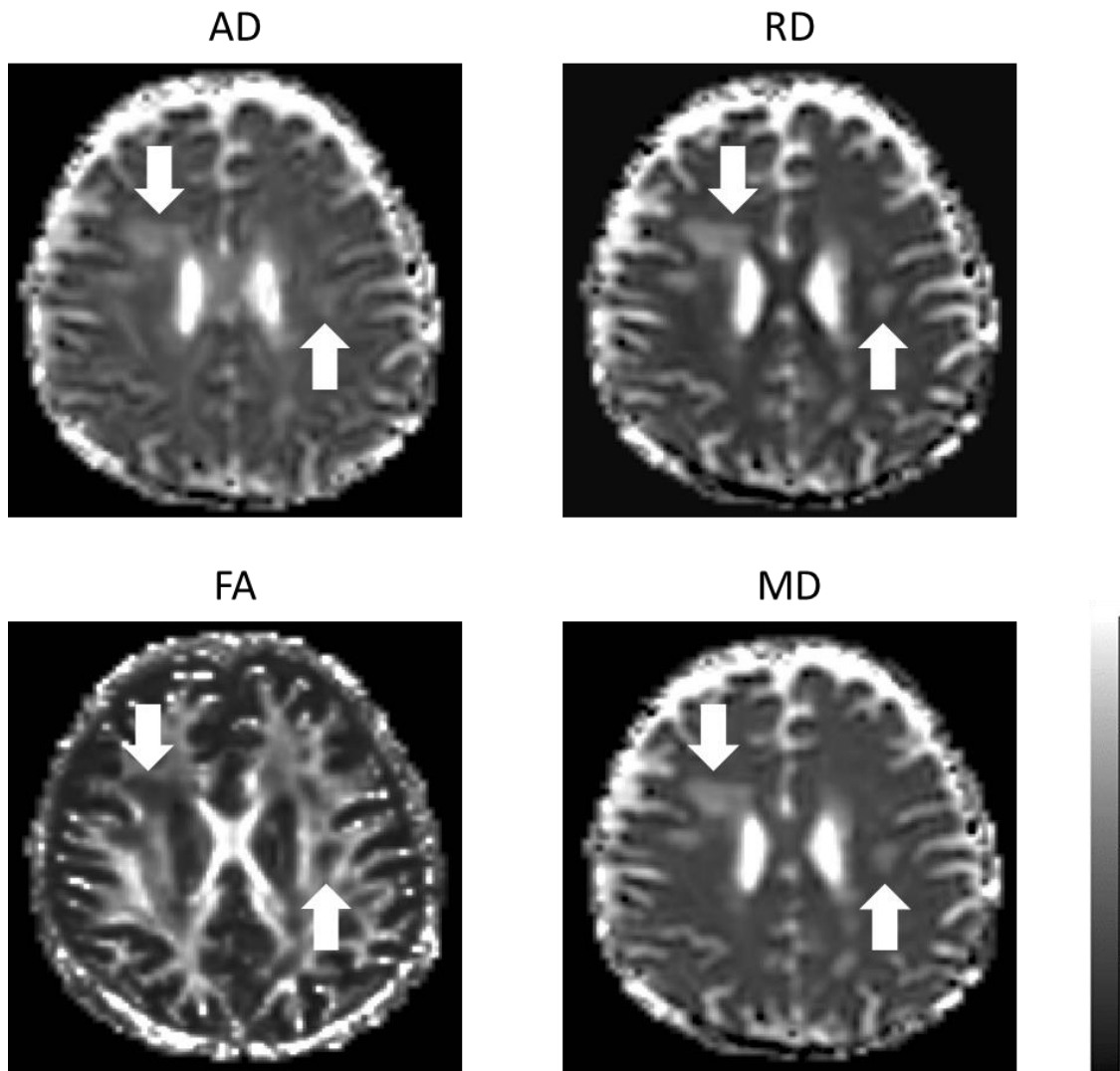


Figure 2.9: Example of an AD, RD, FA and MD maps from an MS patient with reduced FA and increased diffusivity seen in lesional tissue (white arrows). These images are from the DTI data acquired as part of the NODDI study in Chapter IV of this thesis.

Overall, the simple measures associated with DTI (FA, MD, RD, AD), provide crude measurements of the underlying complex environment (Assaf *et al.*, 2000, Assaf *et al.*, 2008). Animal studies suggest that axial diffusivity is a marker of neuroaxonal damage and radial diffusivity is a marker of demyelination (Song *et al.*, 2003; Zhang *et al.*, 2009; Budde *et al.*, 2009), although this has to be applied with caution when interpreting these measures in the human brain. However, it

has been suggested that a number of physical parameters can influence diffusion metrics such as demyelination, axonal density and fibre orientation, therefore making the diffusion tensor an imperfect model (Wheeler-Kingshott *et al.*, 2014).

The main limitations of the DTI model are that it based on a single fibre orientation in each voxel, therefore it fails in areas of heterogenous white matter, such as fibre crossing (Alexander *et al.*, 2001) and the DTI microstructural indices lack specificity. Another limitation of the diffusion tensor model is that diffusion is generally not Gaussian and it does not reflect the real displacement behaviour of water molecules due to the presence of membranes and myelin (Enzinger *et al.*, 2015). Longer diffusion times, which are typical in clinical application, increases the likelihood of hindrance and restriction due to the underlying tissue microstructure, which interferes with the ideal Gaussian behaviour of free water (Enzinger *et al.*, 2015). As a result of this, a number of more complex DWI techniques have been proposed, which are thought to reflect more accurately what actually happens at the tissue level (Enzinger *et al.*, 2015). These newer diffusion techniques can be divided into (i) a model free and (ii) a model based methods. Quite a number of these newer diffusion techniques have been developed and as part of this thesis, I chose to study a model free diffusion technique – Q-space imaging (QSI) and a model based diffusion technique – neurite orientation dispersion and density imaging (NODDI), with the NODDI method designed and optimised to be performed in clinical settings (Zhang *et al.*, 2012). These two newer diffusion techniques have been used in two of the studies presented in Chapters IV and V, and these techniques will be discussed in the following section.

2.7.5 Q-Space Imaging

The diffusion tensor model, described above, assumes that the displacement distribution function has a Gaussian probability of displacement, related to the diffusion of water molecules (Schneider *et al.*, 2014a). QSI is a model free diffusion weighted imaging technique (Callaghan *et al.*, 1988), which employs a Fourier transformation of the signal attenuation curve to determine the displacement distribution without assuming a Gaussian distribution.

Diffusion weighted imaging (DWI) is typically performed in the low b – value range, usually $< 1500\text{s/mm}^2$, where the signal decay is essentially monoexponential (Farrell *et al.*, 2008). In the CNS, the degree to which diffusion is reduced, compared to free water arises due to microstructural barriers, which includes multiple compartments in vivo (Farrell *et al.*, 2008). When restriction between compartments is large, the exchange is slow on the MR time scale and as a result the signal attenuation will become non-monoexponential (Farrell *et al.*, 2008). This effect is seen with higher b – values ($>1500\text{s/mm}^2$). When the signal attenuation curve is Fourier transformed, it is possible to obtain the probability density distribution of the diffusion from which summary statistics are derived, specifically the full width of half maximum (FWHM) and zero displacement probability (P_0). These steps are outlined in **Figure 2.10**.

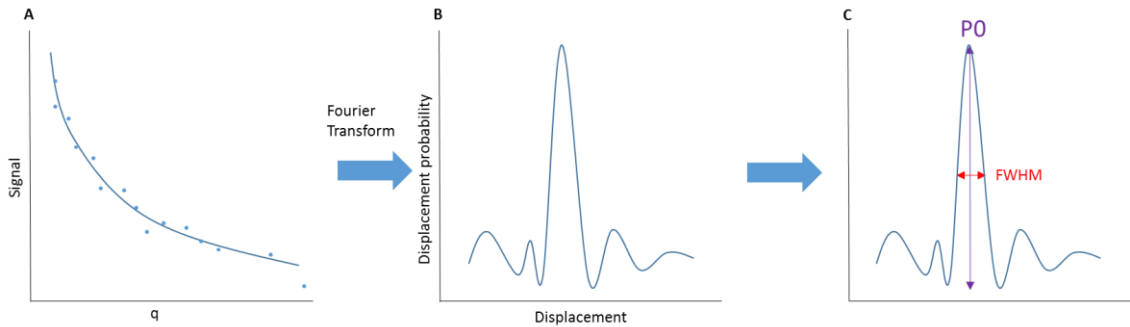


Figure 2.10: Steps involved in Q-space analysis. (A) The signal attenuation curve from the raw Q-space data is Fourier transformed. (B) This gives the probability density function. (C) Summary statistics (P0 and FWHM) are derived from the probability density function.

FWHM and P0 describes the height and width of the displacement distribution function. Typically, a high P0 and a low FWHM is an indicator of more hindered diffusion, while a low P0 and a wide FWHM indicates freer or less hindered diffusion (Farrell *et al.*, 2008). As Q-space metrics are contributed to from areas with non-Gaussian diffusion, it is thought to be a more sensitive technique for detecting restricted diffusion (Assaf *et al.*, 2000; Assaf *et al.*, 2002). Therefore, high b-value Q-space imaging, which measures slower diffusion within compartments, such as intra-axonal fluid, may contribute more to Q-space metrics than standard DTI (Schneider *et al.*, 2014b) and may be more specific for axonal injury (Assaf *et al.*, 2005).

2.7.5.1 Clinical application of Q-space imaging in MS

Patient studies on clinical scanners have been limited to date due to hardware limitations with the large gradients and short gradient pulses. Increasing the gradient pulses to compensate for the low gradients has enabled experiments on clinical scanners (Assaf *et al.*, 2005; Latt *et al.*, 2007). One study found that Q-space imaging was more sensitive at detecting pathophysiological changes

within lesions and NAWM, when compared to DTI in the brain of MS patients (Assaf *et al.*, 2002). The study by Assaf *et al.*, 2002 found broadening of the FWHM and a decrease in the amplitude (P_0) was more pronounced in lesional tissue, than NAWM and when compared to control tissue. Chapter V of this thesis will present the results of longitudinal changes in Q-space metrics in a cohort of patients with PPMS.

2.7.6 NODDI (Neurite Orientation Dispersion and Density Imaging)

Newer MRI sequences are needed to evaluate the microstructural changes in the brain and spinal cord, in order to give us a better understanding of the pathological changes taking place in MS. The quantification of neurite morphology in respect to its density and orientation distribution, gives us an insight into the structural basis of brain function (Zhang *et al.*, 2012). A new technique called NODDI which has recently been developed at UCL (Zhang *et al.*, 2012) addresses this. DTI provides sensitivity to tissue microstructure, but lacks specificity for individual tissue microstructural features. NODDI is designed to overcome the limitations of DTI, achieving higher sensitivity and specificity (Zhang *et al.*, 2012). Diffusion is based on water displacement patterns, which is influenced by the underlying tissue microstructure. Diffusion MRI measures these displacement patterns, and therefore provides information on different microstructural environments (Zhang *et al.*, 2012). During a typical diffusion MRI scan, two types of diffusion are seen, either hindered or restricted and these relate to two kinds of microstructural environments (Assaf *et al.*, 2000). The NODDI model consists of three compartments: intra-neurite, extra-neurite and cerebrospinal fluid (CSF). The extra-neurite compartment refers to the space around neurites (refers to both axons and dendrites), which is occupied by

various types of glial cells, the extracellular matrix and neuronal somas in grey matter. Diffusion in this compartment is hindered but not restricted. Restricted diffusion is the diffusion of water with a non-Gaussian pattern of displacement, with restricted geometries and this describes the water in the intra-neurite compartment. The intra-neurite compartment is modelled as a set of cylinders of zero radius, which reflects the restricted diffusion perpendicular to axons and free diffusion along their length. The CSF component is modelled using isotropic diffusion. The differentiation of intra-neurite and extra-neurite water forms the basis of measuring neurite morphology with diffusion MRI (Zhang *et al.*, 2012).

The NODDI model provides three summary statistics: Orientation dispersion index (ODI), neurite density index (NDI) and isotropic volume fraction (isoVF). Examples of these NODDI metrics as shown in the NODDI maps in **Figure 2.11**.

ODI quantifies the variability of neurite orientations (Zhang *et al.*, 2011). ODI values range from 0 – 1, with increasing ODI reflecting increasing variability of the underlying neurite orientations. As ODI approaches 0, neurites are all parallel; as ODI approaches 1, neurites are uniformly randomly orientated as can be seen in **Figure 2.12**.

NDI is used to estimate neurite density and, with axonal loss a likely pathological substrate for disability in MS, NDI may be a useful marker of axonal loss in MS. Normal brain development is associated with an increase in the dispersion of neurite orientation distribution (Conel, 1939), while the aging brain is associated with a reduction in the dendritic density of the brain (Jacobs *et al.*, 1997). Based on this, the NODDI model, may provide additional information to DTI, in a clinical

feasible setting and it may help to explain the key factors which contribute to physical disability.

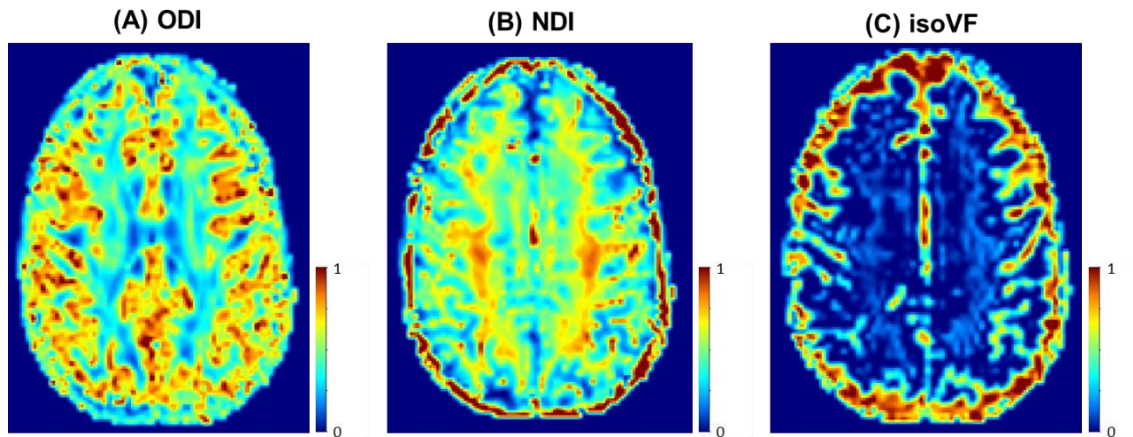


Figure 2.11: Example of NODDI maps from an MS patient (A) orientation dispersion index (ODI), (B) neurite density index (NDI) and (C) isotropic volume fraction (isoVF).

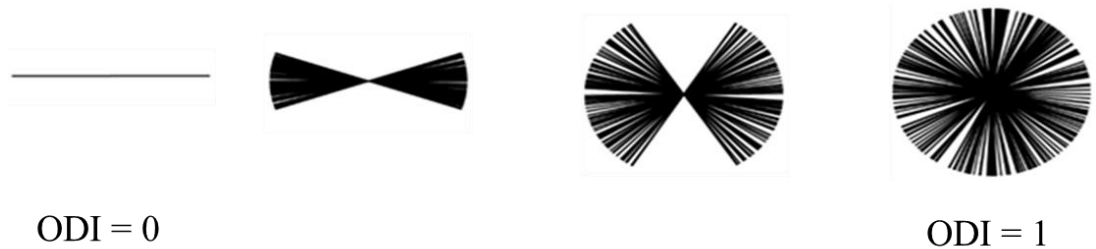


Figure 2.12: Orientation dispersion index (ODI), which is the spread of neurite orientations, ranging from 0 (on the left) and 1 (on the right). (Figure reproduced with permission from Dr. Francesco Grussu).

2.7.6.1 Clinical application of NODDI in MS

To date one pilot study has been carried out in the brain of MS patients (Schneider *et al.*, 2014b). Results from this study found reduced NDI and ODI in MS lesions compared to healthy control white matter tissue and reduced NDI and increased ODI in NAWM of MS patients compared to normal white matter in controls, reflecting axonal loss and loss of fibre integrity in MS lesions (Schneider *et al.*, 2014b). More recently the NODDI technique has been successfully applied to the spinal cord in healthy controls (Grussu *et al.*, 2015b). NODDI in the brain has been used in the study presented in Chapter IV of this thesis, in patients with RRMS.

2.8. Brain atrophy

2.8.1 Background

Brain atrophy is a global marker of neuroaxonal loss (Fillipi & Agosta, 2010). Brain volume loss is well recognised in MS from the very earliest stages and in a complex disease like MS, it reflects a generalised process involving various tissue compartments (Giorgio *et al.*, 2008). It is reported that brain volume loss occurs at a rate of 0.5-1.0% per year in MS patients (Bermel *et al.*, 2006), compared to healthy controls who have a rate of brain volume loss of 0.1-0.3% per year (Coffey *et al.*, 1992; Pfefferbaum *et al.*, 1994). The brain volume loss in controls is likely related to changes associated with age. The mechanisms which lead to brain atrophy are not fully understood and may arise due to a combination of demyelination, inflammation, and axonal damage and loss which may lead to retrograde neurodegeneration (Giorgio *et al.*, 2008). A number of pathological studies have found that neuroaxonal damage and loss may occur independent of

demyelination, and this may be related to the presence of an abnormal glia-axonal interaction in the absence of very little inflammation (Garbern *et al.*, 2002).

2.8.2 Technical

In order to capture temporal patterns of structural brain changes, adequate MRI protocols as well as accurate and robust image analysis tools are required. Brain atrophy is generally measured on 2D/3D T1-weighted images. A number of MRI based methods are available to detect brain atrophy.

Segmentation based methods are suitable for single time point analysis and are designed to analyse regional volumes. Brain parenchymal fraction (BPF) is one example which assesses global brain atrophy, which provides a ratio of volume of parenchymal brain tissue to the total volume within the outer surface of the brain, and it has been demonstrated that this measure is highly reproducible with a coefficient of variation of less than 0.2% (Rudick *et al.*, 1999). Segmentation based methods are not recommended for longitudinal analysis.

Registration based methods are sensitive to changes over time and are therefore recommended for longitudinal studies. An example of a registration based method is SIENA (structural image evaluation using normalisation of atrophy) (Smith *et al.*, 2001). This method assesses brain volume changes by estimating directly the local shifts in brain edges across the entire brain. Firstly, the brain and skull are extracted from the two time points, the two brains are aligned to each other and both brains are then resampled into the halfway space between the two images, in order to avoid bias (Smith *et al.*, 2004). Tissue type segmentation is then performed in order to find the brain/non-brain edge points and perpendicular edge displacement is then estimated at these edge points

(Smith *et al.*, 2004). The mean edge displacement is then converted into a global estimate of percent brain volume change (PBVC) between the two time points (Giorgio *et al.*, 2008). Another well-established registration based method is Boundary Shift Integral (BSI) (Freeborough & Fox, 1997), which is similar to SIENA as it uses linear registration to align the baseline and repeat images and then tracks the shift of the brain boundary location (Prados *et al.*, 2015).

It has been demonstrated that registration based techniques are more precise and sensitive compared to segmentation based methods for longitudinal data analysis (Anderson *et al.*, 2007).

Prior to any brain atrophy measurements, be it registration or segmentation based methods, lesion filling of the hypointense lesions on T1-weighted scan is performed in order to prevent misclassification of tissue during brain volume calculations. One study found 52% of lesion voxels were misclassified as grey matter (Chard *et al.*, 2010), and as a result, an increase in lesion volume causes a false increase in grey matter volume.

2.8.3 Clinical application

Global brain atrophy has been demonstrated at all stages of MS (Bermel *et al.*, 2006). It has been demonstrated that those patients with CIS who have significantly greater ventricular enlargement develop MS when compared to those that remain stable (Dalton *et al.*, 2002). Global brain atrophy measures predict disability and disability progression (Fisher *et al.*, 2002). More recently it has been found that grey matter, but not white matter volumes, decreased with advancing disease in MS (Roosendaal *et al.*, 2011) and disability and cognitive

impairment are better predicted by grey matter than white matter volume or T2 lesion volume (Roosendaal *et al.*, 2011).

Regional measures of brain atrophy also vary with frontal, temporal and parietal lobes the most frequently involved cortical grey matter regions in MS patients (Calabrese *et al.*, 2007). Atrophy of the deep grey matter structures also occurs, with the thalamus the most consistently involved grey matter region in MS. Thalamic atrophy occurs within the first five years of MS onset, when most patients are minimally disabled (Henry *et al.*, 2009) and it is also associated with conversion from CIS to clinically definite MS over 2 years (Zivadinov *et al.*, 2013). Thalamic atrophy is associated with cognitive dysfunction, motor disability, fatigue and pain syndromes (Minagar *et al.*, 2013).

Brain atrophy has been used as an outcome measure in clinical trials in MS. Patients participating in clinical trials often have active disease with clinical relapses and evidence of gadolinium enhancing lesions on MRI. Resolution of this inflammation results in an initial accelerated decrease in brain volume during the first year of treatment, which is termed pseudoatrophy (Zivadinov *et al.*, 2008). It is not known if the effects of pseudoatrophy continue to occur after one year. This needs to be further investigated to determine the full extent of pseudoatrophy after the initiation of certain therapies which may be related to resolution of inflammation as opposed to neurodegeneration (De Stefano and Arnold, 2015).

Some of the newer disease modifying agents available (natalizumab, dimethyl-fumarate, fingolimod, alemtuzumab) for the treatment of RRMS, have incorporated brain volume as an outcome measure and have shown to improve brain atrophy accrual when compared to placebo or another treatment (Vidal-

Jordana *et al.*, 2015; Miller *et al.*, 2007b; Miller *et al.*, 2015; Radue *et al.*, 2012; Coles *et al.*, 2008; Cohen *et al.*, 2012). To date only one phase II clinical trial in SPMS have had positive effects on brain atrophy (Chataway *et al.*, 2014).

2.9 Spinal cord imaging

Most of the above techniques can also be applied to the spinal cord; however overall spinal cord imaging is technically very challenging. The spinal cord is a small structure, motion artefacts can arise in the cervical cord due to cardiac systole (Mikulis *et al.*, 1994) and truncation artefact can arise at the interface between high and low signal which can cause misrepresentation at the interface of the CSF/spinal cord surface within the image, which overall can degrade the image quality (Bronskill *et al.*, 1988). Motion artefacts can be significantly reduced with the use of cardiac triggering and saturation bands. As well as this, fast imaging techniques have made spinal cord imaging more reliable which has, overall improved the quality of spinal cord data (Filippi and Rocca, 2011). The technical improvements which have been made to spinal cord imaging, have resulted in more spinal cord imaging studies taking place in MS. Lesions in the spinal cord are most commonly seen in the cervical cord and they are mostly located peripherally. Up to 90% of patients with MS have asymptomatic spinal cord lesions, whilst 30-40% of CIS subjects have asymptomatic lesions (Lycklama *et al.*, 2003).

2.9.1 Spinal cord ¹H-MR spectroscopy

Over the last decade, improvements in data acquisitions and post-processing, have made spinal cord spectroscopy possible. As discussed previously, NAA is a marker of neuroaxonal integrity and in the spinal cord a number of studies have

demonstrated reduced NAA in both acute and chronic lesions (Ciccarelli *et al.*, 2007; Marliani *et al.*, 2010; Abdel-Aziz *et al.*, 2015).

One study demonstrated that following a spinal cord relapse, NAA levels are initially low and the NAA levels starts to recover as the patient recovers from the relapse (Ciccarelli *et al.*, 2010). Cord area was then used as a surrogate marker of axonal density and it was found that changes in NAA levels were not entirely a result of axonal loss, but may also reflect mitochondrial dysfunction. These findings suggest that the recovery of NAA is partially explained by the recovery of mitochondrial function (Ciccarelli *et al.*, 2010).

Ins is a marker of glial function. One study demonstrated marginally increased Ins at the start of a spinal cord relapse, which correlated with disability (Ciccarelli *et al.*, 2007). Reduced Ins was found in the spinal cord of patients with neuromyelitis optica when compared to MS patients, reflecting astrocytic loss, in keeping with the pathological hallmark of neuromyelitis optica (astrocytic necrosis) (Ciccarelli *et al.*, 2013).

Glx (the sum of glutamate and glutamine) represents the excitatory neurotransmitter pool. In the cervical cord Glx was lower in patients with PPMS compared to controls, which may be explained by neuro-axonal degeneration (Abdel-Aziz *et al.*, 2015).

2.9.2 Q-space imaging in the spinal cord

Very few Q-space imaging studies have been performed in the spinal cord of MS patients. The change in the shape of the displacement distribution function in MS lesions in the spinal cord represents the loss of axonal and/or myelin barriers to

diffusion, as demonstrated in one study in patients with RRMS (Farrell *et al.*, 2008). This study demonstrated the feasibility of using high b-value Q-space imaging in four patients with MS in the spinal cord, as well as improved detection of abnormal diffusion compared to apparent diffusion coefficient (ADC) measurements (Farrell *et al.*, 2008). A study in healthy controls demonstrated good reproducibility in perpendicular and parallel diffusivity in the ascending and descending tracts in the cervical cord (Schneider *et al.*, 2011). More recently, Abdel-Aziz *et al.*, 2015 found significantly higher perpendicular diffusivity in the whole cervical cord, anterior, posterior and lateral columns of the cervical cord in early PPMS compared to healthy controls. This is likely to reflect a breakdown of myelin and axonal membranes, which act as a microstructural barrier to perpendicular diffusivity (Abdel-Aziz *et al.*, 2015). They also found Q-space imaging metrics were more sensitive at detecting microstructural injury within the spinal cord than standard ADC measures (Abdel Aziz *et al.*, 2015).

2.9.3 Spinal Cord Atrophy

2.9.3.1 Background

Irreversible and progressive disability in MS is thought to be due to ongoing neuroaxonal loss and demyelination in white matter lesions (Trapp *et al.*, 1998), NAWM (Evangelou *et al.*, 2000) and grey matter (Kutzelnigg *et al.*, 2005). Spinal cord involvement in MS often results in progressive locomotor disability. Demyelinating plaques are the characteristic feature of MS in the spinal cord. However, spinal cord neuropathological studies have demonstrated that axonal loss rather than plaques represent the main pathological substrate of irreversible physical disability (DeLuca *et al.*, 2006; Lovas *et al.*, 2000). It is reported that axonal density can be reduced by as much as 65% in the spinal cord in patients

with MS (Lovas *et al.*, 2000). To date, clinical trials of anti-inflammatory therapies in progressive MS have generally been negative (Fox *et al.*, 2012). There is an urgent need to develop biomarkers to measure important events in the neuronal injury pathway and correlate these with clinical disability (Fox *et al.*, 2012) in progressive MS in order to facilitate development of neuroprotective agents.

MRI is the most sensitive technique for detecting in vivo measurements of spinal cord cross sectional area. A reduction in spinal cord cross sectional area can be used as an approximate marker of axonal loss (Losseff *et al.*, 1996; Bot *et al.*, 2004). Demyelination can also contribute to reduction in cord volume (Bot *et al.*, 2004). To date only a few clinical trials have used spinal cord cross sectional area as an exploratory endpoint in clinical trials due to the challenges in developing sensitive and reproducible methods (Kearney *et al.*, 2014a). The rate of cord atrophy in MS is thought to be ~1% per year with substantial inter-subject variation (Rashid *et al.*, 2006). As these changes are overall quite small, a very reproducible method is required to detect these changes longitudinally.

2.9.3.2 Technical

Initially spinal cord area was measured using manual outlining of the axial images of the cord (Kidd *et al.*, 1993). A semiautomatic edge-detection method was then developed (Losseff *et al.*, 1996). This method involved drawing two regions of interest, one around the spinal cord and one around the outer border of the CSF. A mean signal intensity of the cord and CSF was calculated and a signal intensity threshold halfway between the cord and CSF was used to define the edge of the spinal cord (Losseff *et al.*, 1996). The newest method, the active surface model, is more automated and allows rapid measurement of spinal cord area (Horsfield *et al.*, 2010). This method involves the placement of cord markers centrally in the

cord on a number of axial slices. Then an outline of the cord is created automatically, allowing for the detection of atrophy in the cervical cord as shown in **Figure 2.13**. The C2/C3 region is used to measure spinal cord area using the active surface model as the CSF space is wide at this level so the cord tends to lie centrally, there is little variability in cross-sectional area at this level and it is not a common site for disc protrusion (Losseff *et al.*, 1996). As well as this, post-mortem work has demonstrated that as a result of flexion and extension of the head, the spinal cord can move up to 1.8 cm. However, this effect is least evident in the high cervical region (Reid, 1960).



Figure 2.13: Example of an axial 3D-FFE image (resolution $0.5 \times 0.5 \times 5 \text{ mm}^3$) through the C2/3 intervertebral disc from a healthy control showing the cord volume using the active surface model.

A highly reproducible method is required to detect these small changes in the spinal cord over time in order for it to be a feasible outcome measure in clinical trials. The active surface model (ASM) is a rapid and reproducible semi-automatic measure of spinal cord area (Horsfield *et al.*, 2010). The active surface model has been demonstrated to be more reproducible than the Losseff technique (Losseff *et al.*, 1996), with lower inter and intra-observer coefficients of variation compared to the Losseff technique (inter-observer coefficient of variation = 1.07% for the ASM versus 7.95% for the Losseff technique; intra-observer coefficient of variation = 0.44% for the ASM versus 2.15% for the Losseff technique) (Horsfield *et al.*, 2010). The feasibility of spinal cord cross sectional area quantification in the context of a multicentre study has been demonstrated using the active surface model in subgroups of MS patients (Rocca *et al.*, 2011).

2.9.3.3 Clinical application

Spinal cord atrophy is seen in all stages of MS, with volume loss most marked in the progressive forms of MS. Cord atrophy has been detected in patients with a CIS, even in the absence of spinal cord symptoms (Brex *et al.*, 2001). Several studies in MS subjects with a long disease duration found that cord atrophy is independently related to disability (Daams *et al.*, 2014) (Kearney *et al.*, 2014b) (Kidd *et al.*, 1993). The study by Losseff *et al.*, 1996, found a strong correlation between EDSS score and cord area with a reduction in cord area associated with increased levels of disability. It has been demonstrated both in-vivo (Bergers *et al.*, 2002) and ex-vivo (Ganter *et al.*, 1999), that cord atrophy occurs independently of focal lesions. It has been found that the rate of spinal cord atrophy does not correlate with the rate of brain atrophy which raises the possibility of independent disease processes causing brain and spinal cord

atrophy (Lukas *et al.*, 2015). Cord atrophy has the potential to be used as an imaging biomarker to monitor disease progression in MS, as well as a primary outcome measure in neuroprotective clinical trials to evaluate the effects of treatment. Chapter VI of this thesis presents the results of a study which investigated the changes in spinal cord atrophy in a progressive MS cohort.

2.10 Conclusion

The following Chapters III-VI will present the results of studies which have used a number of the above advanced imaging techniques in MS.

Chapter III

Gamma-aminobutyric acid concentration in progressive multiple sclerosis

3.1 Introduction

There is a need to understand the mechanisms of neurodegeneration in progressive MS (Fox *et al.*, 2012), as described in Chapter I. SPMS develops after an initial RRMS course (typically 10-15 years), with or without acute exacerbations during the progressive course (Lublin *et al.*, 2014). This results in irreversible and continuous neurological decline. There is a decrease in the development of new inflammatory lesions, but disability accumulation continues, which is likely to be due to ongoing neuroaxonal loss, the mechanisms for which include degeneration of chronically demyelinated white matter axons (Trapp *et al.*, 1999) and progressive cortical demyelination (Kutzelnigg *et al.*, 2005). SPMS results in significant motor and cognitive impairment in affected patients. Cognitive dysfunction is common, with prevalence rates of between 43% and 70% (Langdon *et al.*, 2012), affecting information processing speed (Amato *et al.*, 2010), episodic memory and executive function (Strober *et al.*, 2009). The pathological processes underlying clinical disability in MS are complex, and include neuronal and glial changes with associated structural and metabolic abnormalities. These abnormalities may be detected in vivo by metabolic and molecular imaging (Ciccarelli *et al.*, 2014). A recent study found that in MS patients, reduced concentrations of grey matter Glu, the main excitatory neurotransmitter of the human brain, correlated with worse memory function (Muhlert *et al.*, 2014), suggesting that abnormalities in the neurotransmitter pathways may play a role in neurodegeneration, which underpins disability in MS.

Gamma-aminobutyric acid (GABA) is the major inhibitory neurotransmitter in the brain (DeFelipe, 1993) and is produced from glutamate by L-glutamic acid

decarboxylase within GABAergic neurons (Chang *et al.*, 2003), as described in *Section 2.6.5*. GABA is needed for normal brain function, synaptic plasticity, cortical adaptation and reorganisation (Stagg, 2014). Altered GABA concentrations, either increases or decreases, have been detected in a number of conditions, including epilepsy (MacDonald *et al.*, 2010), and schizophrenia (Reynolds *et al.*, 2002). GABAergic inhibition may be one of the mechanisms involved in use-dependent plasticity in the intact human motor cortex (Stagg *et al.*, 2011; Levy *et al.*, 2002). Changes in GABA concentration in the sensorimotor cortex during motor learning have been demonstrated (Floyer-Lea *et al.*, 2006). One pilot study in RRMS (Bhattacharyya *et al.*, 2013) found that reduced motor performance correlated with increased GABA levels in the sensorimotor cortex. The increased GABA concentration was also associated with increased motor activation on functional MRI. Despite limitations, these in vivo results suggest that cortical reorganisation occurring in the sensorimotor cortex in patients with RRMS, as reflected by increased functional MRI response, is linked with increased GABA levels, and is a possible compensatory mechanism that maintains motor function (Bhattacharyya *et al.*, 2013).

Magnetoencephalography (MEG) is a method of providing measures of neural activity and it is thought to reflect the effects of synchronous post-synaptic activity (Hari *et al.*, 2010). The peak frequency of gamma oscillations in the primary motor cortex measured using MEG, which was induced by a button press task was positively correlated with GABA concentrations in this region in controls (Gaetz *et al.*, 2011). This has also been demonstrated in the visual cortex (Muthukumaraswamy *et al.*, 2009). This suggests that the frequency of gamma oscillations is determined by the GABA/glutamate ratio, with a low ratio

associated with efficient inhibition of relevant neural activity, therefore producing more precise task performance (Atallah & Scanziani, 2009; Takei *et al.*, 2016). In vivo quantification of GABA using ^1H -MR spectroscopy is challenging due to the spectral overlap of GABA with more abundant metabolites, such as N-acetyl-aspartate (NAA) at 2 ppm (Puts and Edden, 2012). MEGA-PRESS (MEscher-GARwood Point RESolved Spectroscopy) is a spectral editing method that allows the discrimination of GABA from these metabolites (Mescher *et al.*, 1998), as described in *Section 2.5.6*; it also allows quantification of tNAA, which, when reduced, indicates neuronal loss and/or metabolic dysfunction (Moffett *et al.*, 2007), and Glx, which has been found to be reduced in the spinal cord of PPMS patients compared to healthy controls, suggesting dysfunction in the glutamatergic pathway and neuroaxonal loss (Abdel-Aziz *et al.*, 2015).

Single voxel MRS using MEGA-PRESS has been used in a number neurological conditions to date as mentioned above. Specifically, the sensorimotor cortex has been studied in RRMS and demonstrated the MEGA-PRESS sequence is a reproducible method for the detection of GABA in this region (Bhattacharrya *et al.*, 2013). One study carried out in controls successfully measured GABA in the hippocampus using the same protocol used in this study and also demonstrated good reproducibility of the measure in this region (Solanky *et al.*, 2013b).

Thus, the finding of: (i) reduced concentrations of Glu, which is the precursor of GABA, as observed in post-mortem (Wegner *et al.*, 2006) and in vivo MR spectroscopy studies in progressive multiple sclerosis (Sastre-Garriga *et al.*, 2005); (ii) reduced GABA-related gene transcripts and density of inhibitory neuronal processes in the motor cortex of autopsied MS brains (Dutta *et al.*,

2006); and (iii) impaired compensatory mechanisms occurring in SPMS compared with RRMS (Rocca *et al.*, 2005), lead us to hypothesise that GABA levels are reduced in SPMS patients when compared with healthy controls and that they correlate with increased clinical disability. This is the first in-vivo study performed to date, to investigate reduced GABA levels in SPMS and its association with clinical disability. In order to test these two hypotheses, I measured the concentrations of GABA in the prefrontal cortex, right hippocampus (involved in visual and verbal memory) and left sensorimotor cortex using MEGA-PRESS MR spectroscopy. I investigated whether there was an association between memory function and GABA concentration in the grey matter regions of the prefrontal cortex and hippocampus, and between sensory and motor function and GABA concentration in the left sensorimotor cortex. I examined if these associations were independent of imaging measures of structural damage, such as those sensitive to axonal loss and demyelination, derived from the same areas, and of tNAA and Glx, obtained within the same spectroscopic voxels.

3.2 Materials and methods

3.2.1 Subjects

Patients with a diagnosis of SPMS who were not taking any medication that affects the GABAergic systems (e.g. Baclofen), for a minimum of 6 months prior to the time of scanning, and with an EDSS of between 4.0 - 6.5, were recruited into this cross-sectional stand-alone study. Healthy controls were also recruited. All the SPMS patients recruited into this study were recruited from the MS clinics ran on a weekly basis at The National Hospital of Neurology and Neurosurgery, Queen Square London. All healthy controls recruited into this study, were work

colleagues, friends and family as well as friends and family of the MS patients. Written informed consent was obtained for participants in the study, which was approved by our local research ethics committee (Study reference: 05/Q0502/101).

I recruited the SPMS patients from the MS clinics at Queen Square, I obtained the consent on the day of the scanning and I carried out all the clinical and cognitive testing on the day of the scan. The radiographers at the Institute of Neurology performed the actual MRI scans (Marios Yiannakas, Chichi Ugorji and Luke Hoy). I carried out the post-processing in TARQUIN and reviewed the results of each patient individually. If there were any issues with the data, I discussed and reviewed the results with Dr Bhavana Solanky, the Physicist who optimised the protocol. I assimilated the data in a spreadsheet, including all clinical, cognitive and MRI data. Dr. Dan Altmann and Dr. Carmen Tur performed the statistical analysis for this study. I interpreted the results from the statistical analysis performed and the results are presented below.

3.2.2 Cognitive Tests

Patients and controls were assessed using a range of cognitive tests. Speed of information processing was assessed using the Symbol-Digit Modalities Test (SDMT) (Lezak *et al.*, 2004), and the 3-second Paced Auditory Serial Addition Test (PASAT) (Rao *et al.*, 1990), for which z-scores were obtained with reference to published norms (Fischer *et al.*, 1999). Executive function was measured using the Stroop colour-word interference test (Trenerri *et al.*, 1989) and Hayling sentence completion test (Burgess and Shallice., 1997). Verbal memory was assessed using The California Verbal Learning Test – II (CVLT-II) for immediate

and delayed recall (Delis *et al.*, 2000) and visuospatial memory was assessed using the Brief Visuospatial Memory Test Revised (BVM-T-R) (Benedict *et al.*, 1997). Working memory was assessed using the digit span from the Wechsler Adult Intelligence Scale-III (Wechsler *et al.*, 1997). Premorbid IQ was measured using the National Adult Reading Test (Nelson, 1982). Levels of anxiety and depression were measured using with the Hospital Anxiety and Depression Scale (HADS) (Zigmond *et al.*, 1983).

Failure of a test (SDMT, Stroop, PASAT, Hayling Sentence Completion, Digit Span, CVLT-II and BVM-T-R), was defined as a score of two or more SDs below the mean of the controls. Patients with significant cognitive impairment were defined as those showing failure on at least two tests.

3.2.3 Clinical Assessments

All patients were assessed using the EDSS (Kurtzke, 1983). All patients and controls were also assessed using the 9-Hole Peg Test (9-HPT) (Goodkin *et al.*, 1988), Timed 25-Foot Walk Test (TWT) (Cutter *et al.*, 1999), and the Medical Research Council (MRC) scoring system for muscle strength of the right upper and lower limb (Medical Research Council, 1943; Dyck *et al.*, 2005). Z-scores were calculated for the 9-HPT and TWT from normative values displayed in the National Multiple Sclerosis Society Task Force database (Fischer *et al.*, 1999). Mean grip strength from the right upper limb was measured using the Jamar hydraulic dynamometer (Sammons Preston. Incorporated, Bolingbrook, IL, USA) (Svens and Lee, 2005). The average of two trials for the TWT and the average of two trials for the 9-HPT were calculated (Fischer *et al.*, 1999). Vibration perception thresholds (VPTs) were measured using the biothesiometer (Bio-

Medical Instrument Company, Newbury, Ohio) from both the right lateral malleolus and the right ulnar styloid process. Mean VPTs were calculated and used in the analysis. The right upper and lower limb scores from the motor and sensory tests were only included in the analysis as GABA concentration was estimated in the left sensorimotor cortex.

3.2.4 Magnetic Resonance Imaging Protocol

All scans were performed using a 3T Achieva system (Philips Medical Systems, Best, Netherlands) with a 32-channel head coil.

3.2.4.1 Structural MR Imaging

All participants underwent structural imaging, which included: (i) axial PD / T2-weighted imaging using a 2D dual-echo turbo spin echo (TSE) sequence (TR = 3500 ms; TE = 19/85 ms; flip angle $\alpha = 90^\circ$; FOV = 240 x 180 mm²; with spatial resolution of 1x1x3mm³); (ii) 3D MPRAGE (T1-weighted magnetisation-prepared rapid acquisition gradient-echo sequence) (TR = 6.9 ms; TE = 3.1 ms; flip angle $\alpha = 8^\circ$; FOV = 256 x 256 mm²; voxel size = 1 x 1 x 1 mm³); and (iii) axial 2D DIR (double inversion recovery) scan (voxel-size = 1 x 1 x 3 mm³, TR = 16000 ms; TE = 9.9 ms).

We outlined hyperintense lesions in all SPMS participants on the axially acquired T2-weighted images using a semi-automated edge finding tool in JIM v. 6, then recorded the volume of T2-weighted lesions in millilitres for each subject.

Hypointense lesions on the T1-weighted volume scan were marked and filled with values consistent with NAWM signal intensity to prevent misclassification of tissue during segmentation (Chard *et al.*, 2010). Segmentation of the lesion-filled image was then performed using SPM8 (statistical parametric mapping;

Wellcome Trust Centre for Neuroimaging, University College London (UCL) Institute of Neurology, London). The brain parenchymal fraction (the sum of white and grey matter relative to total intracranial volume) was then recorded for each subject. For calculation of brain tissue volumes, the grey matter, white matter and CSF masks were obtained by segmentation of the volumetric T1-weighted scans. DIR lesions were marked for each patient following consensus recommendations (Geurts *et al.*, 2011).

3.2.4.2 Single-Voxel Spectroscopy

Sagittal T1-, coronal T2- and axial PD-weighted scans were used for voxel placement in the three grey matter regions (prefrontal cortex, right hippocampus and left sensorimotor cortex).

Due to the significant overlapping signals of GABA with other metabolites, non-invasive measures of GABA in the brain were acquired using the widely used MEGA-PRESS editing sequence (Mescher *et al.*, 1998), with parameters TR= 2000ms, TE = 68ms, MOIST water suppression, pencil-beam automated shimming, and editing pulses centred at 1.9 and 7.5ppm on each alternate scan. The dimensions and averages for the volume of interest were as follows: (1) right hippocampus: dimensions 30 x 19.2 x 16 mm³, volume = 9.22 mls, 576 averages; (2) prefrontal cortex: dimensions 28 x 30 x 22 mm³, volume = 18.48 mls, 432 averages; and (3) left sensorimotor cortex: dimensions 35 x 34 x 22 mm³, volume = 26.18 mls, 400 averages. The acquisition and analysis protocol used in this study followed recently published guidelines for GABA-edited MR spectroscopy at 3 T using MEGA-PRESS (Mullins *et al.*, 2014). Example placements of each volume of interest can be seen in **Figure 3.1**.

A non-water suppressed scan was also acquired with the same parameters (24 averages in one block), to provide an internal water reference to metabolite concentrations. TARQUIN (Totally Automatic Robust Quantification in NMR), was used to estimate the concentrations of GABA, tNAA and Glx (Wilson *et al.*, 2011).

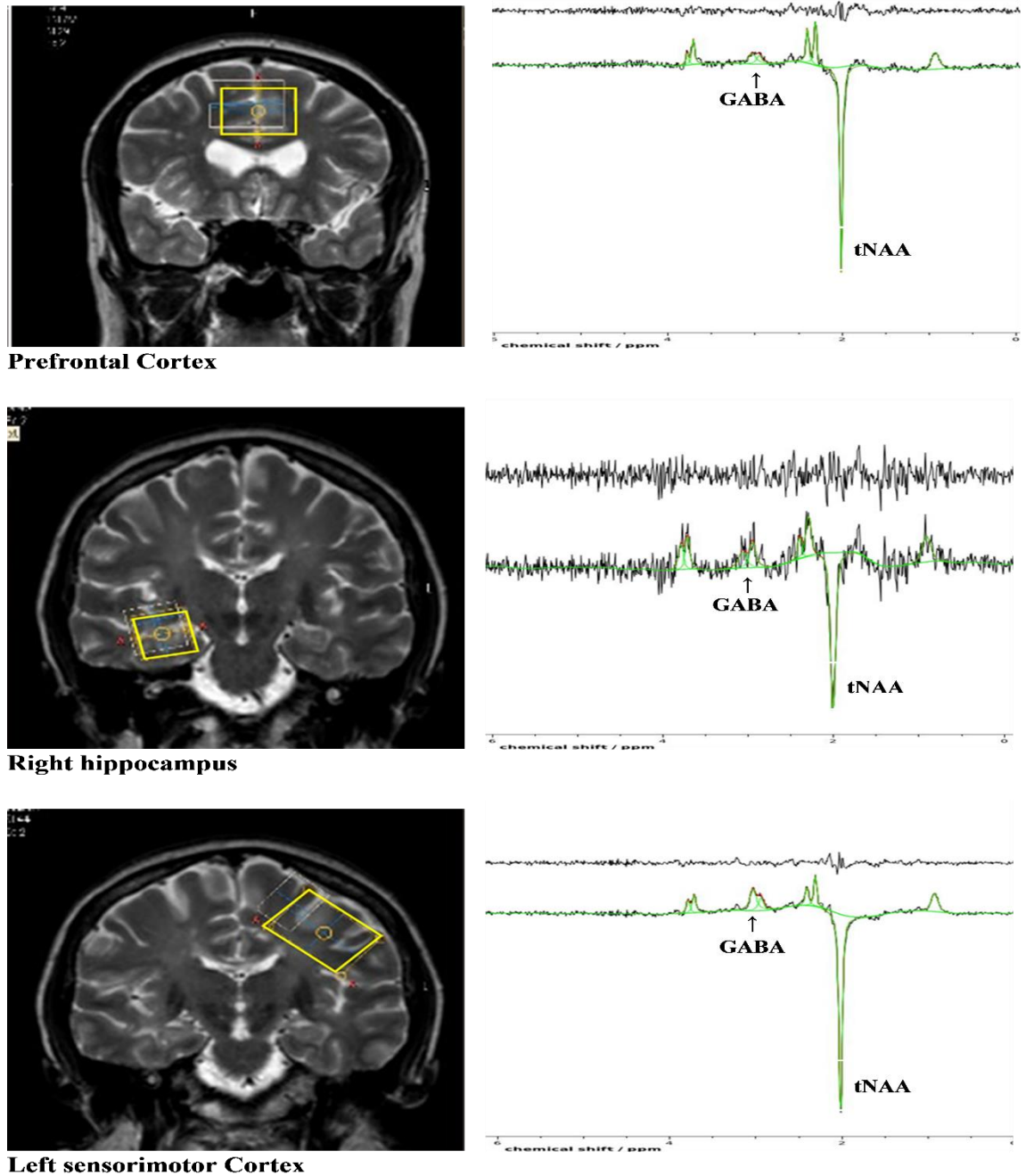


Figure 3.1: Placement of MR Spectroscopy (MRS) voxels (left) with their example MRS spectra (right) in the prefrontal cortex (A), right hippocampus (B) and the left sensorimotor cortex (C).

3.2.5 Spectral Quantification

Spectral quantification was carried out using TARQUIN, which provides a fully automatic analysis of in-vivo spectra (Wilson *et al.*, 2011). The analysis package uses a linear combination of basis functions to fit spectra (Wilson *et al.*, 2011). For MEGA-PRESS data, TARQUIN uses a simple predefined basis set which models the GABA peak as two single Gaussian peaks (Mullins *et al.*, 2014). The reliability of TARQUIN has been demonstrated to be comparable to other spectral quantification methods e.g LCmodel (O’Gorman *et al.*, 2011). The non-water suppressed scan was used as an internal reference of known concentration to find the absolute concentrations of GABA.

Spectral quality was assessed using Cramér-Rao-Lower-Bounds (Rao, 1946) values provided by TARQUIN, which represent the minimum possible variance on a fit parameter. Only data that had Cramér-Rao-Lower-Bounds values of $\leq 20\%$ were included in the analysis. From the participants, datasets for 6 controls and 14 patients had to be excluded from the hippocampus due to Cramér-Rao-Lower-Bounds values larger than 20% (Near, 2014), and one patient’s dataset was excluded from the hippocampus due to time constraints. The hippocampus is technically very challenging due to its small size, the strong susceptibility to effects of nearby cranial air and bone, as well as the pulsatile cerebrospinal fluid surrounding it (Solanky *et al.*, 2013b). In the prefrontal cortex, datasets from 3 controls and 1 patient were excluded due to Cramér-Rao-Lower-Bounds values greater than 20%. In the sensorimotor cortex, 2 controls and 1 patient were excluded due to Cramér-Rao-Lower-Bounds values greater than 20% and 4 patient datasets were not acquired due to time constraints.

The fractional content of grey matter and white matter within each spectroscopic voxel was calculated. In order to count the number of T2 and DIR lesions within each spectroscopic voxel, we created a binary mask of the spectroscopic voxel by using the absolute scan geometry of the PD/T2 and DIR volumes as a reference.

3.2.6 Statistical analysis

3.2.6.1 Differences in cognitive and clinical performance and metabolite concentrations between groups

Differences between patients and controls were examined using independent-sample t-tests. For GABA measures, differences were examined for each region separately using multiple linear regression to adjust for age, gender, grey matter and white matter fraction. Since the concentrations of tNAA and Glx can also be estimated within the same voxel using the same protocol, we completed the investigation by looking at these metabolites in the model.

3.2.6.2 Associations between clinical disability and regional GABA levels in patients and controls

Associations between GABA levels and clinical disability were examined in patients and controls combined using multiple regressions of the clinical variables on GABA predictors with interaction terms (i.e. group x GABA measure) to allow different associations between patients and controls to be estimated. These models allowed adjustment for covariates, such as age, gender, and premorbid IQ (when appropriate). Potential confounders, such as grey matter lesions within the spectroscopic volume of interest, anxiety and depression were also examined by including these as covariates. Grey matter lesions within the spectroscopic volume of interest were not included in the final model, as they did not contribute

to the model. In these models, variables describing executive function and information processing speed were regressed on prefrontal GABA concentration, those describing memory (visual and verbal) functions on hippocampus GABA concentration, and those describing right upper and lower limb motor and sensory ability on sensorimotor cortex GABA concentration.

In patients only, to assess independence of GABA concentration from tNAA or Glx as predictors, tNAA or Glx was added to models with GABA in cases where GABA was significantly or borderline significantly associated with a clinical score.

Where regression residuals showed deviation from normality, we used bias-corrected nonparametric bootstrap with 1,000 replicates to obtain confidence intervals (CIs) and p-values. Significance was set at 5% level. All analyses were performed in Stata 13.1 (Stata Corporation, College Station, Texas, USA).

3.7 Results

3.7.1 Participant demographics and characteristics

Thirty patients with SPMS (mean age = 51.3 years (SD9.6), 23 females, median EDSS=6 (range 4 – 6.5)) and 17 healthy controls (mean age = 46.3 years (SD11.7), 9 females) were studied. Overall patients had a short duration of progressive disease (mean duration of progressive disease = 4 years) and a moderate level of disability. Further details on patient demographic characteristics and disability are summarised in **Table 3.1**.

3.7.2 Clinical disability

As expected, patients had significantly slower processing speed on the SDMT ($p < 0.001$) and had worse verbal memory than controls, with significantly worse

immediate ($p = 0.01$) and 30 minute delayed recall ($p = 0.02$) of the list, after adjusting for age and gender (**Table 3.1**). In contrast, patients and controls did not differ in their executive function (Stroop $p = 0.65$, Hayling sentence completion $p = 0.08$), working memory ($p = 0.26$), visuospatial memory ($p = 0.23$), premorbid IQ ($p = 0.09$), or on the PASAT ($p = 0.14$). 63% of patients ($n = 19$) were categorised as cognitively preserved, with only 37% ($n = 11$) categorised as cognitively impaired.

Patients performed significantly worse on all motor and sensory tests, when compared to controls, specifically, grip strength ($p = 0.001$), muscle strength ($p = 0.001$), 9-HPT ($p = 0.001$), TWT ($p = 0.001$) and VPTs ($p = 0.001$), after adjusting for age and gender (**Table 3.1**).

Physical disability tests	Controls	Patients	Adjusted difference* (95% CI)	P-value
Median EDSS (range)	NA	6 (4 – 6.5)	-	-
Mean 9-HPT (right arm, z score)	1.19 (0.53)	-0.33 (1.29)	-1.69 (-2.36 to -1.01)	<0.001
Mean TWT (z score)	0.41 (0.02)	0.06 (0.33)	-0.340 (-0.52 to -0.16)	<0.001
Mean Grip Strength (right upper limb, kg force)	28.13 (13.53)	12.83 (6.99)	-11.99 (-18.12 to -5.85)	<0.001
Mean Vibration perception Threshold (VPT) (right upper and lower limb)	7.83 (3.64)	18.24 (10.88)	10.86 (4.59 to 17.13)	<0.001
Mean MRC Strength (right upper and lower limb)	70.00 (0.00)	61.38 (4.81)	-8.52 (-11.22 to -5.83)	<0.001

Cognitive Tests	Controls	Patients	Adjusted difference* (95% CI)	P-value
Mean Anxiety (HADS)	5.12 (3.79)	7.10 (5.45)	2.36 (-0.81 to 5.54)	0.14
Mean Depression (HADS)	3.47 (1.81)	5.67 (3.51)	2.45 (0.51 to 4.39)	0.0
Mean Digit Span (scaled score)	11.47 (2.74)	10.73 (3.32)	-1.12 (-3.10 to 0.84)	0.25
Mean Stroop (seconds to complete)	127.69 (25.77)	148.22 (78.72)	10.35 (-35.09 to 55.78)	0.65
Mean SDMT (total score)	60.00 (12.35)	45.63 (14.06)	-15.27 (-23.30 to -7.24)	<0.001
List Learning	Controls	Patients	Adjusted difference* (95% CI)	P-value
Mean Learning (total words)	62.00 (12.28)	53.94 (10.18)	-8.30 (-16.72 to 0.11)	0.05
Mean Recall after distraction	14.18 (1.83)	11.69 (3.14)	-2.73 (-4.64 to -0.82)	0.01
Mean 30 minute delayed recall	14.18 (2.60)	11.69 (3.14)	-2.69 (-4.87 to -0.52)	0.02
Mean PASAT (z score)	0.15 (1.07)	-0.38 (1.24)	-0.53 (-1.25 to 0.18)	0.14
Mean Visual recall – BVMT-R	28.73 (7.73)	25.69 (9.22)	-3.49 (-9.38 to 2.39)	0.23
Mean Hayling Sentence Completion	5.93 (1.27)	5.43 (1.25)	-0.72 (-1.51 to 0.08)	0.08

Table 3.1: Mean (SD) demographics, clinical and cognitive performance of patients and controls. * A linear regression model was used adjusting for age and gender.

3.7.3 Structural MRI Measures

Total grey matter DIR lesions in patients ranged from 0 – 32, with a median of 16 lesions. The median number of grey matter lesions within each of the spectroscopic volumes of interest was 0 (**Table 3.2**).

Patients showed significant whole brain white matter atrophy when compared with controls (white matter fraction: 0.32 vs. 0.34, $p < 0.0001$), after adjusting for

age and gender. There was no significant difference in total brain grey matter fraction ($p = 0.74$), or in the grey matter or white matter tissue volumes within the spectroscopic voxels between patients and controls (all p values > 0.05) (**Table 3.2**).

	Controls	Patients	Adjusted difference* (95% CI)	P-value
Total brain GMF	0.47 (0.02)	0.47 (0.01)	0.001 (-0.01 to 0.01)	0.74
Total brain WMF	0.34 (0.01)	0.32 (0.02)	-0.02 (-0.03 to -0.01)	0.001
BPF	0.81 (0.02)	0.80 (0.02)	-0.02 (-0.03 to -0.004)	0.01
GMF in the hippocampus spectroscopic VOI	0.54 (0.10)	0.58 (0.09)	0.05 (-0.03 to 0.12)	0.21
WMF in the hippocampus spectroscopic VOI	0.44 (0.09)	0.38 (0.08)	-0.06 (-0.13 to 0.01)	0.07
GMF in the prefrontal cortex spectroscopic VOI	0.50 (0.06)	0.50 (0.03)	0.02 (-0.01 to 0.05)	0.24
WMF in the prefrontal cortex spectroscopic VOI	0.35 (0.07)	0.33 (0.08)	-0.02 (-0.08 to 0.03)	0.33
GMF in the sensorimotor cortex spectroscopic VOI	0.32 (0.04)	0.35 (0.10)	0.03 (-0.02 to 0.09)	0.26
WMF in the sensorimotor cortex spectroscopic VOI	0.58 (0.07)	0.53 (0.14)	-0.05 (-0.13, 0.03)	0.18
DIR lesions (median (range))	Controls	Patients		
Total brain grey matter lesions	NA	16 (0 – 32)	-	-
Grey matter lesions in the prefrontal spectroscopic VOI	NA	0 lesions (range 0-4)	-	-
Grey matter lesions in the hippocampal spectroscopic VOI	NA	0 lesions (range 0 - 1)	-	-
Grey matter lesions in the sensorimotor cortex spectroscopic VOI	NA	0 lesions (range 0 - 2)	-	-

Table 3.2: MRI measures in patients and controls. * Adjusted for age and gender. WMF-white matter fraction; GMF-mrey matter fraction.

3.7.4 GABA concentration in the hippocampus and sensorimotor cortex was lower in patients than controls

Patients had significantly reduced GABA concentration in the hippocampus (lower by 0.41mM (95% CIs -0.79, -0.01, $p = 0.04$)), and in the sensorimotor cortex (lower by 0.39mM (95% CIs -0.67, -0.10, $p = 0.01$)), when compared with healthy controls, after adjusting for age, gender, grey matter and white matter fractions within the spectroscopic voxel (**Table 3.3**). However, there was no significant difference in GABA concentration in the prefrontal cortex ($p = 0.096$) between patients and controls.

Patients also showed a significantly reduced tNAA concentration in the sensorimotor cortex (lower by 2.46mM ($p = 0.01$)), when compared with healthy controls, after adjusting for age, gender, grey matter and white matter fractions within the spectroscopic voxel. There were no significant differences in tNAA levels in the hippocampus ($p = 0.51$) and prefrontal cortex ($p = 0.58$) between groups after adjusting for the above-mentioned covariates (**Table 3.3**).

There were no significant difference in Glx in the prefrontal cortex, hippocampus and sensorimotor cortex between patients and controls (**Table 3.3**).

	Controls	Patients	Adjusted difference (95% CI)	P-value
Hippocampus				
GABA	1.46 (0.47)	1.08 (0.33)	-0.41 (-0.792 to -0.014)	0.04
tNAA	5.52 (1.645)	3.62 (2.74)	-1.08 (-4.51 to 2.35)	0.51
Glx	8.12 (4.59)	7.03 (3.57)	1.01 (-12.47 to 14.43)	0.86
Sensorimotor Cortex				
GABA	1.51 (0.46)	1.17 (0.35)	-0.39 (-0.67, -0.10)	0.01
tNAA	9.14 (1.99)	7.28 (2.76)	-2.46 (-4.17, -0.74)	0.01
Glx	4.86 (1.89)	4.32 (2.24)	-0.71 (-2.36, 0.93)	0.38
Prefrontal Cortex				
GABA	0.89 (0.25)	0.98 (0.22)	0.13 (-0.02, 0.29)	0.10
tNAA	7.76 (3.25)	7.93 (2.34)	0.57 (-1.54, 2.67)	0.59
Glx	5.48 (1.57)	5.32 (1.62)	0.03 (-1.21, 1.27)	0.97

Table 3.3: Comparison of GABA, tNAA and Glx concentration (mean (SD) in mM) in the prefrontal cortex, right hippocampus and left sensorimotor cortex between the control group and the patient group. P-values given for adjusted group comparisons after correcting for age, gender, GMF and WMF within the spectroscopic VOI.

3.7.5 Associations between GABA levels in the sensorimotor cortex and clinical scores

In patients, worse motor function in the right upper and lower limb was significantly associated with lower GABA levels in the sensorimotor cortex, after correcting for age and gender. In particular, for each unit decrease in GABA

levels, there was a predicted -10.86 (95% CIs -17.79, - 4.48) decrease in grip strength (kg force) ($p < 0.001$) and -8.74 (95% CIs -13.94, -3.02) decrease in muscle strength of the right upper and lower limb ($p < 0.006$), according to the corresponding regression models. In addition, per unit decrease in GABA levels, there was a predicted borderline significant decrease in the 9-HPT of -1.26 (95% CIs -2.78, 0.26) ($p < 0.10$). These significant associations did not show any substantial change (i.e., their regression coefficients did not change) when tNAA and Glx levels in the sensorimotor cortex were included into the model. Repeating the regression models including age, gender, depression, and premorbid IQ did not change the pattern of results. There were no significant associations between GABA concentration in the sensorimotor cortex and the remaining physical disability scores, such as EDSS, TWT, and VPTs, and between GABA concentration in either the hippocampal or prefrontal volumes of interest and any of the cognitive tests.

3.7.6 Associations between tNAA levels in the sensorimotor cortex and clinical scores

In patients, lower tNAA in the sensorimotor cortex was also significantly associated with worse motor function, after correcting for age and gender. For each unit decrease in tNAA levels, there was a predicted -1.20 (95% CIs -0.48, -1.98) decrease in grip strength ($p < 0.02$), -0.94 (95% CIs -0.73, -1.83) decrease in muscle strength ($p < 0.05$) and -0.14 (95% CIs -0.12, -0.30) decrease in 9-HPT ($p < 0.04$) according to the corresponding regression models. When the models regressing clinical scores on tNAA were adjusted for GABA, the direction and magnitude of the regression coefficients for tNAA completely changed (for grip strength: -1.20 vs. 0.56; muscle strength: -0.94 vs. 0.18; 9-HPT: -0.14 vs. 0.02),

while the direction and magnitude of those for GABA remained similar, before and after adjusting for tNAA (-10.86 vs. -15.26, -8.74 vs. -10.31, and -1.26 vs. -1.30, respectively). There was no significant association between tNAA concentration in the sensorimotor cortex and EDSS, TWT and VPTs.

3.8 Discussion

This study provides evidence that (i) GABA levels are reduced in the hippocampus and sensorimotor cortex in patients with SPMS and (ii) lower GABA concentration in the sensorimotor cortex correlates with reduced motor function of the contralateral limbs. We will discuss each of these results in turn.

3.8.1 Evidence of GABAergic dysfunction in SPMS

The observed reduced GABA levels in the hippocampus and sensorimotor cortex in patients with SPMS when compared with healthy controls raises the possibility that GABA may be a marker of neurodegeneration in the brain. The reduction in GABA levels may reflect a combination of reduced GABA receptor levels and decreased density of inhibitory interneuron processes in the motor cortex in patients with progressive MS, which have been described by a previous histological study (Dutta *et al.*, 2006). A positron emission tomography (PET) imaging study in MS using ¹¹C-flumazenil (Freeman *et al.*, 2010), which binds the benzodiazepine site on the GABA_A receptor, reported that the uptake of ¹¹C-flumazenil was lower (indicating reduced GABA_A receptor levels) in the cortex of patients with MS (RRMS and SPMS) compared with healthy controls (Freeman *et al.*, 2010), suggesting the loss of dendrites and synapses as seen in post-mortem analysis (Wegner *et al.*, 2006), which may precede the development of measurable brain atrophy. A previous study reported reduced Glu levels in grey

matter (cingulate and parietal cortices) in RRMS patients compared to controls, suggesting that a reduced availability of the precursor glutamate may contribute to reduced synthesis of GABA. The significant decrease in tNAA concentration in the sensorimotor cortex in patients compared to controls confirms that there was significant neuronal loss and/or dysfunction in this region, since tNAA is a well-established marker of neuroaxonal integrity, viability and metabolism (Moffett *et al.*, 2007).

In addition to being a marker of neurodegeneration, decreases in GABA levels may contribute to the ongoing neurodegenerative process in progressive MS. Although spectroscopic measurements *in vivo* do not allow us to draw firm conclusions about possible changes in the neurotransmitter pool and/or GABAergic pathway, there is some evidence from preclinical studies that MR spectroscopy-derived GABA levels reflect extra-synaptic GABA tone, rather than synaptic GABA activity (Mason *et al.*, 2001). Therefore, the observed reduced GABA levels may reflect a reduction in inhibitory innervation of cortical neurons, which, in turn, upregulates the firing rate of demyelinated axons, resulting in higher energy demands, as proposed by Dutta *et al.*, 2006; this may ultimately result in progressive axonal loss and neurodegeneration. Additionally, there is evidence that GABA mediates neuroprotection by delaying neuronal death (Saji & Reis, 1987).

There was no difference in GABA levels in the prefrontal cortex between patients and controls, indicating a regional variation in altered GABA levels. This is likely to reflect regional variation in both the reduced synaptic density and neuronal loss, and in the possible role of altered GABA concentration, as a mechanism of

plasticity and functional reorganization, as explained below. Overall the GABA concentration was lower in controls than in patients in the prefrontal cortex, but this did not reach statistical significance. The study carried out by Bhattacharyya *et al.*, 2011 found reduced GABA in the sensorimotor cortex in controls compared to RRMS patients. It has been demonstrated that in healthy controls, reduced GABA levels were observed in the prefrontal cortex during a working memory task and it is thought that this is related to synaptic plasticity (Michels *et al.*, 2012). In the healthy brain, reduced GABA levels are thought to be associated with facilitating long-term potentiation like plasticity (Stagg *et al.*, 2011), which may reflect the results in the prefrontal cortex in this study. The higher GABA levels in the SPMS patients in the prefrontal cortex may reflect loss of some of the adaptive mechanisms associated with plasticity.

3.8.2 Association between lower GABA levels and physical disability

In this study, there were associations between decreased muscle strength and worse performance on the 9-HPT, and lower sensorimotor GABA concentration. This suggests that greater loss of inhibitory neurons (and their processes) is an important contributor to clinical disability. Additionally, reduced GABA levels may represent a mechanism through which progressive axonal degeneration leads to progressive neurological disability. Patients with SPMS may have a loss of compensatory mechanisms associated with cortical reorganisation and adaptation, due to a reduction in synapses and neurons, resulting in the loss or deterioration in function.

The observed correlation between worse 9-HPT scores and lower GABA levels in the sensorimotor cortex is in contrast to a study by Bhattacharyya *et al* (2013),

as previously mentioned. Bhattacharyya *et al.*, found that a worsening of performance on the 9-HPT was associated with increased GABA levels in patients with RRMS. These conflicting findings may reflect differences between patient populations (SPMS compared to RRMS). Patients with SPMS may have loss of the compensatory mechanisms associated with cortical reorganisation (Rocca *et al.*, 2005), as a result of ongoing loss of inhibitory GABA neurotransmission, ultimately resulting in progressive neurodegeneration and progressive disability. In contrast, in RRMS, reduced GABA levels are associated with improved motor performance, as a result of adaptation of cortical grey matter. The inclusion, in the Bhattacharyya's study, of patients currently taking GABAergic medications at the time of scanning is a limitation.

I found no significant associations between GABA levels in the sensorimotor cortex and VPTs, TWT or EDSS. This may be due to the role of regions other than the sensorimotor cortex in contributing to the clinical function that is captured by these scores, the small range of EDSS (4-6.5) in the patient group, and the impact of changes in regionally specific GABA levels on function.

It is surprising that patients' performance on cognitive tests were not associated with GABA levels in relevant brain regions. It is difficult to say why I did not see a relation between memory function and GABA levels in the prefrontal cortex and hippocampus grey matter regions, but this may be due to a number of reasons. First, the patients recruited into this study were relatively early in their progressive disease course (mean duration = 4 years) and had no significant grey matter atrophy. Second, 63% of patients (n = 19) were categorised as cognitively preserved, with only 37% (n = 11) categorised as cognitively impaired. Third, a

sample size calculation with 80% power, at 5% significance, requires an N of 85 to detect a significant association between GABA levels and the cognitive tests, which is substantially more than the number recruited into this study. Finally, GABA differences may be more widespread and so have an effect in relation to memory that is not evident in the single volume of interest studied.

3.8.3 Association between lower tNAA levels and physical disability

The observed reduction in tNAA in the sensorimotor cortex in patients compared to controls is in keeping with previous studies of reduced tNAA in MS (Kirov *et al.*, 2013; Achnichts *et al.*, 2013). tNAA is a well-established marker of neuronal loss and/or metabolic dysfunction as discussed in *Section 2.6.5* (Moffett *et al.*, 2007). tNAA correlated with grip strength, muscle strength and the 9-HPT. Several studies in MS have demonstrated consistent correlations with tNAA and physical disability (De Stefano *et al.*, 1997; Aboul-Enein *et al.*, 2010). These studies confirm neuroaxonal damage as a mechanism of disability in MS. Nevertheless, the fact that tNAA was not a significant factor in the models including GABA, and that the regression coefficients for GABA did not materially change when adjusting for tNAA, indicates that the relationship between lower GABA and poorer clinical performance is confirmed and independent of the levels of tNAA.

3.8.4 Limitations and future directions

One limitation of this study is the shape of the spectroscopic volumes of interest and the linear relationship between the volume of interest and spectroscopic signal to noise ratio. As the regions of interest were small, it was necessary to use volumes of interest that encompassed the grey matter of interest, rather than

being completely contained within the specific region, in order to achieve reliable measurements of metabolite concentrations in acceptable acquisition times. Whilst every effort was made to limit the MR spectroscopy voxel to hippocampal grey matter, the size and shape of the volumes of interest meant this included some white matter from surrounding tissue, and small parts of neighbouring medial temporal lobe structures. This was necessary in order to attain a sufficient signal to noise ratio, in an acceptable acquisition time. The correction for white matter fraction and grey matter fraction within the spectroscopic voxel in the statistical models will have reduced the possibility that differences in these measures between groups were responsible for differences in GABA. One study (Bhattacharyya *et al.*, 2011) measured GABA in the sensorimotor cortex with similar grey matter fraction (37+/-7%) and white matter fraction (52+/-12%) as to those reported in **Table 3.2**. They found that the concentrations of GABA within the grey matter and white matter were up to nine times greater in grey matter compared to white matter (2.87+/-0.61mM versus 0.33+/-0.11mM) (Bhattacharyya *et al.*, 2011), which suggests that the majority of the GABA concentration quantified with MR spectroscopy derives from the grey matter.

From a technical point of view, the spectral editing cannot separate the GABA signal from the macromolecule component, which may be clinically relevant (Cudalbu *et al.*, 2012). A number of approaches have been proposed to separate GABA from co-edited macromolecule signals, including metabolite nulling (Behar *et al.*, 1994), and symmetric editing-based suppression of macromolecules (Henry *et al.*, 2001). Each of these methods have significant detrimental effects on the quality of the data as well as the acquisition time (Mullins *et al.*, 2014), and macromolecule contamination is frequently accepted as a limitation of this most

commonly applied approach (Mullins *et al.*, 2014). It has also been reported in the literature, that occipital cortex GABA concentration is modulated during the menstrual cycle, with reduced GABA during the follicular phase of the cycle (Epperson *et al.*, 2002). I did not correct for menstrual cycle in our analysis, but note that this variable would not be relevant as 14 out of 23 female patients and 4 of 9 female controls were menopausal.

3.8.5 Conclusion

Using ¹H-MR spectroscopy, I provide the first in vivo evidence that GABA neurotransmission in the hippocampus and sensorimotor cortex is reduced in patients with SPMS when compared with healthy controls. Lower GABA levels in the sensorimotor cortex of MS patients are associated with reduced motor performance. These findings raise the possibility that altered GABA neurotransmission may be a marker of neurodegeneration, but it may also suggest that GABA is a mechanism of neurodegeneration in progressive MS patients. If I put these findings together with the evidence that GABA may mediate neuroprotection, targeting GABA may be a productive strategy that should be further explored in multiple sclerosis.

After discussing metabolic imaging in SPMS in this Chapter, the next Chapter looks at a novel quantitative MRI technique, to explore its ability to detect more global microstructural changes in the brain of patients with RRMS.

Chapter IV

Application of NODDI, a novel diffusion MRI technique in RRMS

4.1 Introduction

In order to give us a better understanding of the pathological changes taking place in lesional tissue and normal appearing tissue newer MRI sequences are needed to evaluate the microstructural changes in the brain. A new technique called NODDI (neurite orientation dispersion and density imaging) has been developed to address this. NODDI is designed to overcome the limitations of DTI, achieving higher sensitivity and specificity (Zhang *et al.*, 2012). It provides new opportunities to study diseases, such as MS, which alter neural tissue microstructure.

DTI provides sensitivity to tissue microstructure, but lacks specificity for individual tissue microstructural features. The NODDI model consists of three compartments: intra-neurite, extra-neurite and cerebrospinal fluid (CSF), as described in *Section 2.7.6*. The intra-neurite compartment is modelled as a set of cylinders of zero radius, which reflects the restricted diffusion perpendicular to axons and free diffusion along their length. The extra-neurite compartment is modelled as simple Gaussian anisotropic diffusion as in the DTI model, where diffusion is hindered but not restricted. The extra-neurite compartment refers to the space around neurites (refers to both the axons and dendrites), which is occupied by various types of glial cells, the extracellular matrix and neuronal somas in grey matter. Lastly the CSF compartment is modelled using isotropic diffusion and it is designed to capture CSF contamination and account for other potential sources of free water such as oedema.

The NODDI model provides three summary statistics: Orientation dispersion index (ODI), neurite density index (NDI) and the isotropic volume fraction (isoVF).

ODI quantifies the variability of neurite orientations (Zhang *et al.*, 2011). Values range from 0 to 1, with increasing ODI implying increasing variability of the underlying neurite orientations. For instance, for ODI approaching 0, neurites are all parallel; on the other hand, for ODI approaching 1, neurites are uniformly randomly oriented. Unlike DTI, NODDI estimates orientation dispersion and neurite density, with both contributing to conventional DTI metrics such as FA (Schneider *et al.*, 2016). One study carried out in epilepsy found that the NODDI metrics increased the contrast over DTI for the detection of focal cortical abnormalities (Winston *et al.*, 2014). NDI is used to estimate neurite density and, as axonal loss is a likely pathological substrate for disability in MS (Bonati *et al.*, 2011) and cervical myelopathy (Freund *et al.*, 2011), NDI may be a useful marker of axonal loss in vivo in patients with these disorders.

To date a number of preliminary studies using NODDI in MS have been performed by our group here at UCL. These studies have found increased ODI and reduced NDI in NAWM in RRMS patients when compared to white matter in control subjects (Schneider *et al.*, 2014b; Schneider *et al.*, 2016; Brownlee *et al.*, 2016). The increase in ODI is thought to reflect loss of fibre coherence (i.e. an increase in dispersion) in the NAWM of RRMS patients (Schneider *et al.*, 2014b), while a reduction in NDI is thought to arise due to axonal loss and/or demyelination (Grussu *et al.*, 2015a). In lesions, a reduction of both ODI and NDI and an increase in isoVF have been demonstrated when compared to NAWM in MS subjects (Schneider *et al.*, 2016; Schneider *et al.*, 2014b). The reduction in ODI in lesions, has been preliminary confirmed by histology in the spinal cord (Grussu *et al.*, 2015a; Grussu *et al.*, 2016). Significantly lower NDI in NAWM has been found in SPMS when compared to RRMS (Brownlee *et al.*, 2016), with lower

NDI significantly associated with EDSS, suggesting NDI may reflect reduced density of axons and/or demyelination in NAWM which may contribute to disability in MS (Brownlee *et al.*, 2016). A number of studies carried out by our group at UCL have found similar results in MS patients using the NODDI protocol used in this study and have demonstrated that this is a reproducible method (Schneider *et al.*, 2014b).

It has been demonstrated that in traumatic spinal cord injury patients there is disruption in the axonal architecture and information flow between the spinal cord and brain is interrupted, which results in significant clinical disability (Dietz *et al.*, 2011). As well as spinal cord atrophy, cortical atrophy and cortical reorganisation of the primary motor and sensory cortex have been demonstrated in the brain of spinal cord injury patients (Freund *et al.*, 2011).

One study investigated the relationship between microstructural white matter changes measured with standard DTI using voxel based morphometry, spinal changes and brain activation in spinal cord injury patients (Freund *et al.*, 2012). This study found significant differences (reduced FA) in the corticospinal tract of the spinal cord injury subjects compared to controls, specifically in the pyramids, the internal capsule, the cerebral peduncle and the hand area (Freund *et al.*, 2012). These results suggest that microstructural changes in the brain are specific to the sensorimotor cortex in spinal cord injury (Freund *et al.*, 2012). To date, NODDI has not been applied to cervical myelopathy patients.

In this study I recruited a cohort of patients with RRMS, a cohort of cervical myelopathy patients and a healthy control group, to undergo the same brain NODDI protocol, in order to (i) investigate differences between groups and (ii)

look at the relationship between NODDI parameters and disability in both patient groups, and thus obtain insights into the factors that may contribute to disability. To complete the analysis, standard DTI parameters were also obtained from the same dataset.

My objectives were as follows:

- (i) To determine if ODI, NDI and isoVF (NODDI summary statistics) applied to the brain can help differentiate between MS patients and controls.
- (ii) To determine if ODI, NDI and isoVF (NODDI summary statistics) applied to the brain can help differentiate between cervical myelopathy patients and controls.
- (iii) To correlate these MRI measures with physical disability in these two patient cohorts.

4.2 Materials & Methods

4.2.1 Study

I recruited subjects with RRMS, cervical myelopathy and healthy controls into the study. Inclusion criteria for RRMS patients were: age between 18-65 years; and absence of a relapse or a course of corticosteroids in the three months prior to imaging. Inclusion criteria for cervical myelopathy patients were aged between 18-65 years, previous cervical decompression (with or without an implant) at the level of C3/C4 or C4/C5 in the previous five years, and with or without signal change in the cervical cord. Exclusion criteria for cervical myelopathy patients: presence of a spinal implant at C2/C3.

All the RRMS patients recruited into this study were recruited from the MS clinics ran on a weekly basis at The National Hospital of Neurology and Neurosurgery, Queen Square London. The cervical myelopathy patients were obtained from Mr. David Choi, Consultant Neurosurgeon at The National Hospital of Neurology and Neurosurgery, Queen Square, as these patients were under his care for their cervical myelopathy. All healthy controls recruited as part of this study, were work colleagues, friends and family as well as friends and family of the MS patients.

Written informed consent was obtained for participants in the study, which was approved by our local research ethics committee (Study Reference: 14/LO/0608).

For this study one of my clinical research colleagues, Dr Luke Kipp helped out with getting the consent on the day of the scan and doing the clinical assessments. Overall he performed 20-30% of the assessments and I performed the remainder of the assessments on the subjects recruited into this study. The radiographers at the Institute of Neurology performed the actual MRI scans (Marios Yiannakas, Chichi Ugorji and Luke Hoy). For the NODDI analysis, I used the relatively automated scripts which were developed by Dr Ferran Prados, Dr Torben Schneider and Dr Francesco Grussu, for the processing of the NODDI data. I assimilated the data in a spreadsheet, including all clinical, cognitive and MRI data. Dr. Carmen Tur performed the statistical analysis for this study. I interpreted the results from the statistical analysis performed and the results are presented below.

4.2.2 Cognitive Assessments

All patients (both MS and myelopathic) and controls were assessed using a range of cognitive tests. Speed of information processing was assessed using the SDMT (Lezak *et al.*, 2004), and the 3-second PASAT (Rao *et al.*, 1990), for which z-scores were obtained with reference to published norms (Fischer *et al.*, 1999). Verbal memory was assessed using the CVLT-II for immediate recall (Delis *et al.*, 2000) and visuospatial memory was assessed using the BVMR (Benedict *et al.*, 1997).

4.2.3 Clinical Assessments

All patients (MS and cervical myelopathy) and controls were also assessed using the 9-HPT (Goodkin *et al.*, 1988) and TWT (Cutter *et al.*, 1999). Z-scores were calculated for the 9-HPT and TWT from normative values displayed in the National Multiple Sclerosis Society Task Force database (Fischer *et al.*, 1999). The average of two trials for the TWT and the average of two trials for the 9-HPT were calculated (Fischer *et al.*, 1999). MS patients were also assessed using the EDSS (Kurtzke, 1983). Cervical myelopathy patients were also assessed using the ASIA (American Spinal Injury Association) impairment scale (Maynard *et al.*, 1997).

4.2.4 MRI protocol

Subjects were scanned at 3T using a Philips Achieva MRI system with RF multi-transmit technology (Philips Healthcare, Best, the Netherlands). Brain scans were performed using a 32 – channel coil. A polystyrene filled bag was placed behind the neck of all participants to minimise motion artefacts.

The following scans were performed:

For calculation of brain T2 lesion volumes, PDT2 weighted images were acquired using a dual-echo turbo spin echo (TSE) sequence [parameters; TR = 4900ms; TE = 15/85ms; flip angle $\alpha = 90^\circ$; FOV = 240 x 180mm²; voxel size = 0.5 x 0.5 x 2mm³].

For calculation of brain tissue volumes, a 3D T1-weighted magnetisation – prepared gradient – echo sequence was used [TR = 6.9ms; TE = 3.1ms; flip angle $\alpha = 8^\circ$; FOV = 256 x 256mm²; voxel size = 1 x 1 x 1mm³; NEX = 1; 180 sagittal contiguous slices].

The brain NODDI diffusion-weighted images were acquired using a spin echo-planar imaging sequence. The imaging parameters were; FOV = 192 x 222mm²; TR = 12000ms; TE = 91ms; flip angle $\alpha = 90^\circ$, voxel size = 2.5 x 2.5 x 2.5 mm³, b-values 300/1000/2855s/mm² with 6/30/60 isotropically distributed gradient directions and 10 interleaved non-diffusion weighted (b=0) images.

4.3 Image Post Processing

4.3.1 T2 hyperintense lesions

T2 hyperintense lesions were manually outlined from the T2-weighted images using the semi-automated edge finding tool from (JIM v6.0, Xinapse systems, Aldwinckle, UK). Afterwards the volume of T2-weighted lesions in millilitres was recorded for each subject.

4.3.2 Brain segmentation

The PD-weighted lesion masks were co-registered to the 3D-T1 images using a pseudo-T1 image generated by subtracting the PD from the T2-weighted image (Hickman *et al.*, 2002). Lesion masks were transformed from native space to 3DT1 space using linear interpolation. The 3DT1 images were filled using a non-local patch match lesion filling technique (Prados *et al.* 2014).

For brain extraction, tissue segmentation and parcellation, we used Geodesical Information Flows (GIF) (Cardoso *et al.*, 2015). In brief, GIF is a segmentation technique that uses imaging databases as sources of information. GIF is able to propagate voxel-wise annotations, such as tissue segmentation or parcellation, between morphologically dissimilar images by diffusing and mapping the available examples through intermediate steps. A spatially-variant graph structure connecting morphologically similar subjects is introduced over the database of images, enabling the gradual diffusion of information to all the subjects, even in the presence of large-scale morphological variability. The database of images used for this study has 95 neuroanatomically labelled MRI brain scans following the Neuromorphometrics protocol. GIF is part of NiftySeg (<http://niftyseg.sf.net>) software package and is available as an online tool at <http://cmictig.cs.ucl.ac.uk/niftyweb>.

4.3.4 NODDI processing

Each diffusion-weighted image was corrected for eddy current-induced distortions and subject movements using FSL (FMRIB, Oxford, UK) (Andersson *et al.* 2016). For the NODDI fitting, the Matlab (The MathWorks, Inc., Natick, Massachusetts, USA) NODDI toolbox using the default settings was used to

generate ODI, NDI and isoVF maps (http://nitrc.org/projects/noddi_toolbox) (Zhang *et al.*, 2012). The NODDI maps were then registered to the segmented tissue masks and T2 lesion masks to extract the tissue specific NODDI values. To complete the analysis, standard DTI parameters were obtained from the same dataset using the open-source Camino toolbox (Cook *et al.*, 2006), (<http://camino.cs.ucl.ac.uk/>), using only the $b=0$ and $b=1000$ s/mm² data for each subject. Specifically, we derived the following DTI metrics: fractional anisotropy (FA), radial diffusivity (RD), axial diffusivity (AD) and mean diffusivity (MD).

4.4 Statistical Analysis

Linear regression models were used to look for differences in clinical scores between patient groups and controls, correcting for age, gender and BPF, with the clinical score used as the dependent variable.

Differences in NODDI measures and standard DTI measures in NAWM, cortical grey matter and deep grey matter were examined between RRMS and controls and cervical myelopathy patients and controls using multiple linear regression adjusting for age, gender and the specific tissue fraction (WMF or GMF), with the MRI measure used as the dependent variable and group as the independent variable. The models were also repeated adjusting for T2 lesion load but it was not included in the final model, as it did not contribute to the model.

Paired t-tests were used to look at the differences in NODDI metrics between T2 lesions and normal appearing white matter in the RRMS group.

Associations between NODDI metrics and clinical disability were examined in RRMS patients using multiple linear regressions, correcting for age, gender and

the specific tissue fraction (WMF or GMF), with the clinical disability score used as the dependent variable and the MRI measure as the independent variable. Statistical significance was considered when p values were below 0.05. All analyses were performed using SPSS 21 (IBM).

4.5 Results

4.5.1 Participant demographics and characteristics

Twenty-five patients with a diagnosis of RRMS (mean age = 39.4 years (SD 6.6), 20 females, median EDSS 2.5 (range 1.0 – 6.5)), 15 cervical myelopathy patients (mean age = 48.9 years (SD 7.3), 7 females) and 20 healthy controls (mean age = 36.6 years (SD 12.5), 13 females) were recruited into the study. Overall the MS patients had a mean duration of disease of almost eight years (**Table 4.1**) and a median EDSS of 2.5. Seven of the cervical myelopathy patients had signal change in the cervical cord. Further details on patient demographic characteristics and disability are summarised in **Table 4.1**.

	RRMS	Cervical myelopathy	Controls
N	25	15	20
Mean age (yrs)	39.4 (6.6)	48.9 (7.3)	36.6 (12.5)
Gender (M:F)	5:20	8:7	7:13
Mean disease duration (yrs)	7.96 (5.59)	-	-
Median EDSS (range)	2.5 (1.0 – 6.5)	-	-
Mean ASIA – motor	-	98.60 (2.35)	-
Mean ASIA – pin prick	-	110.93 (1.71)	-
Mean ASIA – light touch	-	109.20 (4.16)	-
Mean T2 lesion volume (mls)	12.67 (13.68)	-	-
WMF	0.30 (0.01)	0.32 (0.01)	0.31 (0.02)
GMF	0.45 (0.01)*	0.44 (0.01)	0.46 (0.01)
BPF	0.75 (0.02)*	0.76 (0.01)	0.77 (0.01)

Table 4.1: Mean (SD) demographics and clinical characteristics of patients and controls. * $p < 0.05$, significant difference between RRMS and controls after performing a linear regression model correcting for age and gender.

4.5.2 Clinical disability

Patients with RRMS had significantly slower processing speed on the SDMT ($p < 0.02$), worse visual ($p < 0.01$), and verbal memory ($p < 0.04$), and were significantly impaired in the TWT ($p < 0.01$) when compared to controls, after correcting for age, gender and BPF. There was no significant impairment in the PASAT ($p < 0.06$) and 9-HPT ($p < 0.07$) (**Table 4.2**).

Patients with cervical myelopathy had worse verbal memory ($p < 0.03$) when compared to controls, after adjusting for age, gender and BPF (**Table 4.3**). They did not differ from controls in the TWT, 9-HPT, PASAT, SDMT and BVMT-R. There was no significant difference demonstrated between the RRMS and cervical myelopathy patients in any of the clinical and cognitive assessments.

Physical disability tests	RRMS	Healthy controls	Adjusted difference*	
			Estimate RC (95% CI)	P-value
Mean 9-HPT (z score)	0.31 (0.39)	0.50 (0.05)	-0.09 (-0.19 to 0.01)	0.07
Mean TWT (z score)	0.17 (0.93)	0.79 (0.54)	-0.34 (-0.58 to -0.09)	0.01
Cognitive Tests	RRMS	Controls	Estimate RC (95% CI)	P-value
Mean SDMT (total score)	54.56 (11.19)	62.13 (10.15)	-3.72 (-6.74 to -0.71)	0.02
Mean PASAT (z score)	-0.42 (1.18)	0.29 (0.80)	-0.33 (-0.67 to 0.02)	0.06
Mean Visual recall – BVMT-R	22.28 (7.50)	28.29 (3.87)	2.91 (0.80 to 5.02)	0.01
Mean Californian Verbal Learning test – CVLT-II (Immediate Recall)	57.80 (11.33)	63.27 (8.19)	-3.36 (-6.59 to -0.14)	0.04

Table 4.2: Mean (SD) clinical and cognitive performance of RRMS patients and controls. * A linear regression model was used adjusting for age, gender and brain parenchymal fraction (BPF). RC – regression coefficient.

Physical disability tests	Cervical myelopathy	Healthy controls	Adjusted difference*	
			Estimate RC (95% CI)	P – Value
Mean 9-HPT (z score)	0.20 (0.56)	0.50 (0.05)	-0.21 (-0.54 to 0.12)	0.21
Mean TWT (z score)	0.41 (0.11)	0.79 (0.54)	-0.21 (-0.53 to 0.10)	0.18
Cognitive Tests	Cervical myelopathy	Controls	Estimate RC (95% CI)	P – Value
Mean SDMT (total score)	52.80 (8.56)	62.13 (10.15)	-4.06 (-10.77 to 2.65)	0.23
Mean PASAT (z score)	-0.19 (1.03)	0.29 (0.80)	-0.25 (-1.00 to 0.50)	0.50
Mean Visual recall – BVMT-R	24.64 (7.70)	28.29 (3.87)	-2.37 (-8.01, 3.27)	0.39
Mean Californian Verbal Learning test – CVLT-II (Immediate Recall)	52.13 (12.64)	63.27 (8.19)	-10.41 (-19.61 to -1.22)	0.03

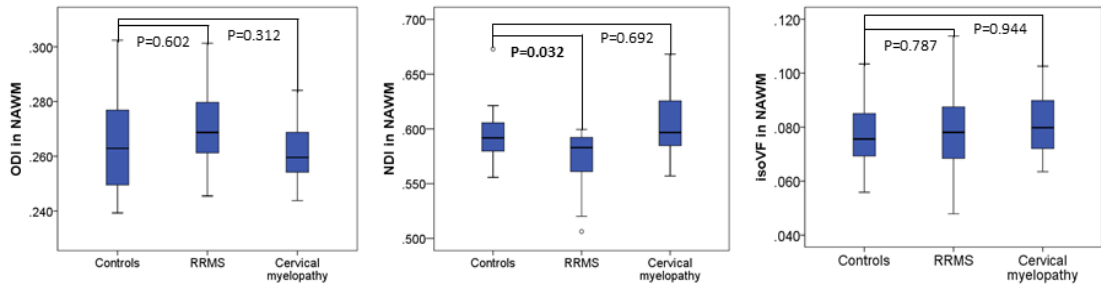
Table 4.3: Mean (SD) clinical and cognitive performance of cervical myelopathy subjects and controls. * A linear regression model was used adjusting for age, gender and BPF.

4.5.3 Difference in MRI metrics between RRMS and controls

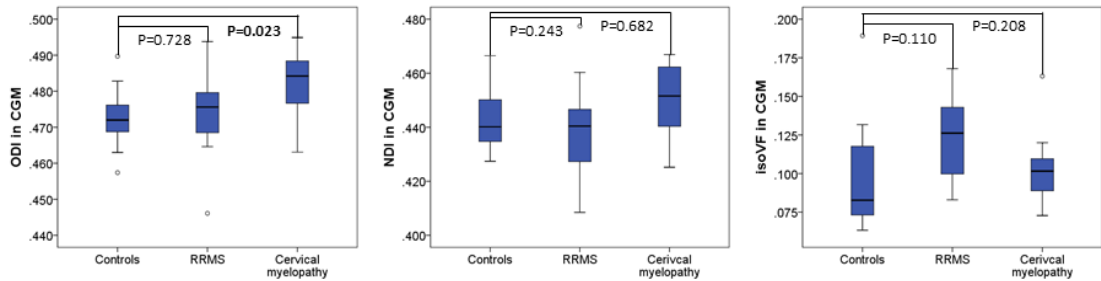
There was a significant decrease in NDI in the NAWM in RRMS patients compared to controls (regression coefficient (RC) -0.02, 95% confidence intervals (CI) -0.04 to -0.002, $p = 0.03$) after correcting for age, gender and WMF (**Figure 4.1 & Table 4.4**). There was no significant difference in any of the other NODDI parameters (**Figure 4.1 & Table 4.4**) or standard DTI parameters in the NAWM, cortical and deep grey matter (**Table 4.4**).

There was a significant decrease in the GMF ($p=0.01$) and brain parenchymal fraction (BPF) ($p=0.02$) in RRMS patients compared to controls after correcting for age and gender (**Table 4.1**).

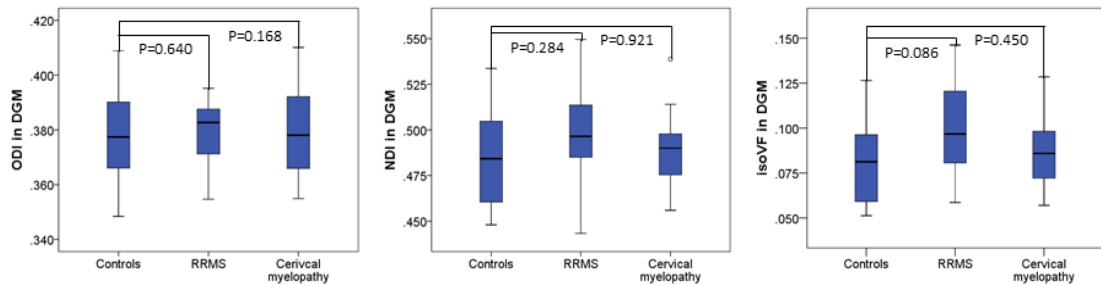
(A) Normal appearing white matter



(B) Cortical grey matter



(C) Deep grey matter



(D) Normal appearing white matter and T2 lesions

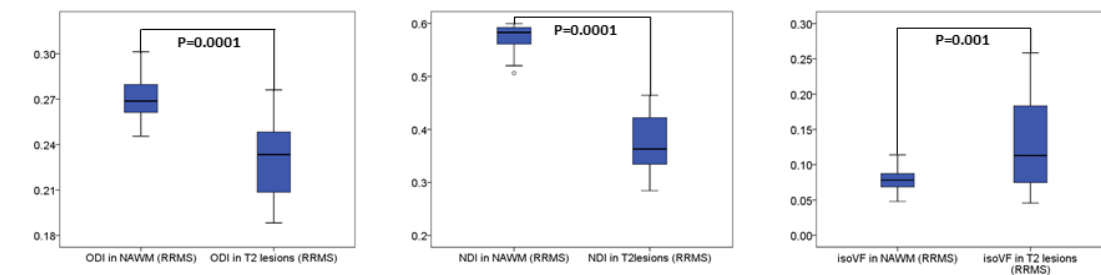


Figure 4.1: Boxplots of the NODDI metrics (ODI, NDI and isoVF) in: (A) normal appearing white matter (NAWM), (B) cortical grey matter (CGM), (C) deep grey matter (DGM) in RRMS and cervical myelopathy patients when compared to healthy controls, and (D) in NAWM compared to T2 lesions in RRMS patients only. P values adjusted for age, gender and WMF or GMF.

MRI Metric	RRMS N = 25	Controls N = 20	P-value	Adjusted difference (95% CI)
Normal appearing white matter				
ODI	0.27 (0.02)	0.27 (0.02)	0.60	0.003 (-0.009 to 0.015)
NDI	0.5733 (0.0264)	0.5949 (0.0280)	0.03*	-0.02 (-0.04 to -0.002)
isoVF	0.08 (0.02)	0.08(0.02)	0.79	0.001 (-0.012 to 0.009)
FA	0.42 (0.02)	0.43 (0.02)	0.12	-0.009 (-0.02 to 0.003)
MD (mm ² /s)	0.00078 (0.00003)	0.00076 (0.00002)	0.11	1.42 x 10 ⁻⁵ (-0.000001 to 0.00003)
AD (mm ² /s)	0.0012 (0.00003)	0.0011 (0.00002)	0.37	9.33 x 10 ⁻⁶ (-0.00001 to 0.00003)
RD (mm ² /s)	0.00059 (0.000030)	0.00057 (0.000029)	0.07	1.66 x 10 ⁻⁵ (-0.0000001 to 0.00004)
Cortical grey matter				
ODI	0.47 (0.01)	0.47 (0.01)	0.73	0.001 (-0.006 to 0.008)
NDI	0.44 (0.02)	0.44 (0.01)	0.24	-0.006 (-0.017 to 0.005)
isoVF	0.12 (0.03)	0.10(0.03)	0.11	0.01 (-0.003 to 0.031)
FA	0.19 (0.01)	0.19 (0.01)	0.34	-0.003 (-0.010 to 0.004)
MD (mm ² /s)	0.00096 (0.000044)	0.00092 (0.00005)	0.06	2.88 x 10 ⁻⁵ (-0.000001 to 0.00006)
AD (mm ² /s)	0.0011 (0.00005)	0.0011 (0.00005)	0.08	2.84 x 10 ⁻⁵ (-0.000001 to 0.00006)
RD (mm ² /s)	0.00086 (0.00004)	0.00084 (0.00005)	0.07	2.90 x 10 ⁻⁵ (-0.000001 to 0.00006)

Deep grey matter				
ODI	0.38 (0.01)	0.38 (0.02)	0.64	0.002 (-0.007 to 0.012)
NDI	0.50 (0.02)	0.48 (0.03)	0.28	0.01 (-0.009 to 0.028)
isoVF	0.10 (0.03)	0.08 (0.02)	0.09	0.013 (-0.002 to 0.028)
FA	0.27 (0.02)	0.26 (0.02)	0.57	0.003 (-0.009 to 0.016)
MD (mm ² /s)	0.00089 (0.000052)	0.00086 (0.00005)	0.22	1.95 x 10 ⁻⁵ (-0.00001 to 0.00005)
AD (mm ² /s)	0.0011 (0.00006)	0.0011 (0.00007)	0.27	2.15 x 10 ⁻⁵ (-0.00002 to 0.00006)
RD (mm ² /s)	0.00077 (0.00005)	0.00074 (0.00004)	0.22	1.85 x 10 ⁻⁵ (-0.00001 to 0.00005)

Table 4.4: Mean (SD) of diffusion MRI measures in RRMS patients and controls. P-values based on linear regression models comparing RRMS to controls, adjusting for age, gender and the specific tissue fraction for the region (either WMF or GMF). * Significant p-value.

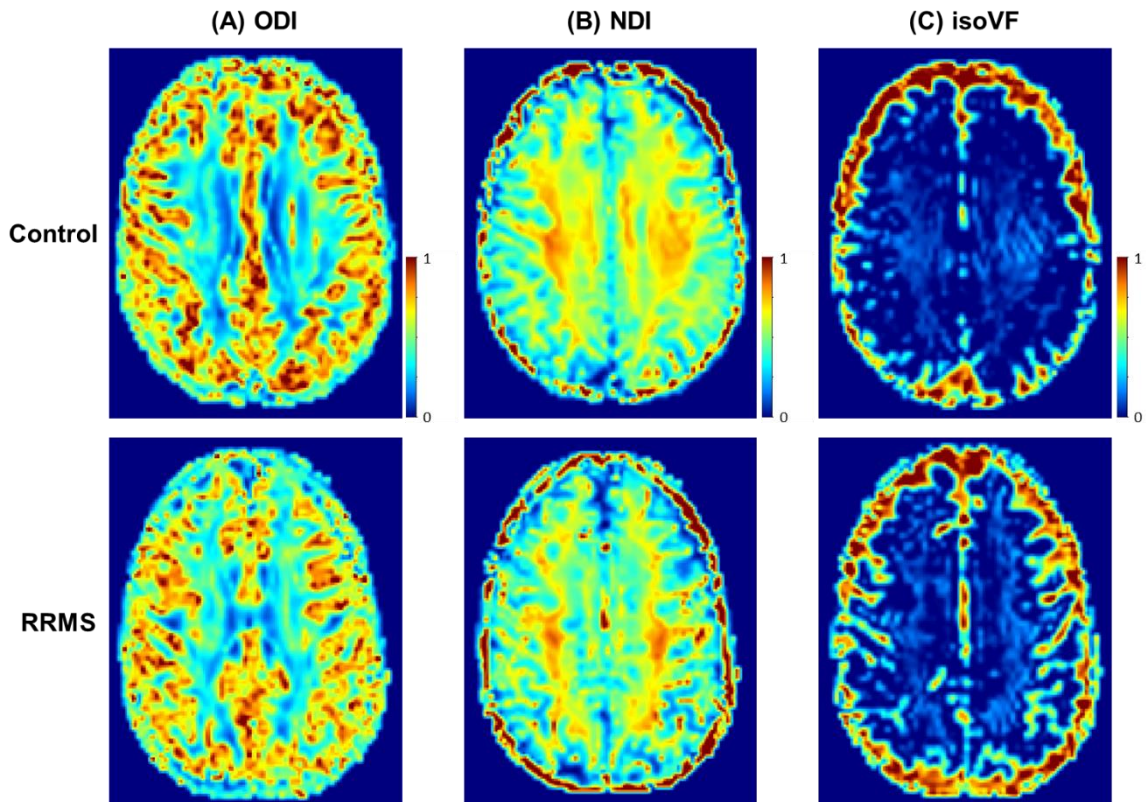


Figure 4.2: Example of NODDI maps from a control (top row) and a patient with RRMS (bottom row) (27-year-old male, with an EDSS of 3.5), (A) orientation dispersion index (ODI), (B) neurite density index (NDI) and (C) isotropic volume fraction (isoVF). Visually there is a reduction in NDI in the normal appearing white matter of the RRMS subject when compared to the control. Absolute values of NDI in the NAWM in the control is 0.5839 and 0.5642 in the RRMS patient.

4.5.4 Difference in MRI metrics between cervical myelopathy subjects and controls

There was a significant increase in ODI in the cortical grey matter in cervical myelopathy patients when compared to controls (RC 0.005, 95% CI 0.001 to 0.008, $p=0.02$) (**Figure 4.1 & Table 4.5**). There was a significant decrease in MD (RC -2.17×10^{-5} , 95% CI -0.00004 to -0.00001 , $p=0.02$), AD (RC -2.56×10^{-5} , 95% CI -0.00004 to -0.00001 , $p=0.009$) and RD (RC -1.97×10^{-5} , 95% CI -0.00004 to -0.00001 , $p=0.02$) in the cortical grey matter of the brain in cervical myelopathy patients compared to controls after correcting for age, gender and GMF (**Table 4.5**).

MRI Metric	Cervical Myelopathy N = 15	Controls N=20	P-value	Adjusted difference (95% CI)
Normal appearing white matter				
ODI	0.26 (0.01)	0.27 (0.02)	0.31	-0.003 (-0.009 to 0.003)
NDI	0.60 (0.03)	0.60 (0.03)	0.69	0.003 (-0.011 to 0.016)
isoVF	0.08 (0.01)	0.08 (0.02)	0.94	0.002 (-0.006 to 0.005)
FA	0.44 (0.02)	0.43 (0.02)	0.24	0.005 (-0.003 to 0.013)
MD (mm^2/s)	0.00075 (0.00002)	0.00076 (0.00002)	0.15	-6.16×10^{-6} (-0.00001 to 0.000001)
AD (mm^2/s)	0.0011 (0.00002)	0.0011 (0.00002)	0.41	-4.02×10^{-6} (-0.00001 to 0.000001)
RD (mm^2/s)	0.0005 (0.00003)	0.00057 (0.00003)	0.15	-7.23×10^{-6} (-0.00002 to 0.000001)

Cortical grey matter				
ODI	0.48 (0.009)	0.47 (0.007)	0.02*	0.005 (0.001 to 0.008)
NDI	0.45 (0.014)	0.44 (0.01)	0.68	0.001 (-0.005 to 0.007)
isoVF	0.10 (0.02)	0.10 (0.03)	0.21	0.007 (-0.004 to 0.018)
FA	0.19 (0.009)	0.19 (0.007)	0.52	-0.001 (-0.005 to 0.003)
MD (mm ² /s)	0.00090 (0.00004)	0.00092 (0.00005)	0.02*	-2.17 x 10 ⁻⁵ (-0.00004 to - 0.00001)
AD (mm ² /s)	0.00106 (0.00004)	0.00108 (0.000052)	0.009*	-2.56 x 10 ⁻⁵ (-0.00004 to - 0.00001)
RD (mm ² /s)	0.00082 (0.00004)	0.00084 (0.000049)	0.02*	-1.97 x 10 ⁻⁵ (-0.00004 to - 0.00001)
Deep grey matter				
ODI	0.38 (0.017)	0.38 (0.017)	0.17	0.005 (-0.002 to 0.012)
NDI	0.49 (0.02)	0.48 (0.03)	0.92	0.001 (-0.010 to 0.011)
isoVF	0.09 (0.02)	0.08 (0.02)	0.45	0.003 (-0.006 to 0.012)
FA	0.26 (0.01)	0.26 (0.019)	0.31	-0.003 (-0.010 to 0.003)
MD (mm ² /s)	0.00084 (0.00005)	0.00086 (0.000052)	0.06	-2.00 x 10 ⁻⁵ (-0.00004 to 0.000001)
AD (mm ² /s)	0.0011 (0.00007)	0.0011 (0.00007)	0.06	-2.77 x 10 ⁻⁵ (-0.00005 to 0.000001)
RD (mm ² /s)	0.00074 (0.00005)	0.00073 (0.00005)	0.09	-1.606 x 10 ⁻⁵ (-0.00003 to 0.000001)

Table 4.5: Mean (SD) of diffusion MRI measures in cervical myelopathy patients and controls. P-values based on linear regression models comparing cervical myelopathy subjects to controls, adjusting for age, gender and the specific tissue fraction for that region (either WMF or GMF). * Significant p-value.

4.5.5 Differences between MRI parameters in T2 lesions and normal appearing white matter in RRMS

There was a significant decrease in NDI ($p=0.0001$, 95% CI -0.22 to -0.17) and ODI ($p=0.0001$, 95% CI -0.06 to -0.03) and a significant increase in isoVF ($p=0.001$, 95% CI 0.02, 0.08) in T2 lesions compared to NAWM in RRMS patients (**Table 4.6, Figure 4.1 & 4.3**).

There was a significant decrease in FA ($p=0.0001$, 95% CI -0.10 to -0.07) and a significant increase in MD ($p=0.0001$, 95% CI 0.0003 to 0.0004), AD ($p=0.0001$, 95% CI 0.0003 to 0.0004) and RD ($p = 0.0001$, 95% CI 0.0003 to 0.0004) in T2 lesions when compared to NAWM in RRMS patients (**Table 4.6**).

MRI metric	T2 lesions	Normal appearing white matter	P-value
ODI	0.23 (0.03)	0.27 (0.02)	0.0001
NDI	0.38 (0.06)	0.57 (0.03)	0.0001
isoVF	0.13 (0.07)	0.08 (0.02)	0.001
FA	0.33 (0.05)	0.42 (0.02)	0.0001
MD (mm ² /s)	0.001 (0.0001)	0.0008 (0.00003)	0.0001
AD (mm ² /s)	0.0015 (0.0001)	0.0011 (0.00003)	0.0001
RD (mm ² /s)	0.00089 (0.0001)	0.00059 (0.00003)	0.0001

Table 4.6: Mean (SD) of NODDI MRI measures in T2 lesions and in NAWM in RRMS patients. P-values based on paired sample t-tests comparing T2 lesions to NAWM in RRMS patients.

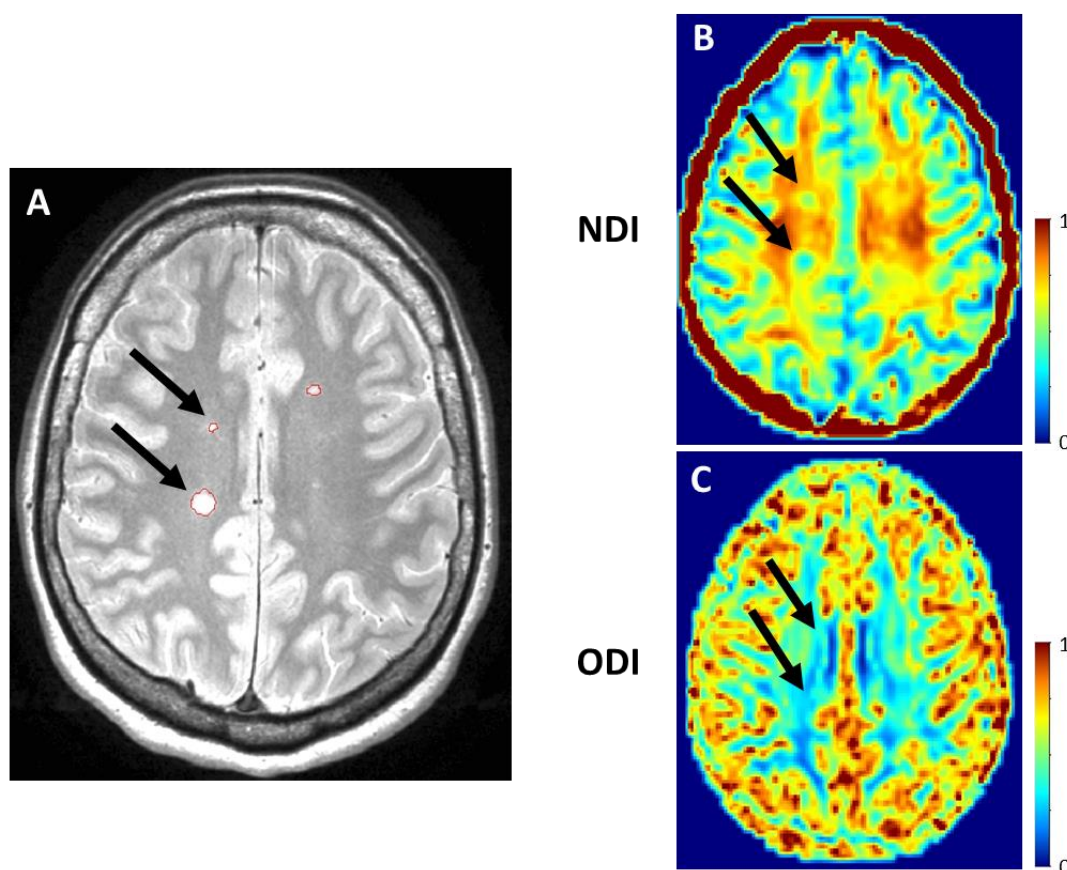


Figure 4.3: Example of NODDI maps from T2 lesions of an MS subject. (A) Axial T2 scan with T2 hyperintense lesions outlined in red, (B) an NDI map of the T2 lesions demonstrating a reduction in NDI and (C) an ODI map of the T2 lesions demonstrating a reduction in ODI.

4.5.6 Associations between MRI metrics and clinical disability scores in patients with RRMS and cervical myelopathy

A) NODDI metrics

There was no significant association between NDI in the NAWM and any clinical scores despite a significant reduction in NDI in RRMS patients when compared to controls.

NDI and isoVF were associated with clinical scores: (i) there was a significant association between NDI in the deep grey matter and scores obtained in the CVLT-II, such that, per unit decrease in NDI, there was a predicted decrease in

verbal memory (CVLT-II) of -169.96 (95% CI -335.04 to -4.85, $p = 0.04$), after correcting for age, gender and GMF in RRMS patients, (ii) isoVF in the cortical grey matter was independently associated with EDSS and TWT after adjusting for age, gender and GMF. In particular, per unit increase in isoVF, was associated with a predicted 44.80 (95% CI 10.51 to 79.10, $p=0.01$) increase in EDSS and a predicted -26.64 (95% CI -45.15 to -8.13, $p=0.008$) decrease in TWT and, (iii) isoVF in the deep grey matter was independently associated with the TWT, such that, per unit increase in isoVF, was associated with a predicted -26.48 (95% CI -48.68 to -4.29, $p=0.02$) decrease in TWT, after correcting for age, gender and GMF.

There was no significant association between the NODDI metrics and clinical disability scores in cervical myelopathy patients.

B) DTI metrics

There was a significant association between the TWT and RD (RC -16,831.79mm², 95% CI -27,775.97 to -5,887.68, $p=0.005$), AD (RC -12,159.29mm², 95% CI -20,137.64 to -4,180.93, $p=0.005$) and MD (RC -15,440.53mm², 95% CI -25,232.51 to -5,648.56, $p=0.004$) in the cortical grey matter and between the TWT and RD (RC -19,858.36mm², 95% CI -33,825.13 to -5,891.58, $p=0.008$), AD (RC -14,394.52mm², 95% CI -26,425.81 to -2,363.23, $p=0.042$) and MD (RC -20,087.56mm², 95% CI -33,753.69 to -6,421.44, $p=0.007$) in the deep grey matter in RRMS patients.

In the cervical myelopathy patients, there was no significant difference in RD, AD and MD in the deep grey matter when compared to controls, but there was a significant association between visual memory assessed using the BVMT-R and

RD (RC $-160,973.95\text{mm}^2$, 95% CI $-298,895.95$ to $-23,051.46$, $p=0.03$), AD (RC $-116,451.31\text{mm}^2$, 95% CI $-213,991.13$ to $-18,911.50$, $p=0.024$) and MD (RC $-148,562.93\text{mm}^2$, 95% CI $-270,199.16$ to $-26,926.70$, $p=0.02$) in the deep grey matter in cervical myelopathy patients, such that an increase in diffusivity in the deep grey matter is associated with a reduction in visual memory scores.

The very high regression coefficients obtained in this analysis arose due to the very small numbers obtained for the diffusivity measures e.g 0.0007 or 0.0008 mm^2/s .

4.6 Discussion

NODDI is a multi-compartment, model-based diffusion weighted MRI technique, which reflects in-vivo neuronal morphology, such as the density and dispersion of neurites. NODDI has the potential to provide specific biomarkers of tissue injury in MS and in clinically feasible settings.

In this pilot study, I aimed to investigate differences in NODDI metrics between RRMS and controls and cervical myelopathy patients and controls and to look at the relationship between NODDI parameters and disability in both patient cohorts, in order to obtain insights into the key factors that may contribute to disability.

Based on this pilot study, there was a significant decrease in NDI (believed to reflect a reduction in the density of axons and/or demyelination) in NAWM in RRMS patients compared to controls. In T2 lesions, there was a significant decrease in NDI and ODI and a significant increase in isoVF compared to NAWM in the RRMS cohort, which is thought to reflect axonal loss and/or demyelination, reduction in neural tissue complexity and increased free water respectively. In

cervical myelopathy patients, there was a significant increase in ODI in cortical grey matter when compared to controls.

Despite no significant change in NDI in the deep grey matter between MS patients and controls, there was a significant correlation between NDI in the deep grey matter and verbal memory in MS patients, raising the possibility that NODDI measures may reflect pathological abnormalities which may be responsible for cognitive impairment. I will discuss each of these results in turn.

4.6.1 Difference in MRI metrics between RRMS and controls

4.6.1.1 Normal appearing white matter

There was a significant reduction in NDI in NAWM in RRMS patients compared to controls. NDI represents the amount of neural tissue occupied by neurites and a reduction in NDI is likely to represent axonal loss in NAWM in MS. This is in keeping with the results presented by Schneider *et al.*, 2014b and Brownlee *et al.*, 2016. Interestingly, a recent histological-MRI study performed by our colleagues (Grussu *et al.*, 2015a), has shown that reduced NDI can also occur in the presence of demyelination, without axonal loss. Demyelination increases the amount of MRI-visible water. As a result, NDI, which is the ratio of the amount of water inside axons to the total MRI visible water, also decreases, even if there is no evidence of axonal loss, due to loss of myelin (Grussu *et al.*, 2015a). Therefore, these findings from the histological study raise the possibility that NDI is unable to distinguish between demyelination of axons and axonal loss.

There was a trend towards increased ODI in the NAWM in RRMS patients compared to controls, but this did not reach statistical significance. An increase

in ODI is thought to arise due to a loss of fibre coherence, with consequent increased dispersion of the orientation of the neurites (Schneider *et al.*, 2014b).

There was no significant difference in any of the standard DTI metrics in the NAWM. Results from previous studies carried out in RRMS have found significant decreases in FA, increases in RD (diffusivity along the principle diffusion direction), AD (diffusivity across the principle diffusion direction) and MD (mean amount of diffusion) in NAWM in MS subjects compared to controls, which is thought to arise due to axonal loss and/or demyelination (Roosendaal *et al.*, 2009). A previous post-mortem study in MS brains found that myelin content and to a lesser extent axonal loss are associated with FA and MD (Schmierer *et al.*, 2007). It has been suggested that standard DTI may be sensitive to microstructural changes in the brain but lacks specificity, which may account for the fact that multiple DTI indices have been implicated in explaining the same pathological process in MS (Pierpaoli and Basser, 1996). These findings suggest NODDI is sensitive to microstructural changes in the NAWM, which was not detected by any of the DTI indices.

4.6.1.2 T2 lesions

In T2 lesions, there was a reduction in ODI and NDI and an increase in isoVF, and these results are in keeping with the results presented by Schneider *et al.*, 2014. A reduction in ODI may arise for a number of reasons: (i) in MS lesions small axonal fibres are more likely to be lost, compared to large fibres, therefore a reduction in ODI may be due to the presence of axons with less undulations and therefore a reduction in overall neural tissue complexity (DeLuca *et al.*, 2006; Muhlert *et al.*, 2013; Grussu *et al.*, 2015a) and (ii) as a result of axonal loss, there is expansion of the extracellular space and gliosis, raising the possibility that

gliosis may alter neurite architecture and therefore cause a reduction in ODI (Klawiter *et al.*, 2011). Results from an ex-vivo study found similar results of reduced ODI in MS spinal cord lesions (Grussu *et al.*, 2015a). An increase in isoVF may arise due to higher CSF contamination as a result of lesional tissue being adjacent to the ventricles with associated tissue loss, increasing the free diffusion compartment represented by isoVF, and also the presence of oedema at the site of lesions may lead to an increase in isoVF.

There was a significant decrease in FA, with significant increases in RD, AD and MD in T2 lesions compared to NAWM in RRMS subjects. Reduction in FA and increased MD in NAWM has previously been demonstrated in RRMS with the highest degree of diffusion abnormalities found in T1-hypointense lesions (Werring *et al.*, 1999; Werring *et al.*, 2000; Filippi *et al.*, 2001). Increases in RD, and AD reflects increased movement of water perpendicular and parallel to the main diffusion direction, as you would expect as a result of axonal loss and/or demyelination (Schmierer *et al.*, 2007).

Work carried out by Grussu *et al.*, (Grussu *et al.*, 2015a) found that a decrease in FA can be related independently by an increase in ODI or by a decrease in NDI. These two contrasting effects have very different biological meaning, which cannot be distinguished by using FA alone and therefore indicates that DTI FA is a somewhat non-specific measure of tissue integrity (Grussu *et al.*, 2015a). Thus NODDI metrics have the potential to disentangle two of the main microstructural changes contributing to FA - the density and the orientation complexity of neuronal processes (Grussu *et al.*, 2015a).

4.6.2 Difference in MRI metrics between cervical myelopathy subjects and controls

There was a significant increase in ODI in cortical grey matter in cervical myelopathy patients when compared to controls but there was no difference in any of the other NODDI metrics in this patient population. To explain this, it may be useful to look at spinal cord injury, which results in the disintegration of axons, which disrupts pathways mediating efferent and afferent information flow between the brain and spinal cord (Freund *et al.*, 2011). It has been demonstrated that following spinal cord injury, there is the development of spinal cord atrophy (Lundell *et al.*, 2011), cortical atrophy (Wrigley *et al.*, 2009) and cortical reorganisation (within the sensorimotor cortex) (Kokotilo *et al.*, 2009). It has been suggested that cortical reorganisation in spinal cord injury may arise from regenerative sprouting of axons in order to reintegrate injured neurons (Henderson *et al.*, 2011). The increase in ODI may reflect a loss of fibre coherence (i.e. more dispersed) due to increased synaptic complexity, which may occur as an adaptive mechanism to preserve function. Overall the size of the myelopathy cohort is small and greater numbers will be required to confirm these findings.

There was a significant decrease in the standard DTI metrics, specifically RD, AD and MD in the cortical grey matter, in cervical myelopathy patients compared to controls. Decreases in RD, AD and MD are thought to reflect a reduction in the movement of water perpendicular and parallel to the principle diffusion direction and a reduction in mean diffusion respectively. It is difficult to say why these changes occurred as overall the sample size for the cervical myelopathy patients is very small. One study carried out in spinal cord injury patients (where the

subjects were more physically impaired than our cohort of myelopathy patients in this study) found an increase in RD in the corticospinal tract which was likely due to axonal loss and/or demyelination (Freund *et al.*, 2012). Our findings in the brain are in the opposite direction to these results (decrease in MD, AD and RD). The decrease in MD, AD and RD may arise due to increased synaptic complexity in the cortical grey matter, in keeping with the ODI results. These mechanisms are presently only speculative and requires further investigation.

4.6.3 Associations between MRI metrics and clinical disability scores in RRMS

There was no significant reduction in NDI in the deep grey matter in MS patients compared to controls, although this may be due to the small sample size; there was a significant association between a reduction in neurite density in the deep grey matter and impaired verbal memory. I know cognitive dysfunction in MS is associated with grey matter pathology. The findings in this study may reflect axonal loss and/or demyelination contributing to cognitive dysfunction, raising the possibility that this NODDI metric may detect pathological changes occurring in the deep grey matter that contributes to cognitive disability. isoVF in the cortical grey matter was associated with EDSS and TWT and in the deep grey matter with TWT in MS patients, which is likely to reflect higher CSF contamination, increasing the free diffusion compartment, which may arise due to atrophy of the cortical and deep grey matter. This is reflected in the significant decrease in GMF in RRMS patients when compared to controls.

RD, AD and MD in the cortical and deep grey matter was significantly associated with the TWT z-scores in MS patients, reflecting an increase in perpendicular,

parallel and mean diffusivity respectively, which may arise due to axonal loss and/or demyelination. A number of DTI studies in cortical and deep grey matter in MS patients have found increased diffusivity in these regions, associated with clinical (Vrenken *et al.*, 2006) and cognitive disability (Rovaris *et al.*, 2002).

4.6.4 Associations between MRI metrics and clinical disability scores in cervical myelopathy patients

Cervical myelopathy patients were significantly impaired on testing of verbal memory when compared to controls. There appears to be quite limited data to explain this but one study carried out in cervical myelopathy patients before and after decompression surgery demonstrated improvements in cognitive function after surgery (Hoshimaru *et al.*, 2010). There is also evidence of cognitive impairment in spinal cord injury patients ranging from reduced attention, executive function, learning ability and processing speed (Davidoff *et al.*, 1992; Roth *et al.*, 1989; Murray *et al.*, 2007). One study in an animal model of spinal cord contusion demonstrated cognitive deficits which they suspected were related to microglial activation (Wu *et al.*, 2014). It is an interesting finding that needs to be further explored. There was no significant association with any of the NODDI indices and physical or cognitive function tests in the cervical myelopathy patients. There were significant associations between RD, AD and MD in the deep grey matter and visual memory in the cervical myelopathy patients, such that an increase in diffusivity in the deep grey matter is associated with impaired visual memory. The DTI metrics may be detecting pathological changes in these regions which may explain some of the previous documented cognitive difficulties in cervical myelopathy patients but this needs further investigation.

4.7 Conclusion

Based on this pilot study, there was a significant reduction in NDI and ODI in T2 lesions and in NDI in NAWM in RRMS. In cervical myelopathy patients there was a significant increase in ODI in cortical grey matter. It is likely that NODDI can provide additional information on neural tissue microstructure and tissue complexity which standard DTI cannot disentangle and it may be a useful imaging technique to complement other imaging modalities.

4.8 Limitations

Overall, the numbers recruited into this study is small, and this might explain the lack of significant results in more of the NODDI metrics in the RRMS cohort. The recruitment for this study is ongoing, to increase the number of RRMS and cervical myelopathy patients recruited into the study. NODDI in the spinal cord is also being acquired as part of this study. This may provide more information in relation to intrinsic changes occurring in the cervical cord in both MS and cervical myelopathy patients and how this influences the NODDI metrics.

In the MS patients only, I performed the EDSS, which is a well known clinical assessment carried out in MS. While in the cervical myelopathy patients I carried out the ASIA scale only and not the EDSS. The ASIA was designed for spinal cord injury patients to capture specifically the degree of sensory and motor impairment in the upper and lower limbs in these patients. In hindsight, I probably should have performed the EDSS in the cervical myelopathy patients as well, to compare the degree of disability between the two patient groups. The remainder of the clinical and cognitive assessments were the same in both groups.

In **Figure 4.1 (A)**, there was an outlier in ODI in normal appearing white matter in the RRMS group and in **Figure 4.1 (B)** there was an outlier in ODI in cortical grey matter in the control group and the RRMS group. When the statistical analysis was initially performed, it was re-ran again excluding these outliers and it did not change the pattern of results. Therefore, it was felt that these outliers were not contributing significantly to the overall results and so I did not exclude them in the final model.

In **Table 4.2**, two of the clinical and cognitive assessments, specifically the 9-HPT ($p=0.07$) and PASAT ($p=0.06$), were very close to reaching statistical significance in RRMS patients compared to controls. It is very likely that these tests would have reached significance if a few more subjects were recruited into the study.

Another limitation of this study is the fact that the DTI metrics were obtained from recycled NODDI data. In one sense this is good as it reduces the scan time for the patients, however, the DTI metrics were acquired with a TE which is longer, than the TE you would use if acquiring only DTI. The same echo time was used for each b-shell in order to achieve the same T2-weighting for the three tissue compartments (Grussu *et al.*, 2015b). The signal decreases as you increase the TE, therefore the signal to noise ratio may be sub-optimal for the DTI data (Grussu *et al.*, 2015b).

Longitudinal changes in NODDI metrics have not yet been investigated in MS to date. The next Chapter will explore the longitudinal changes in a number of advanced spinal cord imaging techniques, in order to establish whether changes are seen over time in these MRI metrics and if they can predict disability progression in a cohort of patients with early PPMS.

Chapter V

Longitudinal changes in advanced imaging measures in the cervical cord in PPMS

5.1 Introduction

PPMS is characterised by sustained disability progression from disease onset and, as mentioned earlier, the rate of deterioration, both clinically and radiologically is variable (Khaleedi *et al.*, 2008; Ingle *et al.*, 2003; Confavreux *et al.*, 2003). To date, MRI is not well established as a prognostic marker in PPMS. Biomarkers, which are linked to the pathological processes underlying progression, are key to the successful development of treatments in progressive MS (Thompson, 2015).

High b-value Q-space imaging (QSI) is one such advanced quantitative MRI (qMRI) technique. It is a model free diffusion weighted imaging (DWI) technique (Callaghan *et al.*, 1998), which is thought to be specific for axonal injury (Assaf *et al.*, 2005), with better sensitivity for detecting pathological changes in lesions and NAWM, compared to standard diffusion tensor imaging (DTI) (Assaf *et al.*, 2002). QSI has been discussed in more detail in *Section 2.7.5*.

One study demonstrated the feasibility of using high b-value Q-space imaging in four patients with MS in the spinal cord, as well as improved detection of abnormal diffusion compared to apparent diffusion coefficient (ADC) measurements (Farrell *et al.*, 2008). A study in healthy controls demonstrated good reproducibility in perpendicular and parallel diffusivity in the ascending and descending tracts in the cervical cord (Schneider *et al.*, 2011).

¹H-MRS quantifies metabolites, which can reflect quite specific microstructural processes occurring in the spinal cord and can complement standard structural MRI (Ciccarelli *et al.*, 2014), discussed in *Section 2.6.5* and *Section 2.9.1*. Metabolites frequently quantified in the spinal cord include: tNAA - a marker of

neuronal structure and neuronal metabolism (Moffett *et al.*, 2007), Ins - a marker of astrocytic activation and proliferation (Brand *et al.*, 1993), tCr – a marker of gliosis, and tCho - a marker of membrane phospholipids, which are released during myelin breakdown (Henning *et al.*, 2008). More recently, the glutamate-glutamine (Glx) complex, a marker of neuronal integrity and the excitatory neurotransmitter has been successfully quantified in the spinal cord (Solanky *et al.*, 2013a) (Abdel-Aziz *et al.*, 2015).

In our recent study in early PPMS (Abdel-Aziz *et al.*, 2015), we demonstrated significant changes in spinal cord spectroscopy (¹H-MRS) (significantly reduced tNAA and Glx) and Q-space metrics (significantly increased perpendicular diffusivity in all spinal cord columns) between patients and controls, and interpreted these abnormalities as indicating neurodegeneration. This raises the possibility that these imaging metrics may be reliable imaging biomarkers of spinal neurodegeneration, and may have a role in predicting clinical outcome and treatment responses in PPMS.

The aim of the study was to investigate if (i) changes in advanced MRI techniques occur over 1 year in the baseline cohort reported by Abdel-Aziz *et al.*, 2015, (ii) if changes in these MRI metrics correlate with clinical changes over 1 year and (iii) if baseline MRI metrics predict clinical status at 1 year.

In addition to using these advanced pathologically specific MRI techniques, I selected clinical function tests, which are more sensitive at detecting clinical changes mediated by spinal pathways than conventional clinical tests used in MS studies.

5.2 Materials and Methods

5.2.1 Study participants

Twenty-one patients with an established diagnosis of PPMS (Polman *et al.*, 2005) (13F, median EDSS 5 (range 3-6.5)) and 24 healthy controls (21F) were recruited into the initial study at baseline (Abdel-Aziz *et al.*, 2015) and invited to come back after 1 year. Two patients were not scanned at one year due to the insertion of devices which would have been affected by the MRI scan – in one the insertion of an intrathecal baclofen pump and in the other a cardiac device. Six healthy control subjects did not undergo the one-year follow-up study - four subjects had moved away and two subjects were not contactable. Patients were clinically assessed on the day of the MRI at baseline and at 1 year.

All the PPMS patients recruited into this study were recruited from the MS clinics ran on a weekly basis at The National Hospital of Neurology and Neurosurgery, Queen Square, London. All healthy controls recruited into this study were work colleagues, friends and family as well as friends and family of the MS patients.

All subjects recruited into the study provided written informed consent prior to taking part in the study, which was approved by the local research ethics committee (Study Reference: 10/H0713/74).

Dr. Abdel-Aziz carried out all the baseline study in the PPMS cohort as reported in Abdel-Aziz *et al.*, 2015. I then completed the 1 year follow-up study for this cohort of patients. Dr Abdel-Aziz obtained the consent at baseline. I then contacted (by phone and e-mail) the patients and healthy controls at 1 year and arranged for them to comeback for the 1 year follow-up. I carried out all the clinical

testing on the day of the scan. The radiographers at the Institute of Neurology performed the MRI scans at the two time points (Marios Yiannakas, Chichi Ugorji and Luke Hoy). I carried out the post-processing for the spectroscopy data using the LCModel and reviewed the results of each patient individually. I also performed the Q-space analysis, spinal cord and brain atrophy measurements. If there were any issues with the data, I discussed and reviewed the results with Dr Bhavana Solanky and Dr Torben Schneider, the Physicists who optimised the protocol. I assimilated the data in a spreadsheet, including all clinical, cognitive and MRI data. Dr. Dan Altmann and Dr. Carmen Tur performed the statistical analysis for this study. I interpreted the results from the statistical analysis performed and the results are presented below.

5.2.2 Clinical Assessments

All patients were assessed using standard clinical assessments commonly performed in MS studies including the EDSS (Kurtzke et al., 1983), 9-HPT (Goodkin et al., 1988), TWT (Cutter et al., 1999), ASIA impairment scale (Maynard *et al.*, 1997), Multiple Sclerosis Walking Scale – 12 (MSWS – 12) (Hobart et al., 2003) and Modified Ashworth Scale (MAS) (Bohannon and Smith, 1987). For the statistical analysis, the average of two trials of the TWT and the average of four trials of the 9-HPT (averaged as reciprocals of the mean times from two trials for each hand) (Fischer *et al.*, 1999) were calculated. The MAS values from 16 muscle groups in the upper and lower limbs were converted from a 0-4 scale (which includes a value of 1+ between scores of 1 and 2), to a 0-5 scale, with the resulting values summated to obtain an overall score ranging from 0-80 (Stein *et al.*, 2007).

I also used a number of clinical measures which are more sensitive at detecting correlations between MRI abnormalities in the spinal cord and clinical disability (Oh et al., 2013; Zackowski et al., 2009), specifically grip strength from both upper limbs was measured using the dynamometer (mean grip strength from both limbs was used in the analysis) (Sammons Preston. Incorporated, Bolingbrook, IL, USA) (Svens and Lee, 2005), Vibration perception thresholds (VPTs) were measured from all 4 limbs at the lateral malleoli and ulnar styloid processes, using the biosthesiometer (mean VPTs were calculated and then used in the analysis) (Bio – medical Instrument Company, Newbury, Ohio) and postural stability was assessed using a modified version of a recently developed protocol for quantifying stance stability (Bunn *et al.*, 2013). Individuals were requested to stand relaxed and still, facing a blank wall at a distance of 1m, for 40s long trials. Three trials each of four conditions were recorded, consisting of two stance widths (inter – malleolar distance of 32cm and 4cm) and two visual conditions (eyes open (EO) and eyes closed (EC)). Body sway was measured using a 3-D orientation sensor (MTx: Xsens, Enschede, NL), which was fixed to the skin, just below the C7 spinous process. The device measured the instantaneous angular position of the trunk in the anteroposterior (pitch) and mediolateral (roll) planes. Summary measures were made in these signals using custom scripts written in Matlab (The Mathworks, Natick, MA USA). The amount of angular motion was then calculated separately from the roll and pitch body sway data and from the combined motion given by square root ($\text{pitch-motion}^2 + \text{roll-motion}^2$), termed total sway. All three signals were summarized by summing the sample – to – sample absolute change in signal and then dividing by the duration of the trial to yield average angular speeds of body sway reported in degrees/second. The mean of

the three trials per condition were used for statistical analysis. An index of exacerbation of sway on eye closure was obtained from the Romberg quotient calculated as sway eyes closed/sway eyes open at both stance widths.

5.2.3 MRI Protocol

The MRI protocol at 1-year follow-up was exactly the same as that used for the baseline study (Abdel-Aziz *et al.*, 2015). All scans were performed using a 3T Achieva system (Philips Medical Systems, Best, Netherlands). To reduce motion artefacts during scanning and improve image quality, an MR compatible cervical collar was worn by all subjects (Yiannakas *et al.*, 2012). The scans performed included single voxel ¹H-MRS and Q-space imaging of the cervical cord, PD/T2 of the brain and cervical cord, volumetric 3D-T1 of the brain and 3D fast-field echo for cervical cord area measurement.

5.2.3.1 MRS protocol

Using the manufacturer's 16 – channel neurovascular coil (Philips Healthcare Systems), single voxel MRS was performed using a recently optimised protocol (Solanky *et al.*, 2013a). Conventional turbo spin – echo sequences (TSE) were used to acquire structural images for radiological reading and to guide voxel placement. T2w images were acquired in the coronal plane [parameters: TR = 4000ms; TE = 100ms; FOV = 160 x 250 mm²; voxel size = 0.6 x 0.6 x 3.0 mm³; NEX = 2; 13 contiguous slices] and PD/T2w images were acquired in the sagittal plane using a dual echo TSE [parameters: TR = 4000ms; TE = 15/80ms; FOV = 256 x 160mm²; echo train length (ETL) = 12; voxel size = 1.0 x 1.0 x 3.0 mm³; NEX = 2; 12 contiguous slices].

For spectroscopy, volumes of interest (VOI) with dimensions of approximately 5.4 x 7.76 x 55mm³ (2.3mls) were prescribed using the reference images. The dimensions of the VOI were adjusted in the anterior-posterior (AP) direction dependent on the size of each volunteer's spinal cord (Ciccarelli et al., 2007; Marliani et al., 2010). Care was taken in positioning of the voxel at baseline and then at 1 year follow-up. The same voxel sizes were used at both time points for each subject and the voxel was centred on C2/C3 at each time. MRS data was acquired using a point resolved spectroscopy (PRESS) localisation sequence, previously published (Solanky *et al.*, 2013a) [parameters: TE = 30ms; 376 averages with triggered first order iterative shimming, multiple obtained insensitive suppression train (MOIST) water suppression, 4 outer volume suppression (OVS) slabs in the AP and rostrocaudal directions and cardiac gating (TR = 3RR ~ 3000ms) using a peripheral pulse unit (350ms delay)]. An example of a spectroscopy voxel placement is shown in **Figure 5.1**.

5.2.3.2 Spinal cord atrophy protocol

The cervical cord was imaged in the axial plane, perpendicular to the longitudinal axis of the cord, to measure the cord mean cross – sectional area (CSA) and for confirmation of lesion location. The imaging volume was centred on the C2/3 intervertebral disc, using a fat – suppressed 3D slab-selective fast field echo (FFE) sequence [parameters; TR = 23ms; TE = 5ms; flip angle $\alpha = 7^\circ$; FOV = 240 x 180mm²; voxel size = 0.5 x 0.5 x 5 mm³; NEX = 8; 11 axial contiguous slices]. In order to match the position and orientation of the volumetric scan to the spectroscopy voxel, the prescription values used for the MRS acquisition were copied and manually entered by the operator when setting up the 3D-FFE scan.

5.2.3.3 QSI protocol

Using the manufacturer's 32 – channel head coil (Philips Medical Systems, Best, Netherlands), each subject underwent a cardiac gated DWI acquisition [parameters; voxel size = $1 \times 1 \times 5 \text{ mm}^3$ (interpolated in k-space to a $0.5 \times 0.5 \text{ mm}^2$ in-plane resolution), FOV = $64 \times 64 \text{ mm}^2$; TR = 9RR, TE = 129ms], performed with the volume centred on the C2/C3 disc to ensure similar coverage as the spectroscopy voxel. 12 axial contiguous slices covering a 60mm length of the cervical cord, typically giving coverage of the C1-C3 spinal segments. The 32 channel head coil was used because it gave superior SNR during QSI sequence optimisation experiments (Schneider *et al.*, 2011). A ZOOM (zonal oblique multi-slice) sequence in combination with outer-volume suppression was used to minimise artefacts (Wilm *et al.*, 2007). Thirty DWI volumes with equally spaced Q-values (Farrell *et al.*, 2008) and two non-diffusion weighted (b_0) volumes were acquired with diffusion weighting in two perpendicular (x and y) and one parallel (z) direction to the main axis of the spinal cord [parameters: diffusion pulse duration $\delta = 11.4 \text{ ms}$, diffusion time $\Delta = 75 \text{ ms}$, gradient strength G linearly increased in 31 steps from 0 to 87.5 mT/m in x and y direction and 62 mT/m in z direction]. An example of the diffusion weighted image volume is shown in **Figure 5.1**.

5.2.3.4 Brain MRI protocol

For calculation of brain T2 lesion volumes, PD2 weighted images were acquired using a dual-echo TSE sequence [parameters; TR = 3500ms; TE = 15/85ms; flip angle $\alpha = 90^\circ$; FOV = $240 \times 180 \text{ mm}^2$; voxel size = $1 \times 1 \times 3 \text{ mm}^3$; NEX = 1; 50 axial contiguous slices]. For calculation of brain tissue volumes, a 3D T1-weighted magnetisation – prepared gradient – echo sequence was used [TR = 6.9ms; TE

= 3.1ms; flip angle $\alpha = 8^\circ$; FOV = 256 x 256mm²; voxel size = 1 x 1 x 1mm³; NEX = 1; 180 sagittal contiguous slices].

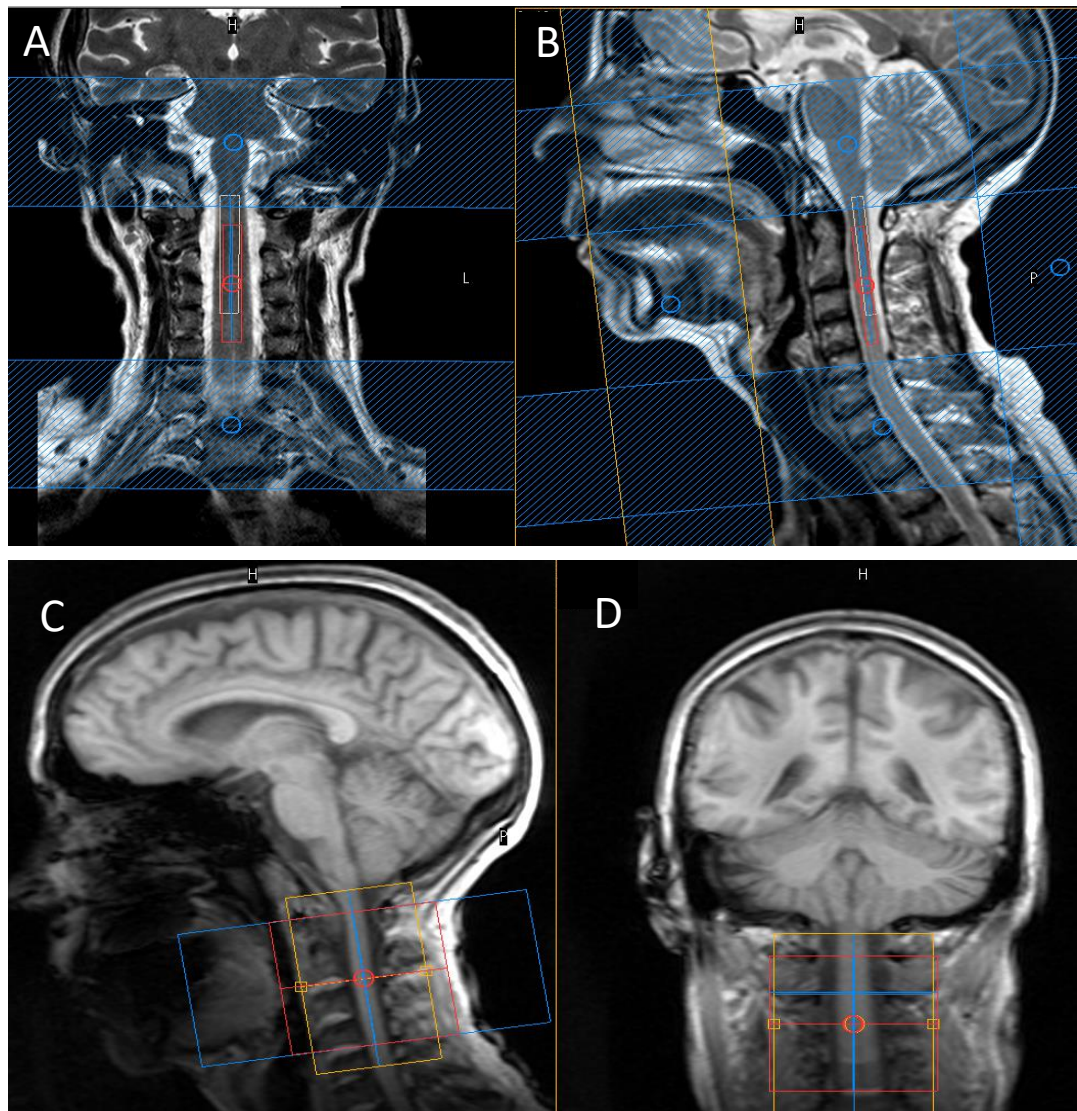


Figure 5.1: Example of the spectroscopy voxel placement in the coronal (A) and sagittal planes (B) and the diffusion weighted image volume in the sagittal (C) and coronal plane (D) in the cervical cord.

5.3 Image Post Processing

5.3.1 Spinal cord metabolite quantification

Metabolite concentrations were quantified using the user-independent LCModel (version 6.3) package (Provencher, 1993) and a set of basis spectra, comprising seventeen metabolites including macromolecules, as previously described (Solanky *et al.*, 2013a). tNAA, tCho, tCr, Ins and Glx concentrations were quantified using the unsuppressed water signal obtained from the same voxel as a reference (Gasparovic *et al.*, 2006) and formed the focus of our analysis. Corrections for T2 values were not performed because the TE used is relatively short, compared to the T2 relaxation times of the metabolites under study (Wansapura *et al.*, 1999; Edden *et al.*, 2007) and therefore, it is expected that changes in T2 would be negligible. Measuring T2 values for each metabolite would not have been possible in a patient cohort within clinically feasible scan times.

5.3.2 Spectral Quality

Overall spectral quality was assessed using the full width at half maximum (FWHM) and signal – to – noise ratio (SNR) provided by LCModel. CRLB values were used to confirm the reliability of each metabolite. CRLB values of <20% for tNAA, tCr, tCho and Ins and <30% for Glx were used to confirm the reliability of the spectral fit (Provencher *et al.*, 2014). Poor quality spectra were excluded from the analysis with poor water suppression or FWHM > 0.13 and SNR < 3. The FWHM and SNR estimated by the LCModel (mean +/-SD) were 0.110+/-0.027

ppm and 3.874 ± 0.859 respectively for the 1-year data. The mean CRLBs values for each metabolite were: tNAA (12.76%), tCr (13.46%), Ins (11.12%), Glx (13.70%) and Cho (13.46%).

5.3.3 Spinal cord cross sectional area measurement

Image segmentation and CSA measurements were performed using the 3D-FFE dataset in Jim 6.0 Software (Xinapse systems, Northants, England). Three contiguous 5mm axial slices, centred on the C2/3 disc were segmented using the active surface model (Horsfield *et al.*, 2010). The mean cross – sectional area of the three slices was then calculated.

5.3.4 Spinal cord QSI and ROI analysis

The QSI indices represent the diffusion properties of water and can be derived from the displacement probability density function (dPDF). This is the average probability of a spin moving a certain distance during a given diffusion time. A tall, narrow dPDF is associated with a low apparent diffusion coefficient, suggesting more hinderance or restriction of diffusing water molecules. A broad, low dPDF suggests a high apparent diffusion coefficient with more free diffusion of water molecules and/or a more unrestricted diffusion (Farrell *et al.*, 2008; Cohen & Assaf, 2002; Schneider *et al.*, 2014a).

Assuming axial symmetry of diffusion along the main axis of the spinal cord, the two perpendicular (x,y) diffusion directions were averaged before analysis to increase the signal – to – noise ratio. The measurements were then extrapolated in to 128 data points in q-space to avoid cut-off artifacts (Cohen & Assaf, 2002)

and the voxel-wise dPDF was computed using inverse Fast Fourier Transformation.

Data was corrected for motion using “reg_aladin” from the NiftyReg toolbox (Ourselin et al., 2000). Registration was performed between the interleaved b=0 acquisitions of the xy and z protocol using the first b=0 of the xy protocol as reference. The estimated registration was then applied to the intermediate DWI images. The quality of the motion correction was assessed in each subject and mis-registered slices/subjects were excluded from the study.

Voxel maps of the FWHM and the zero displacement probability (P0) were calculated from the dPDF. The FWHM represents the width of the displacement distribution function and the P0 represents the height of the displacement distribution function. We also acquired conventional apparent diffusion coefficient (ADC) maps, from the low b – value part of the decay curve ($b < 1100\text{s/mm}^2$), for both the xy and z directions, using a constrained non – linear least squared fitting algorithm.

To look at region specific differences in QSI metrics, the full length (60mm) of the cervical spinal cord was initially extracted, excluding the CSF and other tissue types. Four regions of interest were created using the ROI tool in JIM 6.0 and drawn on the average b0 image on each axial slice. From this the ADC and QSI indices were measured from the anterior, posterior, right lateral and left lateral columns of the spinal cord, as well as over the whole cord. There were no statistical differences between q-space indices between the right and left lateral columns, so the mean values from both columns were calculated for each of the q-space indices.

5.3.5 Brain T2 Lesion Volumes and grey matter and white matter volumes

Brain T2 lesion volume (T2LV) was calculated by outlining lesions on T2 – weighted MRI scans using a semi – automated edge finding tool (JIM v. 6.0) by a single observer (NC). Total lesion volume was recorded in mls for each subject.

Hypointense lesions on the T1-weighted volume scan were marked and filled with values consistent with NAWM signal intensity to prevent misclassification of tissue during segmentation (Chard *et al.*, 2010). Segmentation of the lesion-filled image was then performed using the 'new_segment' function in SPM8 (statistical parametric mapping; Wellcome Trust Centre for Neuroimaging, University College London (UCL) Institute of Neurology, London). This reduces the impact of lesion-associated segmentation bias on GM and WM segmentation (Chard *et al.*, 2010). WM and GM fractional (WMF and GMF) volumes, relative to total intracranial volume, were calculated. The sum of white and grey matter relative to total intracranial volume (BPF) was also recorded for each subject.

5.3.6 Brain atrophy

To avoid segmentation errors due to white matter lesions, an automated lesion-filling technique was employed (Chard *et al.*, 2010). Lesions masks were created based on the 3D-T1 weighted sequences without reference to previously created masks on T2-weighted images.

Probabilistic whole brain segmentations were obtained using STEPS1, a multi-atlas segmentation propagation technique, which uses an atlas library of 682 non-MS patients with associated manual segmentations, of which the 30 most similar

brain templates were used during a locally-weighted label fusion process (Cardoso *et al.*, 2013).

Using these brain masks, Structural Image Evaluation using Normalization of Atrophy (SIENA) were calculated. SIENA is a registration based method which computes atrophy between two aligned scans as the perpendicular edge displacement at each edge point. The mean edge displacement is converted into a global estimate of Percent Brain Volume Change (PBVC) between two time-points, using self-calibration based on registering both time points to the half-way space between them (Smith *et al.*, 2002).

5.4 Statistical Analysis

Analyses were performed in Stata 13.1 (Stata Corporation, College Station, Texas, USA).

Multiple linear regression models were used to (i) estimate differences between patients and controls in terms of change in MRI metrics over time, (ii) estimate association between MRI and clinical changes over the same period of time, in patients only, and (iii) predict clinical outcomes at one-year follow-up based on the MRI metrics at baseline. All models were adjusted for age and gender. Where regression residuals showed deviation from normality, we obtained confidence intervals and p-values using a bias-corrected non-parametric bootstrap with 1000 replicates.

Additionally, to estimate the association between changes in certain highly correlated clinical measures such as postural stability measures and changes in MRI data, we used multivariate multiple linear regression models, which allowed

us to predict several clinical dependent variables at the same time. To build our multivariate multiple linear regression models we used the Stata command 'Structural Equation Modelling'.

Among the advantages of the multivariate regression there were: i) for each MRI predictor (changes over one year), we performed a single joint test, which reflected its ability to jointly predict changes in a set of postural stability measures, with which the MRI predictor showed associations all in the same direction. This reduced the risk of type I error derived from multiple testing; ii) under the assumptions of missing-at-random and multivariate normality, all available data points contributed to the model. This reduced the potential bias from exclusion of patients without complete data on all variables, thus reducing the risk of type II error. These models allowed us to reduce the risk of type I and type II errors. Similar models were built to predict postural stability outcomes at one year of follow-up with MRI variables. All multivariate models were also adjusted for age and gender. Statistical significance was set at 5%.

To build the multivariate models used to predict changes in postural stability measures with changes in MRI metrics over one year, we followed these steps:

- 1) A non-parametric correlation analysis between each clinical variable (changes over one year in a given postural stability measure) and each MRI measure was performed and the sign of the Spearman's correlation coefficient was recorded
- 2) A parametric correlation analysis was performed and only those correlations where the sign of the Spearman's and the Pearson's correlation coefficients were

equal were kept for further analyses (those correlations with different signs were discarded).

3) Postural stability measures were divided into 4 sets, depending on the distance between feet (32 cm or 4 cm) and whether they were obtained with eyes open or closed.

4) For each set of postural stability variables, the signs of the correlation coefficients describing the association between a given MRI metric and the individual clinical measures within the set were examined. In order to comply with the requirements of multivariate linear regression, where all dependent variables were assumed to behave in a similar biological manner, only those sets with all signs equal were kept for further analyses.

5) For each set of postural stability variables selected in step 4), a multivariate analysis was carried out: the clinical variables (change over one year) were jointly considered as dependent variables and a joint test for each set of postural stability variables was performed. Whenever the joint test was significant (at 5% significance level) we considered there was evidence that the changes in a given MRI metric were associated with overall changes in postural stability measures.

Sample size calculations were performed to detect different plausible treatment effects (with 80% power at 5% statistical significance) based on the observed differences between patients and controls.

5.5 Results

5.5.1 Participant demographics and characteristics

Nineteen patients with PPMS and 18 healthy controls were followed-up at one year (**Table 5.1**). Patients had a relatively short disease duration (mean disease duration= 4.65 years, range = 1 – 6.5), and a moderate level of disability (median EDSS 6.0). The PPMS cohort was significantly older than the healthy controls ($p<0.026$). Further details on patient characteristics, disability and conventional brain MRI are summarised in **Table 5.1 and Table 5.2**. Changes in conventional spinal cord and brain MRI measures between baseline and at 1 year in patients are also summarised in **Table 5.1**.

Patients worsened in a number of clinical measures over the follow-up period, specifically: EDSS ($p<0.0001$); TWT ($p<0.01$); 9-HPT ($p<0.008$); ASIA-motor scores ($p<0.003$); and MSWS ($p<0.0001$) (**Table 5.2**).

	Patients	Controls	P – value
N	19	18	
Mean age at baseline	50.8 (8.8)	42.4 (12.6)	0.03
Gender (M:F)	9:10	5:13	
Mean Disease Duration at baseline (years)	4.65 (1.64)	-	
Mean CSA (mm ²) at baseline	77.42 (9.84)*	81.40(9.10)	0.21
Mean CSA (mm ²) at 1 year	74.56 (9.11)*	81.14 (8.62)	0.03
Change in CSA over 12 months (mm ²)	2.86*	0.26	0.0001
PBVC	-1.59 (1.13)*	-0.33 (1.07)	0.02

Table 5.1: Mean (SD) demographics of patients and controls. * Linear regression model comparing patients with controls, correcting for age and gender. CSA – cross sectional cord area.

	Baseline	1 Year
Mean T2 lesion volume	10.73 (9.14)	11.35 (10.14)
EDSS (median) (range)	5.0 (3.0 – 6.5)	6.0 (4.5 – 7.5)*
Mean TWT (z-score)	0.28 (0.20)	0.18 (0.33)*
Mean 9-HPT (z-score)	-0.67 (1.04)	-0.99 (1.16)*
Mean grip strength (lbs force)	54.93 (25.97)	45.29 (25.36)
Mean vibration perception threshold	13.52 (9.56)	16.95 (8.14)
ASIA-motor baseline	96.22 (4.57)	90.00 (8.61)*
ASIA-light touch	111.50 (1.20)	111.56 (1.34)
ASIA-pin prick	111.61 (0.70)	107.89 (1.22)
Mean summated MAS	7.37 (8.87)	6.47 (6.77)
Mean MSWS-12	46.63 (10.41)	72.19 (24.01)*
Mean sway, 32cm, EO	0.80 (0.30) deg/sec	0.91 (0.40) deg/sec
Mean sway, 32cm, EC	0.97 (0.44) deg/sec	1.10 (0.56) deg/sec
Mean sway, 4cm, EO	0.94 (0.39) deg/sec	1.09 (0.49) deg/sec
Mean sway, 4cm, EC	1.20 (0.43) deg/sec	1.29 (0.43) deg/sec
Mean Romberg 32cm	1.19 (0.23)	1.22 (0.34)
Mean Romberg 4cm	1.19 (0.14)	1.33 (0.32)

Table 5.2: Mean (SD) clinical characteristics of patients. P-values for paired t-tests comparing baseline with 1-year follow-up, * p<0.05.

5.5.2 Cross-sectional difference in spinal cord measures between patients and controls at 1 year

All QSI-derived indices of perpendicular diffusivity involving the anterior columns (**Table 5.3**), lateral columns (**Table 5.4**) and whole cord (**Table 5.5**) were significantly higher (reflected by increased ADC_{xy} and $FWHM_{xy}$ and reduced $P0_{xy}$) in patients than in controls at 1-year follow-up after adjusting for age and gender, which is similar to the baseline results by Abdel-Aziz *et al.*, 2015. There was no significant difference in the Q-space metrics in the posterior columns (**Table 5.6**).

Patients had significantly lower spinal tNAA concentration compared to controls at 1 year follow-up, after correcting for age and gender (regression coefficients (RC) -1.22, 95% confidence interval (CI) -2.37 to 0.08, $p < 0.04$). There was no significant difference in Ins ($p < 0.58$), Glx ($p < 0.82$), tCr ($p < 0.72$) and tCho ($p < 0.77$) between patients and controls at 1-year follow-up after correcting for age and gender (**Table 5.7**).

There was a significant difference in spinal cord area between patients and controls at 1-year follow-up (RC -7.39, 95% CI -14.12 to -0.66, $p < 0.03$) after adjusting for age and gender (**Table 5.1**).

An example of these findings are demonstrated in **Figure 5.2**.

Anterior column QSI indices at 0 and 12 months

QSI Index	Time points (months)	PPMS	Controls	Adjusted difference		
				Estimate (RC)	95%CI	P-value
ADCxy (um ² /ms)	0	0.48 (0.14)	0.39 (0.12)	0.09	-0.01, 0.19	0.09
	12	0.52 (0.11)	0.38 (0.07)	0.16	0.08, 0.24	0.0001
FWHMxy (um x 10 ²)	0	0.26 (0.04)	0.23 (0.02)	0.04	0.12, 0.06	0.004
	12	0.26 (0.04)	0.24 (0.01)	0.03	0.01, 0.05	0.001
POxy (a.u)	0	0.19 (0.03)	0.22 (0.03)	-0.03	-0.05, -0.005	0.02
	12	0.18 (0.02)	0.20 (0.01)	-0.03	-0.04, -0.01	0.0001
ADCz (um ² /ms)	0	1.88 (0.22)	1.87 (0.17)	0.06	-0.07, 0.20	0.36
	12	1.73 (0.12)	1.74 (0.13)	-0.01	-0.11, 0.10	0.92
FWHMz (um x 10 ²)	0	0.55 (0.04)	0.56 (0.04)	0.001	-0.02, 0.03	0.53
	12	0.54 (0.03)	0.54 (0.03)	0.01	-0.02, 0.03	0.48
POz (a.u)	0	0.18(0.03)	0.21 (0.03)	-0.001	-0.006, 0.003	0.50
	12	0.18 (0.02)	0.20 (0.01)	-0.002	-0.006, 0.003	0.52

Table 5.3: Summary of mean (SD) diffusivity from the anterior column of the cervical cord in patients and controls at baseline and at 12 months follow-up. P-values for adjusted group comparisons after correcting for age and gender. RC - regression coefficient.

Lateral column QSI indices at 0 and 12 months

QSI Index	Time points (months)	PPMS	Controls	Adjusted difference		
				Estimate (RC)	95%CI	P-value
ADC _{xy} (µm ² /ms)	0	0.40 (0.11)	0.32 (0.10)	0.09	0.02, 0.16	0.02
	12	0.43 (0.11)	0.36 (0.06)	0.09	0.02, 0.17	0.02
FWHM _{xy} (µm x 10 ²)	0	0.25 (0.04)	0.21 (0.02)	0.04	0.01, 0.06	0.004
	12	0.25 (0.04)	0.22 (0.02)	0.03	0.01, 0.06	0.02
PO _{xy} (a.u)	0	0.19 (0.03)	0.22 (0.03)	-0.03	-0.05, -0.01	0.002
	12	0.19 (0.03)	0.21 (0.02)	-0.02	-0.04, -0.00	0.05
ADC _z (µm ² /ms)	0	1.96 (0.27)	1.76 (0.62)	0.15	-0.12, 0.41	0.28
	12	1.79 (0.11)	1.82 (0.09)	-0.03	-0.12, 0.06	0.51
FWHM _z (µm x 10 ²)	0	0.57 (0.04)	0.58 (0.03)	-0.001	-0.03, 0.02	0.96
	12	0.55 (0.03)	0.55 (0.03)	0.01	-0.01, 0.03	0.19
PO _z (a.u)	0	0.11 (0.01)	0.11 (0.004)	0.002	-0.004, 0.01	0.60
	12	0.11 (0.004)	0.11 (0.003)	0.000082	-0.003, 0.003	0.96

Table 5.4: Summary of mean (SD) diffusivity from the lateral column of patients and controls at baseline and at 12 months follow-up. P-Values for adjusted group comparisons after correcting for age and gender.

Whole cord QSI indices at 0 and 12 months

QSI Index	Time points (months)	PPMS	Controls	Adjusted difference		
				Estimate (RC)	95%CI	P-value
ADC_{xy} ($\mu\text{m}^2/\text{ms}$)	0	0.44 (0.09)	0.39 (0.09)	0.06	-0.002, 0.12	0.06
	12	0.47 (0.12)	0.37 (0.04)	0.13	0.06, 0.20	0.001
FWHM_{xy} ($\mu\text{m} \times 10^2$)	0	0.26 (0.03)	0.24 (0.02)	0.03	0.004, 0.05	0.02
	12	0.25 (0.03)	0.23 (0.02)	0.03	0.006, 0.05	0.02
PO_{xy} (a.u)	0	0.18 (0.02)	0.20 (0.02)	-0.02	-0.04, -0.01	0.01
	12	0.19 (0.02)	0.21 (0.02)	-0.02	-0.04, -0.01	0.008
ADC_z ($\mu\text{m}^2/\text{ms}$)	0	1.81 (0.16)	1.59 (0.55)	0.15	-0.06, 0.35	0.15
	12	1.75 (0.10)	1.76 (0.08)	0.03	-0.04, 0.10	0.42
FWHM_z ($\mu\text{m} \times 10^2$)	0	0.55 (0.03)	0.55 (0.03)	0.01	-0.01, 0.03	0.45
	12	0.55 (0.03)	0.55 (0.03)	0.01	-0.01, 0.03	0.32
PO_z (a.u)	0	0.12 (0.01)	0.11 (0.004)	0.001	-0.003, 0.005	0.71
	12	0.11 (0.004)	0.12 (0.01)	-0.003	-0.01, 0.001	0.12

Table 5.5: Summary of mean (SD) diffusivity from the whole cord of patients and controls at baseline and at 12 months follow-up. P-values for adjusted group comparisons after correcting for age and gender.

Posterior column QSI indices at 0 and 12 months

QSI Index	Time points (months)	PPMS	Controls	Adjusted difference		
				Estimate (RC)	95%CI	P-value
ADC _{xy} (um ² /ms)	0	0.42 (0.11)	0.37 (0.107)	0.05	-0.02, 0.11	0.18
	12	0.42 (0.08)	0.35 (0.09)	0.07	0.00, 0.13	0.05
FWHM _{xy} (um x 10 ²)	0	0.26 (0.06)	0.23 (0.03)	0.02	-0.01, 0.06	0.18
	12	0.24 (0.03)	0.22 (0.03)	0.02	-0.01, 0.04	0.15
PO _{xy} (a.u)	0	0.19 (0.03)	0.21 (0.03)	-0.02	-0.04, 0.01	0.20
	12	0.19 (0.02)	0.22 (0.03)	-0.02	-0.04, 0.004	0.11
ADC _z (um ² /ms)	0	2.03 (0.46)	2.01 (0.40)	-0.07	-0.43, 0.29	0.69
	12	2.01 (0.17)	2.08 (0.11)	-0.01	-0.13, 0.10	0.81
FWHM _z (um x 10 ²)	0	0.60 (0.05)	0.60 (0.04)	0.01	-0.02, 0.04	0.40
	12	0.59 (0.04)	0.60 (0.04)	0.001	-0.03, 0.03	0.97
PO _z (a.u)	0	0.10 (0.01)	0.10 (0.004)	-0.002	-0.01, 0.001	0.18
	12	0.11 (0.01)	0.10 (0.01)	-0.001	-0.01, 0.004	0.70

Table 5.6: Summary of mean (SD) diffusivity from the posterior column of patients and controls at baseline and at 12 months follow-up. P-values for adjusted group comparisons after correcting for age and gender.

Metabolite	Time Point (months)	PPMS	Controls	Adjusted difference		
				Estimate (RC)	95% CI	P-value
tNAA (mmol/l)	0	4.06 (1.16)	5.31 (1.47)	-1.28	-2.36, -0.20	0.02
	12	3.70 (1.57)	5.07 (1.03)	-1.22	-2.37, -0.08	0.04
Glx (mmol/l)	0	4.65 (1.11)	5.93 (1.66)	-1.03	-2.34, 0.29	0.12
	12	6.82 (2.22)	8.09 (2.32)	-4.28	-2.05, 0.19	0.07
Ins (mmol/l)	0	5.59 (1.83)	4.49 (1.23)	0.75	-0.53, 2.03	0.24
	12	6.39 (2.44)	5.52 (1.60)	0.46	-1.24, 2.17	0.58
tCho (mmol/l)	0	1.30 (0.38)	1.32 (0.41)	-0.13	-0.47, 0.22	0.46
	12	1.43 (0.59)	1.29 (0.38)	0.06	-0.37, 0.50	0.77
tCr (mmol/l)	0	3.84 (1.46)	3.76 (1.13)	-0.230	-1.39, 0.79	0.58
	12	3.78 (1.58)	3.57 (1.27)	0.20	-0.94, 1.34	0.72

Table 5.7: Cross-sectional summary of mean (SD) metabolite concentrations (mmol/l) from the cervical cord of patients and controls. P-values for adjusted group comparisons after correcting for age and gender.

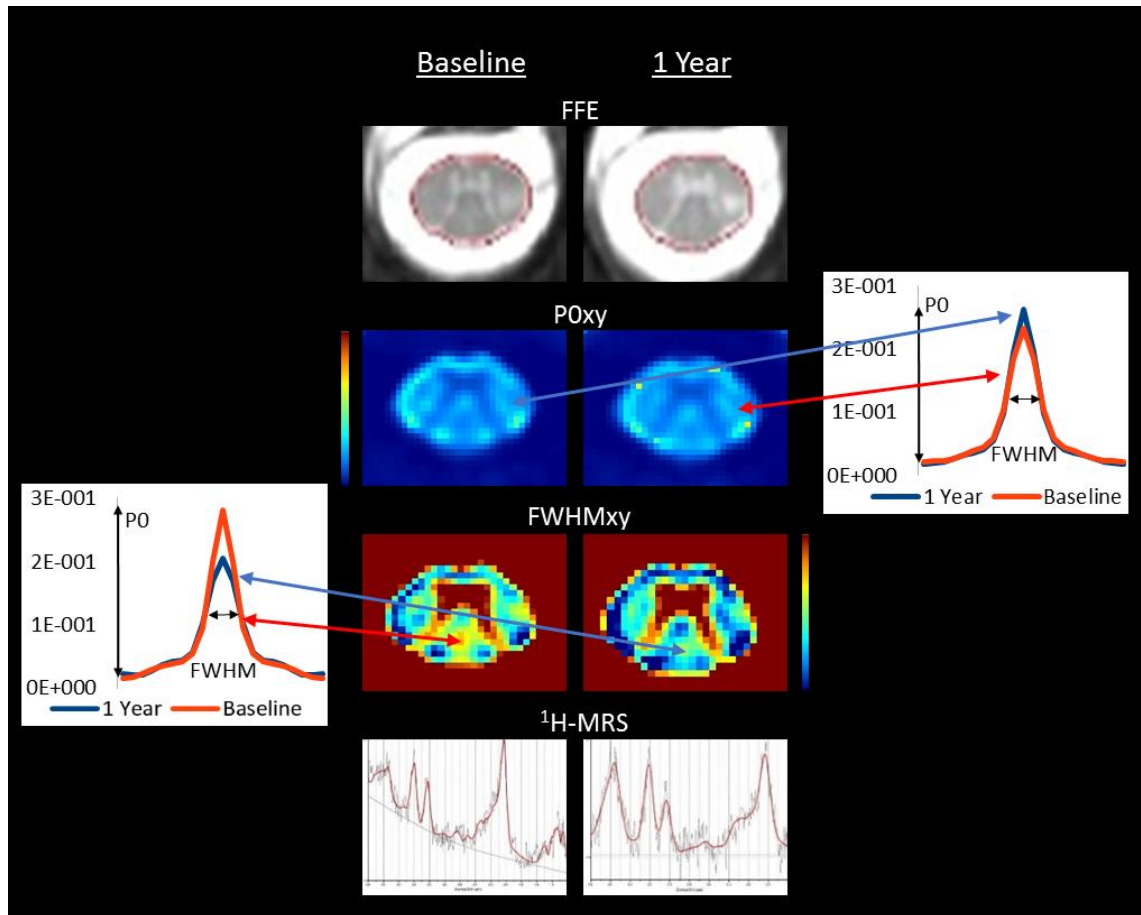


Figure 5.2: Examples of a 3D-FFE axial image of the cervical cord outlined using the active surface model, P0xy map, FWHMxy map and a post processed spectra in a PPMS patient at baseline and then at 1-year follow-up. The graphs represent differences in height and width of the displacement distribution function from the posterior (left) and lateral column (right) from a patient at baseline and 1 year. The FFE image shows a reduction in cross-sectional cord area, increased FWHMxy in the posterior column, reduced P0xy in the lateral columns and reduced tNAA at 1 year.

5.5.3 Longitudinal changes in MRI metrics over 1 year

Spinal cord area was the only MRI metric in the spinal cord which significantly decreased over 1 year, such that the rate of reduction in cord area in the PPMS cohort over one year was 2.86 mm² greater than in controls (RC-2.86, 95% CI - 4.36 to -1.37, $p < 0.0001$), after correcting for age and gender.

The metabolites and Q-space measures did not change significantly over 1 year. Sample size calculations with 80% power using the spectroscopic protocol and Q-space imaging protocol used in this study, demonstrated slightly larger sample sizes would have enabled us to detect significant changes in perpendicular diffusivity in the posterior and lateral cord and in tCho as outlined in **Table 5.8**.

PBVC was significantly greater in the PPMS cohort at -1.59% when compared to controls after adjusting for age and gender over 1 year (95% CI -0.21 to -2.08, $p < 0.02$) (**Table 5.1**).

MRI Metric	Sample size per arm	MRI Metric	Sample size per arm
tNAA	625	Lateral ADCxy	4246
Creatine	96	Lateral ADCz	261
Choline	64	Lateral FWHMxy	61
Ins	671	Lateral FWHMz	138
Glx	445	Lateral POxy	58
Posterior ADCxy	60	Lateral POz	363
Posterior ADCz	82	Anterior ADCxy	88
Posterior FWHMxy	35	Anterior ADCz	75
Posterior FWHMz	100	Anterior FWHMxy	5618
Posterior POxy	990	Anterior FWHMz	694
Posterior POz	129	Anterior POxy	2002
		Anterior POz	142

Table 5.8: Sample size calculations required to detect significant changes in MRI metrics in patients over time compared to changes observed in controls with 80% power. Those numbers highlighted in bold represent sample sizes, which are less than 100 per arm.

The below is a summary table of the significant associations between change in MRI metrics and change in clinical disability scores in PPMS subjects. Each of these results will be discussed in more detail in **Section 5.5.4**, **5.5.6** and **5.5.7**, as well as in **Table 5.9**, **5.10** and **5.11**.

(A) Change in QSI metrics	Change in clinical disability
Cord FWHMxy Cord FWHMz Posterior FWHMz Posterior P0z Lateral FWHMz	Vibration perception thresholds
Cord ADCxy Anterior FWHMz	ASIA-light touch
Posterior P0z Lateral FWHMz Lateral ADCxy	Postural stability (32EO, 32EC, 4EO, 4EC)
(B) Change in metabolites	Change in clinical disability
Ins	EDSS
tNAA tCr	TWT
tCr	Postural stability (32EO, 32 EC, 4EO, 4EC)
(C) MRI measures baseline	Predictors of clinical status at 1 year
Cord FWHMz Anterior FWHMz Posterior FWHMxy Posterior P0xy Posterior ADCxy Lateral FWHMz	EDSS
Cord FWHMxy Cord P0xy Cord ADCxy Anterior FWHMxy Posterior P0xy Lateral FWHMxy Lateral P0xy Lateral ADCxy	Postural stability 32EO
Cord ADCxy Lateral FWHMxy Lateral ADCxy	Postural stability 32EC

Table 5.9: Summary of significant associations between: **(A)** change in QSI metrics and change in clinical disability scores, **(B)** change in metabolites and change in clinical disability scores and **(C)** predictors of clinical status at 1 year with baseline MRI measures. 32EO - 32cm eyes open, 32EC – 32cm eyes closed, 4EO – 4cm eyes open and 4EC – 4cm eyes closed.

5.5.4 Associations between change in Q-space imaging measures and change in clinical disability over 1 year

Despite no significant change in Q-space metrics, over 1 year in patients compared to controls, increased whole cord perpendicular diffusivity (increased FWHM_{xy}) was associated with impaired vibration sensation, such that, per unit increase in FWHM_{xy}, there was a predicted 320.70 (95% CI 28.38 to 984.27) increase in vibration sensation ($p=0.045$). Changes in parallel diffusivity (increased FWHM_z) in the posterior column was associated with a predicted 117.11 (95% CI 20.77 to 198.11) increase in vibration sensation ($p=0.02$), in the lateral columns with a predicted 85.02 (95% CI 2.81 to 261.03) increase in vibration sensation ($p=0.04$) and in the whole cord with a predicted 120.59 (2.53 to 389.60) increase in vibration sensation ($p=0.05$). A scatterplot representing these associations are shown in **Figure 5.3**. In the anterior column, per unit increase in FWHM_z, there was a predicted -34.94 decrease (95% CI -94.25 to -4.60) in ASIA-light touch scores ($p=0.04$). Changes in perpendicular diffusivity in the whole cord (increased ADC_{xy}) were associated with impaired ASIA – light touch scores, such that per unit increase in ADC_{xy} was associated with a predicted -8.15 decrease (95% CI -73.09 to -0.30) in ASIA-light touch scores ($p=0.04$).

Increased parallel diffusivity (decreased P0_z) in the posterior columns and lateral columns (increased FWHM_z) and increased perpendicular diffusivity (increased ADC_{xy}) in the lateral columns were associated with increased postural instability over 1 year. These associations are presented in **Table 5.10**.

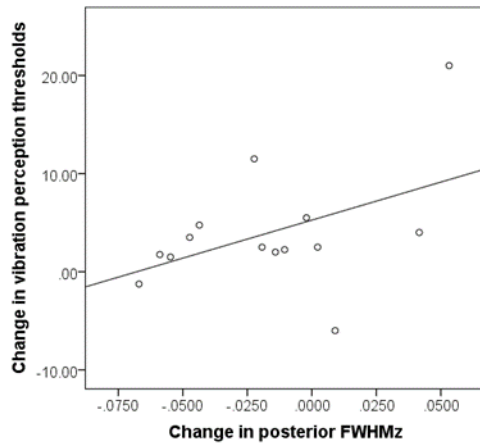


Figure 5.3: Scatter plot demonstrating the association between change in vibration perception thresholds and change in parallel diffusivity in the posterior columns (FWHMz) in patients (unadjusted).

5.5.5 Associations between change in ¹H-MRS measures and change in clinical disability over 1 year

Despite no significant change in metabolites over 1 year, in patients increased tCr was associated with a decrease in TWT z-score (RC -0.07, 95% CI -0.14 to -0.01, p=0.03) and with greater postural instability. Decreased tNAA over 1 year was associated with a borderline significant decrease in TWT z-score in patients (RC 0.07, 95% CI -0.01 to 0.14, p=0.06). There was borderline evidence of increased Ins being associated with an increase in EDSS (RC 0.50, 95% CI -0.04 to 1.04, P=0.07). These associations are presented in **Table 5.11**. There was no significant association between change in cervical spinal cord area and clinical disability.

Predictors Q-space metrics XY Z		Dependent variables							
		EDSS	TWT	VPTs	ASIA-light touch	Postural stability 32cm		Postural stability 4cm	
		Regression coefficients (95%CI) from linear regression, p-value				Standardised regression coefficients (95% CI) from multivariate analysis			
		EO	EC	EO	EC				
Cord FWHM		-9.84 (-71.80, 65.15) P=0.78**	-2.77 (-15.91, 5.81) P=0.62**	320.70 (28.38, 984.27) P=0.05**	-49.86 (-176.17, 22.08) P=0.25**	Sway: -0.42 (-0.81, -0.03) Pitch: -0.39 (-0.77, -0.14) Roll: -0.48 (-0.89, -0.06) P=0.01*	Sway: -0.43 (-0.90, 0.04) Pitch: -0.48 (-0.92, -0.05) Roll: -0.51 (-0.97, -0.04) Romberg: -0.09 (-0.66, 0.48) P=0.07*	Sway: -0.55 (-0.95, -0.15) Pitch: -0.52 (-0.92, -0.11) Roll: -0.59 (-0.99, -0.19) P=0.07*	Sway: -0.58 (-1.27, 0.12) Pitch: -0.69 (-1.33, -0.06) Roll: -0.90 (-1.20, -0.59) Romberg: -0.09 (-0.67, 0.48) P=0.02*
	Cord FWHM	-15.19 (-45.38, 8.24) p=0.24**	-1.32 (-5.37, 3.13) p=0.49**	120.59 (2.53, 389.69) p=0.05**	-24.44 (-74.85, 15.56) p=0.26**	Sway: 0.31 (-0.19, 0.80) Pitch: 0.29 (-0.20, 0.78) Roll: 0.24 (-0.29, 0.77) P=0.35*	Sway: -0.09 (-0.68, 0.40) Pitch: -0.13 (-0.71, 0.45) Roll: -0.11 (-0.72, 0.51) Romberg: -0.40 (-0.92, 0.12) P=0.21*	Sway: 0.13 (-0.50, -0.76) Pitch: 0.21 (-0.39, 0.81) Roll: -0.03 (-0.71, 0.65) P=0.004*	Sway: 0.02 (-0.60, 0.64) Pitch: -0.30 (-0.91, 0.32) Roll: -0.47 (-0.97, 0.03) Romberg: -0.31 (-0.82, 0.20) P=0.01*

Cord ADC		-1.78 (-11.24, 5.56) p=0.76**	-0.45 (-2.42, 1.95) p=0.65**	38.63 (-64.74, 187.95) p=0.57**	-8.15 (-73.09, -0.30) p=0.04**	Sway: -0.31 (-1.44, 0.82) Pitch: -0.05 (-1.51, 1.42) Roll: -0.62 (-1.24, 0.01) P=0.43*	Sway: -0.67 (-1.24, -0.09) Pitch: -0.62 (-1.29, 0.05) Roll: -0.61 (-1.47, 0.25) Romberg: -0.64 (-1.43, 0.16) P=0.72*	Sway: -0.45 (-1.43, 0.53) Pitch: -0.27 (-1.57, 1.03) Roll: -0.67 (-1.20, -0.14) P=0.02*	Sway: 0.67 (0.009, 1.34) Pitch: 0.62 (-0.25, 1.49) Roll: 0.33 (-1.26, 1.92) Romberg: -0.64 (-1.43, 0.16) P=0.12*
	Anterior FWHM	-20.08 (-50.47, 3.99) p=0.15**	-0.64 (-4.66, 3.95) p=0.74**	48.02 (-109.53, 282.19) p=0.61**	-34.94 (-94.25, -4.60) P=0.04**	Sway: 0.05 (-0.43, 0.52) Pitch: 0.07 (-0.40, 0.53) Roll: -0.05 (-0.56, 0.47) P=0.63*	Sway: -0.18 (-0.70, 0.35) Pitch: -0.22 (-0.73, 0.29) Roll: -0.21 (-0.75, 0.34) Romberg: -0.35 (-0.85, 0.15) P=0.30*	Sway: -0.12 (-0.67, 0.42) Pitch: -0.04 (-0.57, 0.49) Roll: -0.27 (-0.80, 0.26) P=0.03*	Sway: 0.01 (-0.64, 0.66) Pitch: -0.24 (-0.91, 0.43) Roll: -0.54 (-0.99, -0.09) Romberg: -0.21 (-0.75, 0.32) P=0.0001*
	Posterior FWHM	-8.76 (-28.50, 5.15) p=0.32**	-0.64 (-4.73, 0.86) p=0.60**	117.11 (20.77, 198.11) P=0.02**	-20.15 (-47.22, 10.26) p=0.22**	Sway: 0.22 (-0.27, 0.71) Pitch: 0.32 (-0.14, 0.78) Roll: -0.009 (-0.54, 0.52) P=0.13*	Sway: -0.52 (-0.93, -0.97) Pitch: -0.47 (-0.90, -0.04) Roll: -0.49 (-0.95, 0.009) Romberg: -0.72 P=0.03*	Sway: -0.09 (-0.80, 0.62) Pitch: 0.02 (-0.68, 0.73) Roll: -0.29 (-0.98, 0.39) P=0.013*	Sway: -0.10 (-0.80, 0.59) Pitch: -0.33 (-1.02, 0.36) Roll: -0.55 (-1.03, -0.07) Romberg: -0.51 (-0.96, -0.06) P=0.0001*

	Posterior P0	-25.70 (-173.70, 116.79) p=0.72**	7.38 (-9.65, 39.46) p=0.54**	-1114.73 (-1915.09, -363.46) p=0.006**	89.10 (-184.76, 282.93) p=0.47**	Sway: -0.17 (-0.27, 0.61) Pitch: -0.03 (-0.43, 0.48) Roll: -0.44 (-0.82, 0.05) P=0.005*	Sway: -0.75 (-0.97, -0.53) Pitch: -0.72 (-0.96, -0.49) Roll: -0.72 (-0.99, -0.46) Romberg: 0.76 (0.49, 1.03) P=0.0001*	Sway: -0.65 (1.00, -0.30) Pitch: -0.59 (-0.99, -0.22) Roll: -0.74 (-1.01, -0.47) P=0.0001*	Sway: -0.47 (-1.07, -0.12) Pitch: -0.26 (-1.03, -0.50) Roll: -0.55 (-1.04, -0.06) Romberg: 0.65 (0.25, 1.05) P=0.0001*
	Lateral FWHM	-12.85 (-30.82, 4.61) P=0.15**	-2.12 (-5.35, 0.39) P=0.14**	85.02 (2.81, 261.03) P=0.04**	-8.07 (-50.56, 23.24) p=0.62**	Sway: 0.20 (-0.28, 0.69) Pitch: 0.20 (-0.27, 0.67) Roll: 0.07 (-0.46, 0.61) P=0.0002*	Sway: 0.02 (-0.54, 0.57) Pitch: 0.01 (-0.54, 0.56) Roll: 0.29 (-0.82, 0.24) Romberg: 0.02 (-0.51, 0.54) P=0.0005*	Sway: 0.36 (-0.22, 0.94) Pitch: 0.47 (-0.03, 0.96) Roll: 0.15 (-0.57, 0.86) P=0.0001*	Sway: 0.57 (0.04, 1.09) Pitch: 0.36 (-0.34, 1.05) Roll: -0.06 (-0.79, 0.67) Romberg: -0.02 (-0.79, 0.67) P=0.0001*
Lateral ADC		0.41 (-4.98, 4.87) P=0.87**	-0.23 (-1.39, 0.40) P=0.61**	18.08 (-19.99, 73.18) P=0.47**	-5.27 (-12.96, 2.42) P=0.18**	Sway: -0.47 (-0.81, -0.12) Pitch: -0.39 (-0.74, 0.06) Roll: -0.64 (-0.92, -0.35) P=0.003*	Sway: -0.76 (-0.98, -0.55) Pitch: -0.77 (-0.98, -0.57) Roll: -0.70 (-0.99, -0.40) Romberg: -0.68 (-1.02, -0.35) P=0.0001*	Sway: -0.71 (-0.94, -0.48) Pitch: -0.69 (-0.92, -0.45) Roll: -0.73 (-0.97, -0.49) P=0.0001*	Sway: -0.79 (-0.99, -0.58) Pitch: -0.36 (-1.29, 0.57) Roll: -0.29 (-1.21, 0.64) Romberg: -0.68 (-1.01, -0.35) P=0.0001*

Table 5.10: Associations between change in Q-space metrics (predictors) and change in clinical scores (dependent variable) in patients. * Joint tests of association used for the postural stability measures. Significant differences are reported for each stance distance (32cm and 4cm) with eyes open (EO) and eyes closed (EC) if three or more of the stance conditions (32cm EO, 32cm EC, 4cm EO, 4cm EC) were significant. ** Linear regression performed with the change in MRI measure used as the predictor and the clinical measure as the dependent variable correcting for age and gender. Significant results highlighted in bold.

Predictors	Dependent variables							
	EDSS	TWT	VPTs	ASIA-light touch	Postural stability 32cm		Postural stability 4cm	
					EO	EC	EO	EC
	Regression coefficients (95%CI) from linear regression, p-value				Standardised regression coefficients (95% CI) from multivariate analysis			
Myo-inositol	0.50 (-0.04, 1.04) P=0.07**	0.02 (-0.43, 0.09) p=0.44**	-1.03 (-6.39, 4.32) p=0.64**	0.65 (-0.23, 1.53) p=0.44**	Sway: -0.91 (-1.50, -0.32) Pitch: -0.90 (-1.48, -0.33) Roll: -0.62 (-1.34, 0.10) P=0.0001*	Sway: -0.15 (-1.02, 0.72) Pitch: -0.20 (-1.06, 0.66) Roll: 0.32 (-0.57, 1.21) Romberg: 0.34 (-0.53, 1.22) P=0.0001*	Sway: -0.33 (-1.12, 0.46) Pitch: -0.47 (-1.21, 0.27) Roll: -0.07 (-0.91, 0.77) P=0.06*	-
N-acetyl-aspartate	-0.17 (-0.75, 0.42) p=0.54**	0.07 (-0.01, 0.14) P=0.06***	-21.91 (-79.88, 36.05) p=0.35**	0.16 (-0.76, 1.08), p=0.69**	Sway: 0.60 (-0.06, 1.27) Pitch: 0.21 (-0.71, 1.13) Roll: 0.99 (0.75, 1.22) P=0.0001*	Sway: 0.47 (-0.007, 0.94) Pitch: 0.34 (-0.17, 0.85) Roll: 0.25 (-0.31, 0.81) Romberg: 0.40 (-0.05, 0.84) P=0.07*	-	-

Creatine	0.14 (-0.49, 0.77) p=0.64**	-0.07 (-0.14, -0.01) P=0.03**	-2.67 (-7.18, 1.84) p=0.20** *	0.17 (-0.66, 0.10) p=0.65**	Sway: 0.52 (0.02, 1.01) Pitch: 0.35 (-0.26, 0.95) Roll: 0.73 (0.42, 1.04) P=0.003*	Sway: 0.87 (0.71, 1.03) Pitch: 0.85 (0.66, 1.03) Roll: 0.78 (0.54, 1.03) Romberg: 0.59 (0.09, 1.10) P=0.0001*	Sway:0.49 (-0.04, 1.02) Pitch: 0.50 (0.00, 1.00) Roll: 0.41 (-0.19, 1.01) P=0.01*	Sway: 0.86 (0.78, 0.93) Pitch: 0.35 (0.21, 0.49) Roll: 0.21 (0.12, 0.30) Romberg: 0.77 (0.67, 0.87) P=0.05*
----------	-----------------------------------	--	---	-----------------------------------	---	--	--	--

Table 5.11: Associations between change in ¹H-MRS metabolites (predictors) and change in clinical scores (dependent variable) in patients. * Joint tests of association used for the postural stability measures. Significant differences are reported for each stance distance (32cm and 4cm) with eyes open (EO) and eyes closed (EC) if three or more of the stance conditions (32cm EO, 32cm EC, 4cm EO, 4cm EC) were significant. ** Linear regression model performed with change in MRI measure used as the predictor and the clinical measure as the dependent variable correcting for age and gender. Significant results highlighted in bold.

5.5.6 Predicting clinical status at 1 year with baseline MRI measures

Perpendicular diffusivity in the posterior columns (increased ADCxy, increased FWHMxy and decreased P0xy), and parallel diffusivity in the anterior columns (increased FWHMz), lateral columns (increased FWHMz) and whole cord (increased FWHMz) at baseline best predicted EDSS at 1 year after correcting for age, gender and EDSS at baseline, as outlined in **Table 5.12**. **Figure 5.4** represents the correlation between perpendicular diffusivity (FWHMxy) in the posterior column at baseline, predicting EDSS at 1 year. In particular, per unit increase in ADCxy and FWHMxy in the posterior columns was associated with a predicted 3.71 (95% CI 0.31 to 8.71) and 5.73 (95% CI 0.35 to 11.82) increase in EDSS respectively at 1 year ($p=0.04$ and $p=0.05$), while per unit decrease in P0xy was associated with a predicted 13.12 (25.07 to 0.09) increase in EDSS ($p=0.04$). Per unit increase in FWHMz in the anterior columns, lateral columns and whole cord was associated with a predicted 12.85 (0.21 to 0.96), 8.02 (0.02 to 18.50) and 13.83 (2.44 to 33.00) increase in EDSS respectively at 1 year. QSI derived metrics of perpendicular diffusivity in the anterior, posterior, lateral columns and whole cord at baseline best predicted postural stability at 1 year, as outlined in **Table 5.12**. None of the other MRI metrics, including spinal cord area and the metabolites at baseline, predicted EDSS at 1-year.

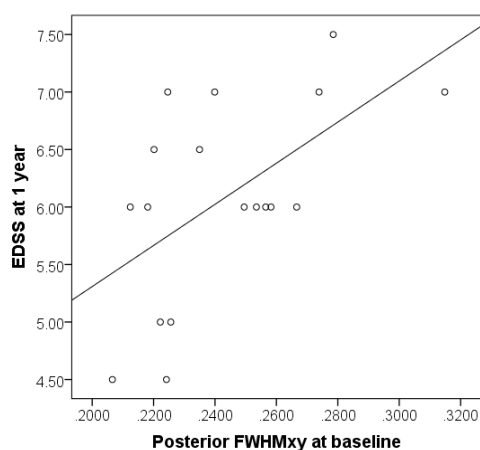


Figure 5.4: Scatter plot demonstrating the association between perpendicular diffusivity (FWHMxy) in the posterior column at baseline predicting EDSS at 1 year (unadjusted).

Clinical measure		EDSS	Postural stability 32cm	
Q-space imaging metrics baseline			EO	EC
XY	Z	Regression coefficients (95% CI), p-value from bootstrap analysis		
Cord FWHM		9.47 (-3.27, 22.59), p=0.17	Sway: 5.90 (0.51, 11.82), p=0.04 Pitch: 4.62 (-3.38, 8.23), p=0.50 Roll: 3.04 (-0.39, 8.08), p=0.18	Sway: 9.56 (-11.20, 28.19), p=0.45 Pitch: 6.80 (-11.48, 21.32), p=0.44 Roll: 5.39 (-1.17, 15.87), p=0.96
	Cord FWHM	13.83 (2.44, 33.00), p=0.03	Sway: 3.97 (-1.69, 16.50), p=0.33 Pitch: 3.10 (-1.76, 13.50), p=0.35 Roll: 2.09 (-1.20, 9.46), p=0.38	Sway: 5.97 (-8.59, 38.68), p=0.55 Pitch: 4.62 (-8.59, 29.83), p=0.60 Roll: 3.59 (-2.39, 17.12), p=0.45
Cord P0		-14.66 (-31.10, 5.93), p=0.10	Sway: -9.23 (-28.26, -4.21), p=0.04 Pitch: -7.31 (-11.35, -2.93), p=0.002 Roll: -4.63 (-18.07, -0.29), p=0.04	Sway: -13.48 (-421.20, 8.67), p=0.49 Pitch: -9.00 (-25.79, 13.21), p=0.44 Roll: -7.97 (-114.14, 0.55), p=0.23
Cord ADC		4.26 (-0.21, 9.58), p=0.09	Sway: 2.72 (-3.13, 4.82), p=0.12 Pitch: 1.94 (-2.32, 3.76), p=0.12 Roll: 1.60 (0.44, 2.88), p=0.03	Sway: 5.47 (-0.38, 10.65), p=0.07 Pitch: 4.04 (0.80, 17.10), p=0.04 Roll: 2.59 (1.23, 7.54), p=0.02
Anterior FWHM		6.66 (-8.54, 15.97), p=0.25	Sway: 4.13 (0.38, 38.69), P=0.04 Pitch: 3.23 (0.65, 17.97), P=0.05 Roll: 2.21 (-0.66, 15.31), p=0.26	Sway: 7.67 (-3.99, 642.69), p=0.72 Pitch: 5.75 (-5.38, 129.67), p=0.42 Roll: 4.02 (-0.92, 13.60), p=0.20
	Anterior FWHM	12.85 (0.21, 0.96), p=0.02	Sway: 3.17 (-1.79, 14.64), p=0.67 Pitch: 2.59 (-2.20, 9.42), p=0.44 Roll: 1.51 (-1.09, 9.91), p=0.87	Sway: 2.81 (-8.55, 34.87), p=0.76 Pitch: 2.11 (-7.27, 26.80), p=0.77 Roll: 2.18 (-2.55, 17.48), p=0.61
Posterior FWHM		5.73 (0.35, 11.82), p=0.05	Sway: 3.14 (-16.36, 6.36), p<0.31 Pitch: 2.45 (-3.24, 6.12), p<0.24 Roll: 1.60 (-0.27, 6.56), p<0.47	Sway: 5.04 (-12.61, 91.21), p<0.63 Pitch: 3.77 (-9.54, 74.95), p<0.56 Roll: 2.73 (-5.07, 65.74), p<0.56
Posterior P0		-13.12 (-25.07, -0.09), p=0.04	Sway: -7.04 (-13.18, -3.97), p=0.02 Pitch: -5.58 (-8.77, 3.35), p=0.15 Roll: -3.42 (-6.80, -0.07), p=0.05	Sway: -10.06 (-93.95, 16.95), p=0.51 Pitch: -6.92 (-26.59, 14.29), p=0.48 Roll: -5.90 (-32.08, 4.72), p=0.39

Posterior ADC		3.71 (0.31, 8.71), p=0.04	Sway: 1.50 (-5.83, 8.87), p=0.68 Pitch: 1.07 (-3.20, 9.91), p=0.68 Roll: 0.90 (-1.94, 5.58), p=0.52	Sway: 4.73 (-7.67, 11.93), p=0.37 Pitch: 3.86 (-18.36, 11.43), p=0.54 Roll: 1.82 (-3.14, 5.57), p=0.46
Lateral FWHM		7.82 (-2.73, 18.72), p=0.16	Sway: 6.02 (3.47, 15.63), p=0.01 Pitch: 4.53 (-2.65, 9.60), p=0.12 Roll: 3.27 (1.27, 9.96), p=0.004	Sway: 10.45 (0.80, 156.07), p=0.04 Pitch: 7.68 (-2.80, 45.36), p=0.40 Roll: 5.44 (1.24, 45.05), p=0.004
	Lateral FWHM	8.02 (0.02, 18.50), p=0.05	Sway: 2.91 (-1.91, 11.97), p=0.32 Pitch: 2.19 (-1.52, 10.03), p=0.39 Roll: 1.69 (-1.66, 5.60), p=0.31	Sway: 4.63 (-6.92, 21.13), p=0.51 Pitch: 3.77 (-5.44, 16.42), p=0.51 Roll: 3.23 (-1.61, 9.87), p=0.25
Lateral P0		-10.03 (-20.27, 7.42), p=0.14	Sway: -8.14 (-22.81, -3.36), p=0.01 Pitch: -6.25 (-14.85, -3.10), p=0.02 Roll: -4.26 (-10.38, -0.91), p=0.01	Sway: -12.54 (-81.08, 1.54), p=0.51 Pitch: -9.05 (-46.03, 3.59), p=0.66 Roll: -6.63 (-24.44, -0.35), p=0.19
Lateral ADC		2.68 (-1.60, 6.62), p=0.19	Sway: 1.96 (0.38, 3.86), p=0.013 Pitch: 1.35 (-1.21, 2.86), p=0.12 Roll: 1.17 (0.79, 2.29), p=0.0001	Sway: 4.12 (1.01, 6.91), p=0.004 Pitch: 3.19 (1.00, 7.38), p=0.008 Roll: 1.90 (1.04, 4.18), p=0.001

Table 5.12: Predictors of clinical status at 1 year with baseline MRI measures. Regression analysis using bootstrapping correcting for age, gender and baseline clinical measure. Significant results highlighted in bold. Multivariate analysis was not possible with this data, which is likely due to the small sample size. Significant results highlighted in bold.

5.7 Discussion

The findings from this study demonstrate that among all MRI metrics, (i) cervical spinal cord area had the greatest and most significant change over 1 year and (ii) there were significant associations between change in Q-space metrics and change in clinical scores. The findings from this follow-up study, demonstrate possible ongoing neurodegeneration in the cervical cord in early PPMS over a short follow-up period detected using spinal cord atrophy. Q-space metrics may detect clinically meaningful pathology within the cervical cord and may help in predicting disability.

5.7.1 Differences in spinal cord area, metabolite concentrations and Q-space imaging measures between patients and controls

There was a significant decrease in cord area over a relatively short follow-up period in patients compared to controls, even though there was no significant difference in spinal cord area at baseline. Cord atrophy is thought to be a measure of the underlying destructive pathological process involved in MS. It has been demonstrated that spinal cord area is a useful imaging biomarker of axonal loss (Kearney *et al.*, 2014a). The significant change in spinal cord area as demonstrated in this study suggests it may be a useful marker of neurodegeneration and further supports its role as an imaging biomarker in clinical trials. Several studies in MS subjects with a long disease duration found that cord atrophy is related to disability independently of brain lesion load and atrophy (Kearney *et al.*, 2014b; Daams *et al.*, 2014; Lin *et al.*, 2004).

tNAA and Glx reduced and Ins, tCho and tCr increased between baseline and 1 year follow up in patients compared to controls. This is in the direction you would

expect for each metabolite, but these changes did not reach statistical significance. The sample size and duration of this follow-up study was small and this may contribute to the lack of a significant change in metabolites. The sample size calculations for tCho (a marker of membrane turn over (Henning *et al.*, 2008)) (N=64) and tCr (a marker of gliosis (Moore *et al.*, 2012)) (N=96) gave acceptable numbers of patients per arm for these metabolites, suggesting tCho and tCr may have a role in explaining the pathological processes underlying disability progression but this needs to be further investigated. The sample size calculations, gave very high numbers for tNAA, which may suggest subtle changes in tNAA are difficult to detect, particularly over a short follow-up period. The three-year longitudinal extension of this study will further investigate the role of tNAA, tCho, tCr and Ins in disease progression.

Glx, which represents the sum of glutamate and glutamine, is the main excitatory neurotransmitter in the central nervous system, with glutamate making up the majority of the Glx signal (Baker *et al.*, 2008). The lower Glx seen in patients compared to controls, at both baseline and 1 year follow up, may arise due to neuro-axonal degeneration with the majority of glutamate located in the synaptic terminals (Kaiser *et al.*, 2005; Muhlert *et al.*, 2014; Abdel-Aziz *et al.*, 2015). The concentration of Glx in both patients and controls was greater at 1 year, when compared to the baseline Glx concentration. It is difficult to say why this occurred as the same protocol was used at both time points. We do not know how Glx fluctuates over time and the variability in the measure may arise due to this in both patients and controls. It does not affect the overall message, of lower Glx in patients compared to controls at 1 year, similar to the baseline results.

Of note the majority of patients followed-up at 1 year had a lesion(s) in the spectroscopic voxel (18 out of 19 subjects), and therefore we were unable to determine if there was a significant difference between patients with and without cervical cord lesions

Next, looking at the Q-space imaging metrics, higher diffusivity perpendicular to the long axis of the spinal cord in patients compared to controls cross-sectionally at 1 year, is in keeping with the results found in the baseline data (Abdel-Aziz *et al.*, 2015) and is likely to reflect increased movement of water perpendicular to the long axis of the cord due to the breakdown of myelin and axonal membranes (Beaulieu *et al.*, 2002; Abdel-Aziz *et al.*, 2015). The lack of a significant change in Q-space metrics in the spinal cord over 1 year may be due to the small sample size. A sample size calculation found that the minimum sample sizes required to detect a significant difference in perpendicular diffusivity metrics between the two groups with 80% power in the posterior and lateral columns gave acceptable numbers of patients per arm (**Table 5.8**). Q-space metrics in the anterior column gave extremely high numbers of subjects per arm. Axonal loss occurs most commonly in the lateral and posterior columns whilst the anterior columns are least affected by axonal loss (Bergers *et al.*, 2002). This is consistent with the smaller sample sizes required to detect significant difference in Q-space metrics in the posterior and lateral columns, which is likely to reflect greater pathological changes occurring within these columns.

5.7.2 Associations between whole cord imaging measures and clinical disability

In this study, I used a number of clinical measures e.g postural stability, vibration perception thresholds and dynamometry, which are thought to be more responsive to clinical damage in the spinal cord than EDSS and they are thought to have increased sensitivity for detecting correlations between MRI abnormalities in the spinal cord and disability (Oh et al., 2013; Zackowski et al., 2009).

The changes in metabolites over 1 year, specifically tNAA, Ins and tCr, were not significant in patients when compared to controls but have correlated with clinical changes over that period. An increase in tCr was associated with deterioration in the TWT, which may suggest the role of gliosis in the spinal cord, contributing to disability progression. Increased tCr over 1 year was associated with increased postural instability, providing further evidence of the possible involvement of a gliotic process in disability progression. An increase in Ins was associated with borderline evidence of an increase in EDSS, which may further suggest the role of gliosis (similar to tCr) in the spinal cord as an important process driving disability progression in early PPMS. These associations require longer follow-up to evaluate the exact meaning of these clinical correlations.

There was no significant change in Q-space metrics over time in patients. However, impaired vibration and light touch sensation were associated with an increase of whole cord QSI-derived perpendicular diffusivity, which may be due to reduced neuronal integrity and/or presence of demyelination (Abdel-Aziz *et al.*, 2015). An increase in whole cord QSI-derived parallel diffusivity over 1 year was

associated with impaired vibration sensation, which may arise due to gliosis and an increase in the extracellular space (Klawiter *et al.*, 2011). Animal models have demonstrated a decrease in parallel diffusivity in the acute setting, which is likely to be due to acute axonal damage (Klawiter *et al.*, 2011). However, after the acute stages, the diffusivity of the remaining axons is overshadowed by increased parallel diffusivity, which may result from gliosis and increased extracellular space (Klawiter *et al.*, 2011). One study in acute versus chronic optic neuritis found a decrease in parallel diffusivity during the acute stage and increased parallel diffusivity at 1 year follow-up in patients compared to controls (Naismith *et al.*, 2009), suggesting an increase in parallel diffusivity in the chronic stage.

The absence of a significant association between change in cord area and change in disability may arise due to the small sample size of this study and the short follow-up period. This is despite a significant difference in cord area between patients and controls.

5.7.3 Associations between change in column-specific q-space imaging measures and change in clinical disability

Increased QSI derived perpendicular and parallel diffusivity in the posterior cord over 1 year was associated with impaired vibration sensation and parallel diffusivity was associated with increased postural instability. This may arise due to a combination of axonal loss and/or demyelination, gliosis and an increase in the extracellular space. A previous study compared diffusion tensor imaging with QSI, and found that QSI-derived metrics had greater sensitivity at detecting abnormalities in lesional tissue and NAWM in MS patients (Assaf *et al.*, 2002) and demonstrated that it was reproducible (Assaf *et al.*, 2005). This latter study

also found that the QSI metrics correlated well with NAA/creatinine ratio, in keeping with axonal loss (Assaf *et al.*, 2005).

5.7.4 Predicting clinical status at 1 year with baseline MRI measures

Out of all the MRI metrics, Q-space imaging was the only MRI metric at baseline that significantly predicted EDSS at 1 year. The microstructural abnormalities detected using Q-space imaging at baseline is likely to reflect reduced neuronal integrity and it may be one of the main pathological processes driving disability progression in early PPMS. We will investigate if these predictors hold true at the 3 year follow-up study planned for this cohort. Postural instability at 1 year was best predicted by Q-space imaging derived metrics at baseline from the whole cord and lateral columns again suggesting neuronal dysfunction driving impairment in postural stability.

5.8 Limitations

The sample size of this study was small, making significant results more difficult to detect. In addition, the short follow-up period (12 months) can make it difficult to detect significant changes longitudinally in MRI metrics. I plan to follow-up this cohort of patients at 3 years, where we hope more significant changes in MRI measurements will be detected, specifically for QSI metrics in the posterior and lateral columns. I will see if correlations with MRI metrics and clinical disability at 1 year are still present at 3 years and if this further elucidates the role of neuronal dysfunction and gliosis in disease progression.

The MRS protocol used in this clinical study reliably quantified Glx. In the brain, it is possible to separate Glutamate from Glutamine using echo time averaged

PRESS (Hurd *et al.*, 2004; Hancu *et al.*, 2009). However, this is technically very challenging in the spinal cord, using a 3T scanner as larger voxel sizes would be needed (Abdel-Aziz *et al.*, 2015). Further developmental work is needed to be able to directly measure Glutamate in the spinal cord.

5.9 Conclusion

There was a significant change in spinal cord cross-sectional area over 1 year. Slightly larger sample sizes may have detected significant changes in perpendicular diffusivity in the posterior and lateral columns and in tCho between patients and controls over time. There was a significant association between change in Q-space metrics and change in clinical status over 1 year. The findings from this follow-up study demonstrates possible evidence of ongoing neurodegeneration in the spinal cord in early PPMS detected using spinal cord atrophy. In addition to this, Q-space metrics may detect clinically meaningful pathological processes occurring in the cervical cord, which contributes to disability progression in early PPMS.

The results presented in this Chapter demonstrate the ability of spinal cord cross-sectional area to detect cord atrophy over a relatively short follow-up period in PPMS. In the next Chapter, I will explore if similar results are seen in a larger cohort of patients with progressive MS and will determine sample sizes required to demonstrate a reduction in spinal cord cross-sectional area as an outcome measure in clinical trials in progressive MS.

Chapter VI

Spinal cord atrophy in progressive multiple sclerosis

6.1 Introduction

There are no effective treatments that modify the disease course in progressive MS, unlike the dramatic progress in the therapeutics of RRMS over the last decade. To date, clinical trials of anti-inflammatory therapies in progressive MS have generally been negative, and no treatment is available to slow progression (Fox *et al.*, 2012). A fundamental element to the successful development of treatments in progressive MS is the identification of biomarkers that reflect the pathological processes underlying progression (Thompson *et al.*, 2015). Phase II trials, which test efficacy and safety, rely on biomarkers that are more sensitive to therapeutic effects than clinical measures. These biomarkers provide a signal for phase III trials, where clinical disability is the primary outcome measure.

Neurodegeneration and, in particular, neuronal and axonal loss, are the main mechanisms leading to irreversible disability in MS and this is perhaps most relevant in the spinal cord where cervical cord atrophy appears to be an independent determinant of EDSS scores (Kearney *et al.*, 2014b). A reduction in spinal cord cross sectional area, an indicator of spinal cord atrophy, can be used as an approximate marker of axonal loss (Losseff *et al.*, 1996; Bot *et al.*, 2004). Several studies in MS subjects with a long disease duration found that cord atrophy is related to disability independently of brain lesion load and atrophy (Kearney *et al.*, 2014b; Daams *et al.*, 2014; Kidd *et al.*, 1993; Lin *et al.*, 2004). Additionally, the rate of atrophy in the cervical cord is greater than that seen in the brain, which is currently used as an outcome measure in progressive MS trials (~1.5% vs. 0.5%-1.0% per year) (Lukas *et al.*, 2015; Furby *et al.*, 2010; De Stefano *et al.*, 2010). In SPMS one study found median rates of cord atrophy of

1.6% per year (De Stefano *et al.*, 2010), while even faster rates of cord atrophy were seen in PPMS (at ~3.75% per year) (Stevenson *et al.*, 2000).

To date, only a few clinical trials have used brain or spinal cord atrophy as an endpoint (Chataway *et al.*, 2014; Kapoor *et al.*, 2010; Yaldizli *et al.*, 2015). This reflects the numerous challenges of detecting minimal changes in a small structure across a large group of patients in a multi-centre setting (Kearney *et al.*, 2015).

In this study, I consider the potential of using spinal cord atrophy as an endpoint in phase II, single-centre, neuroprotective clinical trials in progressive MS. The specific aims of this study are to (i) measure the progression of spinal cord atrophy over time and evaluate its relationship with physical disability in progressive MS; and (ii) determine sample sizes required to demonstrate a reduction in spinal cord area as a primary outcome measure in a phase II clinical trial in progressive MS. For each aim, I first combined our two recent cohorts of PPMS and SPMS into a single progressive MS cohort, as they are thought to share more similarities than differences in their clinical, pathological and imaging characteristics (Fox *et al.*, 2012). Secondly, I looked at each group independently, adjusting for brain atrophy development and changes in lesion loads.

6.2 Methods

6.2.1 Subjects

I retrospectively collected data of patients with SPMS and PPMS who participated in our previous spinal cord imaging studies (Kearney *et al.*, 2015; Abdel-Aziz *et al.*, 2015), and then analysed them separately. Inclusion criteria were a diagnosis of PPMS (Polman *et al.*, 2005) or SPMS, and age between 18 and 65 years. I did not specifically check whether there was “recent” evidence of disability progression. Healthy controls were also recruited. All subjects were invited to come back for a follow-up after 1 year. Patients were clinically assessed on the day of the MRI at each time point.

Of note, none of the PPMS or SPMS patients were on disease modifying therapy at the time of scanning at either baseline or at 1 year follow-up.

All the MS patients recruited into this study were recruited from the MS clinics ran on a weekly basis at The National Hospital of Neurology and Neurosurgery, Queen Square London. All healthy controls recruited were work colleagues, friends and family as well as friends and family of the MS patients. All subjects recruited into the study provided written informed consent prior to taking part in the study, which was approved by the local research ethics committee (Study Reference: 10/H0713/74).

The study in Chapter VI was a retrospective study, based on two previous studies carried out by three of my colleagues (Dr. Abdel-Aziz, Dr. Kearney and Dr. Plantone). Dr Abdel-Aziz and Dr Kearney carried out the baseline studies, including the clinical assessments. Dr Plantone carried out the 1 year follow-ups

for the SPMS patients and some of the PPMS patients and healthy controls (N=7). I carried out the clinical assessments for the remaining PPMS patients (N=19) and healthy controls (N=22) as these were the same PPMS patients involved in the study presented in Chapter V. The radiographers at the Institute of Neurology performed all the MRI scans at the two time points (Marios Yiannakas, Chichi Ugorji and Luke Hoy). I performed the analysis on the spinal cord data and the brain data using the Active Surface Model and SIENA respectively to compute the spinal cord atrophy and brain atrophy measurements at baseline and 1 year follow-up. Dr. Dan Altmann and Dr. Carmen Tur performed the statistical analysis for this study. I interpreted the results from the statistical analysis performed and the results and my interpretation of the results are outlined below.

6.2.2 Clinical Assessments

At the time of the MRI, all patients were clinically assessed with the EDSS (Kurtzke, 1983), 9-HPT (Goodkin *et al.*, 1988) and TWT (Cutter *et al.*, 1999). Z-scores were calculated for the 9-HPT and TWT from normative values displayed in the National Multiple Sclerosis Society Task Force database (Fischer *et al.*, 1999). Mean grip strength from the upper and lower limbs were measured using the Jamar hydraulic dynamometer (Sammons Preston. Incorporated, Bolingbrook, IL, USA) (Svens & Lee, 2005). I also recorded the American Spinal Injury Association (ASIA) motor (m) and sensory (s) scores (Maynard *et al.*, 1997) for all subjects with MS.

6.2.3 MRI acquisition

All subjects were scanned at 3T using a Philips Achieva MRI system at baseline and at 1 year follow-up, using the manufacturer's 16 – channel neurovascular coil (Philips Healthcare Systems, Best, Netherlands). The cervical cord was imaged in the axial plane, perpendicular to the longitudinal axis of the cord, to measure the cord mean cross sectional area. The imaging volume was centred on the C2/3 intervertebral disc, using a fat – suppressed 3D slab-selective fast field echo (FFE) sequence [parameters; TR = 23ms; TE = 5ms; flip angle $\alpha = 7^\circ$; FOV = 240 x 180mm²; voxel size = 0.5 x 0.5 x 5 mm³; NEX = 8; 11 axial contiguous slices].

For calculation of brain volumes, a 3D T1-weighted magnetisation-prepared gradient-echo sequence was used [TR = 6.9 ms; TE = 3.1 ms; flip angle $\alpha = 8^\circ$; FOV= 256 x 256 mm²; voxel size = 1 x 1 x 1 mm³; NEX = 1; 180 sagittal contiguous slices].

For calculation of brain T2 lesion volumes, PD/T2 weighted images were acquired using a dual-echo TSE sequence [parameters: TR = 3500 ms; TE = 15/85 ms; flip angle $\alpha = 90^\circ$; FOV= 240 x 180 mm²; voxel size = 1 x 1 x 3 mm³; NEX = 1; 50 axial contiguous slices].

6.3 MRI analysis

6.3.1 Spinal cord area measurement

For the 3D-FFE images, three contiguous 5mm axial slices, centred on C2/3 disc were segmented using the active surface model (ASM) (Horsfield *et al.*, 2010), as discussed in *Section 2.9.3.2*. Spinal cord cross sectional area measurements were performed using the 3D-FFE dataset in Jim 6.0 Software (Xinapse systems,

Northants, England). The mean cross sectional area of the three slices was then calculated. The ASM involves placing a predetermined size and shape region of interest in the centre of the cord on each slice. The program then uses intensity gradient information to calculate the radius and centre of each slice (Horsfield *et al.*, 2010). The centre line is refined from the initial user estimate and segmentation then involves a multistage approach allowing greater complexity of the cord radius to be calculated (Horsfield *et al.*, 2010). The cord outline is generated automatically for each slice, as shown in **Figure 6.1**.

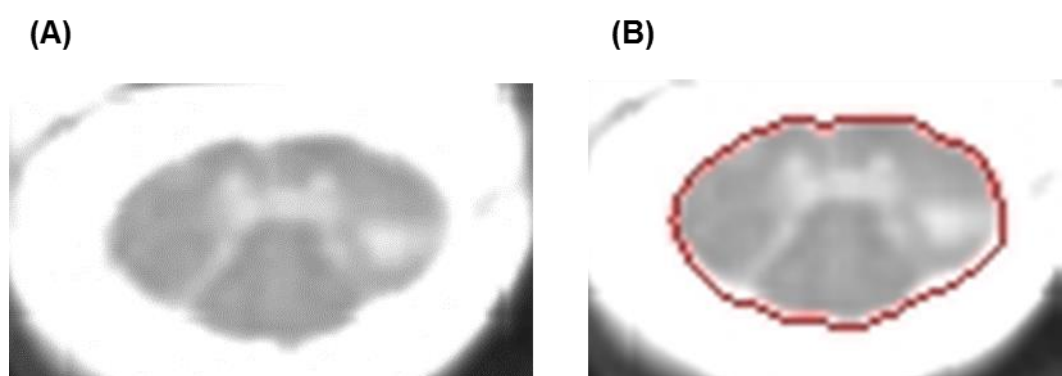


Figure 6.1: Spinal cord outline using the active surface model on the axial FFE images, FFE image in (A) and the cord outline in red using the active surface model (B).

6.3.2 Brain atrophy measurement

To avoid segmentation errors due to white matter lesions, an automated lesion-filling technique was employed (Chard *et al.*, 2010). Lesion masks were created based on 3D-T1 weighted sequences without reference to previously created masks on T2-weighted images. The lesion-filled images were segmented using STEPS (Cardoso *et al.*, 2013). STEPS is a multi-atlas segmentation propagation technique, which uses an atlas library of 682 non-MS patients with associated

manual segmentations, of which the 30 most similar brain templates were used during a locally-weighted label fusion process.

Using these brain masks, Structural Image Evaluation using Normalization of Atrophy (SIENA) were calculated. SIENA is a registration based method which computes atrophy between two aligned scans as the perpendicular edge displacement at each edge point, as discussed in *Section 2.8.2*. The mean edge displacement is converted into a global estimate of Percent Brain Volume Change (PBVC) between two time-points, using self-calibration based on registering both time points to the half-way space between them (Smith et al., 2001). Spinal cord and brain atrophy measures have been annualised.

6.3.3 Brain T2 lesion volume

Brain T2-lesion volume (T2LV) was calculated by outlining lesions on T2-weighted MRI scans using a semi-automated edge finding tool (JIM v. 6.0). Total lesion volume was recorded in ml for each subject.

6.4 Statistical analysis

All analyses were performed in Stata 13.1 (Stata Corporation, College Station, Texas, USA).

Changes in clinical measures over time were assessed through paired t-tests. To assess differences in the rate of change in cord area over time between patients and controls, I first calculated the individual changes in cord area between baseline and 1 year of follow-up. Then I fit a multiple linear regression model with 'change in cord area' as the dependent variable and the binary variable 'group' (patients or controls) as the main predictor variable. This model was adjusted for

age and gender. Changes in lesion load and PBVC over the same period of time were also explored as covariates. To assess differences between the two patient subgroups and controls, similar models were fitted, but using a 3-category variable 'group' (SPMS, PPMS or controls) as the main predictor.

To assess the association between clinical and cord area changes over 1 year, again individual changes in the clinical variable were calculated. Then, multiple linear regression models including the change in the clinical variable as the dependent variable were fitted, including the change in cord area over time as the main predictor variable. These models were fitted for each one of the clinical variables separately using the whole cohort of patients, and were adjusted for age and gender. Afterwards, in order to examine the relationship between clinical and cord area changes in the two patient groups, similar models were fitted but adding a binary variable 'group' (SPMS or PPMS) and an interaction term 'group X cord area changes' among the covariates.

Sample size calculations were performed to detect different plausible treatment effects (with 80% power at 5% statistical significance) based on the observed differences between patients and controls.

Statistical significance was considered when p values were below 0.05.

6.5 Results

6.5.1 Participant demographics and characteristics

Forty-four patients with progressive MS, and 29 healthy controls were studied at baseline and after one year. Out of the 26 PPMS patients included in this retrospective study, 19 of the PPMS patients were from the study presented in

Chapter V. Patient demographics, characteristics and disability of all progressive patients together and of the PPMS and SPMS subgroups are summarised in **Table 6.1**. There was a significant difference in age between the progressive MS cohort and the healthy controls ($p < 0.001$). At baseline, PPMS patients had significantly shorter disease duration ($p < 0.0001$), lower EDSS ($p < 0.004$), lower brain T2 lesion volume ($p < 0.001$) and larger spinal cord area ($p < 0.02$) than SPMS patients. The duration of progressive disease was similar in both PPMS and SPMS (See **Table 6.1**).

	Progressive MS N=44	Healthy controls N=29	PPMS N=26	SPMS N=18
Mean Age (years)	52.02 (9.33)	42.36 (11.16)	50.27 (9.68)	54.88 (8.23)
Gender (F:M)	21:23	11:18	11:15	10:8
Disease duration (years)	14.13 (12.41)	-	7.17 (4.98)	26.20 (12.23)***
Progressive disease duration	7.30 (4.42)	-	7.17 (4.98)	7.92 (3.75)
Median EDSS (range) baseline	6.0 (3.0 – 8.5)	-	5.0 (3.0 – 7.5)	6.0 (4.0 – 8.5)***
Median EDSS (range) 1 year	6.5 (3.0 – 8.5)*	-	6.0 (3.0 – 8.0)*	6.5 (4.5 – 8.5)*
Mean cord area baseline (mm ²)	73.82 (10.33)**	82.49 (8.57)	76.40 (9.90)**	69.78 (10.84)**
Mean cord area 1Y (mm ²)	71.52 (10.16)**	82.05 (8.34)	73.63 (9.30)**	68.29 (10.83)**
% decrease in CSA	-3.11	-0.53	-3.63	-2.14
PBVC	-1.57 (1.03)**	-0.42 (1.03)	-1.65 (1.16)**	-1.40 (0.73)**
T2 lesion load (mls) - baseline	15.71 (13.53)	-	11.09 (10.52)	23.92 (14.66)
T2 lesion load (mls) – 1 year	20.14 (17.34)*	-	13.29 (13.36)*	30.42 (17.87)*

Table 6.1: Mean (SD) of main demographic and clinical findings in the progressive MS, healthy controls, PPMS and SPMS cohorts at 1 year. * Paired sample t-test comparing baseline with 1 year follow-up. ** Linear regression model comparing patients with controls, correcting for age and gender, p<0.05. *** Independent sample t-test comparing PPMS with SPMS. Those numbers highlighted in bold have a significant p-value <0.5. CSA - cross sectional cord area.

6.5.2 Spinal cord atrophy

Patients had a smaller spinal cord area at both baseline and one year follow-up compared to controls (**Table 6.1**). The rate of change in cord atrophy in the progressive MS cohort over this 12-month period was 1.80 mm² greater than in controls after adjusting for age and gender (95% confidence intervals (CI) -3.00 to -0.61, $p < 0.004$). This corresponded to a 3.11% decrease in spinal cord area over one year.

Looking at the sub-group analyses, the rate of change in cord area in the PPMS subgroup was 2.23mm² greater than controls (95% CI -3.55 to -0.91, $p < 0.001$) (percentage decrease in cord area = 3.63%). An example of this is shown in **Figure 6.2**. The rate of change in cord area in the SPMS subgroup was 1.10 mm² greater than controls, but this was not statistically significant (95% CI -2.62 to 0.42, $p < 0.15$) (percentage decrease in cord area = 2.14%). Healthy controls had a reduction in cord area of 0.53%.

(A) Baseline



(B) 1 Year



Figure 6.2: FFE image at baseline **(A)** and 1 year follow-up **(B)** with visible evidence of cord atrophy in a subject with PPMS (47 year old male, baseline: EDSS 4.0, cord area = 85.95mm²; 1 year: EDSS 6.0, cord area = 82.37mm²).

6.5.3 Brain atrophy

PBVC was significantly greater in the progressive MS cohort at -1.57% when compared to controls after adjusting for age and gender over the 12 months (95% CI -0.56 to -1.76, $p < 0.0001$). Looking at the subgroup analysis, the PPMS subgroup had significantly greater PBVC at -1.65% when compared to controls (95% CI -0.56 to -1.97, $p < 0.001$) and the SPMS subgroup also had significantly greater PBVC at -1.40% when compared to controls (95% CI -0.04 to -1.64, $p < 0.04$) after correcting for age and gender. The PBVC for controls over the 12 months was -0.42%. There was also a significant increase in T2 lesion load in the progressive MS cohort over the 12 months (**Table 6.1**).

In order to complete the analysis, all the above models were repeated correcting for T2 lesion load and PBVC. PBVC and T2 lesion load were never significant when included in the models and did not change the direction of the results for the spinal cord atrophy measures, therefore these covariates were not included in the final model.

6.5.4 Associations between change in cord area and change in clinical scores

Patients worsened in all clinical measures during the 12-month follow-up period. In particular, they progressed significantly in EDSS ($p < 0.001$), ASIA-motor scores ($p < 0.013$), 9-HPT ($p < 0.001$) and grip strength ($p < 0.001$), as outlined in **Table 6.2**.

	Progressive MS*	PPMS*	SPMS*
Mean 9-HPT baseline (z score)	-0.88 (1.24)	-0.62 (0.95)	-1.31 (1.55)
Mean 9-HPT 1 year (z score)	-1.26 (1.29)	-1.07 (1.18)	-1.58 (1.44)
Mean TWT baseline (z score)	-2.13 (5.22)	-0.49 (2.91)	-4.84 (6.94)
Mean TWT 1 year (z score)	-3.06 (6.07)	-1.05 (3.98)	-6.36 (7.49)
Mean Grip Strength baseline (kg force)	32.46 (26.45)	45.30 (27.29)	15.33 (11.81)
Mean Grip Strength 1 year (kg force)	17.53 (11.45)	20.13 (12.31)	14.07 (9.50)
ASIA – motor baseline	85.37 (14.78)	88.92 (11.92)	80.44 (17.17)
ASIA – motor 1 year	80.19 (19.99)	85.52 (12.83)	72.78 (25.58)
ASIA – sensory (pin prick) baseline	105.39 (6.40)	108.13 (6.05)	102.65 (6.78)
ASIA – sensory (pin prick) 1 year	103.73 (10.06)	105.46 (11.43)	101.29 (7.38)

Table 6.2: Mean (SD) of clinical scores at baseline and 1 year follow-up. * Paired sample t-test comparing baseline with 1 year follow-up. Those numbers highlighted in bold have a significant p-value <0.5.

No significant associations were demonstrated between change in cord area and change in clinical scores in the progressive MS cohort over the 12-month follow-up period. When I investigated the two patient groups, PPMS patients demonstrated a significant decrease in 9-HPT of 0.11 (95% CIs 0.02, 0.20, $p < 0.02$) for each mm^2 decrease in cord area and borderline evidence of an increase in EDSS of 0.12 (95% CIs -0.25, 0.10, $p = 0.06$), over the 12-month follow-up, after correcting for age and gender. **Figures 6.3** and **6.4** are scatter plots demonstrating the unadjusted correlations between change in cord area and change in EDSS (**Figure 6.3**) and change in 9-HPT (**Figure 6.4**) in the PPMS

subgroup. In SPMS, there was no significant association between change in cord area and change in clinical scores.

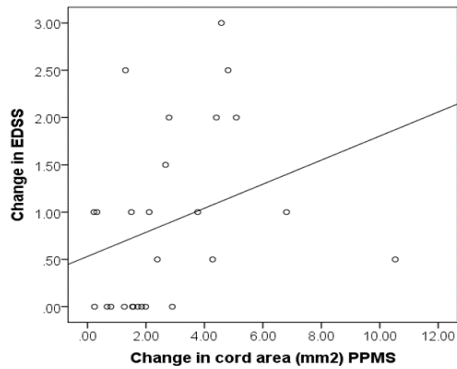


Figure 6.3: Scatterplot showing the association between changes in spinal cord area (mm²) with change in EDSS in the PPMS cohort (unadjusted analysis).

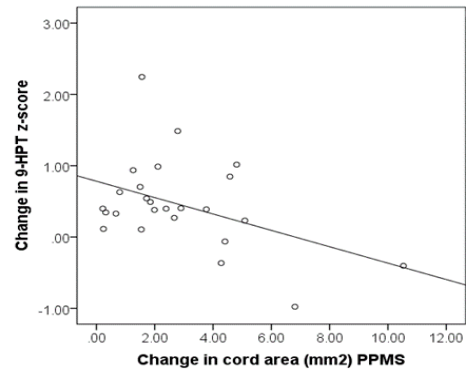


Figure 6.4: Scatterplot showing the association between changes in spinal cord area (mm²) with change in 9-HPT z-scores in the PPMS cohort (unadjusted analysis).

6.5.5 Sample size calculations for a neuroprotective clinical trial

Sample size calculations for the whole group analysis, in a 12-month neuroprotective clinical trial, demonstrated the minimum sample sizes per arm required to detect a 50% treatment effect at 80% power were 157 per arm; when the two cohorts were analysed separately, the minimum sample size per arm reduced to 86 in the PPMS sub-group and increased to 709 in the SPMS sub-group, as seen in **Table 6.3**.

Treatment Effect	Sample size per arm in progressive MS	Sample size per arm in PPMS	Sample size per arm in SPMS
30%	436	238	1968
50%	157	86	709
100%	40	22	178

Table 6.3: Sample size calculations for a neuroprotective clinical trial in progressive MS (80% power, 5% significance).

6.6 Discussion

Our single-centre study was consistent with previous results in showing significant cord atrophy in the progressive MS cohort when compared to healthy controls over 1 year. The PPMS subgroup, who had shorter disease duration, lower EDSS, and larger cord area compared with SPMS, showed the fastest reduction in spinal cord cross sectional area. Sample size calculations gave realistically achievable numbers of patients per arm in the PPMS group, though this was not the case in those with SPMS. Thus spinal cord area shows potential

to be a feasible outcome measure for inclusion in single-centre, placebo-controlled neuroprotective trials in PPMS. We will discuss each of these results in turn.

Decrease in spinal cord area is a marker of cord atrophy, which in turn is an approximate marker of axonal loss. A post-mortem study found that cord atrophy occurred more rapidly in the early stages of progressive MS (Evangelou *et al.*, 2005), underlining the importance of early therapeutic intervention in this population (Evangelou *et al.*, 2005), in order to minimise the amount of axonal loss, in neuroprotective clinical trials. This is reflected in the results from this study, where there was a significant difference in cross sectional cord area between PPMS patients and controls, but not between SPMS patients and controls. This is shown in the better performance of cord atrophy measures in the PPMS subgroup (who were early on in the disease course) compared to the SPMS subgroup. The SPMS subjects were older, had longer disease duration and were more disabled than those with PPMS, they had more marked spinal cord atrophy at the study baseline and had a lower rate in cord area reduction over time than the PPMS subjects (SPMS 2.14% vs. PPMS 3.63%). The PPMS subgroup had less cord atrophy at baseline and therefore had more to lose over time, while the critical loss of axons may have already occurred in the SPMS subgroup. This raises the possibility that cord atrophy may not be a useful biomarker in SPMS. The better performance of cord atrophy measures in the PPMS subgroup compared to the SPMS subgroup may be important in understanding progressive MS as well as in using cord atrophy as an outcome measure in clinical trials. A question arising is whether the rate of spinal cord atrophy has occurred in a non-linear fashion over time in the SPMS cohort and

would have been greater in earlier years. A long term study that follows people from RRMS through to SPMS would be required to clarify the temporal dynamics of spinal cord atrophy in relapse-onset MS.

PBVC in the progressive MS cohort over the 12 months was significantly greater than that observed in the controls. There was a greater increase in PBVC in the PPMS subgroup compared to the SPMS subgroup.

This is in keeping with the spinal cord atrophy measures, demonstrating the faster development of both cord and brain atrophy in the PPMS subgroup. Brain atrophy measures have been demonstrated to be robust outcome measures in phase 2 and phase 3 clinical trials in primary and secondary progressive MS (Chataway et al., 2014; Kapoor et al., 2010).

6.6.1 Clinical correlations

The progressive MS cohort significantly progressed in a number of clinical measures over 1 year, including EDSS, ASIA-motor scores, 9-HPT and grip strength, as expected in a cohort of patients with progressive MS. However, there were no significant associations between change in cord area and change in clinical scores in the progressive MS cohort. This may be due to the very short follow-up period and the small sample size of the study, which makes it difficult to detect significant associations. Also, the patients recruited into this study were not recruited based on clinical progression in the year prior to recruitment, as this was a retrospective study and patients were not selected on the basis of this criterion.

In the PPMS subgroup, change in cord area was significantly associated with change (deterioration) in the 9-HPT and a borderline association with change (increase) in EDSS, which is in keeping with previous studies, reflecting the correlation which has been established between cord area and disability (Bot *et al.*, 2004; Lin *et al.*, 2004). The lack of a significant association between change in clinical measures and change in cord area in the SPMS subgroup, may be due to the smaller sample size of SPMS subjects (N=18) recruited into this study compared to the PPMS (N=26) cohort.

Of note, none of the patients included in this study were on disease modifying therapy at the time of scanning, either at baseline or at 1 year follow-up. Therefore the effects of treatment on atrophy measures is not something which we need to consider with this progressive MS cohort. It has been demonstrated that patients participating in clinical trials often have active disease with clinical relapses and evidence of gadolinium enhancing lesions on MRI, particularly in RRMS cohorts. Resolution of this inflammation results in an initial accelerated decrease in brain volume during the first year of treatment, which is termed pseudoatrophy (Zivadinov *et al.*, 2008). It is not known if the effects of pseudoatrophy continue to occur after one year. This needs to be further investigated to determine the full extent of pseudoatrophy after the initiation of certain therapies which may be related to resolution of inflammation as opposed to neurodegeneration (De Stefano and Arnold, 2015).

A number of newer disease modifying agents available (natalizumab, dimethyl-fumarate, fingolimod, alemtuzumab) for the treatment of RRMS, have incorporated brain volume as an outcome measure and have shown to improve

brain atrophy accrual when compared to placebo or another treatment (Vidal-Jordana *et al.*, 2015; Miller *et al.*, 2007b; Miller *et al.*, 2015; Radue *et al.*, 2012; Coles *et al.*, 2008; Cohen *et al.*, 2012). To date only one phase II clinical trial in SPMS have had positive effects on brain atrophy (Chataway *et al.*, 2014).

To date, the effect of disease modifying therapy on spinal cord atrophy is unknown as spinal cord atrophy has only been used as an outcome measure in one clinical trial in PPMS. The INFORMS trials in PPMS, which investigated the effect of fingolimod on both brain and spinal cord atrophy was negative for both these measures.

6.6.2 Sample size

The overall sample size calculations gave achievable numbers of patients per arm in the progressive MS cohort. The PPMS group, who had shorter disease duration but had a similar progressive disease duration to SPMS, had smaller numbers per arm. The sample size calculations for the SPMS subgroup gave exorbitantly high numbers per arm (N=709), which is not a realistic number for a Phase II clinical trial, unlike the PPMS subgroup (N=86). This highlights the importance of recruiting subjects early in the primary progressive disease course into clinical trials and raises the question if cord atrophy behaves differently in SPMS as a result of the longer disease duration rather than the duration of progressive disease and the more marked spinal cord atrophy at baseline. It is likely that these numbers could be further reduced by recruiting only subjects with a history of disease progression in the previous 12 months.

The active surface model has been used in one large cross-sectional multicentre study in MS, to detect cord atrophy, and confirmed the stability of this measure

among different centres and supports its use as an outcome measure to monitor disease progression in multicentre trials (Rocca *et al.*, 2011). However, the challenges in assessing small absolute changes longitudinally in the size of a small structure should not be underestimated and in the real world setting of large, multicentre, long term, phase III clinical trials, methodological variability includes the use of multiple acquisition sequences and multiple scanner models, software and hardware upgrades and changes in scanners during follow up. Such methodological factors may require larger sample sizes than I have estimated from out single centre/scanner study (Yaldizli *et al.*, 2015). Notwithstanding this, the importance of good image quality and analysis method are crucial for measuring spinal cord atrophy in order to obtain acceptable sample size estimates. Therefore, spinal cord atrophy has the potential to be used as an outcome measure in clinical trials with therapies that target neurodegeneration.

Sample sizes for brain atrophy as an outcome measure in clinical trials in MS using registration based techniques like SIENA or BSI have demonstrated achievable numbers of patients in both RRMS (Anderson *et al.*, 2007) and SPMS (Altmann *et al.*, 2009). This has led to the use of brain atrophy as an outcome measure in multiple clinical trials in MS, both relapsing remitting and progressive forms of MS (Chataway *et al.*, 2014; Kapoor *et al.*, 2010). It has been demonstrated that whole brain atrophy is highly reproducible and sensitive to disease related changes, as well as correlating with disability.

To date, the lack of a registration based method for detecting spinal cord atrophy has limited its ability to be used in a multicentre clinical trial in MS. One clinical trial in PPMS measured spinal cord atrophy in this cohort and results

demonstrated extremely high numbers of patients were required to detect a 50% treatment effect on spinal cord atrophy (Yaldizli *et al.*, 2015). To date segmentation based methods are only available for measuring longitudinal change in spinal cord atrophy unlike brain atrophy where registration based methods are available. This is an ongoing limitation for measuring longitudinal change in spinal cord atrophy. Our research group is working on this and it is looking at developing a BSI technique for the spinal cord, like what is used in the brain (Prados *et al.*, 2016). I await a fully validated registration based technique for measuring spinal cord atrophy and I hope this will give more achievable sample sizes, particularly in a multicentre setting.

6.7 Conclusion

Cord atrophy in progressive MS, especially in PPMS, can be observed over a period of time as short as 1 year. Based on this single centre, single scanner data, sample size calculations gave acceptable numbers of patients per arm, suggesting spinal cord atrophy shows potential to be a feasible outcome measure for placebo-controlled neuroprotective trials in early PPMS. The better performance of cord atrophy measures in the PPMS than the SPMS group, may be due to their earlier stage of disease and less cord atrophy at baseline. This may be important in improving our understanding of cord atrophy in progressive MS, and raises the possibility that cord atrophy may not be a useful outcome measure in SPMS with long disease duration.

CHAPTER VII

Conclusions and future directions

7.1 Conclusions

In this final chapter, the conclusions drawn from the studies presented in this thesis will be summarised in order to address the fundamental aim of this thesis, to investigate the development of new imaging biomarkers in MS.

The United Kingdom Medical Research Council has defined a biomarker as “*an objective measurement that acts as an indicator of normal pathological processes, pathogenic processes or pharmacologic responses to therapeutic intervention*” (<http://www.mrc.ac.uk>). Imaging biomarkers can range from biomarkers associated with diagnosis, biomarkers associated with concurrent and future disability and biomarkers which are endpoints of clinical trials. The studies carried out as part of this thesis are predominantly focused on biomarkers that reflect the underlying pathology and may be responsible for clinical disability.

A combination of innovative MRI techniques, applied to the brain of MS subjects, was explored in Chapter III and Chapter IV. These techniques were single voxel GABA spectroscopy and NODDI respectively. More established imaging measures of the spinal cord were then used in two further studies presented in Chapter V and Chapter VI. These included single voxel spectroscopy, Q-space imaging and spinal cord atrophy measurements. Each of these biomarkers is focused on neurodegeneration, which is a major cause of ongoing, irreversible disability, particularly in the progressive stages of MS.

In the study presented in Chapter III, there was reduced GABA in the sensorimotor cortex and in the hippocampus of patients with SPMS when compared to controls and reduced GABA in the sensorimotor cortex was associated with motor disability. These findings suggest that reduced GABA

levels may reflect pathological abnormalities that may play a role in determining physical disability. These abnormalities may include decreases in the pre- and post-synaptic components of GABA neurotransmission and in the density of inhibitory neurons. Additionally, the reduced GABA concentration may contribute to the neurodegenerative process, resulting in increased firing of axons, with consequent increased energy demands, which may lead to neuroaxonal degeneration and loss of the compensatory mechanisms that maintain motor function. This study supports the idea that modulation of GABA neurotransmission, which can be quantified using MRS, may be an important biomarker of neurodegeneration and a potential target for neuroprotection in MS which needs to be further investigated.

Chapter IV presented the results from a study in RRMS looking at a new advanced diffusion MRI technique, NODDI. The study found there was reduced NDI in NAWM in the brain of RRMS patients when compared to controls, in addition to a reduction in both NDI and ODI in T2 lesions. The results from studies carried out to date in MS using NODDI and in this study, are demonstrating the advantage of NODDI over standard DTI in estimating neurite density and dispersion, both of which are thought to influence FA independently. Therefore, NODDI has the ability to improve the characterisation of microstructural damage in the brain of MS patients. When NODDI was initially developed it was thought that NDI solely represented neurite density, raising the possibility that it may have the potential to be a useful axonal biomarker. However, recent histological work has proved that NDI is influenced by both axonal loss and/or demyelination, therefore disproving its ability to be a sole biomarker of axonal loss.

Chapter V presented a longitudinal follow-up spinal cord study in a cohort of patients with early PPMS, looking at a number of advanced quantitative MRI techniques, specifically Q-space imaging and ¹H-MR spectroscopy in the cervical cord, in addition to spinal cord cross sectional area. Despite no significant difference in spinal cord area between the PPMS patients and the control group at baseline, spinal cord area was the only MRI metric which demonstrated a significant change (reduction) over the 12 month follow-up period. These findings demonstrate evidence of ongoing neurodegeneration in the spinal cord in early PPMS detected using spinal cord atrophy over a relatively short follow-up period. Q-space imaging metrics did not change significantly over the 12 months. However, Q-space imaging metrics at baseline significantly predicted EDSS and postural stability at 1 year, whilst the study also found significant associations between change in Q-space metrics and change in clinical status over 1 year, which may suggest Q-space imaging is a useful biomarker that is capable of detecting clinically meaningful pathology, which requires further investigation. I were surprised that there were no significant changes over time in any of the advanced MRI techniques, as it was hoped, based on previous work, that these techniques may be more sensitive at detecting pathological changes in MS compared with more well established techniques. The short follow-up period may account for the lack of any significant changes in these metrics.

Spinal cord atrophy is an approximate marker of neuroaxonal loss, which is one of the main mechanisms driving irreversible disability in MS. It has been demonstrated that the rate of cord atrophy is greater than the rate of brain atrophy in MS. However, to date brain atrophy has been included as an outcome measure in neuroprotective clinical trials in progressive MS, while spinal cord atrophy has

not. The study in Chapter VI found a significant reduction in cross sectional cord area in a cohort of patients with progressive MS when compared to controls over a 12 month follow-up period. There was a greater rate of cord atrophy in the PPMS subgroup compared to the SPMS subgroup despite both groups having a similar duration of progressive disease. This may be related to the earlier stage of disease in the PPMS cohort and less marked cord atrophy at baseline, which may be important in helping us understand progressive MS. The sample size calculations gave achievable numbers of patients for the PPMS cohort, supporting cord atrophy as a biomarker of neuroaxonal loss in the cord and also an outcome measure in phase II neuroprotective trials, especially in early PPMS. The very large sample size estimates for the SPMS cohort, raises the question if PPMS and SPMS should be kept separate in clinical trials (Lublin *et al.*, 2014), as SPMS may behave differently to PPMS due to longer disease duration. To date, clinical trials have been carried out separately in each cohort.

In relation to the statistical analysis used in the studies carried out as part of this thesis, I used a strict cut-off: any results which had a $p < 0.05$, and therefore confidence intervals did not contain the null value, were determined significant and any results with a $p > 0.05$ and the confidence intervals included the null value were deemed not significant. The main reason for doing this was because I carried out a lot of clinical tests with quite a lot of significant results in the studies. To try and reduce the reporting of a lot of borderline significant results, I focused on those results where there was strong evidence against the null hypothesis.

The use of strict P-values has weaknesses. When multiple independent hypotheses are tested, the risk that at least one of the tests used is falsely positive is high and this risk increases with the number of hypotheses tested.

You may be incurring a type I error: you may consider as significant an association that does not exist. The risk of this type of error is greater if you carry out multiple tests. You may also incur a type II error: where you may consider as non-significant an association that truly exists. The risk of this type of error is greater if the sample size is small.

Multiple comparisons refer to the simultaneous testing of a large number of statistical tests, which increases the likelihood of significant results ($p < 0.05$) purely by chance alone. The commonest approach to the multiple comparison problem is not to set the critical level of significance to $p < 0.05$, but to use a lower critical value of significance. The most common way of doing this is to perform a Bonferroni correction, where you divide the p-value by the number of tests performed. The Bonferroni correction is mainly used when there are a small number of multiple comparisons and one is looking for one or two which may be significant. If one has a large number of multiple comparisons and looking for quite a few significant results, then the Bonferroni correction is conservative and it may lead to a high rate of false negative results, therefore reducing statistical power. There is a lot of debate if a correction should be made or not when there are multiple comparisons. With the Bonferroni correction, as you reduce the risk of a Type I error, you increase the risk of a Type II error, so real differences may not be detected. The interpretation of a single test may depend on a number of other tests performed, therefore the evidence provided by the data is contained

within that specific data. As a result, the conclusions drawn from that dataset should not be altered based on the number of other tests performed. As part of the studies which I did as part of this thesis, I did not perform any Bonferroni corrections due to the limitations associated with it as discussed above.

7.2 Future directions

The studies presented in this thesis demonstrate that novel imaging biomarkers have the potential, to help us improve our understanding of the pathogenesis in progressive and relapsing forms of MS. The International Collaboration in Progressive MS have highlighted that the key to the successful development of therapies in progressive MS is in the development of biomarkers which are directly linked to the underlying pathology (Thompson, 2015). This is particularly important for phase II clinical trials.

To build on the work carried out as part of this thesis, I propose the following research projects as a further stepping stone to help develop improved imaging biomarkers which are accurate, reproducible, sensitive to disease changes, correlates with and predicts relevant clinical measures, are user friendly and quantitative (Filippi & Agosta, 2010), to ultimately improve our understanding of the pathogenesis of MS and to help develop more successful treatments.

For the GABA spectroscopy study in SPMS (Chapter III), in the future, it will be important to follow these patients up over time to see what happens to the GABA concentration in these regions - will GABA continue to decline in the sensorimotor cortex and in the hippocampus and will GABA in the sensorimotor cortex be associated with the progression of motor disability, which may provide further support for the role of GABA in the neurodegenerative process in SPMS. A GABA

spectroscopy study in RRMS is needed, to see how GABA levels differ to patients with progressive MS. Also, it would be very useful to combine PET imaging, in particular ^{11}C -flumazenil, with ^1H -MR spectroscopy, to investigate the co-localisation of the PET signal changes (reflecting GABA_A receptor density), with the ^1H -MR spectroscopy derived GABA changes, to investigate if GABA is reflecting mechanisms in the grey matter that are crucial to disability and therefore may be a potential pharmacological target in SPMS.

Potential future studies which may be useful for the application of NODDI, would be to investigate the longitudinal changes in NODDI metrics over time in MS subjects, to investigate its ability to detect microstructural changes over time using NDI and ODI and its association with clinical disability. Other MRI techniques e.g. magnetisation transfer imaging and myelin water imaging, may complement NODDI and provide a more complete picture of the effects of MS on brain and spinal cord tissue. Ultimately, when developing imaging biomarkers, one question which arises is how applicable is the imaging biomarker to multicentre clinical trials. Overall, to date the evidence suggests NODDI is slightly superior to DTI, but in my opinion, it does not have the ability to be used in a multicentre setting, as standardization and optimization of this technique across centres may be challenging, as well as it lacking a direct link to specific underlying pathology in MS.

Results presented in Chapter V have shown that Q-space imaging metrics may be capable of detecting clinically relevant spinal cord pathology, as well as being a prognostic marker of disability progression. As well as this spinal cord atrophy was the only MRI metric which was significantly different between patients and

controls over time. A three year follow-up study, currently underway, will investigate if these findings are maintained over a longer time period. It will be interesting to see if significant changes in Q-space metrics are detected, particularly in the posterior and lateral columns. Quantitative MRI techniques remain technically challenging in the spinal cord, but can provide very valuable information on the microstructural changes occurring within tissues. Multi-parametric imaging models are very important for the future, to help improve our understanding of the interactions between the structural and metabolic abnormalities occurring in MS.

The spinal cord is a very small structure, making detection of absolute changes in area very difficult to accurately measure particularly in a multicentre setting. The variability between sites including different scanners, different acquisition sequences, upgrade in software and scanners between time points makes spinal cord atrophy as an outcome measure in clinical trials very challenging. There is an urgent need to develop a more standardised and fully automatic method for the detection of spinal cord atrophy over time, similar to what is available for the detection of longitudinal changes in brain atrophy e.g. SIENA. One such method, which is being investigated at UCL, is Boundary Shift Integral (BSI) using non-binary segmentations of the baseline and repeated scans, in order to better localise and capture atrophy. BSI is a well-recognised technique for measuring brain volume change (Freeborough *et al.*, 1997). The method assumes that a change in the volume of tissue must be associated with an exact shift in the boundary of the tissue. The change in volume is then estimated by computing the integral of all boundary shifts between the time points (Fox *et al.*, 1997). However, to date it has not been successfully applied to the spinal cord. In a control group,

there was a smaller confidence interval and coefficient of variation using the BSI technique in the spinal cord when compared to cross-sectional cord area measurements using the active surface model (Prados *et al.*, 2016). This new technique now needs to be applied to a cohort of patients with MS. A voxel-based analysis of spinal cord atrophy has also been carried out (Rocca *et al.*, 2013), which has the potential to provide regional atrophy measurements in MS, which would be very useful. One of the main limitations of BSI and voxel based measurements in the spinal cord, is the accurate registration of the images, which is very difficult to achieve in the spinal cord due to the high prevalence of motion artefacts in spinal cord imaging.

In conclusion, the studies carried out as part of this thesis looked at a number of different imaging biomarkers, to investigate different pathological mechanisms potentially underlying MS and contributing to disability. A combination of different MRI modalities, such as PET imaging, ¹H-MR spectroscopy specifically looking at Ins, Glx and GABA, spinal cord atrophy and newer contrast agents which are specific to different aspects of MS pathology, such as microglial and monocyte activation, gliosis, glutamate mediated excitotoxicity, neurodegeneration and inflammation, may be the best way to proceed in the future, to ultimately improve our understanding of the mechanisms involved in the pathogenesis of MS.

References

- Abdel-Aziz, K., Schneider, T., Solanky, B. S., Yiannakas, M. C., Altmann, D. R., Wheeler-Kingshott, C. A., Peters, A. L., Day, B. L., Thompson, A. J. & Ciccarelli, O. 2015. Evidence for early neurodegeneration in the cervical cord of patients with primary progressive multiple sclerosis. *Brain*.
- Aboul-Enein, F., Krassak, M., Hoftberger, R., Prayer, D. & Kristoferitsch, W. 2010. Reduced NAA-levels in the NAWM of patients with MS is a feature of progression. A study with quantitative magnetic resonance spectroscopy at 3 Tesla. *PLoS One*, 5, e11625.
- Achnichts, L., Gonen, O., Rigotti, D. J., Babb, J. S., Naegelin, Y., Penner, I. K., Bendfeldt, K., Hirsch, J., Amann, M., Kappos, L. & Gass, A. 2013. Global N-acetylaspartate concentration in benign and non-benign multiple sclerosis patients of long disease duration. *Eur J Radiol*, 82, e848-52.
- Alexander, A. L., Hasan, K. M., Lazar, M., Tsuruda, J. S. & Parker, D. L. 2001. Analysis of partial volume effects in diffusion-tensor MRI. *Magn Reson Med*, 45, 770-80.
- Altmann, D. R., Jasperse, B., Barkhof, F., Beckmann, K., Filippi, M., Kappos, L. D., Molyneux, P., Polman, C. H., Pozzilli, C., Thompson, A. J., Wagner, K., Yousry, T. A. & Miller, D. H. 2009. Sample sizes for brain atrophy outcomes in trials for secondary progressive multiple sclerosis. *Neurology*, 72, 595-601.
- Amato, M. P., Portaccio, E., Goretti, B., Zipolli, V., Hakiki, B., Giannini, M., et al. 2010. Cognitive impairment in early stages of multiple sclerosis. *Neurol Sci*, 31, S211-4.
- Anderson, V. M., Fernando, K. T., Davies, G. R., Rashid, W., Frost, C., Fox, N. C. & Miller, D. H. 2007. Cerebral atrophy measurement in clinically isolated syndromes and relapsing remitting multiple sclerosis: a comparison of registration-based methods. *J Neuroimaging*, 17, 61-8.
- Andersson, J. L. & Sotiropoulos, S. N. 2016. An integrated approach to correction for off-resonance effects and subject movement in diffusion MR imaging. *Neuroimage*, 125, 1063-78.
- Andersson, P. B., Waubant, E., Gee, L. & Goodkin, D. E. 1999. Multiple sclerosis that is progressive from the time of onset: clinical characteristics and progression of disability. *Arch Neurol*, 56, 1138-42.
- Ascherio, A. & Munch, M. 2000. Epstein-Barr virus and multiple sclerosis. *Epidemiology*, 11, 220-4.
- Ascherio, A. & Munger, K. L. 2007. Environmental risk factors for multiple sclerosis. Part II: Noninfectious factors. *Ann Neurol*, 61, 504-13.
- Ascherio, A., Munger, K. L. & Simon, K. C. 2010. Vitamin D and multiple sclerosis. *Lancet Neurol*, 9, 599-612.
- Ascherio, A., Munger, K. L., White, R., Kochert, K., Simon, K. C., Polman, C. H., Freedman, M. S., Hartung, H. P., Miller, D. H., Montalban, X., Edan, G., Barkhof,

- F., Pleimes, D., Radu, E. W., Sandbrink, R., Kappos, L. & Pohl, C. 2014. Vitamin D as an early predictor of multiple sclerosis activity and progression. *JAMA Neurol*, 71, 306-14.
- Assaf, Y., Ben-Bashat, D., Chapman, J., Peled, S., Biton, I. E., Kafri, M., Segev, Y., Hendler, T., Korczyn, A. D., Graif, M. & Cohen, Y. 2002. High b-value q-space analyzed diffusion-weighted MRI: application to multiple sclerosis. *Magn Reson Med*, 47, 115-26.
- Assaf, Y., Chapman, J., Ben-Bashat, D., Hendler, T., Segev, Y., Korczyn, A. D., Graif, M. & Cohen, Y. 2005. White matter changes in multiple sclerosis: correlation of q-space diffusion MRI and ¹H MRS. *Magn Reson Imaging*, 23, 703-10.
- Assaf, Y., Mayk, A. & Cohen, Y. 2000. Displacement imaging of spinal cord using q-space diffusion-weighted MRI. *Magn Reson Med*, 44, 713-22.
- Assaf, Y. & Pasternak, O. 2008. Diffusion tensor imaging (DTI)-based white matter mapping in brain research: a review. *J Mol Neurosci*, 34, 51-61.
- Atallah, B. V. & Scanziani, M. 2009. Instantaneous modulation of gamma oscillation frequency by balancing excitation with inhibition. *Neuron*, 62, 566-77.
- Awad, A., Hemmer, B., Hartung, H.P., Kieseier, B., Bennett, J.L. Stuve, O. 2010. Analyses of cerebrospinal fluid in the diagnosis and monitoring of multiple sclerosis. *J Neuroimmunol*, 219, 1-7.
- Babbe, H., Roers, A., Waisman, A., Lassmann, H., Goebels, N., Hohfeld, R., Friese, M., Schroder, R., Deckert, M., Schmidt, S., Ravid, R. & Rajewsky, K. 2000. Clonal expansions of CD8(+) T cells dominate the T cell infiltrate in active multiple sclerosis lesions as shown by micromanipulation and single cell polymerase chain reaction. *J Exp Med*, 192, 393-404.
- Baker, E. H., Basso, G., Barker, P. B., Smith, M. A., Bonekamp, D. & Horska, A. 2008. Regional apparent metabolite concentrations in young adult brain measured by (1)H MR spectroscopy at 3 Tesla. *J Magn Reson Imaging*, 27, 489-99.
- Bakshi, R., Thompson, A. J., Rocca, M. A., Pelletier, D., Dousset, V., Barkhof, F., Inglese, M., Guttmann, C. R., Horsfield, M. A. & Filippi, M. 2008. MRI in multiple sclerosis: current status and future prospects. *Lancet Neurol*, 7, 615-25.
- Barker P.B., Bizzi A., De Stefano N., Gullapalli R., Lui D. (2010) *Clinical MR Spectroscopy*. First edition. Cambridge: Cambridge University Press.
- Barkhof, F., Filippi, M., Miller, D. H., Scheltens, P., Campi, A., Polman, C. H., Comi, G., Ader, H. J., Losseff, N. & Valk, J. 1997. Comparison of MRI criteria at first presentation to predict conversion to clinically definite multiple sclerosis. *Brain*, 120 (Pt 11), 2059-69.

- Basser, P. J., Mattiello, J. & Lebihan, D. 1994. Estimation of the effective self-diffusion tensor from the NMR spin echo. *J Magn Reson B*, 103, 247-54.
- Basser, P. J. & Pierpaoli, C. 1996. Microstructural and physiological features of tissues elucidated by quantitative-diffusion-tensor MRI. *J Magn Reson B*, 111, 209-19.
- Beaulieu, C. 2002. The basis of anisotropic water diffusion in the nervous system - a technical review. *NMR Biomed*, 15, 435-55.
- Behar, K. L., Rothman, D. L., Spencer, D. D. & Petroff, O. A. 1994. Analysis of macromolecule resonances in ¹H NMR spectra of human brain. *Magn Reson Med*, 32, 294-302.
- Benedict RHB. 1997. *The Brief Visuospatial Memory Test Revised (BVRT-R)*. Lutz, FL: Psychosocial Assessment Resources Inc.
- Bergers, E., Bot, J. C., De Groot, C. J., Polman, C. H., Lycklama A Nijeholt, G. J., Castelijns, J. A., Van Der Valk, P. & Barkhof, F. 2002. Axonal damage in the spinal cord of MS patients occurs largely independent of T2 MRI lesions. *Neurology*, 59, 1766-71.
- Bermel, R. A. & Bakshi, R. 2006. The measurement and clinical relevance of brain atrophy in multiple sclerosis. *Lancet Neurol*, 5, 158-70.
- Bhattacharyya, P. K., Philips, M. D., Stone, L. A., Bermel, R. A. & Lowe, M. J. 2013. Sensorimotor cortex gamma-aminobutyric acid concentration correlates with impaired performance in patients with MS. *AJNR Am J Neuroradiol*, 34, 1733-9.
- Bhattacharyya, P. K., Phillips, M. D., Stone, L. A. & Lowe, M. J. 2011. In vivo magnetic resonance spectroscopy measurement of gray-matter and white-matter gamma-aminobutyric acid concentration in sensorimotor cortex using a motion-controlled MEGA point-resolved spectroscopy sequence. *Magn Reson Imaging*, 29, 374-9.
- Bloch F. 1946. Nuclear Induction. *Phys Rev* 70:460.
- Bohannon, R. W. & Smith, M. B. 1987. Interrater reliability of a modified Ashworth scale of muscle spasticity. *Phys Ther*, 67, 206-7.
- Bonati, U., Fisniku, L. K., Altmann, D. R., Yiannakas, M. C., Furby, J., Thompson, A. J., Miller, D. H. & Chard, D. T. 2011. Cervical cord and brain grey matter atrophy independently associate with long-term MS disability. *J Neurol Neurosurg Psychiatry*, 82, 471-2.
- Bot, J. C., Blezer, E. L., Kamphorst, W., Lycklama, A. N. G. J., Ader, H. J., Castelijns, J. A., IG, K. N., Bergers, E., Ravid, R., Polman, C. & Barkhof, F. 2004. The spinal cord in multiple sclerosis: relationship of high-spatial-resolution quantitative MR imaging findings to histopathologic results. *Radiology*, 233, 531-40.

- Bottomley, P. A. 1987. Spatial localization in NMR spectroscopy in vivo. *Ann N Y Acad Sci*, 508, 333-48.
- Brand, A., Richter-Landsberg, C. & Leibfritz, D. 1993. Multinuclear NMR studies on the energy metabolism of glial and neuronal cells. *Dev Neurosci*, 15, 289-98.
- Brex, P. A., Leary, S. M., O'Riordan, J. I., Miszkiet, K. A., Plant, G. T., Thompson, A. J. & Miller, D. H. 2001. Measurement of spinal cord area in clinically isolated syndromes suggestive of multiple sclerosis. *J Neurol Neurosurg Psychiatry*, 70, 544-7.
- Bronskill, M. J., McVeigh, E. R., Kucharczyk, W. & Henkelman, R. M. 1988. Syrinx-like artifacts on MR images of the spinal cord. *Radiology*, 166, 485-8.
- Browne, P., Chandraratna, D., Angood, C., Tremlett, H., Baker, C., Taylor, B. V. & Thompson, A. J. 2014. Atlas of Multiple Sclerosis 2013: A growing global problem with widespread inequity. *Neurology*, 83, 1022-4.
- Brownlee W., Da Mota P., Prados F., Schneider T., Cardoso G., Altmann D., Ourselin S., Gandini Wheeler-Kingshott C., Ciccarelli O., Miller D. 2016. Neurite Orientation Dispersion and Density Imaging (NODDI) is sensitive to microstructural damage related to disability in relapse-onset MS, S41.03 American Academy of Neurology.
- Budde, M. D., Xie, M., Cross, A. H. & Song, S. K. 2009. Axial diffusivity is the primary correlate of axonal injury in the experimental autoimmune encephalomyelitis spinal cord: a quantitative pixelwise analysis. *J Neurosci*, 29, 2805-13.
- Bunn, L. M., Marsden, J. F., Giunti, P. & Day, B. L. 2013. Stance instability in spinocerebellar ataxia type 6. *Mov Disord*, 28, 510-6.
- Burgess, P. W., & Shallice, T. (1997). *The Hayling and Brixton Tests*. Thurston, Suffolk: Thames Valley Test Company.
- Cader, S., Johansen-Berg, H., Wylezinska, M., Palace, J., Behrens, T. E., Smith, S. & Matthews, P. M. 2007. Discordant white matter N-acetylaspartate and diffusion MRI measures suggest that chronic metabolic dysfunction contributes to axonal pathology in multiple sclerosis. *Neuroimage*, 36, 19-27.
- Calabrese, M., Atzori, M., Bernardi, V., Morra, A., Romualdi, C., Rinaldi, L., McAuliffe, M. J., Barachino, L., Perini, P., Fischl, B., Battistin, L. & Gallo, P. 2007. Cortical atrophy is relevant in multiple sclerosis at clinical onset. *J Neurol*, 254, 1212-20.
- Calabrese, M., Filippi, M. & Gallo, P. 2010a. Cortical lesions in multiple sclerosis. *Nat Rev Neurol*, 6, 438-44.
- Calabrese, M., Rocca, M. A., Atzori, M., Mattisi, I., Favaretto, A., Perini, P., Gallo, P. & Filippi, M. 2010b. A 3-year magnetic resonance imaging study of cortical lesions in relapse-onset multiple sclerosis. *Ann Neurol*, 67, 376-83.

- Callaghan, P. T., Eccles, C. D. & Xia, Y. 1988. NMR microscopy of dynamic displacements: k-space and q-space imaging. *J Phy E Sc Instrum*; 21(8): 820.
- Capkun, G., Dahlke, F., Lahoz, R., Nordstrom, B., Tilson, H. H., Cutter, G., Bischof, D., Moore, A., Simeone, J., Fraeman, K., Bancken, F., Geissbuhler, Y., Wagner, M. & Cohan, S. 2015. Mortality and comorbidities in patients with multiple sclerosis compared with a population without multiple sclerosis: An observational study using the US Department of Defense administrative claims database. *Mult Scler Relat Disord*, 4, 546-54.
- Cardoso, M.J., Leung, K., Modat, M., Keihaninejad, S., Cash, D., Barnes, J., Fo, N. C. & Ourselin, S. 2013. STEPS: Similarity and Truth Estimation for Propagated Segmentations and its application to hippocampal segmentation and brain parcellation. *Med Image Anal*, 17, 671-84.
- Cardoso J., Modat M., Wolz R., Melbourne A., Cash D., Rueckert D., and Ourselin S. (2015). Geodesic Information Flows: Spatially-Variant Graphs and Their Application to Segmentation and Fusion. *IEEE TMI* vol. 34(9), 1976-88.
- Carr, H. Y. & Purcell, E. M. 1954. Effects of Diffusion on Free Precession in Nuclear Magnetic Resonance Experiments. *Physical Review* 94(3): 630-638.
- Carswell J. *Pathological anatomy: illustrations on elementary forms of disease.* 1838 London: Longman.
- Chang, L., Cloak, C. C. & Ernst, T. 2003. Magnetic resonance spectroscopy studies of GABA in neuropsychiatric disorders. *J Clin Psychiatry*, 64 Suppl 3, 7-14.
- Charcot JM. *Lecons sur les maladies du systeme nerveux faites a la salpetriere* 1880 pp. 189-220 Paris: Cerf et fils.
- Chard, D. T., Jackson, J. S., Miller, D. H. & Wheeler-Kingshott, C. A. 2010. Reducing the impact of white matter lesions on automated measures of brain gray and white matter volumes. *J Magn Reson Imaging*, 32, 223-8.
- Chard, D. T., Griffin, C. M., McLean, M. A., Kapeller, P., Kapoor, R., Thompson, A. J. & Miller, D. H. 2002. Brain metabolite changes in cortical grey and normal-appearing white matter in clinically early relapsing-remitting multiple sclerosis. *Brain*, 125, 2342-52.
- Chataway, J., Schuerer, N., Alsanousi, A., Chan, D., MacManus, D., Hunter, K., Anderdson, V., Bangham, C. R., Clegg, S., Nielsen, C., Fox, N. C., Wilkie, D., Nicholas, J. M., Calder, V. L., Greenwood, J., Frost, C. & Nicholas, R. 2014. Effect of high-dose simvastatin on brain atrophy and disability in secondary progressive multiple sclerosis (MS-STAT): a randomised, placebo-controlled, phase 2 trial. *Lancet*, 383, 2213-21.
- Chiaravalloti, N. D. & DeLuca, J. 2008. Cognitive impairment in multiple sclerosis. *Lancet Neurol*, 7, 1139-51.

- Ciccarelli, O., Barkhof, F., Bodini, B., De Stefano, N., Golay, X., Nicolay, K., Pelletier, D., Pouwels, P. J., Smith, S. A., Wheeler-Kingshott, C. A., Stankoff, B., Yousry, T. & Miller, D. H. 2014. Pathogenesis of multiple sclerosis: insights from molecular and metabolic imaging. *Lancet Neurol*, 13, 807-22.
- Ciccarelli, O. & Thompson, A. 2016. Multiple sclerosis in 2015: Managing the complexity of multiple sclerosis. *Nat Rev Neurol*.
- Ciccarelli, O., Altmann, D. R., McLean, M. A., Wheeler-Kingshott, C. A., Wimpey, K., Miller, D. H. & Thompson, A. J. 2010. Spinal cord repair in MS: does mitochondrial metabolism play a role? *Neurology*, 74, 721-7.
- Ciccarelli, O., Thomas, D. L., De Vita, E., Wheeler-Kingshott, C. A., Kachramanoglou, C., Kapoor, R., Leary, S., Matthews, L., Palace, J., Chard, D., Miller, D. H., Toosy, A. T. & Thompson, A. J. 2013. Low Myo-inositol indicating astrocytic damage in a case series of neuromyelitis optica. *Ann Neurol*, 74, 301-5.
- Ciccarelli, O., Werring, D. J., Barker, G. J., Griffin, C. M., Wheeler-Kingsott, C. A., Miller, D. H. & Thompson, A. J. 2003. A study of the mechanisms of normal-appearing white matter damage in multiple sclerosis using diffusion tensor imaging--evidence of Wallerian degeneration. *J Neurol*, 250, 287-92.
- Ciccarelli, O., Wheeler-Kingsott, C. A., McLean, M. A., Cercignani, M., Wimpey, K., Miller, D. H. & Thompson, A. J. 2007. Spinal cord spectroscopy and diffusion-based tractography to assess acute disability in multiple sclerosis. *Brain*, 130, 2220-31.
- Coffey, C. E., Wilkinson, W. E., Parashos, I. A., Soady, S. A., Sullivan, R. J., Patterson, L. J., Figiel, G. S., Webb, M. C., Spritzer, C. E. & Djang, W. T. 1992. Quantitative cerebral anatomy of the aging human brain: a cross-sectional study using magnetic resonance imaging. *Neurology*, 42, 527-36.
- Cohen, Y. & Assaf, Y. (2002). High b-value q-space analyzed diffusion-weighted MRS and MRI in neuronal tissues - a technical review. *NMR Biomed* 15(7-8): 516-542.
- Cohen, J. A., Coles, A. J., Arnold, D. L., Confavareux, C., Fox, E. J., Hartung, H. P., Havrdova, E., Selmaj, K. W., Weiner, H. L., Fisher, E., Brinar, V. V., Giovannoni, G., Stojanovic, M., Ertik, B. I., Lake, S. L., Margolin, D. H., Panzara, M. A. & Compston, D. A. 2012. Alemtuzumab versus interferon beta 1a as first-line treatment for patients with relapsing-remitting multiple sclerosis: a randomised controlled phase 3 trial. *Lancet*, 380, 1819-28.
- Coles, A. J., Compston, D. A., Selmaj, K. W., Lake, S. L., Moran, S., Margolin, D. H., Norris, K. & Tandon, P. K. 2008. Alemtuzumab vs. interferon beta-1a in early multiple sclerosis. *N Engl J Med*, 359, 1786-801.
- Compston, A. 2006. Making progress on the natural history of multiple sclerosis. *Brain*, 129, 561-3.

- Compston, A. & Coles, A. 2002. Multiple sclerosis. *Lancet*, 359, 1221-31.
- Compston, A. & Coles, A. 2008. Multiple sclerosis. *Lancet*, 372, 1502-17.
- Compston, D. A., Batchelor, J. R. & McDonald, W. I. 1976. B-lymphocyte alloantigens associated with multiple sclerosis. *Lancet*, 2, 1261-5.
- Conel, J.L., 1939. The postnatal development of the human cerebral cortex. Harvard University Press, Cambridge, USA.
- Confavreux, C., Aimard, G. & Devic, M. 1980. Course and prognosis of multiple sclerosis assessed by the computerized data processing of 349 patients. *Brain*, 103, 281-300.
- Confavreux, C., Vukusic, S. & Adeleine, P. 2003. Early clinical predictors and progression of irreversible disability in multiple sclerosis: an amnesic process. *Brain*, 126, 770-82.
- Cook P.A., Bai Y., Nedjati-Gilani S.K.K.S., Seunarine K.K., Hall M.G., Parker G.J., and Alexander D.C. 2006. "Camino: Open-Source Diffusion-MRI Reconstruction and Processing." In 14th Scientific Meeting of the International Society for Magnetic Resonance in Medicine. Vol. 2759. Seattle WA, USA.
- Cruveilhier J.1841. Anatomie pathologique du corps humaine. Paris: Balilliere.
- Cudalbu, C., Mlynarik, V. & Gruetter, R. 2012. Handling macromolecule signals in the quantification of the neurochemical profile. *J Alzheimers Dis*, 31 Suppl 3, S101-15.
- Cutter, G. R., Baier, M. L., Rudick, R. A., Cookfair, D. L., Ficsher, J. S., Petkau, J., Syndulko, K., Weinshenker, B. G., Antel, J. P., Confavreux, C., Ellison, G. W., Lublin, F., Miller, A. E., Rao, S. M., Reingold, S., Thompson, A. & Willoughby, E. 1999. Development of a multiple sclerosis functional composite as a clinical trial outcome measure. *Brain*, 122 (Pt 5), 871-82.
- Daams, M., Weiler, F., Steenwijk, M. D., Hahn, H. K., Geurts, J. J., Vrenken, H., Van Schijndel, R. A., Balk, L. J., Tewarie, P. K., Tillema, J. M., Killestein, J., Uitdehaag, B. M. & Barkhof, F. 2014. Mean upper cervical cord area (MUCCA) measurement in long-standing multiple sclerosis: relation to brain findings and clinical disability. *Mult Scler*, 20, 1860-5.
- Dalton, C. M., Brex, P. A., Jenkins, R., Fox, N. C., Miszkiel, K. A., Crum, W. R., O'Riordan, J. I., Plant, G. T., Thompson, A. J. & Miller, D. H. 2002. Progressive ventricular enlargement in patients with clinically isolated syndromes is associated with the early development of multiple sclerosis. *J Neurol Neurosurg Psychiatry*, 73, 141-7.
- Davidoff, G. N., Roth, E. J. & Richards, J. S. 1992. Cognitive deficits in spinal cord injury: epidemiology and outcome. *Arch Phys Med Rehabil*, 73, 275-84.

- DeFelipe, J. 1993. Neocortical neuronal diversity: chemical heterogeneity revealed by colocalization studies of classic neurotransmitters, neuropeptides, calcium-binding proteins, and cell surface molecules. *Cereb Cortex*, 3, 273-89.
- Delis D.C., Kramer J.H., Kaplan E., Ober B.A. 2000. California Verbal Learning Test, second edition (CVLT-II). San Antonio, TX: Psychological Corporation.
- DeLuca, G. C., Williams, K., Evangelou, N., Ebers, G. C. & Esiri, M. M. 2006. The contribution of demyelination to axonal loss in multiple sclerosis. *Brain*, 129, 1507-16.
- De Stefano, N. & Arnold, D. L. 2015. Towards a better understanding of pseudoatrophy in the brain of multiple sclerosis patients. *Mult Scler*, 21, 675-6.
- De Stefano, N., Filippi, M., Miller, D., Pouwels, P. J., Rovira, A., Gass, A., Enzinger, C., Matthews, P. M. & Arnold, D. L. 2007a. Guidelines for using proton MR spectroscopy in multicenter clinical MS studies. *Neurology*, 69, 1942-52.
- De Stefano, N. & Filippil, M. 2007b. MR spectroscopy in multiple sclerosis. *J Neuroimaging*, 17 Suppl 1, 31S-35S.
- De Stefano, N., Giorgio, A., Battaglini, M., Rovaris, M., Sormani, M. P., Barkhof, F., Korteweg, T., Enzinger, C., Fazekas, F., Calabrese, M., Dinacci, D., Tedeschi, G., Gass, A., Montalban, X., Rovira, A., Thompson, A., Comi, G., Miller, D. H. & Filippi, M. 2010. Assessing brain atrophy rates in a large population of untreated multiple sclerosis subtypes. *Neurology*, 74, 1868-76.
- De Stefano, N., Matthews, P. M., Narayanan, S., Francis, G. S., Antel, J. P. & Arnold, D. L. 1997. Axonal dysfunction and disability in a relapse of multiple sclerosis: longitudinal study of a patient. *Neurology*, 49, 1138-41.
- Dietz, V. 2010. Behavior of spinal neurons deprived of supraspinal input. *Nat Rev Neurol*, 6, 167-74.
- Di Pauli, F., Reindl, M., Ehling, R., Schautzer, F., Gneiss, C., Lutterotti, A., O'Reilly, E., Munger, K., Deisnhammer, F., Ascherio, A. & Berger, T. 2008. Smoking is a risk factor for early conversion to clinically definite multiple sclerosis. *Mult Scler*, 14, 1026-30.
- Disanto, G., Chaplin, G., Morahan, J. M., Giovannoni, G., Hypponen, E., Ebers, G. C. & Ramagopalan, S. V. 2012. Month of birth, vitamin D and risk of immune-mediated disease: a case control study. *BMC Med*, 10, 69.
- Dobson, R., Ramagopalan, S., Davis, A. & Giovannoni, G. 2013. Cerebrospinal fluid oligoclonal bands in multiple sclerosis and clinically isolated syndromes: a meta-analysis of prevalence, prognosis and effect of latitude. *J Neurol Neurosurg Psychiatry*, 84, 909-14.
- Dutta, R., McDonough, J., Yin, X., Peterson, J., Chang, A., Torres, T., et al. 2006. Mitochondrial dysfunction as a cause of axonal degeneration in multiple sclerosis patients. *Ann Neurol*. 2006/01/05.

Dyck PJ, Boes CJ, Mulder D, Millikan C, Winderbank, et al. History of standard scoring, notation, and summation of neuromuscular signs. A current survey and recommendation. *J Peripher Nerv Syst* 2005; 10: 158–73.

Dyment, D. A., Yee, I. M., Ebers, G. C. & Sadovnick, A. D. 2006. Multiple sclerosis in stepsiblings:

Ebers, G. C., Sadovnick, A. D. & Risch, N. J. 1995. A genetic basis for familial aggregation in multiple sclerosis. Canadian Collaborative Study Group. *Nature*, 377, 150-1.

Edden, R. A., Bonekamp, D., Smith, M. A., Dubey, P. & Barker, P. B. 2007. Proton MR spectroscopic imaging of the medulla and cervical spinal cord. *J Magn Reson Imaging*, 26, 1101-5.

Enzinger, C., Barkhof, F., Ciccarelli, O., Filippini, M., Kappos, L., Rocca, M. A., Ropele, S., Rovira, A., Schneider, T., De Stefano, N., Vrenken, H., Wheeler-Kingshott, C., Wuerfel, J. & Fazekas, F. 2015. Nonconventional MRI and microstructural cerebral changes in multiple sclerosis. *Nat Rev Neurol*, 11, 676-86.

Epperson, C. N., Haga, K., Mason, G. F., Sellers, E., Gueorguieva, R., Zhang, W., et al. 2002. Cortical gamma-aminobutyric acid levels across the menstrual cycle in healthy women and those with premenstrual dysphoric disorder: a proton magnetic resonance spectroscopy study. *Arch Gen Psychiatry*, 59, 851-8.

Evangelou, N., DeLuca, G. C., Owens, T. & Esiri, M. M. 2005. Pathological study of spinal cord atrophy in multiple sclerosis suggests limited role of local lesions. *Brain*, 128, 29-34.

Evangelou, N., Esiri, M. M., Smith, S., Palace, J. & Matthews, P. M. 2000. Quantitative pathological evidence for axonal loss in normal appearing white matter in multiple sclerosis. *Ann Neurol*, 47, 391-5.

Farrell, J. A., Smith, S. A., Gordon-Lipkin, E. M., Reich, D. S., Calabresi, P. A. & Van Zijl, P. C. 2008. High b-value q-space diffusion-weighted MRI of the human cervical spinal cord in vivo: feasibility and application to multiple sclerosis. *Magn Reson Med*, 59, 1079-89.

Fernandez-Menedez, S., Fernandez-Moran, M., Fernandez-Vega, I., Perez-Alvarez, A. & Villafani-Echazu, J. 2016. Epstein-Barr virus and multiple sclerosis. From evidence to therapeutic strategies. *J Neurol Sci*, 361, 213-9.

Fernando, K. T., McLean, M. A., Chard, D. T., MacManus, D. G., Dalton, C. M., Miszkiel, K. A., Gordan, R. M., Plant, G. T., Thompson, A. J. & Miller, D. H. 2004. Elevated white matter myo-inositol in clinically isolated syndromes suggestive of multiple sclerosis. *Brain*, 127, 1361-9.

Fiddes, B., Wason, J., Kemppinen, A., Ban, M., Compston, A. & Sawcer, S. 2013. Confounding underlies the apparent month of birth effect in multiple sclerosis. *Ann Neurol*, 73, 714-20.

- Filippi, M. & Agoasta, F. 2010. Imaging biomarkers in multiple sclerosis. *J Magn Reson Imaging*, 31, 770-88.
- Filippi, M. & Rocca, M. A. 2011. MR imaging of multiple sclerosis. *Radiology*, 259, 659-81.
- Filippi, M., Rocca, M. A. & Comi, G. 2003. The use of quantitative magnetic-resonance-based techniques to monitor the evolution of multiple sclerosis. *Lancet Neurol*, 2, 337-46.
- Filippi, M. & Inglese, M. 2001. Overview of diffusion-weighted magnetic resonance studies in multiple sclerosis. *J Neurol Sci*, 186 Suppl 1, S37-43.
- Fischer, J. S., Rudick, R. A., Cutter, G. R. & Reingold, S. C. 1999. The Multiple Sclerosis Functional Composite Measure (MSFC): an integrated approach to MS clinical outcome assessment. National MS Society Clinical Outcomes Assessment Task Force. *Mult Scler*, 5, 244-50.
- Fisher, E., Rudick, R. A., Simon, J. H., Cutter, G., Baier, M., Lee, J. C., Miller, D., Weinstock-Guttman, B., Mass, M. K., Dougherty, D. S. & Simonian, N. A. 2002. Eight-year follow-up study of brain atrophy in patients with MS. *Neurology*, 59, 1412-20.
- Fitzgerald, K. C., Munger, K. L., Kochert, K., Arnason, B. G., Comi, G., Cook, S., Goodin, D. S., Filippi, M., Hartung, H. P., Jeffery, D. R., O'Connor, P., Suarez, G., Sandbrink, R., Kappos, L., Pohl, C. & Ascherio, A. 2015. Association of Vitamin D Levels With Multiple Sclerosis Activity and Progression in Patients Receiving Interferon Beta-1b. *JAMA Neurol*, 1-8.
- Floyer-Lea A, Wylezinska M, Kincses T, Matthews PM. Rapid modulation of GABA concentration in human sensorimotor cortex during motor learning. *Journal of neurophysiology*. 2006 Mar;95(3):1639-44.
- Fox, R. J., Thompson, A., Baker, D., Baneke, P., Brown, D., Browne, P., Chandraratna, D., Ciccarelli, O., Coetzee, T., Comi, G., Feinstein, A., Kapoor, R., Lee, K., Salvetti, M., Sharrock, K., Toosy, A., Zaratin, P. & Zuidwijk, K. 2012. Setting a research agenda for progressive multiple sclerosis: the International Collaborative on Progressive MS. *Mult Scler*, 18, 1534-40.
- Frahm, J., Bruhn, H., Gyngell, M. L., Merboldt, K. D., Hanicke, W. & Sauter, R. 1989. Localized high-resolution proton NMR spectroscopy using stimulated echoes: initial applications to human brain in vivo. *Magn Reson Med*, 9, 79-93.
- Freeborough, P. A. & Fox, N. C. 1997. The boundary shift integral: an accurate and robust measure of cerebral volume changes from registered repeat MRI. *IEEE Trans Med Imaging*, 16, 623-9.
- Freeman L., Leory C., & Galanaud D. 2010. Early neuronal damage in patients with MS detected by PET imaging [11C]-flumazenil. *Multiple Sclerosis*. 16 (suppl): S7-S39 (abstr 117).

- Freund, P., Weiskopf, N., Ward, N. S., Hutton, C., Gall, A., Ciccarelli, O., Craggs, M., Friston, K. & Thompson, A. J. 2011. Disability, atrophy and cortical reorganization following spinal cord injury. *Brain*, 134, 1610-22.
- Freund, P., Wheeler-Kingshott, C. A., Nagy, Z., Gorgoraptis, N., Weiskopf, N., Friston, K., Thompson, A. J. & Hutton, C. 2012. Axonal integrity predicts cortical reorganisation following cervical injury. *J Neurol Neurosurg Psychiatry*, 83, 629-37.
- Frischer, J. M., Bramow, S., Dal-Bianco, A., Lucchinetti, C. F., Rauschka, H., Schmidbauer, M., Laursen, H., Sorensen, P. S. & Lassmann, H. 2009. The relation between inflammation and neurodegeneration in multiple sclerosis brains. *Brain*, 132, 1175-89.
- Frommann C. Untersuchungen über die Gewebsveränderungen bei der Multiplen Sklerose des Gehirns und Rückenmarks 1878 pp. 1-123 Jena: Gustav Fischer.
- Furby, J., Hayton, T., Altmann, D., Brenner, R., Chataway, J., Smith, K. J., Miller, D. H. & Kapoor, R. 2010. A longitudinal study of MRI-detected atrophy in secondary progressive multiple sclerosis. *J Neurol*, 257, 1508-16.
- Gaetz, W., Edgar, J. C., Wang, D. J. & Roberts, T. P. 2011. Relating MEG measured motor cortical oscillations to resting gamma-aminobutyric acid (GABA) concentration. *Neuroimage*, 55, 616-21.
- Ganter, P., Prince, C. & Esiri, M. M. 1999. Spinal cord axonal loss in multiple sclerosis: a post-mortem study. *Neuropathol Appl Neurobiol*, 25, 459-67.
- Garbern, J. Y., Yool, D. A., Moore, G. J., Wilds, I. B., Faulk, M. W., Klugmann, M., Nave, K. A., Siermans, E. A., Van Der Knaap, M. S., Bird, T. D., Shy, M. E., Kamhol, J. A. & Griffiths, I. R. 2002. Patients lacking the major CNS myelin protein, proteolipid protein 1, develop length-dependent axonal degeneration in the absence of demyelination and inflammation. *Brain*, 125, 551-61.
- Gasparovic, C., Song, T., Devier, D., Bockholt, H. J., Caprihan, A., Mullins, P. G., Posse, S., Jung, R. E. & Morrison, L. A. 2006. Use of tissue water as a concentration reference for proton spectroscopic imaging. *Magn Reson Med*, 55, 1219-26.
- Gass, A., Rocca, M. A., Agosta, F., Ciccarelli, O., Chard, D., Valsasina, P., Brooks, J. C., Bischof, A., Eisele, P., Kappos, L., Barkhof, F. & Filippi, M. 2015. MRI monitoring of pathological changes in the spinal cord in patients with multiple sclerosis. *Lancet Neurol*, 14, 443-54.
- Geurts, J. J., Rosendaal, S. D., Calabrese, M., Ciccarelli, O., Agosta, F., Chard, D. T., et al. 2011. Consensus recommendations for MS cortical lesion scoring using double inversion recovery MRI. *Neurology*, 76, 418-24.
- Geurts, J. J., Stys, P. K., Minagar, A., Amor, S. & Zivadinov, R. 2009. Gray matter pathology in (chronic) MS: modern views on an early observation. *J Neurol Sci*, 282, 12-20.

- Gilmore, C. P., Donaldson, I., Bo, L., Owens, T., Lowe, J. & Evangelou, N. 2009. Regional variations in the extent and pattern of grey matter demyelination in multiple sclerosis: a comparison between the cerebral cortex, cerebellar cortex, deep grey matter nuclei and the spinal cord. *J Neurol Neurosurg Psychiatry*, 80, 182-7.
- Giorgio, A., Battaglini, M., Smith, S. M. & De Stefano, N. 2008. Brain atrophy assessment in multiple sclerosis: importance and limitations. *Neuroimaging Clin N Am*, 18, 675-86, xi.
- Giovannoni, G. 2006. Multiple sclerosis related fatigue. *J Neurol Neurosurg Psychiatry*, 77, 2-3.
- Goodkin, D. E., Hertsgaard, D. & Seminary, J. 1988. Upper extremity function in multiple sclerosis: improving assessment sensitivity with box-and-block and nine-hole peg tests. *Arch Phys Med Rehabil*, 69, 850-4.
- Goodin, D. S. 2009. The causal cascade to multiple sclerosis: a model for MS pathogenesis. *PLoS One*, 4, e4565.
- Grussu F, Schneider T, Yates R, Tachrount M, Newcombe J, Zhang H, Alexander D, DeLuca G, and Wheeler-Kingshott C.A.M. 2015a. Quantitative histological validation of NODDI MRI indices of neurite morphology in multiple sclerosis spinal cord". 31st ECTRIMS congress, p.0469, traditional poster presentation.
- Grussu, F., Schneider, T., Zhang, H., Alexander, D. C. & Wheeler-Kingshott, C. A. 2015b. Neurite orientation dispersion and density imaging of the healthy cervical spinal cord in vivo. *Neuroimage*, 111, 590-601.
- Grussu F., Schneider T., Prados F., Tur C., Ourselin S., Zhang H., Alexander D. & Wheeler-Kingshott C. 2016. Axon diameter distribution influences diffusion-derived axonal density estimation in the human spinal cord: in silico and in vivo evidence. ISMRM annual meeting.
- Haase, A., Frahm, J., Hanicke, W. & Matthaei, D. (1985). 1H NMR chemical shift selective (CHESS) imaging. *Phys Med Biol* 30(4): 341-344.
- Hafler, D. A., Compston, A., Sawcer, S., Lander, E. S., Daly, M. J., De Jager, P. L., De Bakker, P. I., Gabriel, S. B., Mirel, D. B., Ivinson, A. J., Pericak-Vance, M. A., Gregory, S. G., Rioux, J. D., McCauley, J. L., Haines, J. L., Barcellos, L. F., Cree, B., Oksenberg, J. R. & Hauser, S. L. 2007. Risk alleles for multiple sclerosis identified by a genomewide study. *N Engl J Med*, 357, 851-62.
- Hahn, E. L. (1950). Spin Echoes. *Physical Review* 80(4): 580-594.
- Hancu, I. 2009. Optimized glutamate detection at 3T. *J Magn Reson Imaging*, 30, 1155-62.
- Hari, R., Parkkonen, L. & Nangini, C. 2010. The brain in time: insights from neuromagnetic recordings. *Ann N Y Acad Sci*, 1191, 89-109.

- Hasler, G., Van Der Veen, J. W., Tumonis, T., Meyers, N., Shen, J. & Drevets, W. C. 2007. Reduced prefrontal glutamate/glutamine and gamma-aminobutyric acid levels in major depression determined using proton magnetic resonance spectroscopy. *Arch Gen Psychiatry*, 64, 193-200.
- Hauser, S. L. & Oksenberg, J. R. 2006. The neurobiology of multiple sclerosis: genes, inflammation, and neurodegeneration. *Neuron*, 52, 61-76.
- Hawker, K., O'Connor, P., Freedman, M. S., Calabresi, P. A., Antel, J., Simon, J., Hauser, S., Waubant, E., Vollmer, T., Panitch, H., Zhang, J., Chin, P. & Smith, C. H. 2009. Rituximab in patients with primary progressive multiple sclerosis: results of a randomized double-blind placebo-controlled multicenter trial. *Ann Neurol*, 66, 460-71.
- Heesen, C., Nawrath, L., Reich, C., Bauer, N., Schulz, K. H. & Gold, S. M. 2006. Fatigue in multiple sclerosis: an example of cytokine mediated sickness behaviour? *J Neurol Neurosurg Psychiatry*, 77, 34-9.
- Henderson, L. A., Gustin, S. M., Macey, P. M., Wrigley, P. J. & Siddall, P. J. 2011. Functional reorganization of the brain in humans following spinal cord injury: evidence for underlying changes in cortical anatomy. *J Neurosci*, 31, 2630-7.
- Henning, A., Schar, M., Kollias, S. S., Boesiger, P. & Dydak, U. 2008. Quantitative magnetic resonance spectroscopy in the entire human cervical spinal cord and beyond at 3T. *Magn Reson Med*, 59, 1250-8.
- Henry, P. G., Dautry, C., Hantraye, P. & Bloch, G. 2001. Brain GABA editing without macromolecule contamination. *Magn Reson Med*, 45, 517-20.
- Henry, R. G., Shieh, M., Amirbekian, B., Chung, S., Okuda, D. T. & Pelletier, D. 2009. Connecting white matter injury and thalamic atrophy in clinically isolated syndromes. *J Neurol Sci*, 282, 61-6.
- Hernan, M. A., Jick, S. S., Logroscino, G., Olek, M. J., Ascherio, A. & Jick, H. 2005. Cigarette smoking and the progression of multiple sclerosis. *Brain*, 128, 1461-5.
- Hickman, S. I., Barker, G. J., Molyneux, P. D. & Miller, D. H. 2002. Technical note: the comparison of hypointense lesions from 'pseudo-T1' and T1-weighted images in secondary progressive multiple sclerosis. *Mult Scler*, 8, 433-5.
- Hobart, J. C., Riazi, A., Lamping, D. L., Fitzpatrick, R. & Thompson, A. J. 2003. Measuring the impact of MS on walking ability: the 12-Item MS Walking Scale (MSWS-12). *Neurology*, 60, 31-6.
- Holick, M. F. 2004. Sunlight and vitamin D for bone health and prevention of autoimmune diseases, cancers, and cardiovascular disease. *Am J Clin Nutr*, 80, 1678S-88S.

- Horsfield, M. A., Larsson, H. B., Jones, D. K. & Gass, A. 1998. Diffusion magnetic resonance imaging in multiple sclerosis. *J Neurol Neurosurg Psychiatry*, 64 Suppl 1, S80-4.
- Horsfield, M. A., Sala, S., Neema, M., Absinta, B., Bakshi, A., Sormani, M. P., Rocca, M. A., Bakshi, R. & FILIPPI, M. 2010. Rapid semi-automatic segmentation of the spinal cord from magnetic resonance images: application in multiple sclerosis. *Neuroimage*, 50, 446-55.
- Horton, R., Wilming, L., Rand, V., Lovering, R. C., Bruford, E. A., Khodiyar, V. K., Lush, M. J., Povey, S., Talbot, C. C., JR., Wright, M. W., Wain, H. M., Trowsdale, J., Ziegler, A. & Beck, S. 2004. Gene map of the extended human MHC. *Nat Rev Genet*, 5, 889-99.
- Hoshimaru, M. 2010. Neuropsychological improvement in patients with cervical spondylotic myelopathy after posterior decompression surgery. *Neurol Med Chir (Tokyo)*, 50, 554-9.
- Hurd, R., Sailasuta, N., Srinivasan, R., Vigneron, D. B., Pelletier, D. & Nelson, S. J. 2004. Measurement of brain glutamate using TE-averaged PRESS at 3T. *Magn Reson Med*, 51, 435-40.
- Gutowsky, H.S., McCall, D.W. 1951. Nuclear magnetic resonance fine structure in liquids. *Phys Rev*; 82: 748–9.
- Hygino Da Cruz, L. C., JR., Batista, R. R., Domingues, R. C. & Barkhof, F. 2011. Diffusion magnetic resonance imaging in multiple sclerosis. *Neuroimaging Clin N Am*, 21, 71-88, vii-viii.
- Hunter, S. F. & Hafler, D. A. 2000. Ubiquitous pathogens: links between infection and autoimmunity in MS? *Neurology*, 55, 164-5.
- Ingle, G. T., Stevenson, V. L., Miller, D. H. & Thompson, A. J. 2003. Primary progressive multiple sclerosis: a 5-year clinical and MR study. *Brain*, 126, 2528-36.
- Inglese, M., Li, B. S., Rusinek, H., Babb, J. S., Grossman, R. I. & Gonen, O. 2003. Diffusely elevated cerebral choline and creatine in relapsing-remitting multiple sclerosis. *Magn Reson Med*, 50, 190-5.
- Jacobs, B., Driscoll, L. & Schall, M. 1997. Life-span dendritic and spine changes in areas 10 and 18 of human cortex: a quantitative Golgi study. *J Comp Neurol*, 386, 661-80.
- Kaiser, L. G., Schuff, N., Cashdollar, N. & Weiner, M. W. 2005. Age-related glutamate and glutamine concentration changes in normal human brain: 1H MR spectroscopy study at 4 T. *Neurobiol Aging*, 26, 665-72
- Kantarci, O. H., LeBrun, C., Siva, A., Keegan, M. B., Azevedo, C. J., Inglese, M., Tintore, M., Newton, B. D., Durand-Dubief, F., Pia Amato, M., De Stefano, N., Pia

- Sormani, M., Pelletier, D. & Okuda, D. T. 2015. Primary Progressive MS evolving from Radiologically Isolated Syndrome. *Ann Neurol*.
- Kapoor, R., Furby, J., Hayton, T., Smith, K. J., Altmann, D. R., Brenner, R., Chataway, J., Hughes, R. A. & Miller, D. H. 2010. Lamotrigine for neuroprotection in secondary progressive multiple sclerosis: a randomised, double-blind, placebo-controlled, parallel-group trial. *Lancet Neurol*, 9, 681-8.
- Kearney, H., Altmann, D. R., Samson, R. S., Yiannakas, M. C., Wheeler-Kingshott, C. A., Ciccarelli, O. & Miller, D. H. 2015. Cervical cord lesion load is associated with disability independently from atrophy in MS. *Neurology*, 84, 367-73.
- Kearney, H., Yiannakas, M. C., Abdel-Aziz, K., Wheeler-Kingshott, C. A., Altmann, D. R., Ciccarelli, O. & Miller, D. H. 2014a. Improved MRI quantification of spinal cord atrophy in multiple sclerosis. *J Magn Reson Imaging*, 39, 617-23.
- Kearney, H., Rocca, M. A., Valsasina, P., Balk, L., Sastre-Garriga, J., Reinhardt, J., Ruggieri, S., Rovira, A., Stippich, C., Kappos, L., Sprenger, T., Tortorella, P., Rovaris, M., Gasperini, C., Montalban, X., Geurts, J. J., Polman, C. H., Barkhof, F., Filippi, M., Altmann, D. R., Ciccarelli, O., Miller, D. H. & Chard, D. T. 2014b. Magnetic resonance imaging correlates of physical disability in relapse onset multiple sclerosis of long disease duration. *Mult Scler*, 20, 72-80.
- Kelly, S. B., Kinsella, K., Duggan, M., Tubridy, N., McGuigan, C. & Hutchinson, M. 2013. A proposed modification to the McDonald 2010 criteria for the diagnosis of primary progressive multiple sclerosis. *Mult Scler*, 19, 1095-100.
- Khaleeli, Z., Altmann, D. R., Cercignani, M., Ciccarelli, O., Miller, D. H. & Thompson, A. J. 2008. Magnetization transfer ratio in gray matter: a potential surrogate marker for progression in early primary progressive multiple sclerosis. *Arch Neurol*, 65, 1454-9.
- Kidd, D., Thorpe, J. W., Thompson, A. J., Kendall, B. E., Moseley, I. F., MacManus, D. G., McDonald, W. I. & Miller, D. H. 1993. Spinal cord MRI using multi-array coils and fast spin echo. II. Findings in multiple sclerosis. *Neurology*, 43, 2632-7.
- Kirov, II, Tal, A., Babb, J. S., Herbert, J. & Gonen, O. 2013. Serial proton MR spectroscopy of gray and white matter in relapsing-remitting MS. *Neurology*, 80, 39-46.
- Klawiter, E. C., Schmidt, R. E., Trinkaus, K., Liang, H. F., Budde, M. D., Naismith, R. T., Song, S. K., Cross, A. H. & Benzinger, T. L. 2011. Radial diffusivity predicts demyelination in ex vivo multiple sclerosis spinal cords. *Neuroimage*, 55, 1454-60.
- Koch, M., Kingwell, E., Rieckmann, P. & Tremlett, H. 2009. The natural history of primary progressive multiple sclerosis. *Neurology*, 73, 1996-2002.

- Koch, M., Kingwell, E., Rieckmann, P. & Tremlett, H. 2010. The natural history of secondary progressive multiple sclerosis. *J Neurol Neurosurg Psychiatry*, 81, 1039-43.
- Koch-Henriksen, N. & Sorensen, P. S. 2010. The changing demographic pattern of multiple sclerosis epidemiology. *Lancet Neurol*, 9, 520-32.
- Kokotilo, K. J., Eng, J. J. & Curt, A. 2009. Reorganization and preservation of motor control of the brain in spinal cord injury: a systematic review. *J Neurotrauma*, 26, 2113-26.
- Kremenchutzky, M., Rice, G. P., Baskerville, J., Wingerchuk, D. M. & Ebers, G. C. 2006. The natural history of multiple sclerosis: a geographically based study 9: observations on the progressive phase of the disease. *Brain*, 129, 584-94.
- Krupp, L. 2006. Fatigue is intrinsic to multiple sclerosis (MS) and is the most commonly reported symptom of the disease. *Mult Scler*, 12, 367-8.
- Kurtzke, J. F. 1975. A reassessment of the distribution of multiple sclerosis. Part one. *Acta Neurol Scand*, 51, 110-36.
- Kurtzke, J. F. 1983. Rating neurologic impairment in multiple sclerosis: an expanded disability status scale (EDSS). *Neurology*, 33, 1444-52.
- Kutzelnigg, A., Lucchinetti, C. F., Stadelmann, C., Bruck, W., Rauschka, H., Bergmann, M., Schmidbauer, M., Parisi, J. E. & Lassmann, H. 2005. Cortical demyelination and diffuse white matter injury in multiple sclerosis. *Brain*, 128, 2705-12.
- Langdon, D. W., Amato, M. P., Boringa, J., Brochet, B., Foley, F., Fredrikson, S., et al. 2012. Recommendations for a Brief International Cognitive Assessment for Multiple Sclerosis (BICAMS). *Mult Scler*, 18, 891-8.
- Lassmann, H. 2011. Review: the architecture of inflammatory demyelinating lesions: implications for studies on pathogenesis. *Neuropathol Appl Neurobiol*, 37, 698-710.
- Lassmann, H. 2014. Mechanisms of white matter damage in multiple sclerosis. *Glia*.
- Lassmann, H., Van Horssen, J. & Mahad, D. 2012. Progressive multiple sclerosis: pathology and pathogenesis. *Nat Rev Neurol*, 8, 647-56.
- Latt, J., Nilsson, M., Rydhog, A., Wirestam, R., Stahlberg, F. & Brockstedt, S. 2007. Effects of restricted diffusion in a biological phantom: a q-space diffusion MRI study of asparagus stems at a 3T clinical scanner. *MAGMA*, 20, 213-22.
- Le Bihan, D., Mangin, J. F., Poupon, C., Clark, C. A., Pappata, S., Molko, N. & Chabriat, H. 2001. Diffusion tensor imaging: concepts and applications. *J Magn Reson Imaging*, 13, 534-46.

Levy, L. M., Ziemann, U., Chen, R. & Cohen, L. G. 2002. Rapid modulation of GABA in sensorimotor cortex induced by acute deafferentation. *Ann Neurol*, 52, 755-61.

Lezak M.D., Howieson D.B., Loring D.W. 2004. *Neuropsychological Assessment*, 4th edn. New York, NY: Oxford University Press.

Lin, A., Ross, B. D., Harris, K. & Wong, W. 2005. Efficacy of proton magnetic resonance spectroscopy in neurological diagnosis and neurotherapeutic decision making. *NeuroRx*, 2, 197-214.

Lin, X., Tench, C. R., Evangelou, N., Jaspán, T. & Constantinescu, C. S. 2004. Measurement of spinal cord atrophy in multiple sclerosis. *J Neuroimaging*, 14, 20S-26S.

Liu, Z., Pardini, M., Yaldizli, O., Sethi, V., Muhlert, N., Wheeler-Kingshott, C. A., Samson, R. S., Miller, D. H. & Chard, D. T. 2015. Magnetization transfer ratio measures in normal-appearing white matter show periventricular gradient abnormalities in multiple sclerosis. *Brain*, 138, 1239-46.

Losseff, N. A., Webb, S. L., O'Riordan, J. I., Page, R., Wang, L., Barker, G. J., Tofts, P. S., McDonald, W. I., Miller, D. H. & Thompson, A. J. 1996. Spinal cord atrophy and disability in multiple sclerosis. A new reproducible and sensitive MRI method with potential to monitor disease progression. *Brain*, 119 (Pt 3), 701-8.

Lovas, G., Szilagyi, N., Majtenyi, K., Palkovitis, M. & Komoly, S. 2000. Axonal changes in chronic demyelinated cervical spinal cord plaques. *Brain*, 123 (Pt 2), 308-17.

Lublin, F. D., Reingold, S. C., Cohen, J. A., Cutter, G. R., Sorensen, P. S., Thompson, A. J., Wolinsky, J. S., Balcer, L. J., Banwell, B., Barkhof, F., Bebo, B., JR., Calabresi, P. A., Clanet, M., Comi, G., Fox, R. J., Freedman, M. S., Goodman, A. D., Inglese, M., Kappos, L., Kieseier, B. C., Lincoln, J. A., Lubetzki, C., Miller, A. E., Montalban, X., O'Connor, P. W., Petkau, J., Pozzilli, C., Rudick, R. A., Sormani, M. P., Stuve, O., Waubant, E. & Polman, C. H. 2014. Defining the clinical course of multiple sclerosis: The 2013 revisions. *Neurology*.

Lublin, F. D. & Reingold, S. C. 1996. Defining the clinical course of multiple sclerosis: results of an international survey. National Multiple Sclerosis Society (USA) Advisory Committee on Clinical Trials of New Agents in Multiple Sclerosis. *Neurology*, 46, 907-11.

Lukas, C., Knol, D. L., Sombekke, M. H., Bellenberg, B., Hahn, H. K., Popescu, V., Weier, K., Radue, E. W., Gass, A., Kappos, L., Naegelin, Y., Uitdehaag, B. M., Geurts, J. J., Barkhof, F. & Vrenken, H. 2015. Cervical spinal cord volume loss is related to clinical disability progression in multiple sclerosis. *J Neurol Neurosurg Psychiatry*, 86, 410-8.

Lundell, H., Barthelemy, D., Skimminge, A., Dyrby, T. B., Biering-Sorensen, F. & Nielsen, J. B. 2011. Independent spinal cord atrophy measures correlate to motor and sensory deficits in individuals with spinal cord injury. *Spinal Cord*, 49, 70-5.

- Lycklama, G., Thompson, A., Filippi, M., Miller, D., Polman, C., Fazekas, F. & Barkhof, F. 2003. Spinal-cord MRI in multiple sclerosis. *Lancet Neurol*, 2, 555-62.
- MacDonald, R. L., Kang, J. Q. & Gallagher, M. J. 2010. Mutations in GABAA receptor subunits associated with genetic epilepsies. *J Physiol*, 588, 1861-9.
- Mackenzie, I. S., Morant, S. V., Bloomfield, G. A., MacDonald, T. M. & O'Riordan, J. 2014. Incidence and prevalence of multiple sclerosis in the UK 1990-2010: a descriptive study in the General Practice Research Database. *J Neurol Neurosurg Psychiatry*, 85, 76-84.
- Magliozzi, R., Howell, O., Vora, A., Serafini, B., Nicholas, R., Puopolo, M., Reynolds, R. & Aloisi, F. 2007. Meningeal B-cell follicles in secondary progressive multiple sclerosis associate with early onset of disease and severe cortical pathology. *Brain*, 130, 1089-104.
- Magliozzi, R., Howell, O. W., Reeves, C., Roncaroli, F., Nicholas, R., Serafini, B., Aloisi, F. & Reynolds, R. 2010. A Gradient of neuronal loss and meningeal inflammation in multiple sclerosis. *Ann Neurol*, 68, 477-93.
- Mahad, D. H., Trapp, B. D. & Lassmann, H. 2015. Pathological mechanisms in progressive multiple sclerosis. *Lancet Neurol*, 14, 183-93.
- Manouchehrinia, A., Tench, C. R., Maxted, J., Bibani, R. H., Britton, J. & Constantinescu, C. S. 2013. Tobacco smoking and disability progression in multiple sclerosis: United Kingdom cohort study. *Brain*, 136, 2298-304.
- Marliani, A. F., Clementi, V., Albin Riccioli, L., Agati, R., Carpenzano, M., Salvi, F. & Leonardi, M. 2010. Quantitative cervical spinal cord 3T proton MR spectroscopy in multiple sclerosis. *AJNR Am J Neuroradiol*, 31, 180-4.
- Marrie, R. A., Elliott, L., Marriott, J., Cossoy, M., Blanchard, J., Leung, S. & YU, N. 2015. Effect of comorbidity on mortality in multiple sclerosis. *Neurology*, 85, 240-7.
- Marrie, R. A., Horwitz, R., Cutter, G., Tyry, T., Campagnolo, D. & Vollmer, T. 2009. Comorbidity delays diagnosis and increases disability at diagnosis in MS. *Neurology*, 72, 117-24.
- Marrie, R. A., Rudick, R., Horwitz, R., Cutter, G., Tyry, T., Campagnolo, D. & Vollmer, T. 2010. Vascular comorbidity is associated with more rapid disability progression in multiple sclerosis. *Neurology*, 74, 1041-7.
- Mason, G. F., Martin, D. L., Martin, S. B., Manor, D., Sibson, N. R., Patel, A., Rothman, D. L. & Behar, K. L. 2001. Decrease in GABA synthesis rate in rat cortex following GABA-transaminase inhibition correlates with the decrease in GAD(67) protein. *Brain Res*, 914, 81-91.
- Maynard, F. M., JR., Bracken, M. B., Creasey, G., Diyunno, J. F., JR., Donovan, W. H., Ducker, T. B., Garber, S. L., Marino, R. J., Stover, S. L., Tator, C. H.,

Waters, R. L., Wilberger, J. E. & Young, W. 1997. International Standards for Neurological and Functional Classification of Spinal Cord Injury. American Spinal Injury Association. *Spinal Cord*, 35, 266-74.

McDonald, W. I., Compston, A., Edan, G., Goodkin, D., Hartung, H. P., Lublin, F. D., McFarland, H. F., Paty, D. W., Polman, C. H., Reingold, S. C., Sandberg-Wollheim, M., Sibley, W., Thompson, A., Van Den Noort, S., Weinshenker, B. Y. & Wolinsky, J. S. 2001. Recommended diagnostic criteria for multiple sclerosis: guidelines from the International Panel on the diagnosis of multiple sclerosis. *Ann Neurol*, 50, 121-7.

Medical Research Council. Aids to the investigation of the peripheral nervous system. London: Her Majesty's Stationary Office; 1943.

Meinl, E., Krumbholz, M., Derfuss, T., Junker, A. & Hohfeld, R. 2008. Compartmentalization of inflammation in the CNS: a major mechanism driving progressive multiple sclerosis. *J Neurol Sci*, 274, 42-4.

Mescher, M., Merkle, H., Kirsch, J., Garwood, M. & Gruetter, R. 1998. Simultaneous in vivo spectral editing and water suppression. *NMR Biomed*, 11, 266-72.

Michels, L., Martin, E., Klaver, P., Edden, R., Zelaya, F., Lythgoe, D. J., Luchinger, R., Brandeis, D. & O'Gorman, R. L. 2012. Frontal GABA levels change during working memory. *PLoS One*, 7, e31933.

Mikulis, D. J., Wood, M. L., Zerdoner, O. A. & Poncelet, B. P. 1994. Oscillatory motion of the normal cervical spinal cord. *Radiology*, 192, 117-21.

Miller, D., Barkhof, F., Montalban, X., Thompson, A. & Filippi, M. 2005. Clinically isolated syndromes suggestive of multiple sclerosis, part I: natural history, pathogenesis, diagnosis, and prognosis. *Lancet Neurol*, 4, 281-8.

Miller, D. H. & Leary, S. M. 2007a. Primary-progressive multiple sclerosis. *Lancet Neurol*, 6, 903-12.

Miller, D. H., Fox, R. J., Philips, J. T., Hutchinson, M., Havrdova, E., Kita, M., Wheeler-Kingshott, C. A., Tozer, D. J., MacManus, D. G., Yousry, T. A., Goodsell, M., Yang, M., Zhang, R., Vigiotta, V. & Dawson, K. T. 2015. Effects of delayed-release dimethyl fumarate on MRI measures in the phase 3 CONFIRM study. *Neurology*, 84, 1145-52.

Miller, D. H., Soon, D., Fernando, K. T., MacManus, D. G., Barker, G. J., Yousry, T. A., Fisher, E., O'Connor, P. W., Phillips, J. T., Polman, C. H., Kappos, L., Hutchinson, M., Havrdova, E., Lublin, F. D., Giovannoni, G., Wajgt, A., Rudick, R., Lynn, F., Panzara, M. A. & Sandrock, A. W. 2007b. MRI outcomes in a placebo-controlled trial of natalizumab in relapsing MS. *Neurology*, 68, 1390-401.

Miller, D. H., Thompson, A. J. & Filippi, M. 2003. Magnetic resonance studies of abnormalities in the normal appearing white matter and grey matter in multiple sclerosis. *J Neurol*, 250, 1407-19.

- Minagar, A., Barnett, M. H., Benedict, R. H., Pelletier, D., Pirko, I., Sahraian, M. A., Frohman, E. & Zivadinov, R. 2013. The thalamus and multiple sclerosis: modern views on pathologic, imaging, and clinical aspects. *Neurology*, 80, 210-9.
- Moffett, J. R., Ross, B., Arun, P., Madhavarao, C. N. & Namboodiri, A. M. 2007. N-Acetylaspartate in the CNS: from neurodiagnostics to neurobiology. *Prog Neurobiol*, 81, 89-131.
- Montalban, X., Tintore, M., Swanton, J., Barkhof, F., Fazekas, F., Filippi, M., Frederiksen, J., Kappos, L., Palace, J., Polman, C., Rovaris, M., De Stefano, N., Thompson, A., Yousry, T., Rovira, A. & Miller, D. H. 2010. MRI criteria for MS in patients with clinically isolated syndromes. *Neurology*, 74, 427-34.
- Moore, G. R. & Laule, C. 2012. Neuropathologic correlates of magnetic resonance imaging in multiple sclerosis. *J Neuropathol Exp Neurol*, 71, 762-78.
- Mugler, J. P., 3RD & Brookeman, J. R. 1990. Three-dimensional magnetization-prepared rapid gradient-echo imaging (3D MP RAGE). *Magn Reson Med*, 15, 152-7.
- Muhlert, N., Atzori, M., De Vita, E., Thomas, D. L., Samson, R. S., Wheeler-Kingshott, C. A., Geurts, J. J., Miller, D. H., Thompson, A. J. & Ciccarelli, O. 2014. Memory in multiple sclerosis is linked to glutamate concentration in grey matter regions. *J Neurol Neurosurg Psychiatry*.
- Muhlert, N., Sethi, V., Schneider, T., Daga, P., Cipolotti, L., Haroon, H. A., Parker, G. J., Ourselin, S., Wheeler-Kingshott, C. A., Miller, D. H., Ron, M. A. & Chard, D. T. 2013. Diffusion MRI-based cortical complexity alterations associated with executive function in multiple sclerosis. *J Magn Reson Imaging*, 38, 54-63.
- Mullins, P. G., McGonigle, D. J., O'Gorman, R. L., Puts, N. A., Vidyasagar, R., Evans, C. J. & Edden, R. A. 2014. Current practice in the use of MEGA-PRESS spectroscopy for the detection of GABA. *Neuroimage*, 86:43-52.
- Mumford, C. J., Wood, N. W., Kellar-Wood, H., Thorpe, J. W., Miller, D. H. & Compston, D. A. 1994. The British Isles survey of multiple sclerosis in twins. *Neurology*, 44, 11-5.
- Munger, K. L., Zhang, S. M., O'Reilly, E., Hernan, M. A., Olek, M. J., Willett, W. C. & Ascherio, A. 2004. Vitamin D intake and incidence of multiple sclerosis. *Neurology*, 62, 60-5.
- Munoz-Culla, M., Irizar, H. & Otaegui, D. 2013. The genetics of multiple sclerosis: review of current and emerging candidates. *Appl Clin Genet*, 6, 63-73.
- Murray, R. F., Asghari, A., Egorov, D. D., Rutkowski, S. B., Siddall, P. J., Soden, R. J. & Ruff, R. 2007. Impact of spinal cord injury on self-perceived pre- and postmorbid cognitive, emotional and physical functioning. *Spinal Cord*, 45, 429-36.

- Muthukumaraswamy, S. D., Edden, R. A., Jones, D. K., Swettenham, J. B. & Singh, K. D. 2009. Resting GABA concentration predicts peak gamma frequency and fMRI amplitude in response to visual stimulation in humans. *Proc Natl Acad Sci U S A*, 106, 8356-61.
- Naismith, R. T., Xu, J., Tutlam, N. T., Snyder, A., Benzinger, T., Shimony, J., Shepherd, J., Trinkaus, K., Cross, A. H. & Song, S. K. 2009. Disability in optic neuritis correlates with diffusion tensor-derived directional diffusivities. *Neurology*, 72, 589-94.
- Near, J. (2014). Spectral quantification and pitfalls in interpreting magnetic resonance spectroscopic data: what to look out for. In Stagg C.J. & Rothman D.L. (Eds.), *Magnetic Resonance Spectroscopy* (pp. 49-67). London: Elsevier
- Nelson, H. E. (1982). *National Adult Reading Test*. Windsor, UK: NFER-Nelson.
- Noseworthy, J. H., Lucchinetti, C., Rodriguez, M. & Weinshenker, B. G. 2000. Multiple sclerosis. *N Engl J Med*, 343, 938-52.
- Novotna, M., Paz Soldan, M. M., Abou Zeid, N., Kale, N., Tutucu, M., Crusan, D. J., Atkinson, E. J., Siva, A., Keegan, B. M., Pirko, I., Pittock, S. J., Lucchinetti, C. F., Noseworthy, J. H., Weinshenker, B. G., Rodriguez, M. & Kantarci, O. H. 2015. Poor early relapse recovery affects onset of progressive disease course in multiple sclerosis. *Neurology*, 85, 722-9.
- O'Gorman, R. L., Michelsl, L., Edden, R. A., Murdoch, J. B. & Martin, E. 2011. In vivo detection of GABA and glutamate with MEGA-PRESS: reproducibility and gender effects. *J Magn Reson Imaging*, 33, 1262-7.
- Oh, J., Saidha, S., Chen, M., Smith, S. A., Prince, J., Jones, C., Diener-West, M., Van Zijl, P. C., Reich, D. S. & Calabresi, P. A. 2013. Spinal cord quantitative MRI discriminates between disability levels in multiple sclerosis. *Neurology*, 80, 540-7.
- Ourselin, S., Roche, A., Prima, S. & Ayache, N. (2000). Block Matching: A General Framework to Improve Robustness of Rigid Registration of Medical Images. In *Medical Image Computing and Computer-Assisted Intervention – MICCAI 2000*, Vol. 1935, 557-566 (Eds S. Delp, A. DiGoia and B. Jaramaz) Springer Berlin Heidelberg.
- Okuda, D. T., Mowry, E. M., Beheshtian, A., Waubant, E., Baranzini, S. E., Goodin, D. S., Hauser, S. L. & Pelletier, D. 2009. Incidental MRI anomalies suggestive of multiple sclerosis: the radiologically isolated syndrome. *Neurology*, 72, 800-5.
- Olerup, O. & Hillert, J. 1991. HLA class II-associated genetic susceptibility in multiple sclerosis: a critical evaluation. *Tissue Antigens*, 38, 1-15.
- Ontaneda, D., Fox, R. J. & Chataway, J. 2015. Clinical trials in progressive multiple sclerosis: lessons learned and future perspectives. *Lancet Neurol*, 14, 208-23.

- Orbach, R., Gurevich, M. & Achiron, A. 2013. Interleukin-12p40 in the spinal fluid as a biomarker for clinically isolated syndrome. *Mult Scler*.
- Ozawa, K., Suchanek, G., Breitschopf, H., Bruck, W., Budka, H., Jellinger, K. & Lassmann, H. 1994. Patterns of oligodendroglia pathology in multiple sclerosis. *Brain*, 117 (Pt 6), 1311-22.
- Patrick, E., Christodoulou, C. & Krupp, L. B. 2009. Longitudinal correlates of fatigue in multiple sclerosis. *Mult Scler*, 15, 258-61.
- Paty, D. W., Oger, J. J., Kastrukoff, L. F., Hashimoto, S. A., Hooge, J. P., Eisen, A. A., Eisen, K. A., Purves, S. J., Low, M. D. & Brandeys, V. 1988. MRI in the diagnosis of MS: a prospective study with comparison of clinical evaluation, evoked potentials, oligoclonal banding, and CT. *Neurology*, 38, 180-5.
- Pfefferbaum, A., Mathalon, D. H., Sullivan, E. V., Rawles, J. M., Zipursky, R. B. & Lim, K. O. 1994. A quantitative magnetic resonance imaging study of changes in brain morphology from infancy to late adulthood. *Arch Neurol*, 51, 874-87.
- Pierpaoli, C. & Basser, P. J. 1996. Toward a quantitative assessment of diffusion anisotropy. *Magn Reson Med*, 36, 893-906.
- Polman, C. H., Reingold, S. C., Banwell, B., Clanet, M., Cohen, J. A., Filippi, M., Fujihara, K., Havrdova, E., Hutchinson, M., Kappos, L., Lublin, F. D., Montalban, X., O'Connor, P., Sandberg-Wollheim, M., Thompson, A. J., Waubant, E., Weinshenker, B. & Wolinsky, J. S. 2011. Diagnostic criteria for multiple sclerosis: 2010 revisions to the McDonald criteria. *Ann Neurol*, 69, 292-302.
- Polman, C. H., Reingold, S. C., Edan, G., Filippi, M., Hartung, H. P., Kappos, L., Lublin, F. D., Metz, L. M., McFarland, H. F., O'Connor, P. W., Sandberg-Wollheim, M., Thompson, A. J., Weinshenker, B. G. & Wolinsky, J. S. 2005. Diagnostic criteria for multiple sclerosis: 2005 revisions to the "McDonald Criteria". *Ann Neurol*, 58, 840-6.
- Poser, C. M., Paty, D. W., Scheinberg, L., McDonald, W. I., Davis, F. A., Ebers, G. C., Johnson, K. P., Sibley, W. A., Silberberg, D. H. & Tourtellotte, W. W. 1983. New diagnostic criteria for multiple sclerosis: guidelines for research protocols. *Ann Neurol*, 13, 227-31.
- Prados, F., Cardoso, M. J., Leung, K. K., Cash, D. M., Modat, M., Fox, N. C., Wheeler-Kingshott, C. A. & Ourselin, S. 2015. Measuring brain atrophy with a generalized formulation of the boundary shift integral. *Neurobiol Aging*, 36 Suppl 1, S81-90.
- Prados, F., Cardoso, M.J., MacManus, D., Wheeler-Kingshott, C. A. M., Ourselin, S. 2014. A modality agnostic patch-based technique for lesion filling in Multiple Sclerosis. *Medical Image Computing and Computer-Assisted Intervention - MICCAI. Lecture Notes in Computer Science Volume 8674, 2014, pp 781-788.*

- Prados, F., Yiannakas, M., Cardoso, M.J., Grussu, F., DeAngelis F., Plantone D., Miller, D., Ciccarelli, O., Gandini Wheeler-Kingshott, C.A.M., & Oureslin, S. 2016. Atrophy computation in the spinal cord using Boundary Shift Imaging. ISMRM.
- Proctor, W.G., Yu, F.C. 1950. The dependence of a nuclear magnetic resonance frequency. *Phys Rev*; 77: 717.
- Provencher, S. W. 1993. Estimation of metabolite concentrations from localized in vivo proton NMR spectra. *Magn Reson Med*, 30, 672-9.
- Provencher SW. LCMModel & LCMgui User's Manual. Vol. 2014. 2014. Available from <http://s-provencher.com/pub/LCMModel/manual/manual.pdf>.
- Puts, N. A. & Edden, R. A. 2012. In vivo magnetic resonance spectroscopy of GABA: a methodological review. *Prog Nucl Magn Reson Spectrosc*, 60, 29-41.
- Radue, E. W., O'Connor, P., Polman, C. H., Hohlfeld, R., Calabresi, P., Selmaj, K., Mueller-Lenke, N., Agoropoulou, C., Holdbrook, F., De Vera, A., Zhang-Auberson, L., Francis, G., Burtin, P. & Kappos, L. 2012. Impact of fingolimod therapy on magnetic resonance imaging outcomes in patients with multiple sclerosis. *Arch Neurol*, 69, 1259-69.
- Rao C.R. 1946. Minimum variance and the estimation of several parameters. *Proc. Cambridge Phil. Soc.*, 43, 280-283.
- Rao S.M. 1990. A manual for the brief repeatable battery of neuropsychological tests in multiple sclerosis. *Ann Neurol Milwaukee, Wis: Medical College of Wisconsin*.
- Rashid, W., Davies, G. R., Chard, D. T., Griffin, C. M., Altmann, D. R., Gordon, R., Thompson, A. J. & Miller, D. H. 2006. Increasing cord atrophy in early relapsing-remitting multiple sclerosis: a 3 year study. *J Neurol Neurosurg Psychiatry*, 77, 51-5.
- Reid, J. D. 1960. Effects of flexion-extension movements of the head and spine upon the spinal cord and nerve roots. *J Neurol Neurosurg Psychiatry*, 23, 214-21.
- Reynolds, G. P., Beasley, C. L. & Zhang, Z. J. 2002. Understanding the neurotransmitter pathology of schizophrenia: selective deficits of subtypes of cortical GABAergic neurons. *J Neural Transm*, 109, 881-9.
- Reynolds, R., Roncaroli, F., Nicholas, R., Radotra, B., Gveric, D. & Howell, O. 2011. The neuropathological basis of clinical progression in multiple sclerosis. *Acta Neuropathol*, 122, 155-70.
- Rocca, M. A., Amato, M. P., De Stefano, N., Enzinger, C., Geurts, J. J., Penner, I. K., Rovira, A., Sumowski, J. F., Valsasina, P. & Filippi, M. 2015. Clinical and imaging assessment of cognitive dysfunction in multiple sclerosis. *Lancet Neurol*, 14, 302-17.

- Rocca, M. A., Colombo, B., Falini, A., Ghezzi, A., Martinelli, V., Scotti, G., Comi, G. & Filippi, M. 2005. Cortical adaptation in patients with MS: a cross-sectional functional MRI study of disease phenotypes. *Lancet Neurol*, 4, 618-26.
- Rocca, M. A., Horsfield, M. A., Sala, S., Copetti, M., Valsasins, P., Mesaros, S., Martinelli, V., Caputo, D., Stosic-Opincal, T., Drulovic, J., Comi, G. & Filippi, M. 2011. A multicenter assessment of cervical cord atrophy among MS clinical phenotypes. *Neurology*, 76, 2096-102.
- Rocca, M. A., Valsasina, P., Damjanovic, D., Horsfield, M. A., Mesaros, S., Stosic-Opincal, T., Drulovic, J. & Filippi, M. 2013. Voxel-wise mapping of cervical cord damage in multiple sclerosis patients with different clinical phenotypes. *J Neurol Neurosurg Psychiatry*, 84, 35-41.
- Roosendaal, S. D., Bendfeldt, K., Vrenken, H., Polman, C. H., Borgwardt, S., Radue, E. W., Kappos, L., Pelletier, D., Hauser, S. L., Matthews, P. M., Barkhof, F. & Geurts, J. J. 2011. Grey matter volume in a large cohort of MS patients: relation to MRI parameters and disability. *Mult Scler*, 17, 1098-106.
- Roosendaal, S. D., Geurts, J. J., Vrenken, H., Hulst, H. E., Cover, K. S., Castelijns, J. A., Pouwels, P. J. & Barkhof, F. 2009. Regional DTI differences in multiple sclerosis patients. *Neuroimage*, 44, 1397-403.
- Roth, E., Davidoff, G., Thomas, P., Dolianac, R., Dijkers, M., Berent, S., Morris, J. & Yarkony, G. 1989. A controlled study of neuropsychological deficits in acute spinal cord injury patients. *Paraplegia*, 27, 480-9.
- Rovaris, M., Iannucci, G., Falautano, M., Possa, F., Martinelli, V., Comi, G. & Filippi, M. 2002. Cognitive dysfunction in patients with mildly disabling relapsing-remitting multiple sclerosis: an exploratory study with diffusion tensor MR imaging. *J Neurol Sci*, 195, 103-9.
- Rovira, A., Wattjes, M. P., Tintore, M., Tur, C., Yousry, T. A., Sormani, M. P., De Stefano, N., Filippi, M., Auger, C., Rocca, M. A., Barkhof, F., Fazekas, F., Kappos, L., Polman, C., Miller, D. & Montalban, X. 2015. Evidence-based guidelines: MAGNIMS consensus guidelines on the use of MRI in multiple sclerosis-clinical implementation in the diagnostic process. *Nat Rev Neurol*, 11, 471-82.
- Rudick, R. A., Fisher, E., Lee, J. C., Simon, J. & Jacobs, L. 1999. Use of the brain parenchymal fraction to measure whole brain atrophy in relapsing-remitting MS. Multiple Sclerosis Collaborative Research Group. *Neurology*, 53, 1698-704.
- Saji, M. & Reis, D. J. 1987. Delayed transneuronal death of substantia nigra neurons prevented by gamma-aminobutyric acid agonist. *Science*, 235, 66-9.
- Salzer, J., Hallmans, G., Nystrom, M., Syenlund, H., Wadell, G. & Sundstrom, P. 2012. Vitamin D as a protective factor in multiple sclerosis. *Neurology*, 79, 2140-5.

Sargsyan, S. A., Shearer, A. J., Ritchie, A. M., Burgoon, M. P., Anderson, S., Hemmer, B., Stademann, C., Gattenlohner, S., Owens, G. P., Gilden, D. & Bennett, J. L. 2010. Absence of Epstein-Barr virus in the brain and CSF of patients with multiple sclerosis. *Neurology*, 74, 1127-35.

Sastre-Garriga, J., Ingle, G. T., Chard, D. T., Ramio-Torrenta, L., McLean, M. A., Miller, D. H. & Thompson, A. J. 2005. Metabolite changes in normal-appearing gray and white matter are linked with disability in early primary progressive multiple sclerosis. *Arch Neurol*, 62, 569-73.

Sato, F., Martinez, N. E., Stewart, E. C., Omura, S., Alexander, J. S. & Tsunoda, I. 2015. "Microglial nodules" and "newly forming lesions" may be a Janus face of early MS lesions; implications from virus-induced demyelination, the Inside-Out model. *BMC Neurol*, 15, 219.

Saunders, D. E., Howe, F. A., Van Den Boogaart, A., Griffiths, J. R. & Brown, M. M. 1999. Aging of the adult human brain: in vivo quantitation of metabolite content with proton magnetic resonance spectroscopy. *J Magn Reson Imaging*, 9, 711-6.

Sawcer, S. 2008. The complex genetics of multiple sclerosis: pitfalls and prospects. *Brain*, 131, 3118-31.

Sawcer, S., Hellenthal, G., Pirinen, M., Spencer, C. C., Patsopoulos, N. A., Moutsianas, L., Dilthey, A., Su, Z., Freeman, C., Hunt, S. E., Edkins, S., Gray, E., Booth, D. R., Potter, S. C., Goris, A., Band, G., Oturai, A. B., Strange, A., Saarela, J., Bellenguez, C., Fontaine, B., Gillman, M., Hemmer, B., Gwilliam, R., Zipp, F., Jayakumar, A., Martin, R., Leslie, S., Hawkins, S., Giannoulatou, E., D'Alfonso, S., Blackburn, H., Martinelli Boneschi, F., Liddle, J., Harbo, H. F., Perez, M. L., Spurkland, A., Waller, M. J., Mycko, M. P., Ricketts, M., Comabella, M., Hammond, N., Kockum, I., McCann, O. T., Ban, M., Whittaker, P., Kempainen, A., Weston, P., Hawkins, C., Widaa, S., Zajicek, J., Dronov, S., Robertson, N., Bumpstead, S. J., Barcellos, L. F., Ravindrarajah, R., Abraham, R., Alfredsson, L., Ardlie, K., Aubin, C., Baker, A., Baker, K., Barazini, S. E., Bergamaschi, L., Bergamaschi, R., Bernstein, A., Berthele, A., Boggild, M., Bradfield, J. P., Brassat, D., Broadley, S. A., Buck, D., Butzkueven, H., Capra, R., Carroll, W. M., Cavalla, P., Celiuș, E. G., Cepok, S., Chiavacci, R., Clerget-Darpoux, F., Clysters, K., Comi, G., Cossburn, M., Courneu-Rebeix, I., Cox, M. B., Cozen, W., Cree, B. A., Cross, A. H., Cusi, D., Daly, M. J., Davis, E., De Bakker, P. I., Debouverie, M., D'Hooghe M, B., Dixon, K., Dobosi, R., Dubois, B., Ellinghaus, D., Elovaara, I., Esposito, F., et al. 2011. Genetic risk and a primary role for cell-mediated immune mechanisms in multiple sclerosis. *Nature*, 476, 214-9.

Scalfari, A., Neuhaus, A., Degenhardt, A., Rice, G. P., Muraro, P. A., Daumer, M. & Ebers, G. C. 2010. The natural history of multiple sclerosis: a geographically based study 10: relapses and long-term disability. *Brain*, 133, 1914-29.

Schmierer, K., Wheeler-Kingshott, C. A., Boulby, P. A., Scaravilli, F., Altmann, D. R., Barker, G. J., Tofts, P. S. & Miller, D. H. 2007. Diffusion tensor imaging of post mortem multiple sclerosis brain. *Neuroimage*, 35, 467-77.

- Schneider, T. & Wheeler-Kingshott, C. (2014a). Q-Space Imaging: A Model-Free Approach. In *Quantitative MRI of the Spinal Cord* (Eds J. Cohen-Adad and C. Wheeler-Kingshott). Oxford: Elsevier.
- Schneider T, Brownlee W, Zhang Z, Ciccarelli O, Miller DH, and Wheeler-Kingshott CAM. (2014b) Application of multi-shell NODDI in multiple sclerosis. In proceedings of the 22nd meeting of the International Society for Magnetic Resonance in Medicine (ISMRM), page 0019.
- Schneider T., Ciccarelli O., Kachramanoglou C., Thomas D.L. & Wheeler-Kingshott CAM. (2011). Reliability of tract-specific q-space imaging metrics in healthy spinal cord. In ISMRM, Montreal.
- Schneider T., Brownlee W., Zhang H., Ciccarelli O., Miller D.H., Wheeler-Kingshott Gandini C.A.M. 2016. Sensitivity of multi-shell NODDI to Multiple Sclerosis white matter changes. *Function Neurology* (under review).
- Schumacher, G., Beebe, G., Kibler, R., Kurland, L. Problems of experimental trials of therapy in multiple sclerosis: report by the panel on the evaluation of experimental trials of therapy in multiple sclerosis. *Ann NY Acad Sci* 1965; 122:552-568.
- Serafini, B., Rosicarelli, B., Magliozzi, R., Stigliano, E. & Aloisi, F. 2004. Detection of ectopic B-cell follicles with germinal centers in the meninges of patients with secondary progressive multiple sclerosis. *Brain Pathol*, 14, 164-74.
- Simon, K. C., Van Der Mei, I. A., Munger, K. L., Ponsonby, A., Dickinson, J., Dwyer, T., Sundstrom, P. & Ascherio, A. 2010. Combined effects of smoking, anti-EBNA antibodies, and HLA-DRB1*1501 on multiple sclerosis risk. *Neurology*, 74, 1365-71.
- Simpson, S., JR., Taylor, B., Blizzard, L., Ponsonby, A. L., Pittas, F., Tremlett, H., Dwyer, T., Gies, P. & Van Der Mei, I. 2010. Higher 25-hydroxyvitamin D is associated with lower relapse risk in multiple sclerosis. *Ann Neurol*, 68, 193-203.
- Smith, S. M., De Stefano, N., Jenkinson, M. & Matthews, P. M. 2001. Normalized accurate measurement of longitudinal brain change. *J Comput Assist Tomogr*, 25, 466-75.
- Smith, S. M., Jenkinson, M., Woolrich, M. W., Beckmann, C. F., Behrens, T. E., Johansen-Berg, H., Bannister, P. R., De Luca, M., Drobnjak, I., Flitney, D. E., Niazy, R. K., Saunders, J., Vickers, J., Zhang, Y., De Stefano, N., Brady, J. M. & Matthews, P. M. 2004. Advances in functional and structural MR image analysis and implementation as FSL. *Neuroimage*, 23 Suppl 1, S208-19.
- Smith, S. M., Zhang, Y., Jenkinson, M., Chen, J., Matthews, P. M., Federico, A. & De Stefano, N. 2002. Accurate, robust, and automated longitudinal and cross-sectional brain change analysis. *Neuroimage*, 17, 479-89.
- Solanky, B. S., Abdel-Aziz, K., Yiannakas, M. C., Berry, A. M., Ciccarelli, O. & Wheeler-Kingshott, C. A. 2013a. In vivo magnetic resonance spectroscopy

detection of combined glutamate-glutamine in healthy upper cervical cord at 3 T. *NMR Biomed*, 26, 357-66.

Solanky B., Cawley N., Graca A., Edden R., Ciccarelli O., Wheeler-Kingshott C. 2013b. In Vivo Optimisation of GABA measurements in the Hippocampus Using MEGA-PRESS at 3T. ISMRM Salt Lake City. Poster no. 2393.

Song, S. K., Sun, S. W., Ju, W. K., Lin, S. J., Cross, A. H. & Neufeld, A. H. 2003. Diffusion tensor imaging detects and differentiates axon and myelin degeneration in mouse optic nerve after retinal ischemia. *Neuroimage*, 20, 1714-22.

Srinivasan, R., Sailasuta, N., Hurd, R., Nelson, S. & Pelletier, D. 2005. Evidence of elevated glutamate in multiple sclerosis using magnetic resonance spectroscopy at 3 T. *Brain*, 128, 1016-25.

Stagg, C. J. 2014. Magnetic Resonance Spectroscopy as a tool to study the role of GABA in motor-cortical plasticity. *Neuroimage*, 86, 19-27.

Stagg, C. J., Bachtiar, V. & Johansen-Berg, H. 2011. The role of GABA in human motor learning. *Curr Biol*, 21, 480-4.

Stein, J., Narendran, K., McBean, J., Krebs, K. & Hughes, R. (2007). Electromyography-controlled exoskeletal upper-limb-powered orthosis for exercise training after stroke. *Am J Phys Med Rehabil* 86(4): 255-261.

Stejskal, E. O. & Tanner, J. E. (1965). Spin diffusion measurements - spin echoes in presence of a time-dependent field gradient. *J Chem Phys* 42: 5.

Stevenson, V. L., Miller, D. H., Leary, S. M., Rovaris, M., Barkhof, F., Brochet, B., Dousset, V., Filippi, M., Hintzen, R., Montalban, X., Polman, C. H., Rovira, A., De Sa, J. & Thompson, A. J. 2000. One year follow up study of primary and transitional progressive multiple sclerosis. *J Neurol Neurosurg Psychiatry*, 68, 713-8.

Strober, L., Englert, J., Munschauer, F., Weinstock-Guttman, B., Rao, S. & Benedict, R. H. 2009. Sensitivity of conventional memory tests in multiple sclerosis: comparing the Rao Brief Repeatable Neuropsychological Battery and the Minimal Assessment of Cognitive Function in MS. *Mult Scler*, 15, 1077-84.

Stromillo, M. L., Giorgio, A., Rossi, F., Battaglini, M., Hakiki, B., Malentacchi, G., Santangelo, M., Gasperini, C., Bartolozzi, M. L., Portaccio, E., Amato, M. P. & De Stefano, N. 2013. Brain metabolic changes suggestive of axonal damage in radiologically isolated syndrome. *Neurology*, 80, 2090-4.

Stys, P. K., Zamponi, G. W., Van Minnen, J. & Geurts, J. J. 2012. Will the real multiple sclerosis please stand up? *Nat Rev Neurosci*, 13, 507-14.

Sumowski, J. F., Rocca, M. A., Leavitt, V. M., Dackovic, J., Mesaros, S., Drulovic, J., DeLuca, J. & Filippi, M. 2014. Brain reserve and cognitive reserve protect against cognitive decline over 4.5 years in MS. *Neurology*, 82, 1776-83.

- Sumowski, J. F., Rocca, M. A., Leavitt, V. M., Riccitelli, G., Comi, G., DeLuca, J. & Filippi, M. 2013. Brain reserve and cognitive reserve in multiple sclerosis: what you've got and how you use it. *Neurology*, 80, 2186-93.
- Svens, B. & Lee, H (2005). Intra- and inter-instrument reliability of Grip-Strength Measurements: Grip Strength™ and Jamar® hand dynamometers. *The British Journal of Hand Therapy* 10 (2): 47-55.
- Takei, Y., Fujihara, K., Tagawa, M., Hironaga, N., Near, J., Kasagi, M., Takahashi, Y., Motegi, T., Suzuki, Y., Aoyama, Y., Sakurai, N., Yamaguchi, M., Tobimatsu, S., Ujita, K., Tsushima, Y., Narita, K. & Fukuda, M. 2016. The inhibition/excitation ratio related to task-induced oscillatory modulations during a working memory task: A multimodal-imaging study using MEG and MRS. *Neuroimage*, 128, 302-15.
- Tartaglia, M. C., Narayanan, S., Francis, S. J., Santos, A. C., De Stefano, N., Lapierre, Y. & Arnold, D. L. 2004. The relationship between diffuse axonal damage and fatigue in multiple sclerosis. *Arch Neurol*, 61, 201-7.
- Taylor, B. V. 2011. The major cause of multiple sclerosis is environmental: genetics has a minor role--yes. *Mult Scler*, 17, 1171-3.
- Thickbroom, G. W., Sacco, P., Faulkner, D. L., Kermode, A. G. & Mastaglia, F. L. 2008. Enhanced corticomotor excitability with dynamic fatiguing exercise of the lower limb in multiple sclerosis. *J Neurol*, 255, 1001-5.
- Thompson, A. J. 2015. A much-needed focus on progression in multiple sclerosis. *Lancet Neurol*, 14, 133-5.
- Tintore, M., Rovira, A., Martinez, M. J., Rio, J., Diaz-Villoslada, P., Brieva, L., Borrás, C., Grive, E., Capellades, J. & MontalbanO, X. 2000. Isolated demyelinating syndromes: comparison of different MR imaging criteria to predict conversion to clinically definite multiple sclerosis. *AJNR Am J Neuroradiol*, 21, 702-6.
- Tkac, I., Andersen, P., Adriany, G., Merkle, H., Ugurbil, K. & Gruetter, R. 2001. In vivo 1H NMR spectroscopy of the human brain at 7 T. *Magn Reson Med*, 46, 451-6.
- Trapp, B. D., Peterson, J., Ransohoff, R. M., Rudick, R., Mork, S. & Bo, L. 1998. Axonal transection in the lesions of multiple sclerosis. *N Engl J Med*, 338, 278-85.
- Trapp, B. D. & Nave, K. A. 2008. Multiple sclerosis: an immune or neurodegenerative disorder? *Annu Rev Neurosci*, 31, 247-69.
- Trapp, B. D., Ransohoff, R. & Rudick, R. 1999. Axonal pathology in multiple sclerosis: relationship to neurologic disability. *Curr Opin Neurol*, 12, 295-302.
- Trenerry MR. 1989. Stroop neuropsychological assessment manual. Odessa, FL: Psychological Assessment Resources.

- Vidal-Jordana, A., Sastre-Garriga, J., Rovira, A. & Montalban, X. 2015. Treating relapsing-remitting multiple sclerosis: therapy effects on brain atrophy. *J Neurol*, 262, 2617-26.
- Vrenken, H., Pouwels, P. J., Geurts, J. J., Knol, D. L., Polman, C. H., Barkhof, F. & Castelijns, J. A. 2006. Altered diffusion tensor in multiple sclerosis normal-appearing brain tissue: cortical diffusion changes seem related to clinical deterioration. *J Magn Reson Imaging*, 23, 628-36.
- Vukusic, S. & Confavreux, C. 2003. Prognostic factors for progression of disability in the secondary progressive phase of multiple sclerosis. *J Neurol Sci*, 206, 135-7.
- Wansapura, J. P., Holland, S. K., Dunn, R. S. & Ball, W. S., JR. 1999. NMR relaxation times in the human brain at 3.0 tesla. *J Magn Reson Imaging*, 9, 531-8.
- Webb, A. R., Kline, L. & Holick, M. F. 1988. Influence of season and latitude on the cutaneous synthesis of vitamin D3: exposure to winter sunlight in Boston and Edmonton will not promote vitamin D3 synthesis in human skin. *J Clin Endocrinol Metab*, 67, 373-8.
- Wechsler D. The Wechsler Adult Intelligence Scale III. San Antonio, TX: Harcourt Assessment 1997.
- Wegner, C., Esiri, M. M., Chance, S. A., Palace, J. & Matthews, P. M. 2006. Neocortical neuronal, synaptic, and glial loss in multiple sclerosis. *Neurology*, 67, 960-7
- Weinshenker, B. G., Bass, B., Rice, G. P., Noseworthy, J., Carriere, W., Baskerville, J. & Ebers, G. C. 1989a. The natural history of multiple sclerosis: a geographically based study. I. Clinical course and disability. *Brain*, 112 (Pt 1), 133-46.
- Weinshenker, B. G., Bass, B., Rice, G. P., Noseworthy, J., Carriere, W., Baskerville, J. & Ebers, G. C. 1989b. The natural history of multiple sclerosis: a geographically based study. 2. Predictive value of the early clinical course. *Brain*, 112 (Pt 6), 1419-28.
- Weinstock-Guttman, B., Zivadinov, R., Horakova, D., Havrdova, E., Qu, J., Shyh, G., Lakota, E., O'Connor, K., Badgett, D., Tamano-Blanco, M., Tyblova, M., Hussein, S., Bergsland, N., Willis, L., Kranensky, J., Vaneckova, M., Seidl, Z. & Ramanathan, M. 2013. Lipid profiles are associated with lesion formation over 24 months in interferon-beta treated patients following the first demyelinating event. *J Neurol Neurosurg Psychiatry*, 84, 1186-91.
- Werring, D. J., Brassat, D., Droogan, A. G., Clark, C. A., Symms, M. R., Barker, G. J., MacManus, D. G., Thompson, A. J. & Miller, D. H. 2000. The pathogenesis of lesions and normal-appearing white matter changes in multiple sclerosis: a serial diffusion MRI study. *Brain*, 123 (Pt 8), 1667-76.

- Werring, D. J., Clark, C. A., Barker, G. J., Thompson, A. J. & Miller, D. H. 1999. Diffusion tensor imaging of lesions and normal-appearing white matter in multiple sclerosis. *Neurology*, 52, 1626-32.
- Wheeler-Kingshott, C. A. M., Barker, G. J., Steens, S. C. A. & van Buchem, M. A. (2003): *The Diffusion of Water In Quantitative MRI of the Brain* (Ed P. Toft). Chichester, England: John Wiley & Sons Ltd. Williams & Warwick Gray's Anatomy. Churchill Livingstone.
- Wheeler-Kingshott, C. A., Stroman, P. W., Schwab, J. M., Bacon, M., Bosma, R., Brooks, J., Cadotte, D. W., Carlstedt, T., Ciccarelli, O., Cohen-Adad, J., Curt, A., Evangelou, N., Fehlings, M. G., Filippi, M., Kelley, B. J., Kollias, S., MacKay, A., Porro, C. A., Smith, S., Strittmatter, S. M., Summers, P., Thompson, A. J. & Tracey, I. 2014. The current state-of-the-art of spinal cord imaging: applications. *Neuroimage*, 84, 1082-93.
- Willer, C. J., Dyment, D. A., Risch, N. J., Sadovnick, A. D. & Ebers, G. C. 2003. Twin concordance and sibling recurrence rates in multiple sclerosis. *Proc Natl Acad Sci U S A*, 100, 12877-82.
- Willer, C. J., Dyment, D. A., Sadovnick, A. D., Rothwell, P. M., Murray, T. J. & Ebers, G. C. 2005. Timing of birth and risk of multiple sclerosis: population based study. *BMJ*, 330, 120.
- Wilm, B. J., Svensson, J., Henning, A., Pruessmann, K. P., Boesiger, P. & Kollias, S. S. 2007. Reduced field-of-view MRI using outer volume suppression for spinal cord diffusion imaging. *Magn Reson Med*, 57, 625-30.
- Wilson, M., Reynolds, G., Kauppinen, R. A., Arvanitis, T. N. & Peet, A. C. 2011. A constrained least-squares approach to the automated quantitation of in vivo (1)H magnetic resonance spectroscopy data. *Magn Reson Med*, 65, 1-12.
- Winston, G. P., Micallef, C., Symms, M. R., Alexander, D. C., Duncan, J. S. & Zhang, H. 2014. Advanced diffusion imaging sequences could aid assessing patients with focal cortical dysplasia and epilepsy. *Epilepsy Res*, 108, 336-9.
- Wrigley, P. J., Gustin, S. M., Macey, P. M., Nash, P. G., Gandevia, S. C., Macefield, V. G., Siddall, P. J. & Henderson, L. A. 2009. Anatomical changes in human motor cortex and motor pathways following complete thoracic spinal cord injury. *Cereb Cortex*, 19, 224-32.
- Wu, J., Stoica, B. A., Luo, T., Sabirzhanov, B., Zhao, Z., Guancia, K., Nayar, S. K., Foss, C. A., Pomper, M. G. & Faden, A. I. 2014. Isolated spinal cord contusion in rats induces chronic brain neuroinflammation, neurodegeneration, and cognitive impairment. Involvement of cell cycle activation. *Cell Cycle*, 13, 2446-58.
- Yaldizli, Ö., MacManus, D., Stutters J., Haring, D., Lublin, F., Freedman, M., Kappos, L., Cree, B., Wolinsky, J., Weiner, H., Lubetzki, C., Hartung, H.P., Montalban, X., Uitdehaag, B., Merschhemke, M., Li, B., Putzki, N. & Miller, D.H.

2015. Brain and cervical spinal cord atrophy in primary progressive multiple sclerosis: results from a placebo-controlled phase III trial (INFORMS),ECTRIMS.
- Yiannakas, M. C., Kearney, H., Samson, R. S., Chard, D. T., Ciccarelli, O., Miller, D. H. & Wheeler-Kingshott, C. A. 2012. Feasibility of grey matter and white matter segmentation of the upper cervical cord in vivo: a pilot study with application to magnetisation transfer measurements. *Neuroimage*, 63, 1054-9.
- Zackowski, K. M., Smith, S. A., Reich, D. S., Gordon-Lipkin, E., Chodkowski, B. A., Sambandan, D. R., Shteyman, M., Bastian, A. J., Van Zijl, P. C. & Calabresi, P. A. 2009. Sensorimotor dysfunction in multiple sclerosis and column-specific magnetization transfer-imaging abnormalities in the spinal cord. *Brain*, 132, 1200-9.
- Zhang, H., Hubbard, P. L., Parker, G. J. & Alexander, D. C. 2011. Axon diameter mapping in the presence of orientation dispersion with diffusion MRI. *Neuroimage*, 56, 1301-15.
- Zhang, H., Schneider, T., Wheeler-Kingshott, C. A. & Alexander, D. C. 2012. NODDI: practical in vivo neurite orientation dispersion and density imaging of the human brain. *Neuroimage*, 61, 1000-16.
- Zhang, J., Jones, M., Deboy, C. A., Reich, D. S., Farrell, J. A., Hoffman, P. N., Griffin, J. W., Sheikh, K. A., Miller, M. I., Mori, S. & Calabresi, P. A. 2009. Diffusion tensor magnetic resonance imaging of Wallerian degeneration in rat spinal cord after dorsal root axotomy. *J Neurosci*, 29, 3160-71.
- Zigmond, A. S. & Snaith, R. P. 1983. The hospital anxiety and depression scale. *Acta Psychiatr Scand*, 67, 361-70.
- Zivadinov, R., Havrdova, E., Bergsland, N., Tyblova, M., Hagemeier, J., Seidl, Z., Dwyer, M. G., Vaneckova, M., Krasensky, J., Carl, E., Kalincik, T. & Horakova, D. 2013. Thalamic atrophy is associated with development of clinically definite multiple sclerosis. *Radiology*, 268, 831-41.
- Zivadinov, R., Reder, A. T., Filippil, M., Minagar, A., Stuve, O., Lassmann, H., Racke, M. K., Dwyer, M. G., Frohman, E. M. & Khan, O. 2008. Mechanisms of action of disease-modifying agents and brain volume changes in multiple sclerosis. *Neurology*, 71, 136-44.